UNIVERSITÉ DE SHERBROOKE

Faculté des sciences appliquées

Département de génie électrique
et génie informatique

QUANTUM WELL INTERMIXING CONTROLLED BY EXCIMER LASER FOR PHOTONIC DEVICE INTEGRATION

Thèse de doctorat
Spécialité : Génie électrique

Composition du jury:
Vincent AIMEZ
Richard Arès
Jan J. DUBOWSKI
Amr S HELMY

Sherbrooke (Québec), Canada Juin 2008

Résumé

L'intégration de composants discrets sur un système unique, tel une puce électronique, augmente les performances totales du système, fait apparaitre de nouvelles fonctionnalités et diminue les coûts associés à la fabrication des dispositifs. Ces améliorations, appliquées au secteur de la microélectronique, sont grandement responsables des avancements importants qu'ont connus les technologies de l'information et des communications au cours des dernières années. Puisque la fabrication de circuits photoniques intégrés nécessite l'intégration de structures ayant des bandes interdites différentes à partir d'une même puce semiconductrice, leur niveau d'intégration est bien inférieur que celui atteint pour un microprocesseur standard.

Parmi les techniques ayant le potentiel de fabriquer des circuits photoniques intégrés monolithiquement, l'interdiffusion de puits quantique post-expitaxial contrôlée spatialement augmente la bande interdite d'une hétérostructure semiconductrice à l'intérieur de régions définies. Le processus d'interdiffusion, activé thermiquement, est accéléré par la diffusion d'impuretés et de défauts ponctuels tels que les lacunes et les interstitiels. L'hypothèse de départ de mes travaux de doctorat suppose que la radiation laser ultra-violette module la diffusion et la génération de défauts ponctuels dans les hétérostructures reposant sur les technologies à base de GaAs et d'InP et, conséquemment, contrôle spatialement l'interdiffusion de puits quantiques.

Nous avons démontré que lorsque appliquée sur des hétérostructures à base de GaAs, l'irradiation laser excimère l'interdiffusion en favorisant la croissance d'un stresseur de surface qui empêche la diffusion des défauts ponctuels vers les puits quantiques. Nous avons souligné

l'influence de la vapeur d'eau physisorbée sur la croissance du stresseur et avons déterminé la résolution spatiale de la technique. Dans les hétérostructures basées sur les technologies InP, même sous le seuil d'ablation, l'absorption des impulsions laser UV favorise la désorption des atomes de surface ce qui génère des défauts ponctuels en concentration excédentaire. Lors d'un recuit thermique, ces défauts ponctuels participent au processus d'interdiffusion sous les régions irradiées.

Summary

Integration of discrete components into a single system, such as an electronic chip, increases the system total performance; makes new functionalities appear and lowers the overall manufacturing cost. In microelectronics, theses important improvements have been largely responsible for enabling the recent advancements in information and communication technologies. Because the fabrication of photonic integrated circuits requires the integration of multiple bandgap structures within a single semiconductor chip, their integration level is far from the one achieved in a common microprocessor chip.

Among the potential techniques to achieve monolithic photonic integrated circuits postgrowth quantum well intermixing in selected areas locally increases the effective band gap energy of a semiconductor heterostructures. The thermally activated intermixing process is accelerated by the diffusion of impurities and of point defects such as vacancies and interstitials. For this thesis work, we hypothesised that UV laser irradiation modulates point defect diffusion and generation in GaAs and InP based heterostructures and therefore controls quantum well intermixing in specific areas.

This was verified by patterning GaAs and InP quantum well heterostructures with KrF and ArF laser pulses in various gaseous environments at different fluences and number of pulses. The intermixing was then activated during a rapid thermal annealing step.

We demonstrated that in GaAs based heterostructure, excimer laser irradiation inhibits quantum well intermixing by growing a surface stressor which prevents the diffusion of point

defects toward the well. We highlighted the influence of physiorbed water vapour on the stressor growth and determined the spatial resolution of the technique. In InP based heterostructure, even below ablation threshold, UV laser absorption in InP favours desorption of surface atoms which generates an extra concentration of point defects. During the annealing, these point defects participate to the intermixing process under the irradiated areas.

Acknowledgements

Firstly, I would like to thank my thesis advisors Vincent Aimez and Jan Dubowski, professors at the Département de génie électrique et génie informatiques of the Université de Sherbrooke, for the quality of their supervision. Their unconditionnal support and the experience and knowledge they shared with me insured the success of the different phases of my work. Without their guidance, encouragements and, sometime, “cracking-of-the-whip”, I would never have finished.

I would also like to express my deepest thanks to the Amr S. Helmy, professor at the department of Electrical and Computer engineering of the University of Toronto, and Richard Arès of the Département de genie mécanique of the Université de Sherbrooke, for managing to read the whole thesis exhaustively and for the quality of their questions, inputs and comments.

I would like to express my gratitude to Dr Mike Post, of the Institute for Chemical Process and Environmental Technology of the National Research Council of Canada in Ottawa for providing me access to his laser setup and for generously sharing his professional experience during our discussion.

I thank Professor Denis Morris of the département de physique of the Université de Sherbrooke for granting me access to his research laboratory to characterize my samples.

Many thanks also to my fellow PhD colleagues, Romain Béal, Sarah Ghania Farih, Radoslaw Stanoski and Maité Volatier-Ravat for the numerous and enlightening discussion and for their encouragements. Their inputs were always appreciated and helpful.

Thanks to Jean Beerens, Abdelatif Jaouad, and Étienne Grondin, research professionnals at the Université de Sherbrooke, and to Nicolas Pauc, researcher at the Comissariat de l'énergie atomique, for generously sharing their knowledge, experience and opinions on countless topics.

This thesis work would not have been without the excellent technical support offered by Christian Clavet, Guillaume Bertrand, Mélanie Cloutier, Michael Lacerte, Pierre Lafrance and Caroline Roy.

I also thank the rest of the academic and support staff of the Centre de recherche en nanofabrication et nanocaractérisation at the Université de Sherbrooke as well as the other undergraduated and graduated students with whom I had the chance to interact during the last four years.

Finally, I have to say a sincere 'thank-you' to all my friends and family, wherever they are, particularly my parents and most importantly to France, who taught me how to make small problems out of an impossible one.

Jonathan

January 15, 2008

Table of content

List of figures

List of tables

Lexicon

CL	Cathodo-luminescence
CLWI	Cathodo-luminescence wavelength imaging
CMOS	Complementary metal–oxide–semiconductor
DWDM	Dense wavelength division multiplexing
Excimer	Excited dimmer
Exciplex	Excited complexes
FWHM	Full width at half maximum
GRIN	Graded index structure
IDD	Impurity induced disordering
III-V	Three-five semiconductor, semiconductor made of atoms from the third and fifth column of the Mendeleev table
ITU	International telecommunication union
L-I	Luminescence emission versus the injected current
Nd:YAG	Neodymium-doped yttrium aluminum garnet; Nd:$Y_3Al_5O_{12}$
PCB	Printed circuit board
PECVD	Plasma enhanced chemical vapour deposition
PL	Photoluminescence
QW	Quantum well
QWI	Quantum well intermixing
RTA	Rapid thermal annealing
UV	Ultra-violet

UV-QWI	UV laser controlled quantum well intermixing
WDM	Wavelength division multiplexing
XPS	X-ray photo-electron spectroscopy

Chapter 1: Introduction

In the last twenty years, information and communication technologies developed themselves at an intense rate. The development and the democratisation of the World Wide Web and of wireless technologies, the apparition on the market of new services such as the voice-over-IP, telemedicine, video on demand and the accessibility of tons of multimedia files on the web have tremendously increased the bandwidth demand on the telecommunication networks. Since 2000 the global network traffic has been dominated by internet data and has grown at rates in the order of 100% per year [M. Smit 2005]. The key feature to this explosive growth was the introduction of optical technology in the telecommunication network.

Because they can transmit an encoded signal over long distances with minimal losses and without heat dissipation, optical fibres have become the new ideal medium for data transmission. As of 2008, telecommunication systems with optical fibres still are mainly used for long distance connections and they only offer few interconnections and low flexibility. The invention of wavelength division multiplexing (WDM), which consists of transmitting multiple signals on different channels positioned at different wavelengths in a single optical fibre, increased the capacity of optical fibre networks. Moreover, since different wavelengths don't interact with each others, the implementation of wavelength division multiplexing didn't require too many modifications to the actual fibre networks. Only the transmission and reception modules needed to be upgraded. The implementation of WDM technologies adds new functionalities to the networks. For example, specific channels could be attributed to different services.

The WDM grids were defined to address different applications (figure 1-1). The C-band (1528-1561 nm) and the L-band (1561-1620 nm) are mainly used. These two grids use a variation of WDM technologies called dense wavelength division multiplexing (DWDM) and are mainly used in telecommunication system covering long distances such as inter-continental networks. The International telecommunication union (ITU) defines the standard for DWDM networks. The standard grids count between 32 and 160 channels, with an allocated spacing varying between 1.6 and 0.2 nm. In an extreme case, a 128 channels optical transceiver for this system requires 128 lasers, 128 modulators, a series of coupling waveguides and an optical multiplexer to couple the multiplexed signal in the optical fibre.

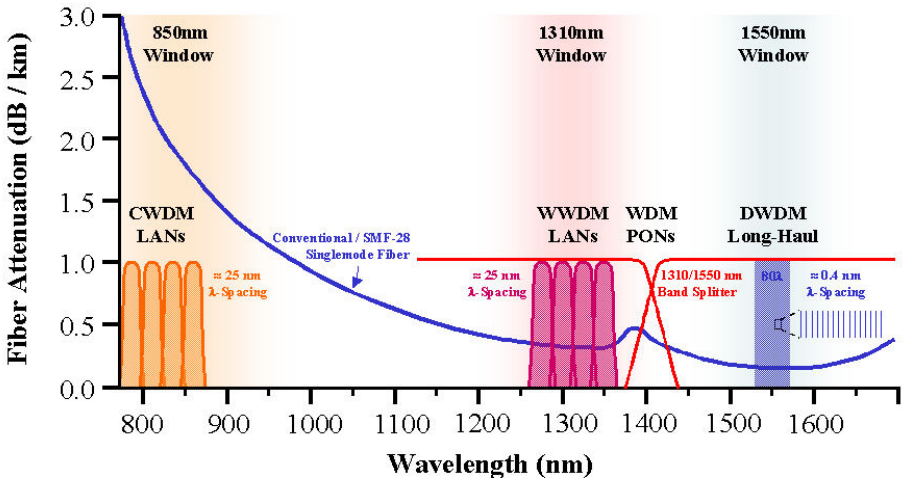

Figure 1-1: Wavelength division multiplexing spectral grids. The blue line represents the attenuation in a regular SMF 28 fibre [RBN 2002].

Although, optical interconnections have tremendous advantages, they only represent 1% of the total number of interconnections and are mainly dedicated to long haul communication [S. Koehl *et al.* 2005]. The remaining 99% are still copper based interconnections and are dedicated to short range communications, to distances going from computer-to-computer to chip-to-chip (figure 1-2). However, as new online services become available and as the bandwidth demand increases, copper-based interconnections need to be denser and problems associated with heat

dissipation and electro-migration start to arise. In such context, optical communication on shorter distance becomes more and more attractive. On the other hand, the high cost related to the installation of optical systems explains their limited use: it only costs few cents to make a copper based interconnection while it costs between few hundreds to few thousand dollars to install an optical transceiver. This is why telecommunication companies limit their installation on optical routes where huge amount of data are transferred from a point A to a point B.

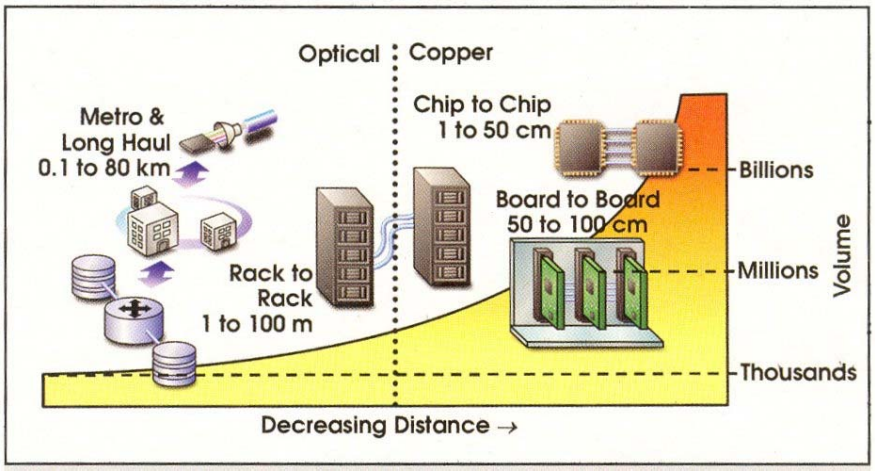

Figure 1-2: Interconnections volume versus the distance over which the data is transmitted [S. Koehl *et al.* 2005].

1.1 Moore's law

In electronics, since the 70s, key features such as processor speed and memory density are doubling every 18 months. This relation, known as the Moore's law [G. Moore 1965], has been mostly driven by the development of microelectronic integration technologies. It has demonstrated that integrating different devices on a single chip not only allowed to reduce the size and the cost of each component but also allowed the mass production of integrated circuits. Furthermore, increasing the complexity and the devices density on a chip resulted in the emergence of new functionalities unavailable with a few discrete electronic devices. This development has allowed the steadily increase of devices performance while systems were

essentially kept at a constant price. This can be illustrated by the fact that we pay our new computers the same price that we paid our previous one three years ago. However, the new ones have four times the speed of the previous ones. This dynamics, which has driven the microelectronics market, would have collapse without constant innovations on integration technologies.

Inspired by the microelectronics example, researchers have already tried, with limited success, to fabricate photonic integrated circuits. The advantages of integrating different photonic devices on a single optical chip are considerable. It reduces the inventory costs, save space, simplify mechanical designs, increase the robustness and it reduces the coupling steps between the different components. According to Jeremy Mills, in 2002, 60 to 90% of the fabrication costs of photonic devices were related to the devices encapsulation [J. Mills 2002]. Therefore the possibility to include many components under a single package is quite attractive. An efficient integration would also ameliorate the devices optical and electronic properties. For example, it would reduce the losses associated with optical interconnection between the discrete devices. From the optoelectronic point of view, bringing the electronic control circuit right next to the modulator would also limit the parasite inductances and would allow the modulators to operate at higher frequencies.

1.2 Integrating passive components

If we want photonic devices to play a more substantial role in the information and communication technologies, photonics needs to follow a similar dynamics as that of microelectronics. Research institutes and industries are putting tremendous effort in finding a solution to this problem. For passive devices such as waveguides, couplers and gratings, the size is the key to the integration: smaller size means more devices on a wafer. In waveguide

technologies, dimensions and bending radii can be reduced by increasing the index contrast between the core and the cladding. Depending on the substrate type (silica-on-silicon, silicon-on-insulator, III-V semiconductor based), this is done ether by increasing the doping level in the waveguide core or by increasing the depth of the etched walls. In both cases, reducing the size also increases the losses and the crosstalk. This is mainly due to increased scattering of light at a rough core/cladding interface. Nevertheless, this technology was used to fabricate highly compact and multifunctional passive photonic integrated circuits. For example, compact array waveguide gratings were fabricated on deeply etched InP and on silicon-on-insulator substrate (figure 1-3a and b).

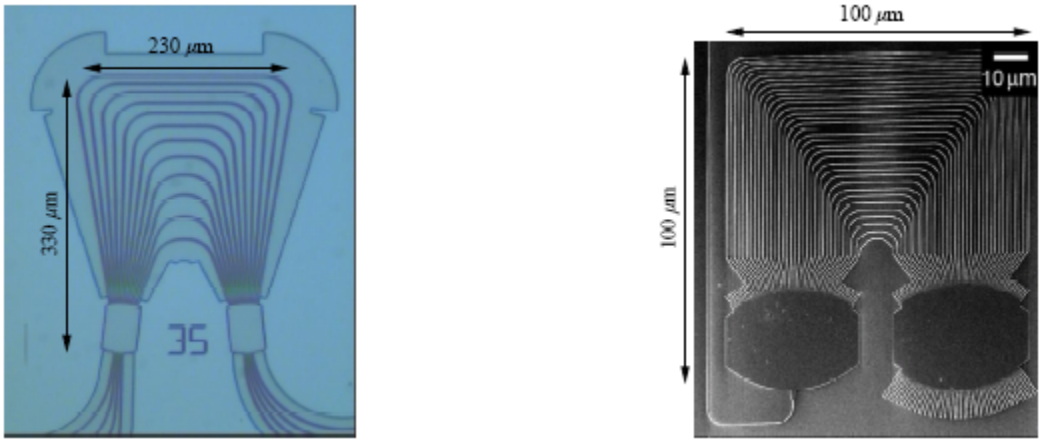

Figure 1-3: Compact array waveguide gratings fabricated a) in deeply etched InP and b) in silicon-on-insulator technology [X. Leijtens *et al.* 2005].

Reducing the device size has significant advantages but the full potential of miniaturization lies in the integration of different components in integrated circuits. Similarly to electronic integrated circuits, theses circuits demonstrate increased functionality. An example of such system is a 40 channels optical channel monitor (figure 1-4). This 0.25 cm^2 chip integrates nine array waveguide gratings and 40 detectors. Furthermore, it is already available commercially.

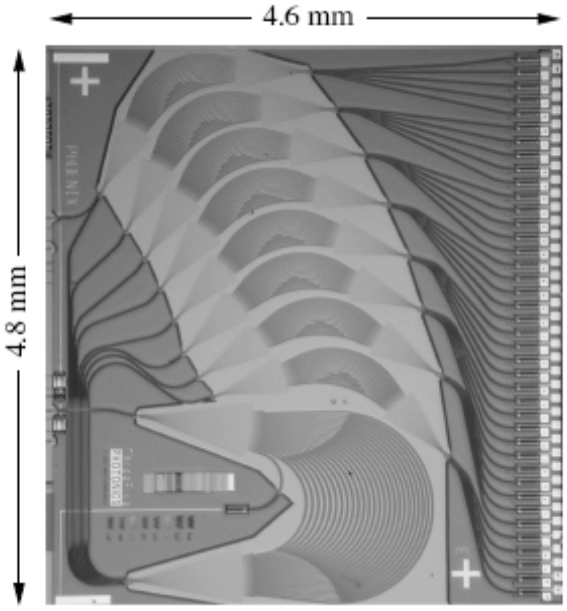

Figure 1-4: A 40 channels optical channel monitor commercially available fabricated by ThreeFive Photonics [X. Leijtens *et al.* 2005].

1.2.1 Emitting the light

To support the integration of almost all the functions required in information and communication technologies, it is imperative that the integrated devices also emit light to transmit data. This explains why researchers from academic institutions, research laboratories and semiconductor companies have invested millions of dollars to fabricate a silicon based laser [S. Coffa 2005]. Because of the indirect bandgap of silicon, to emit light, electrons located at the bottom of the conduction band need to transfer their momentum to phonons as they recombine with holes. Therefore the occurrence of a emitting a photon in silicon is at least one thousand times smaller than in a III-V semiconductor. To overcome this issue, different strategies have been pursued: silicon nanocrystals in SiO_2 [L. Pavesi *et al.* 2000], silicon seeding with rare-earth ions [J. Lee *et al.* 2005] and Raman stimulated emission [R. Claps *et al.* 2002]. The latter approach was used to fabricate the first continuous silicon laser [N. Rong *et al.* 2005]. However, the light emitting devices made in silicon are not very efficient, the best slope efficiency obtained

by Rong was 4.3%, and can rarely be pumped electrically. Because of theses limitations, silicon based technologies are not yet suitable to achieve complete monolithically integrated circuits.

III-V semiconductors technologies, on the other hand, allowed generation and detection of light in various wavelength widows. Moreover, their high refractive index is suitable for the fabrication compact designs thus dense integration.

Up to now, two approaches have been considered to fabricate different active and passive components on a single substrate. The first approach uses the hybridization of components: different devices, fabricated individually, are placed on a supporting substrate. The second approach consists of fabricating all the photonic devices directly from single wafer. This method is called the monolithic integration. It is important to note that theses two approaches are not mutually exclusive: they can be used simultaneously at different extent for the fabrication of a complex photonic integrated circuit.

Figure 1-5 explains the relationship between the appearance of densely integrated photonic devices, maturity of manufacturing technologies and the production volume. As the production volume increases, hybrid and monolithic solutions become more and more appealing because of their lower fabrication costs. On the other hand, complexity slows down the evolution toward monolithically integrated devices. This is because complex device designs make it more difficult to reach the levels of standardization and volume production needed to move to the next stage [J. Mills 2002].

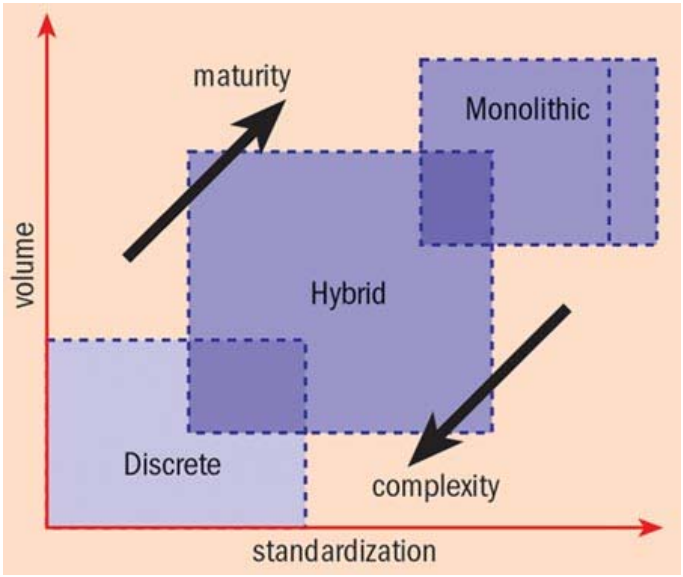

Figure 1-5: As a technology mature and production volume increases, densely integrated devices become the new standard [J. Mills 2002].

1.3 Hybridization

A comparison with electronic device manufacturing method can be made on an example of a printed photonic circuit where different discrete component are connected together on a PCB, as shown in figure 1-6. The substrate contains waveguides which act as data buses between the active components. One of the recent advances of this approach was achieved in 2006 by John E. Bowers and his colleagues [H. Park *et al.* 2005, A.W. Fang *et al.* 2006] and is being developed for the telecom market by Intel. They laminated a series of laser diodes on a silicon substrate on which modulators and waveguides were previous patterned, as shown in figure 1-7. The most important advantage of this approach concerns the use of dedicated substrates for dedicated applications: the electronic control circuit can be fabricated using CMOS electronics on a silicon substrate while the laser diodes can be fabricated on III-V semiconductors heterostructures. However, sticking multiple devices made out of different material on a single substrate can be challenging, especially if light needs to be coupled from a high index material, like a III-V semiconductor, to a lower index material, like silicon.

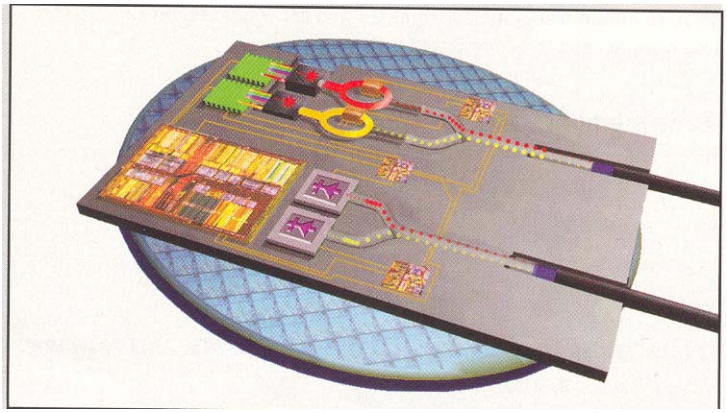

Figure 1-6: Schematic of a complex hybrid photonic integrated circuit [S. Koehl *et al.* 2005].

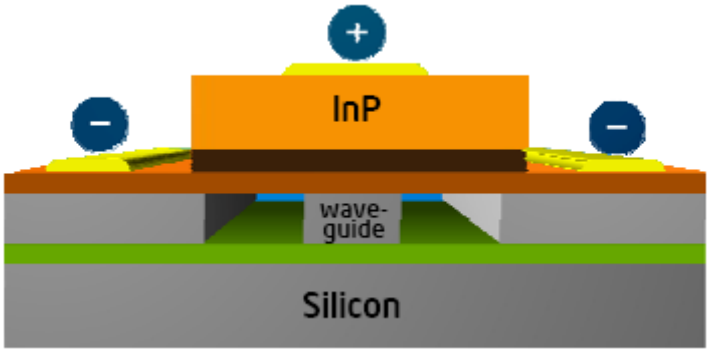

Figure 1-7: Cross section of a hybrid silicon laser [M. Paniccia *et al.* 2006].

1.4 Monolithic integration

The monolithic integration approach has been used successfully in the fabrication of simple photonic integrated devices. Commercially, laser diodes integrated with their modulators, as shown in figure 1-8, have been available commercially. The monolithic integration approach leads to much denser integration and more robust systems than the hybrid one. Since all devices are made from the same substrate, the coupling of light between the devices is much easier. However, monolithic designs, often suffer from very low yields.

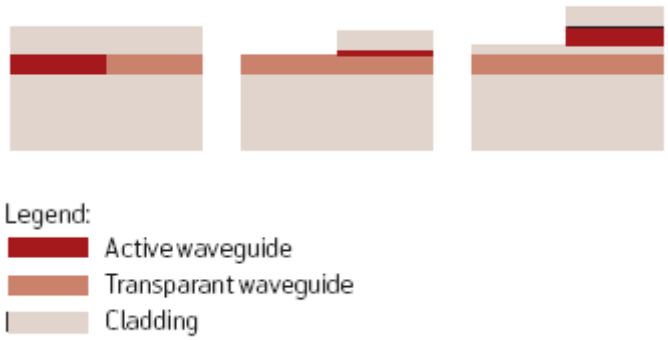

Figure 1-8: Three different avenues to couple active and passive waveguides [M. Smit 2005].

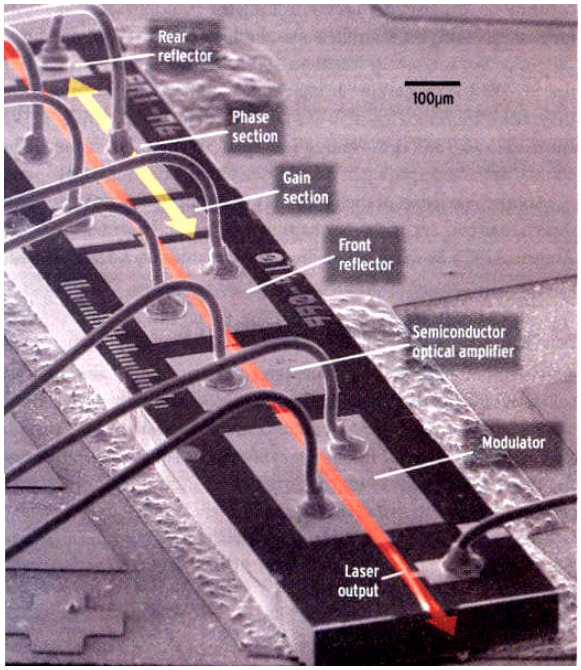

Figure 1-9: An example of a monolithically integrated photonic device. A tuneable laser is integrated with its modulator [E. Bruce 2002].

To address this issue, it is imperative to be able locally change the material properties of the initial substrate. Today, almost all monolithically integrated photonic devices are made by multiple epitaxial growths. This means that after the first growth, lithography and etching steps are applied on the sample before putting it back in the epitaxial reactor to make a second growth (figure 1-10). Since growth processes are long, and the etching treatments can generate a

considerable amount of defects at the surface and edges of the etched wafer, such technique can be costly and demonstrates low production rates. The defects embedded in the interfaces formed during etching procedures often cannot be removed during the consecutive growth and they become responsible for diminishing quality of the device.

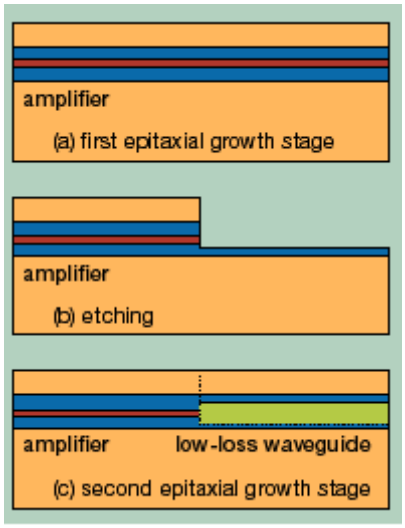

Figure 1-10: Principal steps required to fabricate an active/passive waveguide from an heterostructure [J.H. Marsh 2001].

Problems associated with the cost, low throughput and quality of the wafers fabricated by multiple epitaxial growths and etchings can be avoided if a post-growth process is developed which would allow fabrication of wafers with laterally modulated properties. In that context, quantum well intermixing (QWI) is one of the most promising approaches [E.H. Li 2000]. This process addresses quantum well heterostructure used to fabricate active photonic devices. Because of the heterogeneity in the composition of the heterostructure layers, it is possible to modulate the height of the bandgap by inducing atomic interdiffusion between the well and barrier materials [L.L. Chang *et al.* 1976, J.H. Marsh 1993, E.H. Li 2000].

However, compared with etching and regrowth steps, QWI also has some disadvantages. As it will be discussed, it is controlled by the diffusion of point defects. Theses point defects need

to be created and the technique used to do so can damage the heterostructure leaving it unfit for device fabrication. The residual presence of point defects also affects the device optical and electrical performances. Since the diffusion of point defect is most of the time isometric, the spatial resolution of the intermixing process can be an issue. The resolution then depends on the quantum well depth. Finally most explored QWI techniques do not offer the control and reproducibility needed for industrial applications.

1.5 Project description

This project addresses the need to investigate QWI in the context of known deficiencies of this approach. In particular, it aims at developing an innovative technology of QWI based on the application of UV excimer lasers for modification of surface properties of QW heterostructures and/or controlled introduction of defects required for enhanced intermixing of the QW and barrier materials. The goal is to investigate the potential of such an approach in developing a controllable and reproducible process capable of manufacturing monolithically integrated photonic devices based on the two main III-V semiconductors technologies: GaAs and InP. It also needs to be compatible with the actual micro-fabrication processes. For these reasons, I have chosen to investigate the fundamental mechanisms of UV laser controlled QWI.

Because of their versatility, lasers are a highly attractive tool for post-growth processing of semiconductor wafers. Depending on the emission wavelength and pulse duration, a laser can be used for local heating of semiconductor heterostructure [C.J. McLean *et al.* 1992, J.J. Dubowski *et al.* 2002], generating thermal shock which creates new point defects near the quantum well region [B.S. Ooi *et al.* 2004] or alter the surface chemistry [D.V. Podlesnik *et al.* 1986, J. Genest *et al.* 2007b]. All these effects have an immediate result on the point defects diffusion and thus on the QWI process. This project is based on two hypotheses. The principal

one stipulates that UV laser irradiation can control QWI in AlGaAs/GaAs and InGaAs/InGaAsP/InP laser diode heterostructures. The second one proposes that complex patterns of intermixed areas can be fabricated by developing a lithography technique based on excimer laser irradiation.

This project should allow the advancement of knowledge on the physical mechanisms involved in UV laser controlled QWI. It should evaluate the feasibility of UV excimer QWI in achieving sub-micrometer scale microstructures. Finally the developed technology should allow the fabrication of optoelectronic micro/nanostructures compatible with the actual industrial fabrication processes.

A summary of the theoretical concepts needed to understand this thesis is presented in chapter two. It covers the electronic properties of semiconductor heterostructures and the influence of mechanical strain of their properties. It also discusses the interactions of pulsed lasers with semiconductors. A particular attention is put on laser assisted desorption and ability of the laser to modify chemical composition of irradiated surfaces.

The third chapter reviews the techniques and advances in the QWI field. I introduce the QWI concept and describe the most common intermixing techniques. This chapter also discusses the effect of point defects diffusion in a stressed field.

The fourth chapter presents the methods I used to achieve the goals of this thesis. The excimer laser irradiation setups are described. The characterisation techniques used during my work are also presented in this chapter.

Chapter five presents the results of QWI controlled by UV excimer laser in AlGaAs/GaAs and in InGaAlGaAs/AlGaAs/GaAs laser diodes heterostructures. It contains an article, "Suppressed intermixing in InAlGaAs/AlGaAs/GaAs and AlGaAs/GaAs quantum well heterostructures irradiated with a KrF excimer laser", published in November 2007 [J. Genest *et al.* 2007a].

The lateral resolution of the UV laser suppression of QWI in GaAs-based quantum well heterostructure is discussed in the sixth chapter. The resolution was studied by photoluminescence mapping and cathodoluminescence. This chapter includes an article titled "UV laser controlled quantum well intermixing in InAlGaAs/GaAs heterostructures" [J. Genest *et al.* 2007b].

In the seventh chapter, I demonstrate how UV laser irradiation enhances QWI in InP heterostructures. I describe the enhancement of intermixing by a phenomenological model based on the radiation generation of point defects and assisted interdiffusion. The chapter main body is a manuscript submitted to Applied Physics Letters.

Chapter eight discusses new results which help understand more precisely the UV laser controlled QWI technique. In this chapter, I discuss the influence of the atmosphere during the irradiation procedure on the material surface chemistry and on the QWI extent. The spectral characteristics of laser diodes fabricated from intermixed samples are presented. I also study the potential of UV laser irradiation to achieve quantum dot intermixing.

1.6 Bibliography

Bruce, E. (2002) *Tunable Lasers*, IEEE Spectrum, vol. 39, n° 2, 35-39.

Chang, L. L. and Koma, A. (1976) *Interdiffusion between GaAs and AlAs*, Applied Physics Letters, vol. 29, n° 3, 138-41.

Claps, R., Dimitropoulos, D., et al. (2002) *Observation of Raman emission in silicon waveguides at 1.54 µm*, Optics Express, vol. 10, n° 22.

Coffa, S. (2005) *Ligth from silicon [LED]*, IEEE Spectrum, vol. 42, n° 10, 44-9.

Dubowski, J. J., Feng, Y., et al. (2002) *Monolithic multiple wavelength ridge waveguide laser array fabricated by Nd : YAG laser-induced quantum well intermixing*, Journal of Vacuum Science & Technology A, vol. 20, n° 4, 1426-1429.

Fang, A. W., Hyundai, P., et al. (2006) *A continuous-wave hybrid AlGaInAs-silicon evanescent laser*, IEEE Photonics Technology Letters, vol. 18, n° 10, 1143-5.

Genest, J., Dubowski, J. J., et al. (2007a) *Suppressed intermixing in InAlGaAs/ AlGaAs/GaAs and AlGaAs/GaAs quantum well heterostructures irradiated with a KrF excimer laser*, Applied Physics A: Materials Science & Processing, vol. 89, n° 2, 423-426.

Genest, J., Dubowski, J. J., et al. (2007b) *UV laser controlled quantum well intermixing in InAlGaAs/GaAs heterostructures*, Journal of Physics: Conference Series, vol. 59, n° 1, 605-9.

Koehl, S. and Paniccia, M. (2005) *The Quest fo Siliconize Photonics*, Photonics Spectra, vol. 39, n° 11, 53-66.

Lee, J., Shin, J. H., et al. (2005) *Optical gain at 1.5 µm in nanocrystal Si-sensitized Er-doped silica waveguide using top-pumping 470 nm LEDs*, Journal of Lightwave Technology, vol. 23, n° 1, 19-25.

Leijtens, X. and Smit, M. (2005) *Miniaturization of Passive Devices for Photonic Integration*, Proceedings of SPIE, vol. 6020, n° 60201Q-1.

Li, E. H., Ed. (2000). Semiconductor Quantum Wells Intermixing. Optoelectronic Properties of Semiconductors and Superlattices. Amsterdam, Netherlands, Gordon and Breach Science Publishers, 695 p.

Marsh, J. H. (1993) *Quantum-Well Intermixing*, Semiconductor Science and Technology, vol. 8, n° 6, 1136-1155.

Marsh, J. H. (2001). *Intermixing drives photonic integration (Fiber-Optic Components)*, Retrieved November 20th 2007, from http://compoundsemiconductor.net/cws/article/magazine/11887.

McLean, C. J., Marsh, J. H., et al. (1992) *Layer selective disordering by photoabsorption-induced thermal diffusion in InGaAs/InP based multiquantum well structures*, Electronics Letters, vol. 28, n° 12, 1117-1119.

Mills, J. (2002, Mai). *Photonic integration combats network complexity*, Retrieved November 17th, 2007, from http://www2.fibers.org/articles/fs/6/5/3.

Moore, G. (1965) *Cramming more components onto integrated circuits*, Electronics, vol. 38, n° 8.

Ooi, B. S., Ong, T. K., et al. (2004) *Multiple-wavelength integration in InGaAs-InGaAsP structures using pulsed laser irradiation-induced quantum-well intermixing*, IEEE Journal of Quantum Electronics, vol. 40, n° 5, 481.

Paniccia, M., Krutul, V., et al. (2006). *A Hybrid Silicon Laser - Silicon photonics technology for future tera-scale computing*, Retrieved December 14th, 2007, from http://download.intel.com/research/platform/sp/hl_wp1.pdf.

Park, H., Fang, A. W., et al. (2005) *Hybrid silicon evanescent laser fabricated with silicon waveguide and III-V offset quantum wells*, Optics Express, vol. 13, n° 23.

Pavesi, L., Negro, L. D., et al. (2000) *Optical gain in silicon nanocrystals*, Nature, vol. 408, n° 6811, 440-4.

Podlesnik, D. V., Gilgen, H. H., et al. (1986) *Interaction of Deep-Ultraviolet Laser-Light with GaAs-Surfaces in Aqueous-Solutions*, Journal of the Optical Society of America B-Optical Physics, vol. 3, n° 5, 775-784.

RBN. (2002, Septembre). *CWDM Technology, Standards, Economics & Applications*.

Rong, N., Jones, R., et al. (2005) *A continuous-wave Raman silicon laser*, Nature, vol. 433, n° 7027, 725-8.

Smit, M. (2005) *Photonic integration*, Telektronikk, vol. 05, n° 2, 66-71.

Chapter 2: Theoretical considerations

In this chapter, I present a review of physics principles needed to understand the extent and the implications of my thesis work. In the first section, I describe the bands structure in semiconductor heterostructures comprising quantum wells. I also present how charge carriers recombination can result in the emission of light and how this process is affected by the presence of defects, impurities and mechanical strain. The example of an InGaAs quantum well is used to illustrate these concepts.

In the second section of this chapter, I describe the interaction of a laser beam with semiconductors. I review different light absorption processes and describe the diverse desorption and ablation mechanisms. The influence of laser irradiation on the semiconductor surface morphology and stoichiometry is also discussed.

2.1 Energy band structures in semiconductors

Every crystal has its own energy band structure. This feature describes the wide range of optical and electrical properties in various materials. We can separate solids into three distinct categories following the relative position of the valence and conduction bands: metals, semiconductors and insulators. Metal (figure 2-1c) valence and conduction bands overlap or are only partially filled. In other words, electrons in the conduction band are at the same energy level as empty energy states so they can move freely in the presence of an external force. In semiconductors and in insulators, the bands are separated by an energy gap E_g empty of available energy states. Therefore, the bandgap is an energy barrier that an electron needs to overcome to

jump to the conduction band where it can contribute to the electric conduction. At 0 K, no electron is present in the conduction band of both semiconductors and insulators (figure 2-1a and b). The distinction between these two categories of materials is based on the height of their bandgaps. As a convention, materials with bandgap below 2 eV are considered as semiconductors while insulators have higher bandgap [B.G. Streetman *et al.* 2000]. The relatively small bandgap of semiconductors allows the excitation of electrons to the conduction band by a reasonable amount of thermal or optical energy.

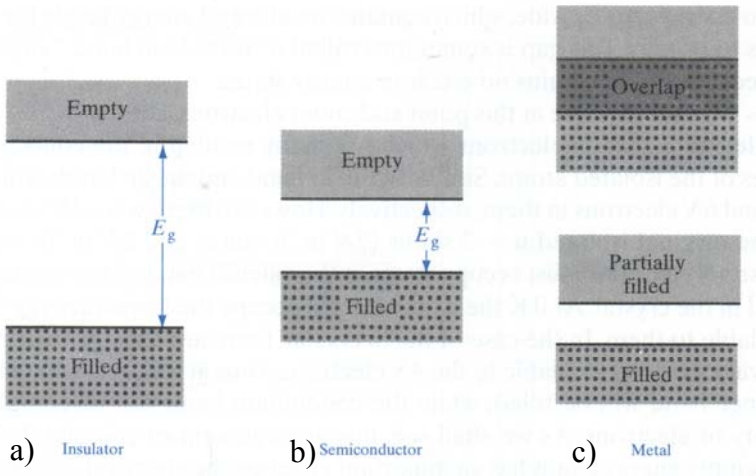

Figure 2-1: Typical bands profiles at 0 K for a) an insulator, b) a semiconductor and c) a metal [B.G. Streetman *et al.* 2000].

The formation and the position of the bands are directly related to the coupling of electronic orbitals in a crystal. All elemental semiconductors (silicon, germanium, carbon) can be found in the fourth column of Mendeleev's periodic table and all have a crystalline structure similar to that of a diamond. Compound semiconductors are made of elements that, when combined, have a mean number of valence electrons equal to four. These compound semiconductors are either made of atoms from the third and fifth columns of the periodic table (III-V semiconductors: GaAs, GaP, GaSb, GaN, InAs, InP, InSb, InN, AlP, AlAs, AlSb, AlN),

from the second and the sixth (II-VI semiconductors: ZnO, ZnS, ZnSe, ZnTe, CdS, CdSe, CdTe, HgS, HgSe, HgTe), from the forth group (IV-IV semiconductors: SiGe, SiC…), or less known semiconductors from the second and the fifth groups (II-V semiconductors: Zn_3As_2, Cd_3As_2, Cd_3P_2…). The combination of more than one binary compounds leads to the formation of ternary and quaternary compound semiconductors such as AlGaAs, InGaAs, InGaAsP and InAlGaAs.

Another distinct property of all semiconductors is their band diagram. It defines the position of the energy states versus the carriers' wave vector **k** (figure 2-2), or carriers' momentum. In most semiconductors, the valence band maximum is positioned at the Γ point of the Brillouin zone. The valence band has three branches, the heavy holes and light holes bands, which overlap at **k** = 0, and the spilt-off band, which maximum also happens at **k** = 0 but at a different energy. The conduction band minimum can be positioned at different wave vector values. A semiconductor has a direct bandgap (figure 2-3a) if the conduction band minimum and the valence band maximum are situated at the same wave vector position. This is the case in most III-V and II-VI compound semiconductors. On the other hand, when there is a momentum difference between the position of the conduction band minimum and the valence band maximum, the gap is considered indirect (figure 2-3b). This is the case in elemental semiconductors (C, Si, Ge) and in some III-V such as GaP, AlAs, AlP and AlSb.

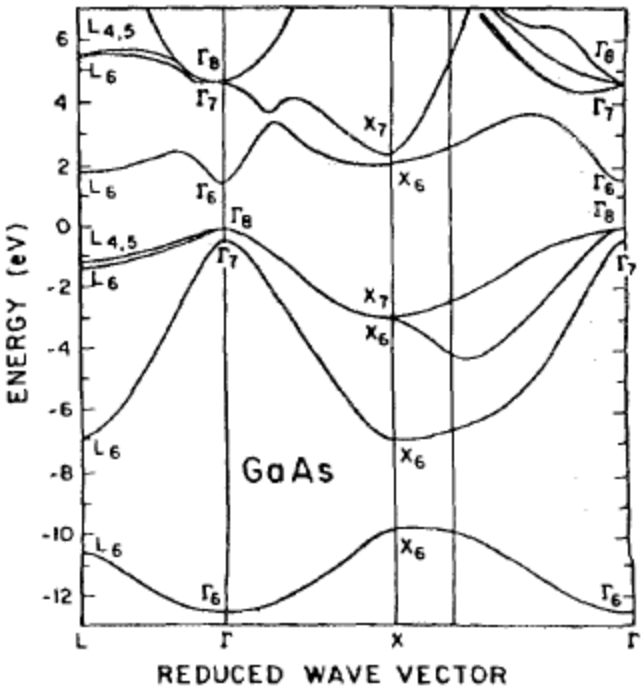

Figure 2-2: Electron energy in GaAs versus the reduced wave vector for the four valence bands and the first conductions bands [C.F. Yu *et al.* 1987]. The energy origin is set at the heavy-light holes maximum.

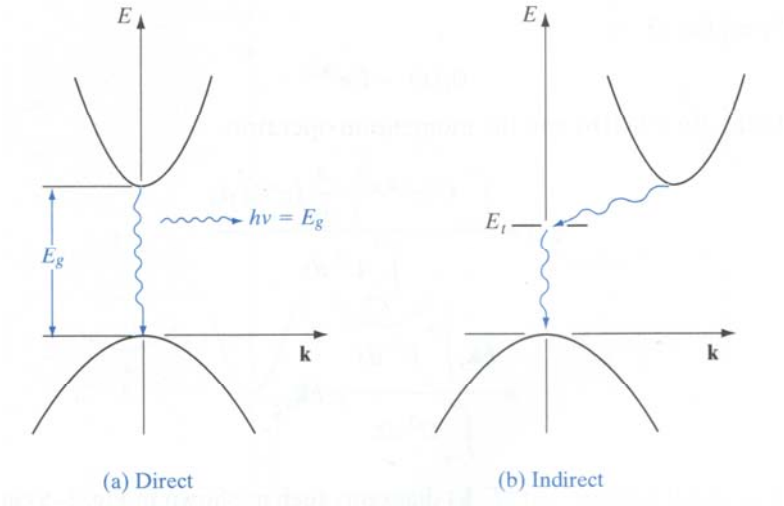

Figure 2-3: a) Direct and b) indirect bandgap in semiconductor [B.G. Streetman *et al.* 2000].

2.1.1 The quantum well

The quantum well is the result of a successive stacking of different materials. The very nature of the quantum well is at the basis of the QWI process. The well is formed if a relatively small bandgap material (e.g. GaAs) is sandwiched between two larger bandgap materials: the

barriers (e.g. AlGaAs). To minimize their energy, charge carriers tend to migrate toward the central region. Since the well thickness is of the order of electron wavelength inside the material, the well confines the charge carriers in the growth direction. The confinement leads to a discretisation of the energy levels inside the well. The levels position depends on the material composition and on the well thickness. By extension, a quantum wire confines the carriers in two dimensions while a quantum dot confines them in three dimensions.

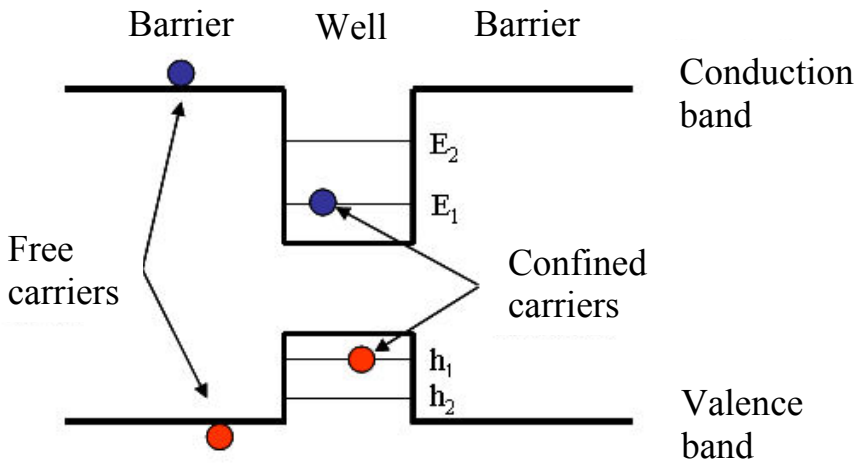

Figure 2-4: Schematic of a type I quantum well band structure

The relative position of the valance band of two different materials depends on there electronic affinity. It also determines the type of quantum well. A type I quantum well confines both electrons and holes in the central section while a type II only confines one type of carrier. Since type I quantum wells are the only type which confines both types of carriers in the well layer they are the only ones allowing direct inter-band recombination. Therefore, type I quantum well heterostructures are largely used for photonic applications in the visible and near/mid infra-red wavelengths. Photonic applications of type II quantum wells are usually based on intra-band transition which leads to the emission of far infra-red photons. Going forward, we'll implicitly consider type I quantum wells unless noted otherwise.

2.1.2 Charge carriers recombination

Since it is impossible to directly measure the band structure of a material, we need to use indirect methods. Most of these methods (absorption, transmission, luminescence, etc) are based on interactions between photons and charge carriers. We distinguish three types of interactions: absorption, spontaneous emission and stimulated emission. Absorption happens when a photon transmits its energy (E_{ph}) to an electron, making it jump from its initial state E_1 to a state E_2 on a higher energy level, so that $E_{ph} = E_2-E_1$. It is also imperative that the E_2 state is empty for the absorption to take place. With semiconductors, if the photons energy is higher than the bandgap energy, most transitions happen as electrons jumps from the valence band to the conduction band [B.G. Streetman *et al.* 2000]. The presence of a carrier vacancy in the valence band reorganises the molecular orbitals which forms a quasi-particle: the hole (figure 2-5a). Spontaneous emission is the inverse process of absorption. An electron relaxes through the emission of a photon of energy $E_{ph} = E_2-E_1$ (figure 2-5c). Since photons have almost nil momentum, this transition cannot be accompanied with a change in the carrier momentum. In other words, material with an indirect bandgap (e.g. silicon) cannot emit light through the simple recombination of an electron and a hole; this can only be done with the interaction of a third particle with a non-nil momentum (e.g. phonon). Since it implies the collision of three particles, the probability of an indirect transition is relatively low compared to relaxation through direct radiative processes.

Since the probability of making a collision with a phonon is higher than the probability of recombination, when an electron is excited to the higher levels of the conduction band, its energy is reduced through interaction with the crystal vibration until it reaches the bottom of the band (figure 2-5b). Finally, if a photon with energy $E_{ph} = E_2-E_1$ passes in the vicinity of an electron on

the energy level E_2, the photon can stimulate the electron hole recombination. This results in the emission of a second photon with the identical energy, direction, polarisation and phase of the first one. The latter transition is called stimulated emission. In contrast, photons emitted through the spontaneous emission process have random phase and direction. Figure 2-6 shows a schematic of absorption, spontaneous emission and stimulated emission in a system with two energy levels.

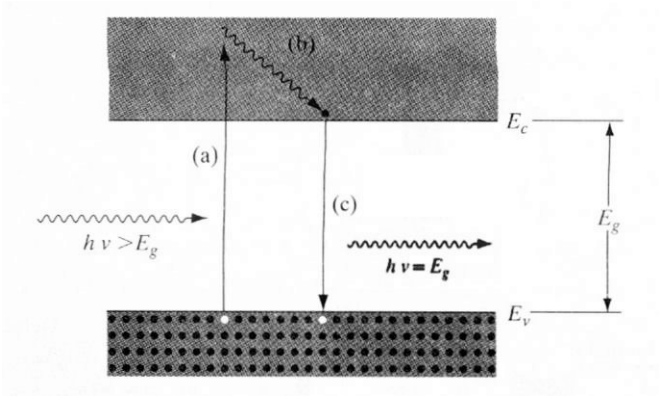

Figure 2-5: Absorption of a photon $h\nu > E_g$: a) Electron jumps to the conduction band and leaves a hole in the valence band b) electron reduces its energy through collisions with phonons c) electron and hole recombination and emission of a photon $h\nu = E_g$ [B.G. Streetman *et al.* 2000].

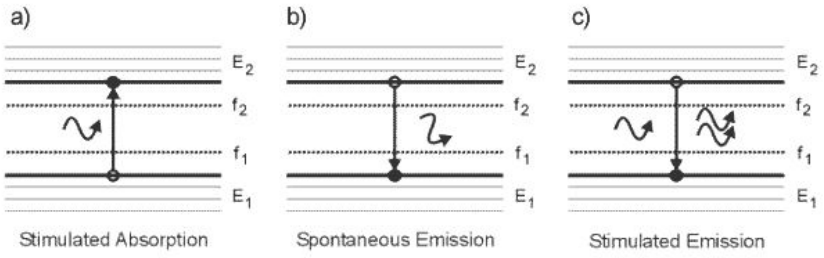

Figure 2-6: Photon and electron interactions in a system with two energy levels, a) absorption, b) spontaneous emission and c) stimulated emission [J.I. Pankove 1975a].

Defects and impurities also affect the electron wave function. This creates accessible energy levels, some of them inside the material bandgap. The related relaxations processes can be radiative or non-radiative. If the position of the energy level of impurities is very near the minimum of the conduction band or the valence band maximum, it is necessary to analyse the

semiconductor at a low temperature to distinguish transition related to impurities from the inter-bands one.

2.1.3 Strain and stress

Strain and stress have a direct influence on the material band structure. Applying a stress field on semiconductors heterostructure modifies the bandgap and the confinement profile. These phenomenon were used by Ahopelto to fabricate strain induced quantum dots from an InGaAs/GaAs quantum well heterostructure [J. Ahopelto *et al.* 1999]. Strained heterostructure are also used to fabricate low current threshold laser diodes because of the lower effective masse of the carriers in stressed materials [J.P. Loehr 1998].

2.1.3.1 Strain

We define strain (**ε**) as the distortion of a material from its position in equilibrium. More generally, if we consider a deformation vector $\vec{u}$, linear strain becomes:

$$\varepsilon_{ii} = \frac{\partial u_i}{dx_i}, \text{ for i = 1,2,3 so that } x_1 = x,\ x_2 = y \text{ and } x_3 = z, \tag{2.1}$$

and the shears strain becomes:

$$\varepsilon_{ij} = \frac{1}{2}\left(\frac{\partial u_i}{\partial x_j} + \frac{\partial u_j}{\partial x_i}\right), \text{ for i} \neq \text{j}. \tag{2.2}$$

All ε_{ii} and ε_{ij} are components of the strain tensor **ε**. The presence of an exclusive shear strain doesn't alter the material volume while linear strain results in compression or dilation. We define the material dilation as $\operatorname{div} \vec{u}$:

$$\operatorname{div} \vec{u} = \varepsilon_{xx} + \varepsilon_{yy} + \varepsilon_{zz}. \tag{2.3}$$

2.1.3.2 Stress

Stress is the force associated with an elastic distortion: $\vec{F} = -\mathrm{div}(\sigma)$. As for strain, we define the stress tensor $\boldsymbol{\sigma}$:

$$\sigma = \begin{bmatrix} \sigma_{xx} & \sigma_{xy} & \sigma_{xz} \\ \sigma_{yx} & \sigma_{yy} & \sigma_{yz} \\ \sigma_{zx} & \sigma_{zy} & \sigma_{zz} \end{bmatrix} \tag{2.4}$$

Strain and stress relate to each other through the Poisson ratio ν, the Young modulus Y_0 and the Shear modulus C':

$$\varepsilon_{xx} = \frac{1}{Y_0}\left[\sigma_{xx} - \nu\left(\sigma_y + \sigma_z\right)\right], \tag{2.5}$$

$$\varepsilon_{xy} = \frac{\sigma_{xy}}{2C'} = \frac{(1+\nu)\sigma_{xy}}{Y_0}. \tag{2.6}$$

Equations (2.5) and (2.6) can be generalised for all components of the strain tensor **ε.**

We can distinguish two specific stress configurations. The hydrostatic stress has identical linear components $\sigma_{xx} = \sigma_{yy} = \sigma_{zz}$ and no shear component. The strain counterpart is a diagonal matrix with all non-null components $\varepsilon_{ii} = \sigma_{ii}(1-2\nu)/Y_0$. The biaxial stress tensor is

$$\sigma_{biaxial} = \begin{bmatrix} \sigma_{\perp} & 0 & 0 \\ 0 & \sigma_{\perp} & 0 \\ 0 & 0 & 0 \end{bmatrix}, \tag{2.7}$$

where $\sigma_{\perp}$ is the strain component in the material plan perpendicular to the growth direction. The corresponding strain tensor is:

$$\varepsilon_{biaxial} = \frac{1}{Y_0}\begin{bmatrix} \sigma_{\perp}(1-\nu) & 0 & 0 \\ 0 & \sigma_{\perp}(1-\nu) & 0 \\ 0 & 0 & -2\nu\sigma_{\perp} \end{bmatrix}. \tag{2.8}$$

2.1.3.3 Effect of strain on the band structure of a crystal

The major effect of strain is mechanical: the sample bends like a common bimetallic strip. Surface distortions can be measured by atomic force microscopy (AFM) or scanning tunnelling microscopy (STM) to determine local strain values in a known material [J.H. Davies 2003]. When the strain is too high, it will also cause samples to break or devices to fail. Microscopically, strain affects the band structure. It shifts the conduction and valence band and it modifies the trapping rate of carriers and excitons by changing their effective masses [J.H. Davies 2003]. It also affects the material refraction index and can induce birefringence.

For direct bandgap, at the Γ point of the Brillouin zone, dilatation decreases the material bandgap by moving the conduction band and valence band closer to each other. Dilatation $\mathrm{div}\,\vec{u}$ reduces the position of the conduction band E_c as:

$$\Delta E_c = a_c \mathrm{div}\,\vec{u}\,, \tag{2.9}$$

where a_c is the deformation potential for the conduction band, typically -5 to -10 eV. Compression increases the position of the conduction band. Similarly, dilation also affects the position of the valence. However, this effect is modulated by the strain induced deviation from the crystal cubic symmetry [J. Micallef *et al.* 1993]. We define the axial strain ε_{ax} as the deviation from hydrostatic strain:

$$\varepsilon_{ax} = \varepsilon_{zz} - \frac{1}{2}\left(\varepsilon_{xx} + \varepsilon_{yy}\right). \tag{2.10}$$

We then define the shifts of the heavy holes band ΔE_{hh} and the light holes band ΔE_{lh} positions:

$$\Delta E_{hh} = a_v \mathrm{div}\,\vec{u} - b_v \varepsilon_{ax} \tag{2.11}$$

$$\Delta E_{lh} = a_v \mathrm{div}\,\vec{u} + b_v \varepsilon_{ax} \tag{2.12}$$

where a_v is the deformation potential for the valence band and b_v is the axial deformation potential. Equations (2.11) and (2.12) show that breaking the crystal cubic symmetry raises the heavy and light holes bands degeneracy at the Γ point of the Brillouin zone. Thus with negative axial strain (tensile biaxial strain), the light hole band becomes the lowest in energy (figure 2-7). It changes the holes' band curvature in the different wave-vector k directions, as described in figure 2-8, which changes the effective mass of heavy and light holes.

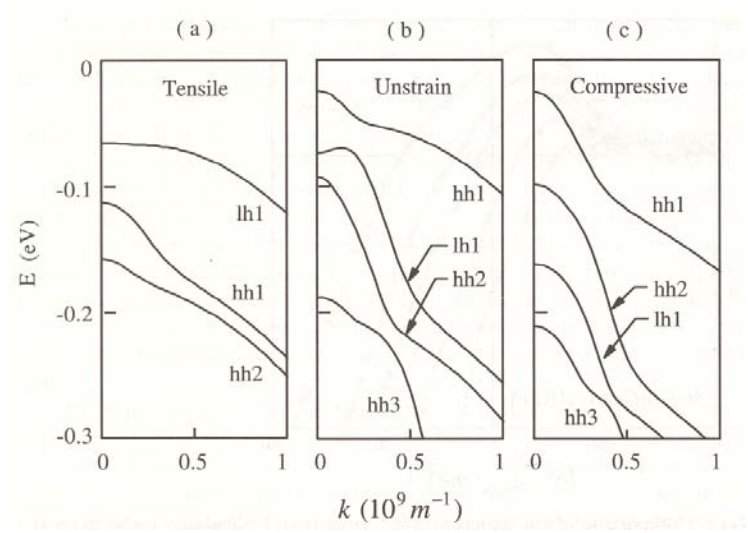

Figure 2-7: Heavy holes and light holes bands in a 5 nm $In_xGa_{1-x}As/InP$ quantum well for different biaxial strain configurations. The strain is controlled by choosing the indium composition in the well: a) tensile strain, x = 0.33, b) lattice matched on InP, x = 0.53, c) compressive strain, x = 0.73 [W.W. Chow *et al.* 1999].

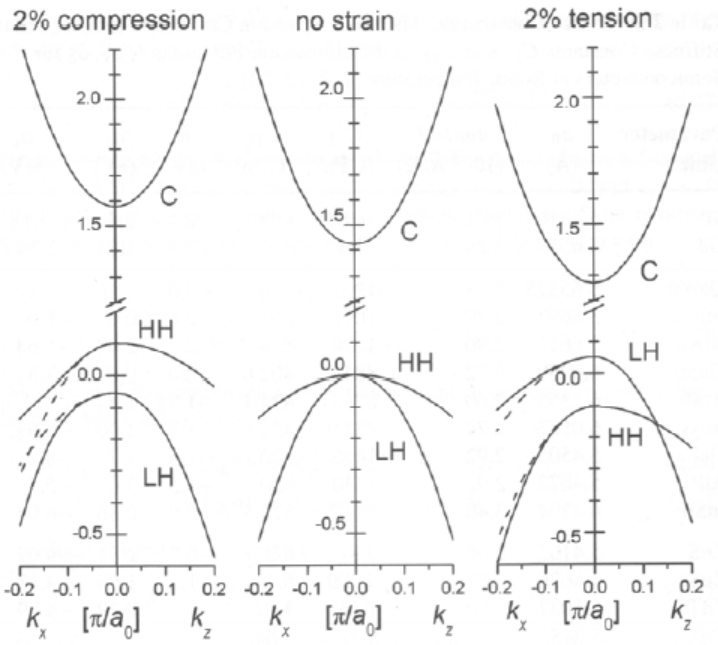

Figure 2-8: Raise of the heavy holes and light holes bands degeneracy at Γ position and change in the band curvature under axial strain [J. Piprek 2003] .

Generally, the refractive index depends on the material bandgap. Compression increases the bandgap and thus increases the index of refraction [P.A. Kirkby *et al.* 1979, M.F. Pereira, Jr. *et al.* 1993]. It can lead to the formation of a waveguide. Breaking the crystal symmetry makes the material birefringent. For a waveguide going in the *y* direction, the change in the dielectric constant for the transverse electric optical mode TE ($\Delta\in_{xx}$) and transverse magnetic TM waves ($\Delta\in_{zz}$) are expressed as [P.A. Kirkby *et al.* 1979]:

$$\Delta\epsilon_{xx} = -\epsilon_{xx}^2 \left\{ \varepsilon_{xx} \left[\frac{1}{2}\left(p_{11} + p_{12} \right) + p_{44} \right] + \varepsilon_{zz} p_{12} \right\}, \tag{2.13}$$

$$\Delta\epsilon_{zz} = -\epsilon_{zz}^2 \left(\varepsilon_{xx} p_{12} + \varepsilon_{zz} p_{11} \right), \tag{2.14}$$

where p_{ij} are a component of the photoelastic tensor.

Example of a InGaAs/GaAs quantum well under biaxial strain

To illustrate the effect of strain and stress on a real heterostructure, we'll consider a single strained InGaAs quantum well grown on a GaAs substrate. In such a case, a very thin layer of

InGaAs with lattice parameter a_f adapts itself to form a pseudomorphic strained layer with a new lattice parameter $a_\perp$ perpendicular to growth direction equal to the one of the substrate a_s. The perpendicular strain in the quantum well is then

$$\varepsilon_\perp = \varepsilon_{xx} = \varepsilon_{yy} = \frac{a_s - a_f}{a_s}. \tag{2.15}$$

Since in this case, $a_s > a_f$, the lattice expands itself in the *xy* plan. As a counterpart, it contracts in the growth direction *z*. To define strain effect on electron-hole recombination, we first need to define the biaxial strain tensor $\boldsymbol{\varepsilon}$, from equation (2.8):

$$\varepsilon = \begin{bmatrix} \varepsilon_\perp & 0 & 0 \\ 0 & \varepsilon_\perp & 0 \\ 0 & 0 & -2[c_{12}/c_{11}]\varepsilon_\perp \end{bmatrix} \tag{2.16}$$

where $\varepsilon_\perp$ is the strain in the plan xy, it is negative for compressive strain and positive for tensile strain and where c_{ij} are elastic deformation constants with $c_{12}/c_{11} = \nu/(1-\nu)$. To establish the dilatation induced change to the conduction band ΔE_c and valence band ΔE_v, we need to define the hydrostatic deformation potentials a_c and a_v for each band:

$$a_c = -\frac{1}{3}[c_{11} + 2c_{12}\frac{dE_c}{dP}], \tag{2.17}$$

$$a_v = -\frac{1}{3}[c_{11} + 2c_{12}\frac{dE_v}{dP}] \tag{2.18}$$

and where dE_c/dP and dE_v/dP are the hydrostatic pressure coefficients for the smallest direct bandgap. The change to the conduction band becomes:

$$\Delta E_c = \frac{2}{3}[c_{11} + 2c_{12}\frac{dE_c}{dP}]\left(1 - \frac{c_{12}}{c_{11}}\right)\varepsilon_\perp \tag{2.19}$$

From the axial strain component, we can establish the splitting of the heavy holes and light holes bands and determine their position:

$$\Delta E_{hh} = \frac{2}{3}[c_{11} + 2c_{12}\frac{dE_v}{dP}]\left(1 - \frac{c_{12}}{c_{11}}\right)\varepsilon_{\perp} - b_v\left[1 + 2\frac{c_{21}}{c_{11}}\right]\varepsilon_{\perp} \qquad (2.20)$$

$$\Delta E_{lh} = \frac{2}{3}[c_{11} + 2c_{12}\frac{dE_v}{dP}]\left(1 - \frac{c_{12}}{c_{11}}\right)\varepsilon_{\perp} + b_v\left[1 + 2\frac{c_{21}}{c_{11}}\right]\varepsilon_{\perp} \qquad (2.21)$$

The b_v, c_{ij}, dE_c/dP and dE_v/dP parameters in equations (2.16) to (2.21) depend directly on the composition profile through the quantum well. Figure 2-9 shows the strain effects on an intermixed InGaAs/GaAs quantum well.

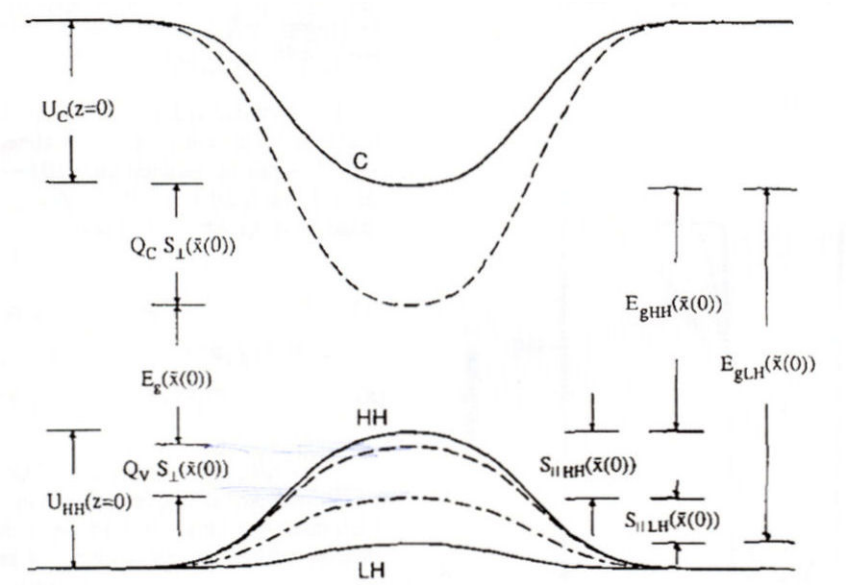

Figure 2-9: Strain influence on an intermixed InGaAs/GaAs quantum well [J. Micallef *et al.* 1993]. The dashed lines show the well original band profile, the dash-dot line shows the effect of the compression while the full lines show the heavy and light holes degeneracy raise due to the axial strain component.

2.2 Laser interaction with semiconductors

The alteration of material surfaces by light is a phenomenon which has been known for centuries. In the nineteenth century, Michel Faraday was the first to comment on the "solarisation" of glass by ultraviolet light. Even prior to Faraday's observation, discoloration, bleaching and cracking of sun exposed surfaces was observed commonly. However, the study of large scale light induced surface alteration over a short period of time had to wait for the development of a high density photon source: the laser.

In this section, I describe the basics of the laser-mater interaction between lasers and III-V semiconductors. I first introduce different photoexcitation processes then follow with a review of the laser induced desorption and ablation mechanisms. Desorption induced by thermal processes and mechanical stress are discussed together with desorption induced by the presence of a dense electron-hole plasma. Finally, I present the effect of laser irradiation on the semiconductor surface stoichiometry.

2.2.1 Photoexcitation and surface response

Depending on the laser wavelength, the material bandgap E_G, the free electrons density n_{ec} and the lifetime of non-radiative states τ_{NR}, we can define four types of absorption mechanism in semiconductors [A.A. Grindberg *et al.* 1967] :

1. Dielectric mechanism ($h\nu << E_g$)

   The absorption results from a direct interaction between photons and the lattice. Under high excitation, the absorption generates coherent hypersonic phonons.

2. Metallic mechanism (n_{ec} high)

   In this absorption type, which happens in material where the density of free carriers is high, conduction band electrons absorb photons energy by direct heating of the charge

carriers gas. The excitation is dissipated by means of collision between the electrons and the lattice.

3. Induced metallic mechanism ($h\nu > E_g$ and τ_{NR} long)

   Heavy excitation of the valence electron is essential to this mechanism. The light is absorbed by the non-equilibrium free carriers. This excitation process is more important than interband transitions.

4. *Pure* semiconductor mechanism ($h\nu > E_g$; τ_{NR} short)

   In this mechanism, the light absorption creates electron-hole pairs. The relaxation mechanism by which the charge carriers recombine, the response of the lattice to the creation and movement of free carriers and electron-hole pairs depend on the photon energy $h\nu$, on the material bandgap E_G, on the electronic structure and on the incorporated defects as illustrated in figure 2-10. The main mechanism of energy conversion to heat is through non-radiative electron-hole recombination.

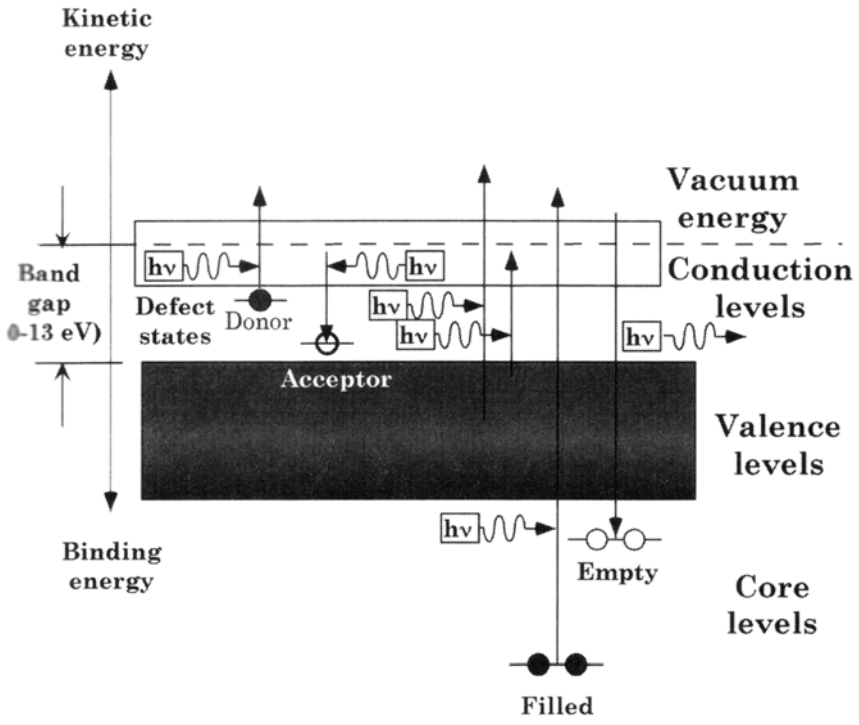

Figure 2-10: Schematic of the photon assisted energy transition process in a nonmetallic solid [J.C. Miller *et al.* 1998]

The laser induced desorption and damage dynamics will depend on the photoexcitation process. As UV photons energy is well above the energy of GaAs and InP bandgap, the absorption mechanisms in those materials must be of type 3 or 4, which means that thermal relaxation has a high influence on the damage generation process.

2.2.2 Laser induced desorption and ablation

When laser irradiation is absorbed by a material, the photon energy is converted to electronic and vibrational energy. The transformation of those photoexcited states into kinetic energy leads to the ejection of atoms, ions, molecules and clusters from the material surface. As a convention *laser induced desorption* is defined as the ejection of particles,

1. "without causing detectable mesoscopic modification to the surface composition or structure,
2. with a particle yield that is a linear function of the density of electronic and vibrational excitation,
3. without any significant gas dynamic effects in the steam of particles leaving the surface" [J.C. Miller *et al.* 1998].

On the other hand, *laser ablation* is defined as the sputtering process in which

1. "material removal rates typically exceed one-tenth monolayer per pulse,
2. surface is structurally or compositionally modified at mesoscopic length scales,
3. particle yields are superlinear functions of the density of excitation" [J.C. Miller *et al.* 1998].

Also, an expanding gas cloud of ablated material, the ablation plume, complicates the picture of laser ablation by adding concepts of plasma-surface interaction, gas dynamics and laser induced photochemistry to the principles of laser-mater interaction. The distinction between laser induced desorption and laser ablation is not very sharp. At low fluences, desorption of the surface may lead to material modification that would allow ablation later on.

It is generally accepted that macroscopic damage induced by a nanosecond laser pulses occurs when the material temperature reaches its fusion threshold [A.V. Kuanr *et al.* 1996b, A. Garg *et al.* 2003b]. In such a case, the rapid expansion of the irradiated material occurring during the phase transition ejects part of the material from its surface. This is also known as phase explosion. Following this definition, it is possible to determine a material theoretical threshold to damage from the heat diffusion equation. Kuanr and Garg teams showed the validity of this

model by analysing pulsed laser irradiated (λ = 1.06 μm, Δt ~ ms) GaAs, Si and Ge samples with scanning electron microscopy and optical reflectivity measurements.

2.2.2.1 Laser pulse absorption and heat transfer processes

The solution to the heat diffusion equation allows the calculation of the heat spatial and time distributions [A.A. Grindberg *et al.* 1967, J.R. Meyer *et al.* 1980, A.V. Kuanr *et al.* 1996a, A. Garg *et al.* 2003a] in the semiconductor. We start from the heat diffusion equation adapted from the Fourier theory:

$$\rho c \frac{\partial T}{\partial t} = k \frac{\partial^2 T}{\partial x^2} + (1-R)\alpha P_0 e^{-\alpha x} \tag{2.22}$$

where ρ is the material density, c is the specific heat, k is the thermal conductivity, R is the reflection coefficient, α, the absorption coefficient, P_0, the applied power density while T, t and x are respectively the temperature, the time and the depth. We also define the thermal diffusion coefficient $D = k/\rho c$. Table 2-1 shows the values of these constants for InP and GaAs for a 248 nm excitation wavelength. By considering a semi-infinite substrate, the border conditions are:

$$1)\ \lim_{x\to\infty} T(x) = 0\,, \quad \left.\frac{\partial T}{\partial x}\right|_{x=0} = 0\,, \quad T(x)_{t=o} = T_0\,,$$

the solution to equation (2.22) is:

$$\begin{aligned} T(x,t) = \frac{(1-R)P_0}{k\alpha}\Bigg[& 2\sqrt{D\alpha^2 t}\ \mathrm{ierf}\left(\frac{x}{2\sqrt{Dt}}\right) - \exp(-\alpha x)... \\ & + \frac{1}{2}\exp\left(D\alpha^2 t - \alpha x\right)\mathrm{erfc}\left(\sqrt{D\alpha^2 t} - \frac{x}{2\sqrt{Dt}}\right)... \\ & + \frac{1}{2}\exp\left(D\alpha^2 t - \alpha x\right)\mathrm{erfc}\left(\sqrt{D\alpha^2 t} + \frac{x}{2\sqrt{Dt}}\right)\Bigg] + T_0. \end{aligned} \tag{2.23}$$

Table 2-1: Thermal, mechanical and optical properties of GaAs and InP

	GaAs	Reference	InP	Reference
k (W/cm-K)	$0.425(300/T)^{1.1}$	Kuanr 1996	0.68 (T=300)	NSM Archive
ρ (g/cm^3)	5.31	NSM Archive	4.81 (T=300)	NSM Archive
c (J/g-K)	0.303+0.015(T/300)	Kuanr 1996	0.31 (T=300)	NSM Archive
D (cm^2/s)	0.25 (T=300)	NSM Archive	0.372 (T=300)	NSM Archive
R^1 (λ = 248 nm)	0.6 (T=300)	Phillip and Ehrenreich 1963	0.6 (T=300)	Aspnes and Studna 1983
R^* (λ = 193 nm)	0.4	Phillip and Ehrenreich 1963	0.4	*Properties of InP* [1991]
α (cm^{-1})* (λ = 248 nm)	2x10^6 (T=300)	Casey et al. 1975	5.05x10^6 (T=300)	Aspnes and Studna 1983
α (cm^{-1})* (λ = 193 nm)	1.4x10^6	Casey et al. 1975	1.3x10^6	*Properties of InP* [1991]
T_{fusion} (K)	1520	Kuanr 1996	1333	NSM Archive
β (°C^{-1})	5.73x10^{-6}	NSM Archive	4.60x10^{-6}	NSM Archive
Y_0 (dyn/cm^2)	8.59x10^{11}	NSM Archive	6.11x10^{11}	NSM Archive
p_0	0.31	NSM Archive	0.36	NSM Archive

2.2.2.2 Mechanical damage

Desorption and defect creation can happen even below the fusion threshold. The huge temperature gradient induces strain inside the material. If the strain value is high enough, the material will relax itself by creating defects. Laser induced surface strain (σ_0) can be expressed with the following equation [Y. Matsuoka 1976]:

$$\sigma_0 \simeq \frac{2\alpha Y_0}{1-\nu}\frac{P_0}{k}\left(\frac{D}{t}\right)^{\frac{1}{2}}\left[-\frac{1}{\sqrt{\pi}}+\frac{2\sqrt{Dt}}{L}-\frac{1}{\sqrt{\pi}}\left(\frac{2\sqrt{Dt}}{L}\right)^2\right] \tag{2.24}$$

where α, Y_0 et ν are respectively the material thermal expansion coefficient, the Yong modulus and the Poisson ratio, while L is the sample total thickness. It is also possible to establish a direct relationship between the induced shear constant and the ablation threshold for most semiconductors having a Zinc-Blend crystalline structure (figure 2-11).

[1] It is important to note that reflection and absorption coefficient also depend on the surface roughness. For example, at 1.06 µm, GaAs reflection coefficient goes from 0.35, for a perfect cleaved surface, to 0.1 for a surface characterised with a mean roughness of 10 µm. Under the same conditions, the absorption coefficient goes from 5 cm^{-1} to 55 cm^{-1}.

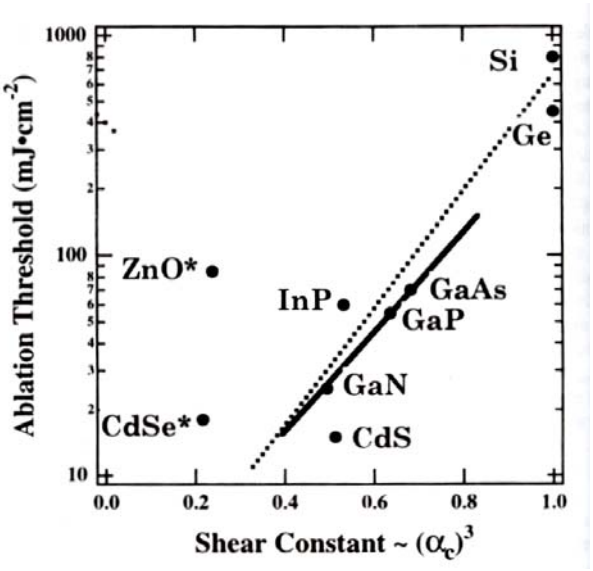

Figure 2-11: Semiconductor ablation threshold as a function of their shear constant [K. Ichige *et al.* 1988].

2.2.2.3 Desorption associated with electron/hole plasma

The non-thermal photo-induced desorption processes depends on competition between localized and delocalized relaxation processes (figure 2-12). This competition depends strongly on the material properties, such as the electron-lattice coupling, laser wavelength and pulse duration. III-V semiconductors compounds are characterized by a weak electron-lattice coupling. In such solids defect induced or plasma generated processes are often the primary mechanisms that lead to desorption or ablation (figure 2-13) [G.S. Khoo *et al.* 1993]. One of the localization mechanisms in weak-coupling solids is called the negative-U – or negative potential – interaction, illustrated in figure 2-14. This negative potential is caused by the elastic distortion in the lattice due to the occupation of a single lattice site by two charge carriers. The total correlation energy $U = U_{electronic} - U_{elastic}$ is negative under different condition depending on the material nature and defects type.

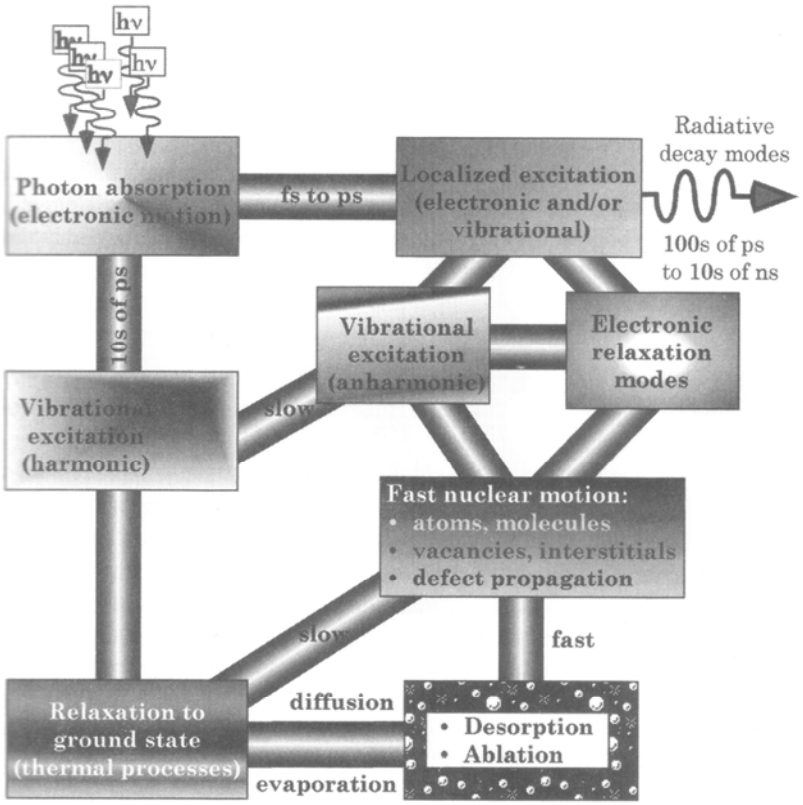

Figure 2-12: Competition between localized and delocalized relaxation mechanisms [J.C. Miller *et al.* 1998].

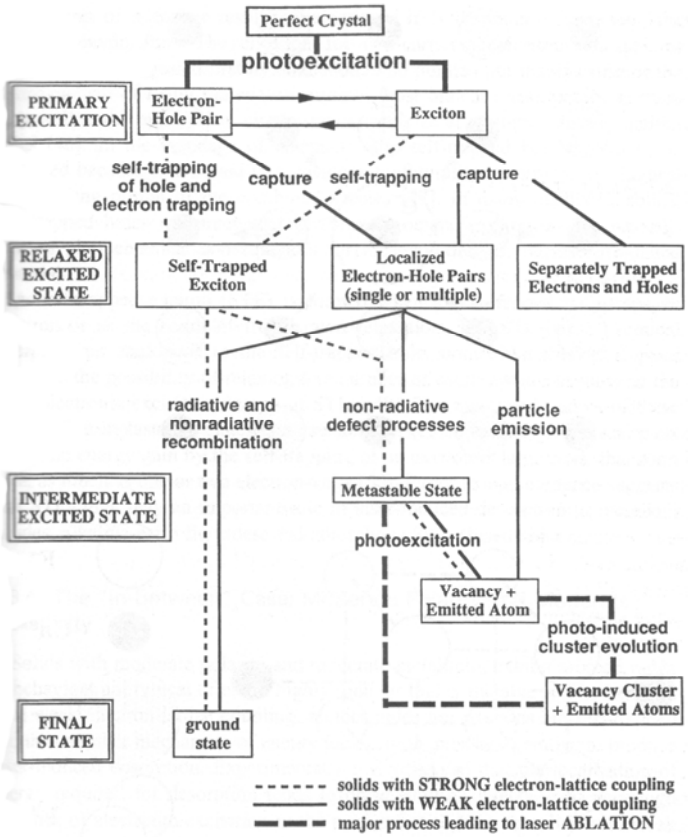

Figure 2-13: Flow diagram showing the intermediary states from photo-excitation to desorption in the cases of strong and weak electron-lattice coupling [J.C. Miller *et al.* 1998].

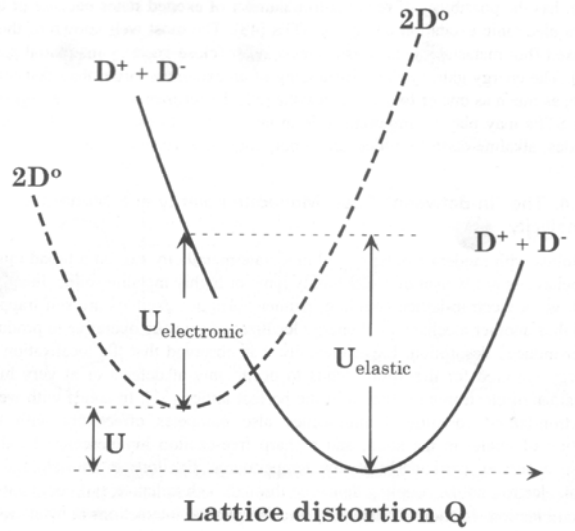

Figure 2-14: Schematic of the potential energy at the surface for a negative-*U* interaction. The lowering of the total energy is done through the localization of two carriers at a single site. D0 represents a singly occupied dangling bond, while D^+ and D^- are respectively unoccupied and doubly occupied dangling bonds [J.C. Miller *et al.* 1998].

Two holes localization by negative-U interaction has been observed in bulk semiconductor on defect sites. Particularly, it was found that such an interaction takes place on *DX* center in GaAs [T.N. Theis *et al.* 1988] and on V^+ center in Si [G.A. Baraff *et al.* 1979, G.D. Watkins *et al.* 1980]. On defect sites on the semiconductor surface, two holes localization is possible if an atom of the surface is displaced outward [M. Raff *et al.* 1994]. This will normally lead to a negative change in the correlation energy U. Normally, two holes localization on a defect site is initiated by carrier trapping, however the localization of two carriers can also results in a sequential excitation of a defect state.

In very dense plasmas of charge carriers, two holes localization can occur without the mediation of a defect site. A possible explanation was proposed by Itoh and Nakayama: two holes could be localized at a single surface site if the energy associated with the Coulomb repulsion was less than the energy gain from the lattice distortion. This model also explains the existence of a fluence threshold for ablation. At this threshold, the density of the electron-hole plasma is too low to effectively screen the charge of the two holes until they both enter the interaction of the negative-U potential. By evaluating the screened Coulomb potential, they were able to calculate the probability of particle emission by the laser induced electron-hole plasma [N. Itoh *et al.* 1985]. Another explanation of this phenomenon proposes that two holes localization is achieved if the density of electron-hole pairs is high enough so the Fermi energy of the degenerated holes is higher than the potential barrier associated with the Coulomb repulsion [H. Sumi 1991, K. Tanimura *et al.* 2006].Such induced desorption by two holes localization on perfect lattice surface site was observed in silicon [K. Tanimura *et al.* 2006] and in InP [T. Gotoh *et al.* 2004]. Surface or near surface vacancies created by the laser induced desorption were analysed by scanning tunnelling microscopy. Even though a dense electron-hole plasma allows the

localization of two holes on the same surface site and subsequent desorption, the probability that such localization occurs near an already existing defect is higher. This results in the clustering of laser induced surface vacancies for a long irradiation period [J. Kanasaki 2006].

Desorption associated with photoemission of electrons

Under UV photon irradiation, desorption can also occur through Coulomb explosion. Since UV photons are absorbed in the first few nanometers of a semiconductor, they generate a high concentration of highly energetic electrons. Theses electrons can be photo-emitted if the photon energy $h\nu$ exceeds the material work function PE [W. Marine *et al.* 2004]:

$$PE = \frac{1}{2}\alpha \frac{I(x,t)}{h\nu} \exp\left(\frac{-x}{l_{PE}}\right), \tag{2.25}$$

where α is the material absorption coefficient and l_{PE} is the electron escape depth. The laser intensity profile can be expressed as:

$$I(x,t) = (1-R)\frac{2F}{\tau} \exp(-\alpha x) \times A(t) \tag{2.26}$$

where R is the reflection coefficient while F and τ are respectively the laser fluence and the pulse duration. The function $A(t)$ describes the laser pulse temporal shape. The number of photo-emitted electrons N_{PE} per surface unit can be estimated:

$$N_{PE} = \frac{\alpha(1-R)F}{2h\nu\left(\alpha + l_{PE}^{-1}\right)}. \tag{2.27}$$

The emitted electrons leave a net positive charge on the sample surface which results in the formation of an electric field E which can be estimated using Gauss law:

$$E\big|_{x=0} = \frac{1}{2\varepsilon\varepsilon_0}\int_0^L q(x)\,dx = \frac{eN_{PE}}{2\varepsilon\varepsilon_0} = \frac{e\alpha(1-R)F}{4\varepsilon\varepsilon_0 h\nu\left(\alpha + l_{PE}^{-1}\right)}, \qquad (2.28)$$

where L is the sample thickness and ε, the material dielectric permittivity. If this electric field is higher than the critical electric field, positive ions will be thrown out of the target, reducing the electrostatic stress. Figure 2-15 shows the electric field generated by electron photoemission induced by an ArF laser on silicon target. Marine *et al.* estimated the critical field E_{th} for silicon from the latent heat of sublimation Λ_{at}: $E_{th}\big|_{x=0} = \sqrt{2\Lambda_{at}/\varepsilon\varepsilon_0 V_0} \approx 2.65\times10^{10}\ \mathrm{V/m}$, where V_0 is the volume occupied by a silicon atom [W. Marine *et al.* 2004].

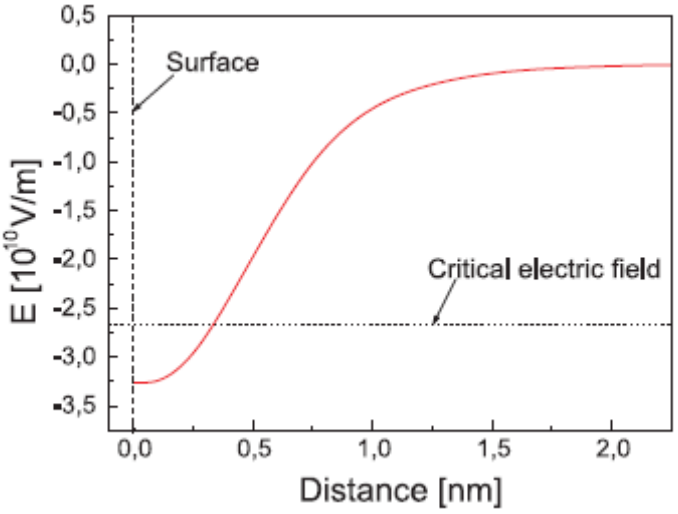

Figure 2-15: Spatial distribution of the electric field in a silicon target under ArF laser irradiation (200 mJ/cm^2) [W. Marine *et al.* 2004].

2.2.2.4 Surface stoichiometry modification and oxidation

In the previous section, I have discussed desorption of surface atoms under laser illumination. Under vacuum, since the vapour pressure of group V elements is higher than that of group III atoms, arsenic and phosphorus desorb predominantly. This results in a change of the stoichiometry at the surface of the semiconductor. Different research teams [L. Vivet *et al.* 1997, J.C. Miller *et al.* 1998] observed the formation of metallic islands after laser irradiation. This tendency for a compound semiconductor to form a metal rich surface under laser ablation is quite

general. However, over a certain time threshold, the group III rich surface reduces the desorption rate of group V atoms which leads to an equal desorption of groups III and V atoms.[M. Raff *et al.* 1994]

Laser irradiation in different atmospheres also affect the desorption rates. For example, a GaAs sample irradiated in a Cl_2 environment will have its gallium and arsenic removed at the same rate [S. Takatani *et al.* 1995]. In an environment containing oxygen or water vapour, laser irradiation also results in enhancing the oxidation rate of gallium arsenide. Naturally, GaAs reacts with the atmosphere and forms a thin layer (~3 nm) of native oxide at its surface. This native oxide is composed primarily of Ga_2O_3 and As_2O_3 but As_2O_5 Ga_2O, $GaAsO_4$, As_2 are also part of the mixture [D.A. Allwood *et al.* 2000]. Different research teams have reported an oxidation rate enhancement when a GaAs [S.A. Schafer *et al.* 1981] or a Si [E.M. Young *et al.* 1983] sample was exposed to laser illumination. Petro *et al.* measured an increase, up to 1000 times, of the GaAs surface absorption of oxygen under Ar^+ (514.5 nm) laser irradiation. They attributed this phenomenon to the photoassisted increase of density of charge carriers at the surface [W.G. Petro *et al.* 1982]. GaAs reconstructed surface has no site available for binding oxygen, however as seen in the previous section, the localisation of the charge carriers on surface defects weakens, or even breaks, the bonds which can make the site available for oxygen adsorption.

UV light also induces an even faster oxidation than visible light (figure 2-16) whether it was done in aqueous solution [D.V. Podlesnik *et al.* 1984] or in air environment [D.V. Podlesnik *et al.* 1986]. In addition to the faster oxidation in aqueous solution, UV light irradiation also leads to arsenic depletion on the surface because of the high solubility of arsenic oxides in water [D.V. Podlesnik *et al.* 1986]. As for regular oxidation, the oxide growth rate saturates because of the oxygen atoms' diffusion through the oxide barrier (figure 2-17a). Figure 2-17b shows that,

because of the smaller size of the H_2O molecule, the oxidation rate is faster in the presence of water vapour than in dry O_2 environment [J.D. Plummer *et al.* 2000].

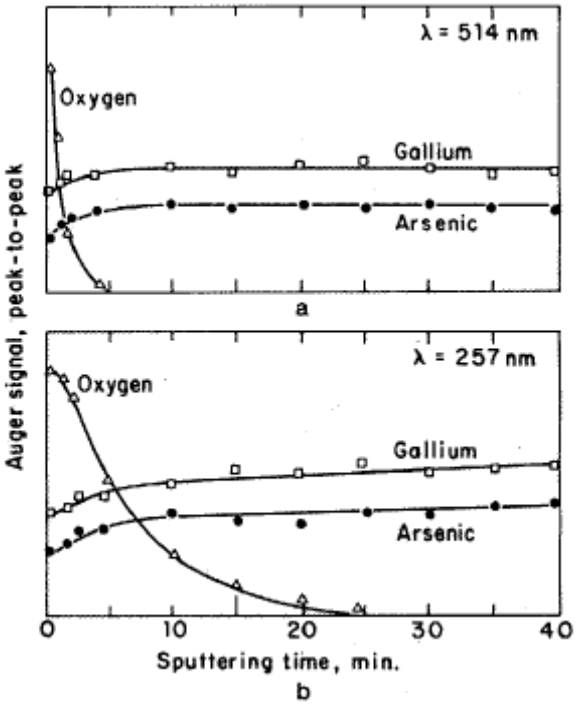

Figure 2-16: Auger electron spectroscopy depth profiles of GaAs sample irradiated with ~100 mW/cm^2 a) 514 nm and b) 257 nm lasers [D.V. Podlesnik *et al.* 1986].

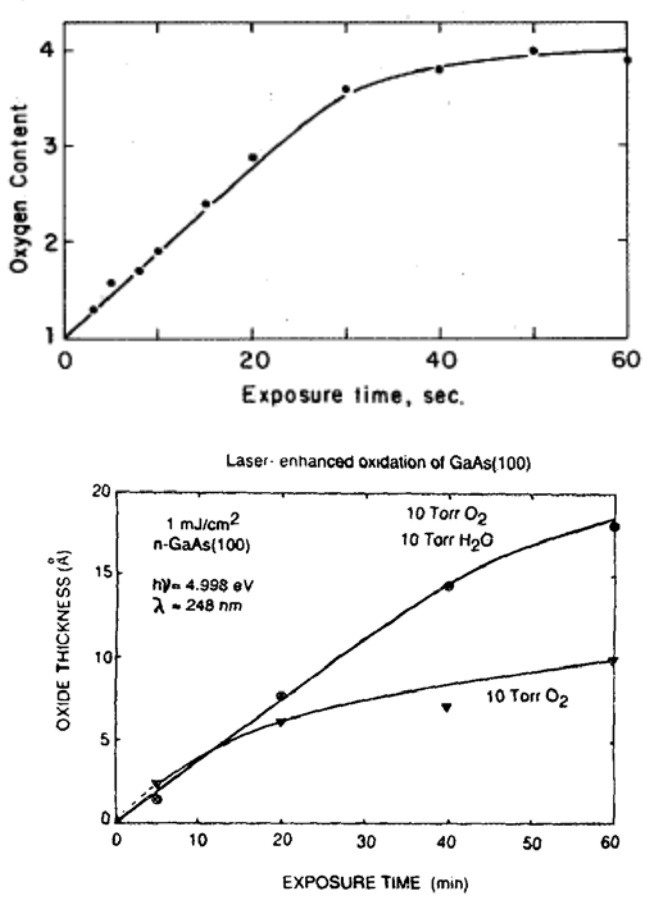

Figure 2-17: a) Relative change of the oxygen content at the GaAs surface versus irradiation time [D.V. Podlesnik *et al.* 1986], b) GaAs oxide thickness as a function of the KrF laser exposure time for dry O_2 and moist O_2 environment [C.F. Yu *et al.* 1987].

To further understand the photo-enhanced oxidation process, Yu *et al*. tested the influence of the incident photons wavelength on the oxidation rate (figure 2-18). The main reason explaining why UV light contributes more efficiently to the oxidation process is the fact that visible and ultraviolet photons are absorbed in different parts of the Brillouin zone, thus generating electrons and holes of different energies [C.F. Yu *et al.* 1987]. When exposing GaAs to light going from visible to deep UV wavelengths, this results in an increase of the absorption coefficient by a factor of 20. Under UV light, the photo-generated carriers are then confined to the surface vicinity. Since they are generated at a distance less than 5 nm from the surface, theses high energetic carriers can diffuse to the surface without completely relaxing. At the surface, most of

the hot holes still have enough energy to access the H_2O of O_2 redox level (0.4 eV below the top of the GaAs valence band) and enhance the reaction rate of oxygen with GaAs [D.V. Podlesnik *et al.* 1986]. Thermalised electrons or holes generated at longer wavelengths can't access the redox level and thus can't stimulate the chemical reaction. With photons energies higher than the dissociation energy of O_2 ($E_{O_2 \rightleftharpoons O^+ + O^-} = 5.13$ eV), the GaAs oxidation is accelerated by the presence of oxygen reactive ions or ozone [S. Ingrey *et al.* 1986]. Similar oxidation results were obtained on indium phosphide [S. Ingrey *et al.* 1987] and silicon [E.M. Young *et al.* 1987].

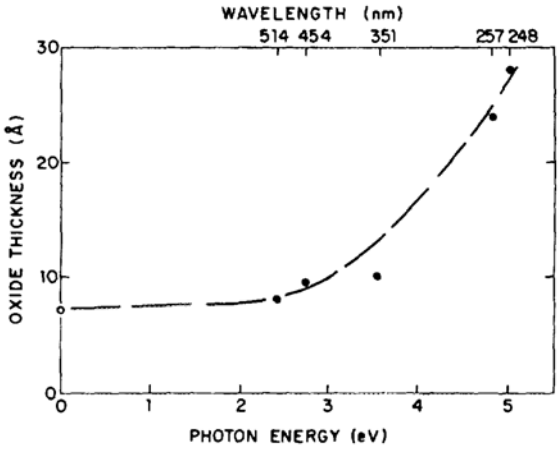

Figure 2-18: GaAs oxide thickness after 20 min irradiations at 50 mW/cm^2 for different wavelengths [C.F. Yu *et al.* 1987].

2.3 Summary

In this chapter, I have presented a review of the physics principles needed to understand the extent and the implications of my thesis work. The nature of semiconductors and their interaction with light was presented. I put an emphasis on the interaction of III-V semiconductors with laser pulses and how it can lead to surface atoms desorption and to changes in the surface stoichiometry because it plays an important role in the research undertaken in this thesis.

I discussed the bands profile influence on the optical properties of semiconductors. I also discussed the quantum well concept, whose nature is at the basis of the QWI process. The thickness and the composition of the well also control the optical properties of optoelectronic devices made from the heterostructure.

The concepts of strain and stress were also introduced. We have seen that they modify the electrical and optical properties of a semiconductor. The dilation decreases the bandgap while deformations that change the crystal symmetry raise the heavy and light holes bands degeneracy at the Γ position of the Brillouin zone. The presence of a pseudomorphic strained layer with a different lattice parameter than the substrate's results in the formation of a biaxial stress.

I distinguished the concepts of desorption and ablation and described their principal sources. They can result from heat transfer from the excited charge carriers, from the mechanical stress induced by the temperature gradient or from the presence of a free electrons and holes plasma. In the latter case, two models describe the desorption process. The first one is valid for all wavelengths with enough energy to excite electrons from the valence band to the conduction band. In very dense plasmas of charge carriers, two holes localization can occur at a surface site where it breaks the atomic bonds, freeing the surface atom. The second model is valid for wavelengths which are absorbed first few nanometers of the irradiated material, such as ultraviolet photons. They generate a high concentration of highly energetic electrons which are emitted from the surface. The resulting Coulomb force expulses surface ions.

Preferential desorption of a specific atom leads to strong deviation from surface stoichiometry. However, UV laser irradiation also acts as a precursor for surface chemical

reaction. When done in air environment or in water vapour, it strongly enhances the oxidation of GaAs and InP.

2.4 Bibliography

Ahopelto, J., Sopanen, M., et al. (1999) *Tailoring of energy levels in strain-induced quantum dots*, Japanese Journal of Applied Physics, Part 1: Regular Papers and Short Notes and Review Papers, vol. 38, n° 2B, 1081-1084.

Allwood, D. A., Carline, R. T., et al. (2000) *Characterization of oxide layers on GaAs substrates*, Thin Solid Films, vol. 364, n° 1-2, 33-39.

Anonymous (1991). *Properties of indium phosphide*, London ; New York, INSPEC, 495 p.

Baraff, G. A., Kane, E. O., et al. (1979) *Silicon vacancy: a possible `Anderson negative-U' system*, Physical Review Letters, vol. 46, n° 13, 956-9.

Chow, W. W. and Koch, S. W. (1999). *Semiconductor laser fundamentals, Physics of the gain materials*, New-York, Springer, 245 p.

Davies, J. H. (2003). Elastic fields in optoelectronic devices. Lausanne.

Garg, A., Kapoor, A., et al. (2003a) *Laser-induced damage studies in GaAs*, Optics and Laser Technology, vol. 35, n° 1, 21-24.

Garg, A., Kapoor, A., et al. (2003b) *Laser-induced damage studies in GaAs*, Optics and Laser Technology, vol. 35, n° 1, 21-4.

Gotoh, T., Kotake, S., et al. (2004) *Photoinduced structural instability of the InP (110)-(1×1) surface*, Physical Review Letters, vol. 93, n° 11, 117401-1.

Grindberg, A. A., Mekhtiev, R. F., et al. (1967) *Absorption of laser radiation and damage in semiconductors*, Soviet Physics – Solid State, vol. 9, n° 5, 1085-1090.

Ichige, K., Matsumoto, Y., et al. (1988). *Laser-induced desorption from compound semiconductors*, Okayama, Japan.

Ingrey, S., Lau, W. M., et al. (1986) *An X-ray photoelectron spectroscopy study on ozone treated GaAs surfaces*, Journal of Vacuum Science & Technology A (Vacuum, Surfaces, and Films), vol. 4, n° 984-8.

Ingrey, S., Lau, W. M., et al. (1987) *An X-ray photoelectron spectroscopy study on ozone treated InP surfaces*, Journal of Vacuum Science & Technology A (Vacuum, Surfaces, and Films), vol. 5, n° 1621-4.

Itoh, N., Nakayama, T., et al. (1985) *Electronic-excitation mechanism in sputtering induced by high density electronic excitation*, Physics Letters A, vol. 108A, n° 9, 480-4.

Kanasaki, J. (2006) *Formation and clustering of surface vacancies under electronic excitation on semiconductor surfaces*, Physica B, vol. 376-377, n° 834-40.

Khoo, G. S., Ong, C. K., et al. (1993) *The multi-hole localization mechanism for particle emission from semiconductor surfaces*, Journal of Physics: Condensed Matter, vol. 5, n° 9, 1187-94.

Kirkby, P. A., Selway, P. R., et al. (1979) *Photoelastic waveguides and their effect on stripe-geometry GaAs/Ga[sub 1 - x]Al[sub x]As lasers*, Journal of Applied Physics, vol. 50, n° 7, 4567.

Kuanr, A. V., Bansal, S. K., et al. (1996a) *Laser induced damage in GaAs at 1.06 μm wavelength: surface effects*, Optics and Laser Technology, vol. 28, n° 1, 25-34.

Kuanr, A. V., Bansal, S. K., et al. (1996b) *Laser induced damage in GaAs at 1.06 @mm wavelength: surface effects*, Optics & Laser Technology, vol. 28, n° 1, 25-34.

Loehr, J. P. (1998). *Physics of strained quantum well lasers*, Boston, Kluwer Academic, x, 255 p.

Marine, W., Bulgakova, N. M., et al. (2004) *Electronic mechanism of ion expulsion under UV nanosecond laser excitation of silicon: Experiment and modeling*, Applied Physics A: Materials Science & Processing, vol. 79, n° 4, 771-774.

Matsuoka, Y. (1976) *Laser-induced damage to semiconductors*, Journal of Physics D: Applied Physics, vol. n° 2, 215.

Meyer, J. R., Bartoli, F. J., et al. (1980) *Optical heating in semiconductors*, Physical Review B (Condensed Matter), vol. 21, n° 4, 1559-68.

Micallef, J., Li, E. H., et al. (1993) *The effects of strain on the cofinement profile of disordered in InGaAs/GaAs single quantum wells*, Superlattices and Microstructures, vol. 13, n° 1, 125-132.

Miller, J. C. and Haglund, R. F., Eds. (1998). Laser ablation and desorption. Experimental methods in the physical sciences. San Diego, Acandemic Press, 647 p.

Pankove, J. I. (1975). *Optical Processes in Semiconductors*, p.

Pereira, M. F., Jr. and Koch, S. W. (1993) *Effects of strain and Coulomb interaction on gain and refractive index in quantum-well lasers*, Journal of the Optical Society of America B (Optical Physics), vol. 10, n° 5, 765-73.

Petro, W. G., Hino, I., et al. (1982) *Effect of low-intensity laser radiation during oxidation of the GaAs(110) surface*, vol. 21, n° 405-8.

Piprek, J. (2003). *Semiconductor Optoelectronic Devices: Introduction to Physics and Simulation*, Amsterdam, Academic Press, 279 p.

Plummer, J. D., Deal, M. D., et al. (2000). *Silicon VLSI Technology : Fundamentals, Practice and Modeling*, Upper Saddle River, NJ, Prentice Hall, 817 p.

Podlesnik, D. V., Gilgen, H. H., et al. (1984) *Deep-ultraviolet induced wet etching of GaAs*, Applied Physics Letters, vol. 45, n° 5, 563-5.

Podlesnik, D. V., Gilgen, H. H., et al. (1986) *Interaction of Deep-Ultraviolet Laser-Light with GaAs-Surfaces in Aqueous-Solutions*, Journal of the Optical Society of America B-Optical Physics, vol. 3, n° 5, 775-784.

Raff, M., Schutze, M., et al. (1994) *Laser-stimulated nonthermal particle emission from InP and GaAs surfaces*, Physical Review B (Condensed Matter), vol. 50, n° 15, 11031-6.

Schafer, S. A. and Lyon, S. A. (1981). *Optically enhanced oxidation of semiconductors*, Williamsburg, VA, USA.

Streetman, B. G. and Banerjee, S. (2000). *Solid State Electronic Devices*, Upper Saddle River, NJ, Prentice Hall, 558 p.

Sumi, H. (1991) *Theory on laser sputtering by high-density valence-electron excitation of semiconductor surfaces*, Surface Science, vol. 248, n° 3, 382-410.

Takatani, S., Yamamoto, S., et al. (1995) *Excimer laser assisted etching of AlGaAs and GaAs*, Journal of Vacuum Science & Technology B, vol. 13, n° 6, 2340-2343.

Tanimura, K., Inami, E., et al. (2006) *Two-hole localization mechanism for electronic bond rupture of surface atoms by laser-induced valence excitation of semiconductors*, Physical Review B (Condensed Matter and Materials Physics), vol. 74, n° 3, 35337-1.

Theis, T. N., Mooney, P. M., et al. (1988) *Electron localization by a metastable donor level in n-GaAs: a new mechanism limiting the free-carrier density*, Physical Review Letters, vol. 60, n° 4, 361-4.

Vivet, L., Dubreuil, B., et al. (1997) *Laser irradiation of GaAs-GaAlAs multi-quantum well structure*, Applied Surface Science, vol. 119, n° 117-126.

Watkins, G. D. and Troxell, J. R. (1980) *Negative-U properties for point defects in silicon*, Physical Review Letters, vol. 44, n° 9, 593-6.

Young, E. M. and Tiller, W. A. (1983) *Photon enhanced oxidation of silicon*, Applied Physics Letters, vol. 42, n° 1, 63-5.

Young, E. M. and Tiller, W. A. (1987) *Ultraviolet light stimulated thermal oxidation of silicon*, Applied Physics Letters, vol. 50, n° 2, 80-2.

Yu, C. F., Schmidt, M. T., et al. (1987) *Wavelength Dependence of Optically Induced Oxidation of GaAs(100)*, Journal of Vacuum Science & Technology B, vol. 5, n° 4, 1087-1091.

Chapter 3: Quantum well intermixing

To monolithically integrate photonic devices, distinct regions demonstrating specific optical and electrical properties must be fabricated on a single wafer. Most, commercially available, active photonic devices are made from quantum well heterostructures. Generally, optical properties of semiconductor heterostructures depend on the material band structure and its bandgap. In contrast with microelectronic devices, where the integration can be achieved by locally doping the semiconductor material, integration of photonic devices requires wafers with buit-in regions of different bandgap material. Quantum well intermixing (QWI) is a process used to fabricate such wafers, without requiring multiple etching and epitaxial re-growth steps.

Intermixing affects the quantum well material composition and bandgap, thus it also influences its optical properties. For example, changing the quantum well shape will result in a modification of the electronic confinement, the refraction index and of the charge carriers' effective masse. Such modification can then be used to fabricate waveguides, to form a region of high optical confinement or to reduce losses in Bragg reflectors [J.H. Marsh 1993, N. Holonyak, Jr. 1998].

QWI can be extended to heterostructures with lower dimensionality than quantum well. Intermixing taking place in quantum wire [S. Yuan *et al.* 1998, X. Liu *et al.* 2000] or quantum dots [R. Leon *et al.* 1996] also alters the bands profiles and position. Furthermore, because intermixing modifies these nanostructures in volume, not just the vertical profile as with QW, its effect on the bandgap is even greater.

In this chapter, I first describe the QWI concept and explain the influence of point defect and stress on diffusion. I then review different QWI techniques and discuss their advantages and weaknesses.

3.1 Description of the quantum well intermixing process

The QWI process takes advantage of the heterogeneity of semiconductor structures used to fabricate photonic devices. We define the active region as the pile up of QW and barrier layers. The operation of photonic devices is defined by the properties of this active region, which is typically tens of nanometers thick. Since QW and barriers are made of different materials, a large atomic concentration gradient exists between them. At sufficiently high temperatures , the diffusion forces associated with concentration gradient initiate the intermixing process [J.E. Haysom *et al.* 2000]. This partially homogenizes the wells and barriers layers and changes the QW shape. Figure 3-1 illustrates the changes in composition and the potential well shape modification associated with the intermixing process. We describe analytically the effect of intermixing on the bands structure profile on a single quantum well by making the assumption that the barrier is thicker than the diffusion length: $L_D = \sqrt{Dt}$, where D is the diffusion coefficient and t is the time. In such case, the intermixing is not influenced by the composition of other layers. For a ternary compound $A_x^{III} B_{1-x}^{III} C^V$, the diffusion equation can be solved analytically and the solution gives the concentration profile $x(z,L_D)$ of a specific constituent atom as an error function profile [E.H. Li 2000]:

$$x\left(z, L_D\right) = x_B + \frac{x}{2}\left[\operatorname{erf}\left(\frac{L_z + 2z}{4L_D}\right) + \operatorname{erf}\left(\frac{L_z - 2z}{4L_D}\right)\right], \tag{3.1}$$

where z is the growth direction, x and x_B are respectively the initial composition inside the well and in the barrier while L_z is the well width centered at z = 0. Such concentration profile evolution is illustrated in figure 3-2.

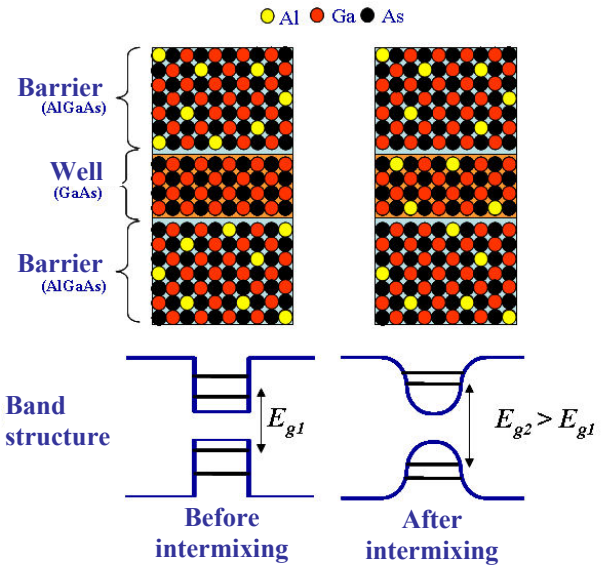

Figure 3-1: Schematic representation of quantum well intermixing in AlGaAs/GaAs heterostructure

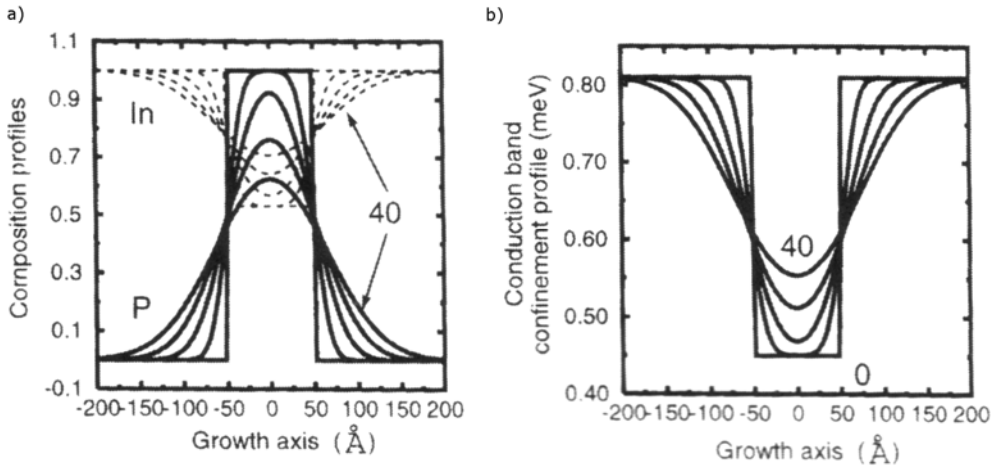

Figure 3-2: a) Simulation of the In and P composition profile in an InGaAs/InGaAsP quantum well for different diffusion length L_D (Å) following the model from equation (3.1), b) conduction band profiles corresponding to the intermixed composition profiles [E.H. Li 2000].

In most GaAs based QW heterostructures ($A_x^{III} B_{1-x}^{III} As / GaAs$), only atoms of the group III sublattice change between the barrier and the well. On the other hand, in most InP based quantum

well heterostructures ($A_x^{III}B_{1-x}^{III}C_y^{V}D_{1-y}^{V}/InP$), there is a concentration gradient between the barriers and the well for both group III and group V atoms. This means that equation (3.1) must be generalize with two uncoupled equations for concentration of group III elements (x) and group V elements (y) and include two different diffusion lengths: L_{III} and L_V:

$$x\left(z, L_{III}\right) = x_B + \frac{x}{2}\left[\operatorname{erf}\left(\frac{L_z + 2z}{4L_{III}}\right) + \operatorname{erf}\left(\frac{L_z - 2z}{4L_{III}}\right)\right] \tag{3.2}$$

$$y\left(z, L_V\right) = x_B + \frac{y}{2}\left[\operatorname{erf}\left(\frac{L_z + 2z}{4L_V}\right) + \operatorname{erf}\left(\frac{L_z - 2z}{4L_V}\right)\right]. \tag{3.3}$$

Except in very specific situations, the different diffusion length L_{III} and L_V between group III and group V atoms induces new strain in the quantum well. Thus, in $In_{0.53}Ga_{0.47}As/InP$ quantum wells, preferential diffusion of group V atoms leads to formation of biaxial tensile strain in the wells, lowering the bandgap energy. The opposite effect is obtained with preferential diffusion of group III atoms. Bollet *et al*. modeled the effect of uneven diffusion length on the bandgap of an intermixed quantum well and demonstrated that quantum well intermixing can lead to redshift when L_V is higher than L_{III} (figure 3-3) [F. Bollet *et al.* 2003]. To simplify to modeling, theorists usually make the assumption that disordered layers stay lattice matched with InP so x and y relate to each other as $x = 1 - 0.47y$ [O. Gunawan *et al.* 2000]. This ensures that the strain related to lattice mismatch is limited to 0.032% [S. Adachi 1982].

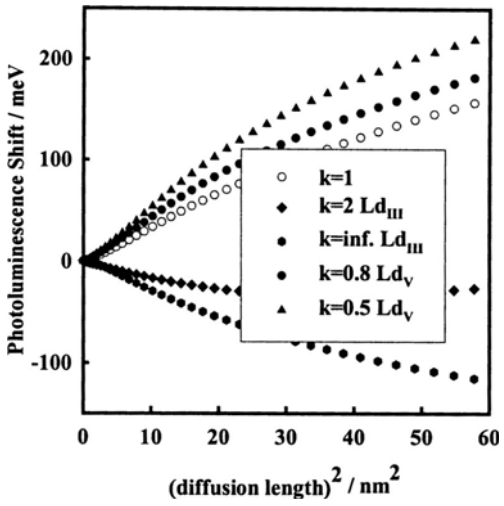

Figure 3-3: Theoretical calculation of photoluminescence blueshift as a function of different diffusion length with k = Ld_{III}/Ld_V. The abscissa is Ld_{III} for k > 1 and Ld_V for k < 1 [F. Bollet *et al.* 2003].

The charge carriers' energy levels in the intermixed well are determined by solving the Schrödinger equation in BenDaniel-Duke approximation [D.J. BenDaniel *et al.* 1966], using an envelope function and approximating the effective mass (m_r^*):

$$\frac{-\hbar^2}{2}\frac{d}{dz}\left[\frac{1}{m_r^*(z)}\frac{d\chi_{rl}(z)}{dz}\right]+U_r(z)\chi_{rl}(z)=E_{rl}\chi_{rl}(z)\,, \qquad (3.4)$$

where z is the growth direction, χ_{rl} is the envelope wave function, E_{rl} is the quantized energy level while $l = p$ or q refers respectively to the level in the electrons and holes sub-band. Solving equation (3.4), we obtain the quantized energy levels E_{Cp} and E_{Vq} and their wave function χ_{Cp} and χ_{Vq}.

3.1.1 Point defects and strain influence on intermixing

At the beginning of the 80s, researchers discovered that it was possible to lower the energy needed to achieve intermixing in AlGaAs/GaAs like heterostuctures by incorporating zinc atoms [W.D. Laidig *et al.* 1981]. They discovered that zinc impurity diffusion activates the quantum well intermixing. This discovery was technological spring board because it allowed the

local modification of semiconductor heterostructures band structure without any need of regrowth step. Controlling how lattice defects diffuse was the key element.

We denote different type lattice defects. They can be separated in categories based on there dimensionality: point, line, planar and bulk defects (respectively 0D, 1D, 2D and 3D). Because of there bigger dimensionality, line, planar and bulk defects need much more energy to diffuse than 0 D defects, therefore their chance to contribute to the intermixing process is quite low. On the other hand, point defects are generally weakly bounded to the rest of the lattice. They can then more easily diffuse over great distance. We identify different type of point points (figure 3-4):

- Vacancies are empty lattice sites,
- Interstitials are atoms which occupy a site in the crystal between the regular lattice sites,
- Frenkel pair or Frenkel defect is a pair of nearby interstitial and vacancy,
- Impurities are atoms which don't belong to the pure crystal, they can occupy interstitial sites or substitute themselves to regular atomic sites,
- Anti-site defect occurs in ordered compound material when an atom of the sublattice A occupies a site on the sublattice B.

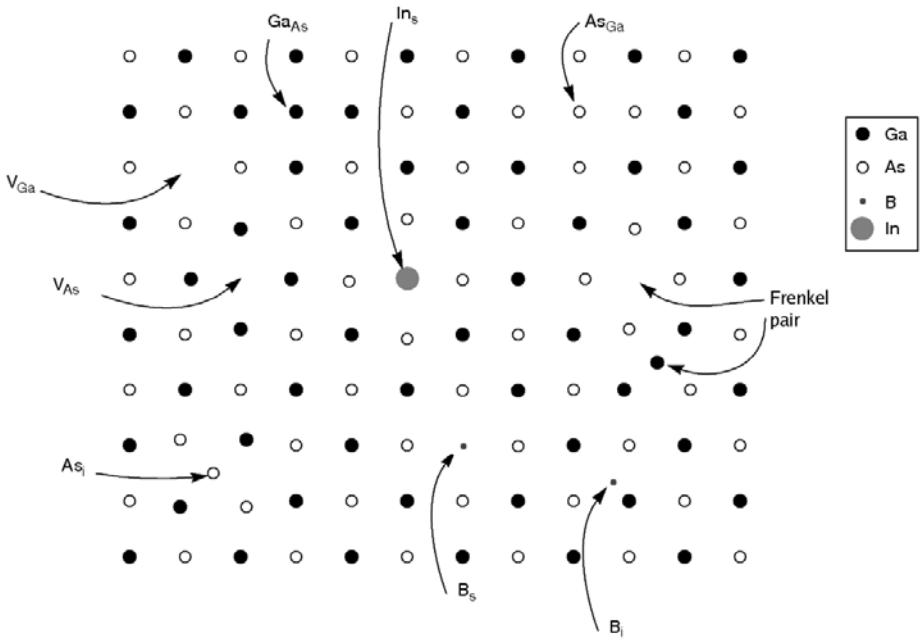

Figure 3-4: Illustration of the different point defects in a GaAs lattice. In this schematic, V stands for vacancy, i for interstitial and s for subtitutionnal, while the notation A_B signifies that the atom A occupies the site of an atom B.

For a given temperature and under given thermodynamic condition, the concentration of a particular type of point defect will tend to reach its thermo-equilibrium concentration [R.M. Cohen 1997]. For example, as we increase the material temperature, vacancies in the near surface area reach their equilibrium concentration by processes such as desorption and generation of Frenkel pairs. The diffusion of the newly created vacancies toward the bulk allows the whole material to reach its equilibrium. This is also the case if a particular region of the material contains an extra concentration of point defect. The material will tend to homogenize its concentration of point defects through diffusion. Point defect diffusion follows the Fick's laws, considering de concentration *c* a type of defect:

$$\vec{J} = -D\nabla c \tag{3.5}$$

and

$$\frac{dc}{dt} = D\nabla^2 c + S \tag{3.6}$$

where $\vec{J}$ is the point defect flux, D is the diffusion coefficient and S is the generation-annihilation term. The passing of point defects through the active region reduces the energy needed to achieve intermixing between barriers and the well. The intermixing coefficient depends on activation energy E_A and follows an Arrhenius law in respect with the temperature T. For example, in an AlGaAs/GaAs heterostructures, we express the intermixing coefficient $D_{Al\leftrightarrow Ga}$ as:

$$D_{Al\leftrightarrow Ga} = D_0 \exp\left(-E_A / k_B T\right), \tag{3.7}$$

where D_0 is the intermixing coefficient at an infinite temperature, k_B is the Boltzmann constant and E_A is the activation energy. The presence of a point defect at the barrier/well interface reduces the activation energy, allowing a faster intermixing rate. Figure 3-5 shows three major processes of point defect assisted diffusion.

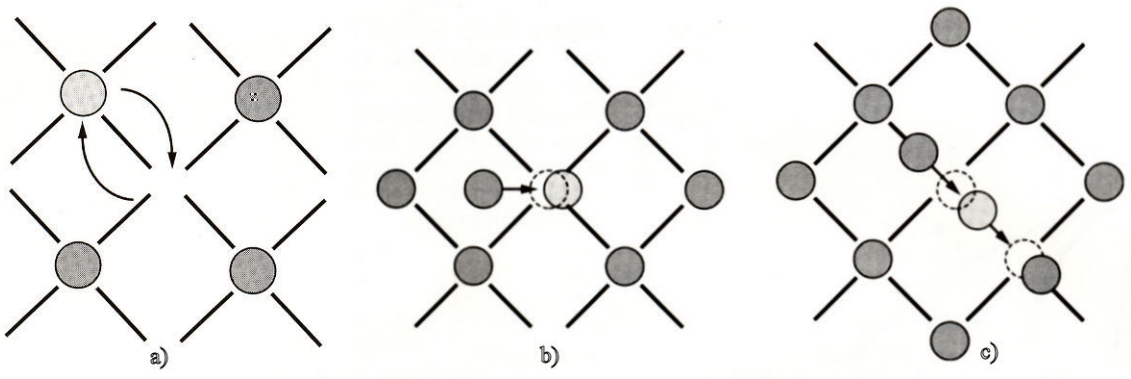

Figure 3-5: Point defect assisted diffusion. a) Vacancy initiated diffusion, b) an interstitial kicks an atom out of its lattice site, c) diffusion channelling through interstitial jumps [J.D. Plummer *et al.* 2000].

The activation energy of intermixing depends on the nature on the material but also on the point defects diffusion processes in the material. This explains why GaAs based heterostructures are stable to temperature up to 800°C while InP based heterostructures usually start to demonstrate intermixing around 600°C. Each point defect diffusion process also affects the reliability QWI techniques with different material type. For example, since interstitials don't

diffuse easily in GaAs, while it's the opposite case in InP, a QWI technique based on the near surface introduction of this type of defect would have a better success in InP than in GaAs based heterostructures.

3.1.1.1 Point defect diffusion under a strain gradient

Most of the time, no external force is applied on the point defects ($\vec{F} = 0$). Thus, the concentration gradient exclusively directs the point defects diffusion. However, if some external force is present, Fick's laws equations (3.5) and (3.6) will change to:

$$\vec{J} = -D\nabla c + \frac{D}{k_B T}\vec{F}c \tag{3.8}$$

and

$$\frac{dc}{dt} = D\left[\nabla^2 c - \left(\nabla c \cdot \nabla \vec{F} + c\nabla^2 \vec{F}\right)\right] + S \tag{3.9}$$

where $\vec{F}$ is the external force applied on the defect. Because point defects can be charged, an electric field would have an effect on them. For a defect with an effective charge Z^*,

$$\vec{F} = Z^* e\vec{E}. \tag{3.10}$$

Similarly, if a temperature gradient (∇T) is present in the structure, the resulting force will be:

$$\vec{F} = -\frac{H_M}{T}\nabla T, \tag{3.11}$$

where H_M is the migration enthalpy.

In contrast with the two precedent forces, the elastic force on a defect depends strongly on the symmetry of the defect itself [J.D. Eshelby 1951]. This is due to the interaction of the applied strain field with the one produced by the defect. In the case of point defects in an isotropic material, the defect symmetry is spherical. We define the defect volume V as a function of the mean atomic site volume V_0 and mismatch parameter α:

$$V = V_0(1+\alpha). \tag{3.12}$$

Using this nomenclature, an interstitial atom constitutes a dilatation center ($\alpha > 0$) while a vacancy causes the lattice to compress on itself ($\alpha < 0$). The applied force on the defect can then be express as:

$$\vec{F} = \alpha \frac{4}{3} r_0^3 \nabla Tr(\sigma), \tag{3.13}$$

where r_0 is the defect radius and $Tr(\sigma)$ is the trace of the stress tensor: $Tr(\sigma) = \sigma_{11} + \sigma_{22} + \sigma_{33}$.

Equation (3.13) demonstrates that 1) shear stress doesn't apply any force on a point defect, 2) a stress gradient needs to be present and 3) under the same conditions, vacancies and interstitials are forced to drift in different direction. Under a stress gradient, Fick's laws are then expressed as:

$$\vec{J} = -D\nabla c + \frac{D}{k_B T} \alpha \frac{4}{3} r_0^3 c \nabla Tr(\sigma) \tag{3.14}$$

and

$$\frac{dc}{dt} = D\left[\nabla^2 c - \frac{4\alpha r_0^3}{3k_B T}\left(\nabla c \cdot \nabla Tr(\sigma) + c\nabla^2 Tr(\sigma)\right)\right] + S. \tag{3.15}$$

This description of point defect diffusion in strained material was used by Britton and his colleagues to simulate the smart-cut process used to fabricate silicon-on-insulator type wafers [D.T. Britton *et al.* 2002]. For such process, high doses of H^+ ions are implanted in a SiO_2 capped silicon wafer [K.V. Srikrishnan 2005]. The implanted atoms are located in a very thin volume where their presence induces a tensile stress in the semiconductor. According to equation (3.15), interstitials are driven away from stress field maximum position while vacancies migrate toward it where they will cluster (figure 3-6). At high temperature, this will allow the top layers of the wafer to be cut away from the substrate.

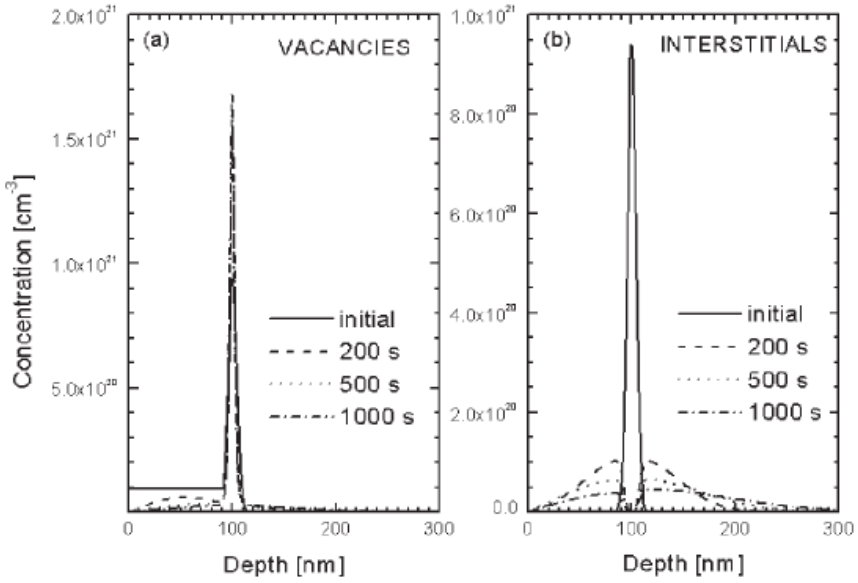

Figure 3-6: Temporal depth profiles of a) center of dilatation (vacancies) and b) center of contraction (interstitials) in a tensile stress field centered at the defects initial position [D.T. Britton *et al.* 2002].

3.2 Review of Quantum well intermixing techniques

Quantum well intermixing can be achieved by heating a quantum well heterostructure over a threshold temperature. At high temperature constituent atoms intermix at each interface between two layers because of the high concentration gradient. The intermixing coefficient $D_{A\leftrightarrow B}$ follows an Arrhenius law as a function of temperature:

$$D_{A\leftrightarrow B} = D_0 \exp\left(\frac{-E_A}{k_B T}\right) \tag{3.16}$$

where D_0 is the intermixing coefficient at an infinite temperature, T is temperature, k_B is the Boltzmann constant, and E_A is an activation energy. We define the *thermal shift* as the blueshift exclusively related to the thermal annealing. This exclude the effect of point defects intentionally introduced in the structure or of stress applied prior to the annealing step. Equilibrium intrinsic point defects contribute to the intermixing and their presence reduces the activation energy E_A. This technique is relatively easy to implement because it only requires a furnace. However, it

doesn't offer any way to define selectively intermixed sites of the same wafer [S. Charbonneau *et al.* 1998]. Furthermore, for the fabrication multi-bandgap material with high contrast, thermal shift is undesired and we usually want to limit this effect to a minimum typically below 5 nm, so that the original characteristics of the heterostructure are conserved.

Different quantum intermixing techniques were developed in the last 25 years. We can classify theses techniques in four different categories: impurity induced intermixing [L.J. Guido *et al.* 1987], impurity-free vacancy diffusion [S. Mitra *et al.* 1991, J. Beauvais *et al.* 1992, A.S. Helmy *et al.* 1998, J.H. Teng *et al.* 2001], quantum well intermixing induced by ion implantation [S. Charbonneau *et al.* 1998, V. Aimez *et al.* 2002] and laser induced QWI [B.S. Ooi *et al.* 1997, J.J. Dubowski *et al.* 2002].

Generally, laterally controlled quantum well intermixing techniques are based on the diffusion of point defects. This is done either by introducing an extra concentration of defects in the material or by applying an external force on the defects.

3.2.1 Impurity induced disordering

At the beginning of the 80s, quantum well intermixing was first studied in AlGaAs/GaAs heterostructures as an undesirable effect occurring during high temperature treatments [W.D. Laidig *et al.* 1981]. The diffusion on zinc during annealing at 600°C increases gallium and aluminum interdiffusion by a factor of 10^5 [J.W. Lee *et al.* 1984]. Other impurities used as dopants, Si, Ge, S, Se, Be, Mg, were also found to increase the Al/Ga interdiffusion [D.G. Deppe *et al.* 1988].

Impurity induced disordering (IID) in (Al)GaAs structures was certainly the most studied of all intermixing techniques. Through its study, the role of group III point defects (vacancies and

interstitials) was identified and so was the effect of the Fermi level [T.Y. Tan 1991] and arsenic overpressure on the intermixing behaviour [D.G. Deppe *et al.* 1988]. Although it is well understood and effective, the impurity induced disordering will always results in increased optical losses due to free carriers trapping by impurities in the active region. Therefore, its application for photonic integration is limited. Since impurities can be introduced in numerous ways such as ion implantation, incorporation during growth, diffusion from surface source, the IID technique can be implemented in numerous ways to achieve localised quantum well intermixing in GaAs based heterostructures but also in InP [R. Lai *et al.* 1991]. However, because it increases optical losses in the intermixed region, this technique is more attractive for application which doesn't directly involve passive light propagation in the intermixed areas [E. Kapon *et al.* 1988].

3.2.2 Impurity-free vacancy disordering

This technique principle is based on the enhanced diffusion of constituent atoms of the heterostructures. In other words, it is done without incorporating new impurities. To achieve intermixing, a dielectric cap, generally SiO_2, is deposited on the heterostructures surface. In most cases, during an annealing step, constituent atoms migrate into the cap which generates new point defects in the surface vicinity. The annealing also makes point defects diffuse toward the active region where they activate the intermixing. The thickness of the capping layer affects the number of vacancies created. For thinner caps, the solubility limit is reached faster than for thicker caps. This means that the maximum concentration of excess point defects is reached faster and smaller interdiffusion coefficient can be achieved.

For example, in AlGaAs/GaAs heterostructures, during annealing, because of its high solubility in SiO_2, gallium out-diffuses in the capping layer, leaving Ga vacancies in the material.

Still under the high temperature influence, theses vacancies diffuse through the quantum well and barrier layers where they contribute to the quantum well intermixing by lowering the activation energy [J.H. Marsh 1993]. Since vacancies diffuse at a temperature below the thermal energy needed to activate the atomic interdiffusion inside the wells, the intermixing is localised to the capped areas.

The nature of the capping material will also influence whether it activates or inhibits the interdiffusion process. For examples, in AlGaAs/GaAs heterostructures, intermixing is accelerated by SiO_2 [J.H. Teng *et al.* 2001], while it is slowed down by SrF_2 [J. Beauvais *et al.* 1992], TiO_2 [L. Fu *et al.* 2003, P.L. Gareso *et al.* 2004] and Ga_2O_3 [L. Fu *et al.* 2002b]. During the annealing procedure, the mismatch in the expansion coefficients α of semiconductor and the dielectric layer induces stress in both materials [P.L. Gareso *et al.* 2004]. In GaAs ($\alpha_{GaAs} = 5.73 \times 10^{-6}$ °C^{-1}), the annealing with a SiO_2 ($\alpha_{SiO2} = 0.5 \times 10^{-6}$ °C^{-1}) cap puts the GaAs under compressive strain which facilitate gallium out-diffusion toward SiO_2 and increases the formation extra gallium vacancies. Annealing under a cap with a higher expansion coefficient than GaAs, e.g. TiO_2 ($\alpha_{TiO2} = 8.2 \times 10^{-6}$ °C^{-1}), has the opposite effect and suppresses thermal shift in InGaAs/AlGaAs/GaAs quantum well heterostructures [P.L. Gareso *et al.* 2004] and in InGaAs/GaAs quantum dots [L. Fu *et al.* 2003]. Furthermore, theses capping materials usually have small gallium solubility, thus under them gallium vacancies are less likely to form in comparison to GaAs free surface. Lithography techniques allows the patterning of a sample with dielectric layer promoting and inhibiting the intermixing (figure 3-7) [B.S. Ooi *et al.* 1995a].

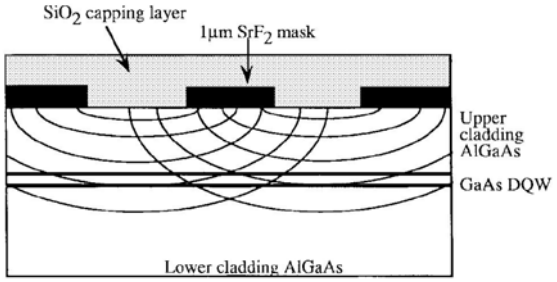

Figure 3-7: Example of dielectric capping to control quantum well intermixing [Ooi'1995]. SiO_2 promotes the interdiffusion while SrF_2 prevents it.

Most of the time, silicon nitride (Si_3N_4) is used to suppress intermixing in GaAs based quantum well heterostructure when using the impurity-free vacancy disordering technique [A. Pepin *et al.* 1997, J.H. Teng *et al.* 2001] because the deposition of high quality Si_3N_4 film is well understood. In 2001, Teng and his colleagues obtained a 135 nm contrast between areas on a InGaAsP/InP heterostructure covered with either SiO_2 and Si_3N_4 after an annealing at 800°C for 100s. Figure 3-8 also shows that covering part of the sample with Si_3N_4 reduced the thermal shift compared to the uncovered area. However, under certain deposition conditions [W.J. Choi *et al.* 1994], Si_3N_4 can also enhanced the interdiffusion. In contrast with most inhibiting materials, Si_3N_4 doesn't induces a tensile stress in the GaAs but a small compressive stress ($\alpha_{Si3N4} = 2.8 \times 10^{-6}$ °C^{-1}). Thus the inhibition mechanism when using Si_3N_4 dielectric cap is purely related its low solubility to gallium. When the porosity of silicon nitride increases, its voids enhance out-diffusion of gallium atoms from GaAs which enhances the quantum well intermixing process [J.S. Yu *et al.* 2002].

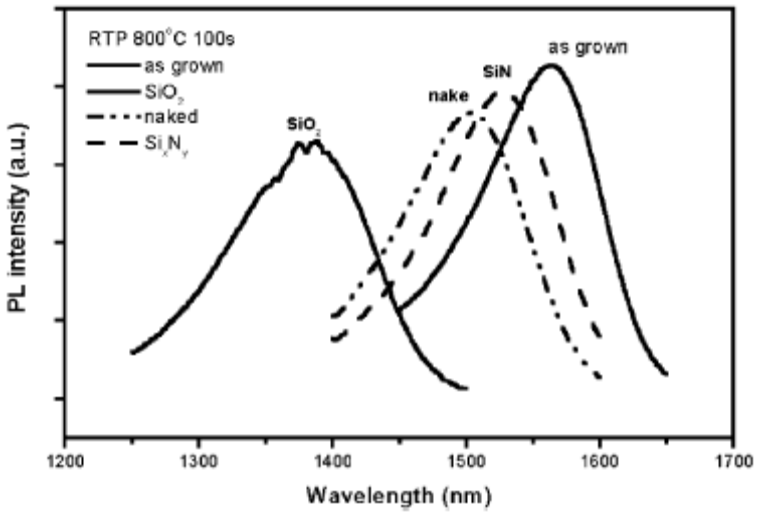

Figure 3-8: Photoluminescence spectra from a disordered and reference InGaAsP multi-quantum-well sample after annealing [J.H. Teng *et al.* 2001].

In some conditions, SiO_2 caps can also inhibits intermixing. With caps of phosphorus doped SiO_2 (SiO_2:P), suppressed intermixing in AlGaAs/GaAs laser structure was observed by [P. Cusumano *et al.* 1997]. They deposited SiO_2:P by plasma enhanced chemical vapour deposition on one p-i-n and one n-i-p double quantum well heterostructures and annealed them at high temperatures (800 to 950°C). They achieved intermixing suppression in both structures and obtained contrasts as high as 40 nm (p-i-n) and 50 nm (n-i-p) with samples covered with SiO_2 and annealed (figure 3-9). The suppression is attributed to the fact that SiO_2:P contains less voids than SiO_2 and that it is denser, thus it has a smaller solubility to gallium. Also, incorporation of phosphorus in SiO_2 increases its expansion coefficient which lowers the induced stress during the annealing, making gallium out-diffusion less favourable.

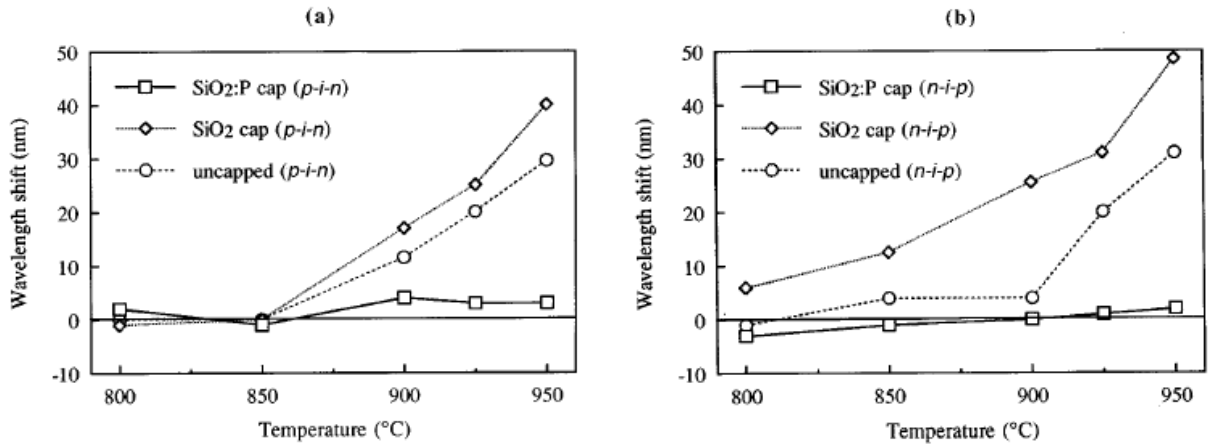

Figure 3-9: Shift of photoluminescence peak position for SiO_2:P capped, SiO_2 capped and uncapped of a) p-i-n and b) n-i-p laser structures [P. Cusumano *et al.* 1997].

Impurity-free vacancy disordering is mainly used to integrate optoelectronic devices fabricated on (In)AlGaAs/GaAs heterostructures [N. Shimada *et al.* 2004]. While this technique has been used with success to integrate devices made on InP based heterostructures [J.H. Teng *et al.* 2001], its use on this type of semiconductor is more problematic than on crystalline systems based on GaAs and usually require the growth of a defect layer. In InP heterostructures, the energy needed to activate the out-diffusion of surface atoms in the dielectric cap is comparable to the interdiffusion activation energy. Furthermore, impurity-free vacancy disordering only offers a limited selectivity and often results in energy shift on the whole sample [E.V.K. Rao *et al.* 1995]. The strain located inside the dielectric layers was suggested to influence the diffusion process and affect its reproducibility [B. Elman *et al.* 1989].

One of the biggest advantages of this technique is the fact that it doesn't introduce impurity inside the material. On heterostructures based on GaAs, the simplicity of this technique and its easy implementation makes it popular. However, dielectric capping induced quantum well intermixing doesn't offer a global solution to fabricate photonic integrate circuits, especially on InP based heterostructures. The deposited dielectric material quality is difficult to control and

such control is crucial to obtain reproducible results. Moreover, this technique doesn't offer practical diagnosis tools allowing *in-situ* measurement of the interdiffusion.

3.2.2.1 Dielectric sputtering induced intermixing

This technique, developed by a team from the University of Glasgow, and also known as "universal damage technique", is also considered impurity-free because it doesn't involve the introduction of foreign atomic species within the heterostructure. It consists in depositing a layer of SiO_2, Si_3N_4 or SiC on top of the substrate by magnetron sputtering [O.P. Kowalski *et al.* 1998]. In addition to create a dielectric cap, the sputtering process damages the heterostructure surface generating shallow point defects. An annealing step activates the quantum well intermixing process. In this technique, two mechanisms are responsible of the interdiffusion. First, sputtering-generated vacancies and interstitials in the surface vicinity diffuse toward the active region and activate the interdiffusion at high temperature. Secondly, in GaAs based materials, during the annealing, the dielectric cap absorbs gallium atoms and generates surface vacancies in the semiconductor. Similarly to the dielectric capping technique, theses new point defects diffuse toward the well and participate to the interdiffusion [S.D. McDougall *et al.* 1998]. Patterned resist can also be used to protect specific areas, limiting the intermixing process under them.

To study the defect generation process, Kowalski *et al.* used heterostructures with five quantum wells of different width (figure 3-10a). They measured the photoluminescence spectra before and after the sputtering. The reduced intensity of the two shallowest peaks suggested that the sputtering process generates damage in the form of mobile point defect, which increased the non-radiative recombination. They measured the damage limit depth to ~550-750 Å [O.P. Kowalski *et al.* 1998]. After annealing, the signal from the first wells was recovered because of

the diffusion of the high concentration of point defect toward the surface and deeper inside the heterostructure.

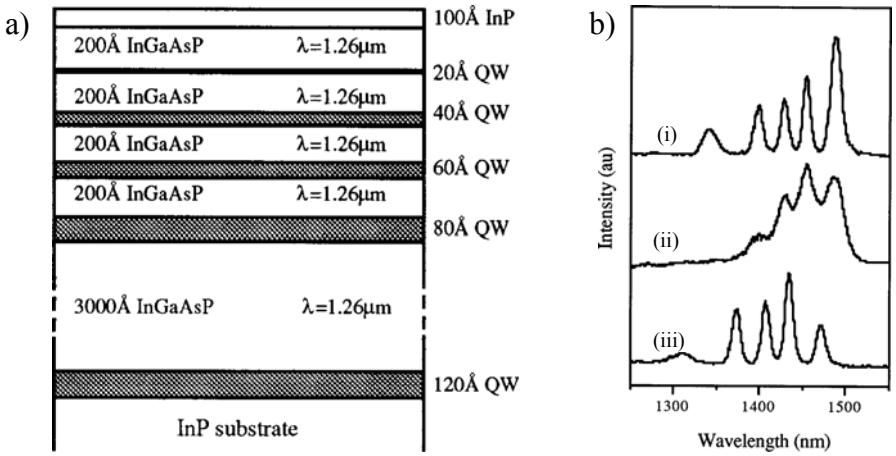

Figure 3-10: a) InGaAs/InP heterostructure with five quantum wells of different width, b) photoluminescence spectra before (i) and after (ii) pulverization and after rapid thermal annealing at 500°C for 60 seconds [O.P. Kowalski *et al.* 1998].

The procedure is almost identical on InP [S.D. McDougall *et al.* 1997] based heterostructure than on GaAs based ones [M. Ying *et al.* 2003]. However, it is difficult to control the amount of generated defects. Reproducibility then becomes a major issue. Annealing temperature and time controls the interdiffusion extent. It is then difficult to achieve regions with more than two different bandgaps. Liu *et al.* tried to address this issue by masking the heterostructure with a stepped SiO_2 layer (figure 3-11a) deposited by PECVD before the sputtering process [X.F. Liu *et al.* 2000]. They observed that the blueshift decreased as the SiO_2 mask thickness increased (figure 3-11b). The SiO_2 mask limited the number of generated point defects during the sputtering process.

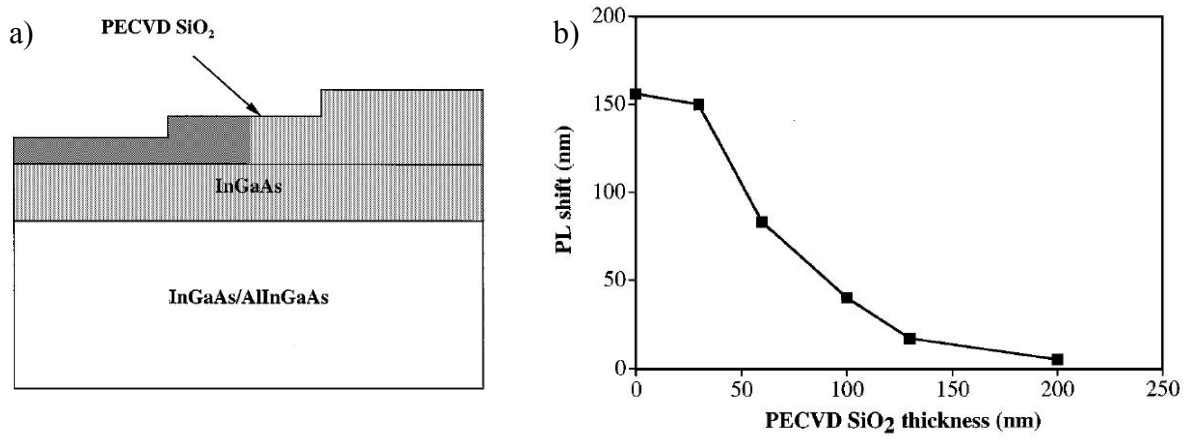

Figure 3-11: a) Schematic of the stepped PECVD SiO_2 mask, b) photoluminescence blueshift as a function of the mask thickness [X.F. Liu *et al.* 2000].

Because this technique creates large amount of sub-surface damage, the quality of the material is significantly compromised. Laser diodes fabricated from such intermixed heterostructures (blueshift = 140 nm) demonstrate a threshold current 300% higher than the one measured for laser diodes made from the untreated material [S.D. McDougall *et al.* 1998, F. Robert *et al.* 2004].

3.2.2.2 Low temperature epitaxial "defect" layer

Enhanced quantum well intermixing through native point defect diffusion can also be achieve by growing a layer containing a high concentration of defects. Such a layer can be grown by a low-temperature epitaxy technique. For instance, a layer containing high concentration of gallium vacancies and arsenic interstitials was obtained by growing GaAs at temperature around 200°C, i.e., well below the temperature required for the growth of high quality GaAs [M. Kaminska *et al.* 1989]. This technique was also used successfully for QWI in InP based heterostructure [J.H. Teng *et al.* 2001] and InAs quantum dots grown on InP [C. Dion *et al.* 2006]. This process does not require any defect introduction following the epitaxial groth of the structure. The localised bandgap shift can be obtained by selective removal of the defect layer

prior to annealing. The main drawback for this process is the requirement for non standard heterostructures with low temperature growth, which can lead to reproducibility issues, and the difficulties to have a gradual control of the bandgap shift.

3.2.3 Ion implantation induced quantum well intermixing

When an ion beam is implanted in a semiconductor, the collision the implanted specie and the lattice atoms displaces the later ones out of the initial site, producing Frenckel's pair defects [D.K. Brice *et al.* 1977]. We distinguish two different category of implantation. The first is done at low acceleration energies (below 500 keV). With such energies, ions are stopped well above the quantum well and the generated defects are limited to the higher layers. This implantation type is similar to the one used for doping semiconductor material when fabricating integrated circuits. The second implantation category is done with high acceleration energies (0.5 to 10 MeV). In the latter case, ions are implanted through the whole heterostructure and the formation of point defects occurs directly in the quantum wells.

The generated defects are the results of multiple collisions of the incident ions with the material atoms. The highly energetic ions propagate through the lattice and they kick atoms out of their lattice sites. Thus, ion implantation generates vacancies as newly vacant lattice site and interstitials which correspond to the displaced atoms and the implanted ions. In both low and high energy implantation, an additional annealing step to allow the defects diffusion and activates quantum well intermixing. The annealing also reconstructs part of the damage done to the lattice [J.F. Ziegler 1992].

The number of point defects introduced in the material depends of different implantation parameters [S. Charbonneau *et al.* 1998]:

1. the dose (ion/cm^2),
2. the mass of the implanted ions,
3. the incident angle,
4. the ion energy,
5. ion flux or ion current density (A/cm^2),
6. the temperature of the substrate during the implantation.

The dose plays a crucial role on the blueshift extent as demonstrated by figure 3-12. On the other hand, the ion energy has an effect on the concentration of point defects generated but also on the defect depth distribution.

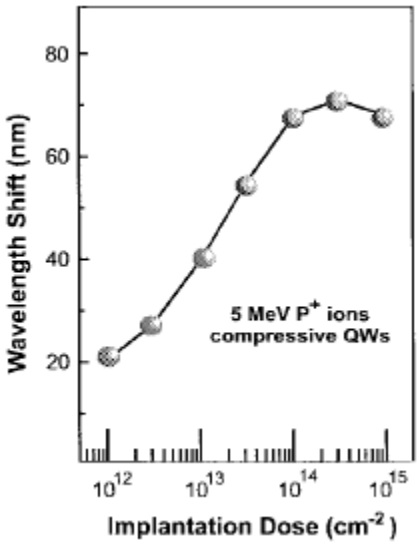

Figure 3-12: Quantum well photoluminescence peak shift as a function of the implantation dose [S. Charbonneau *et al.* 1998].

In AlGaAs/GaAs heterostructures, best results were obtained by implanting constituent atoms directly through the quantum well, i.e. with acceleration energies of the order of few MeV [S. Charbonneau *et al.* 1995]. Because of the fast diffusion of point defects diffusion in InP based semiconductor heterostructures [V. Aimez *et al.* 2002], defects don't need to be created in the active region vicinity. On the contrary, generating them farther from the well induces less

damage. Then, the crystal needs a lower temperature annealing to reconstruct itself which reduces the impurity diffusion in doped heterostructures. Furthermore, since there is less damage near the active region, we can expect better performances of devices fabricated from the intermixed material. Blueshift of the order of 25 nm can be achieved without affecting the threshold current density of the laser diode (Figure 3-13). A sacrificial layer can also be used to further limit the damage to the heterostructure [M. Paquette *et al.* 1997]. The sacrificial layer is etch away after the annealing step, leaving an almost damage free surface for the device fabrication.

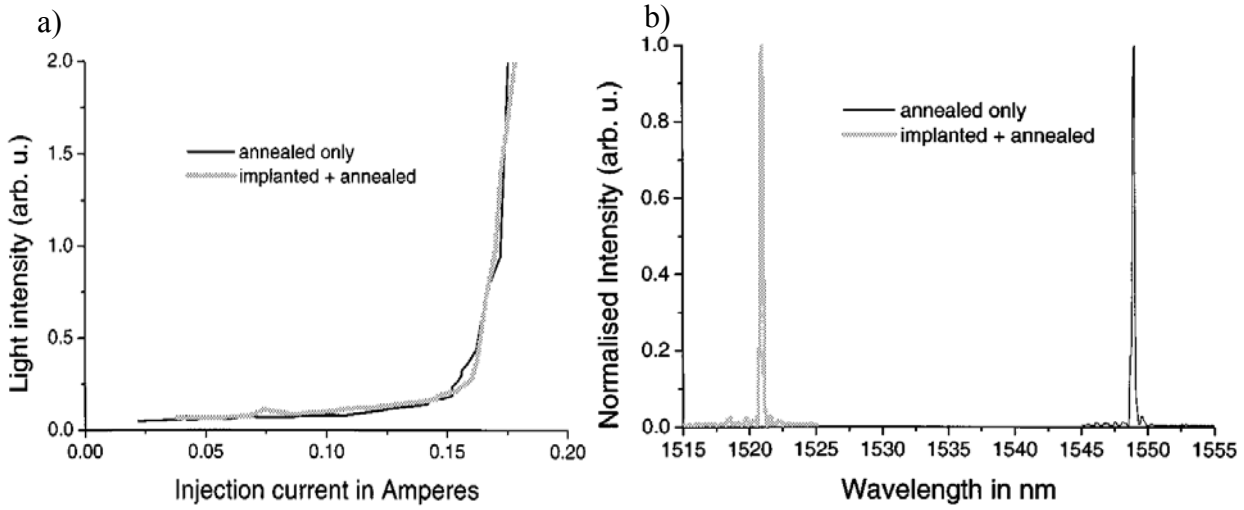

Figure 3-13: Example of laser diode characteristics, a) the implanted and annealed sample showed almost no increase of the threshold current density compared to the annealed only sample b) while the implantation caused the laser diode to shift of 25 nm [V. Aimez *et al.* 2002].

To address photonic device integration, researchers have fabricated multiple bandgap samples. This was done either by masking different areas and doing several implantation steps or by implanting through a single mask with a variable thickness [S.L. Ng *et al.* 2002]. In the latter case, a graded SiO_2 mask was used to slow down the incident ions. Doing so Ng *et al.* achieved an integrated chip on a single InGaAs/InP laser heterostructure with twelve sections of variable bandgaps. A waveguide modulator arrays was fabricated on a single InGaAs/InP wafer chip using this technique [S.L. Ng *et al.* 2003].

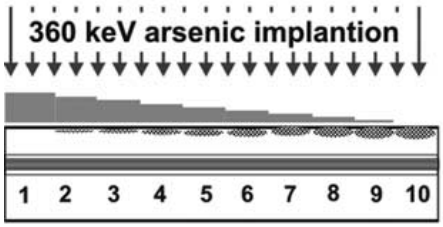

Figure 3-14: Schematic of arsenic implantation through a graded SiO_2 mask [S.L. Ng *et al.* 2003].

Since ion implantation is already present in the microelectronic industry as a doping solution, ion implantation induced quantum well intermixing, especially for low acceleration energies, offer an interesting solution as an integration tool for photonic devices, even though an industrial ion implantation induced QWI process would require a dedicated ion implanter, which is an expensive tool, as substrate sizes and contamination issues would prevent such a tool for ion implanting both Si and InP based devices. For low and high energies implantation, the lattice damage needs to be annealed out so it doesn't affect the devices electrical and optical performances. The main drawback associated with this process is related to multiple bandgap devices fabrication where the bandgap control requires the fabrication of complex SiO_2 masks with controlled thickness steps or multiple masking/implantation Steps, thus yielding to lower yields.

3.2.3.1 Plasma induced defect disordering

Reactive ion etching (RIE) is associated with bombarding the sample with energetic ions. Similarly to low energy ion implantation, the RIE ions generate Frenckel's pair defects when they collide with the atoms of the lattice. A high density of point defects is generated in the surface vicinity, far from the active region, which limits the damage and deterioration of the optical properties of the intermixed material [H.S. Djie *et al.* 2003]. An annealing step is needed to make the mobile point defects diffuse toward the active region and to activate the intermixing. Original work on plasma induced defect disordering was done on AlGaAs/GaAs quantum well structures

treated in a RIE system with a H_2 plasma. A maximum blueshift of 24 nm was obtained after nine exposures and annealing cycles [B.S. Ooi *et al.* 1995b]. The process was also applied for InGaAs/InP quantum well heterostructures and led to 10 nm of maximum blueshift [B.C. Qiu *et al.* 1998b]. In AlGaAs/GaAs systems, when the sample was already covered with a native oxide, H_2 plasma treatment done at room temperature was also found to suppress intermixing [C.J. Hamilton *et al.* 1995]. This was attributed to the strong reducing capacity of hydrogen, which changes the stoichiometry of the native oxide by reducing the As_2O_3 to AsH_3. The liberated oxygen atoms can then react with the GaAs and form Ga_2O_3 [G.M. Mikhailov *et al.* 1992]:

$$As_2O_3 + 2\,GaAs + 12\,H^* \Leftrightarrow Ga_2O_3 + 4\,AsH_3, \qquad (3.17)$$

the H^* are hydrogen radicals. This reaction proceeds to a total coverage of Ga_2O_3 because all free As, Ga and As_2O_3 are forced to form Ga_2O_3 - the most stable product of the reaction [C.J. Hamilton *et al.* 1995]. During the annealing step, the Ga_2O_3 layer acts as a stressor and put the heterostructure under tensile strain. This was reported to prevent vacancies located in the surface vicinity to diffuse toward the active region [L. Fu *et al.* 2002b].

Argon plasma generated by an inductively induced plasma (ICP) generator was also used to introduce point defect in InGaAs/InP quantum well heterostructures [H.S. Djie *et al.* 2003]. Using a patterned SiO_2 mask, Djie and his colleagues achieved a 88 nm differential shift between the masked regions and the plasma treated ones.

Models of defects introduced by plasma treatment [M. Rahman *et al.* 1993] have allowed different research teams to investigate their role and the quantum well intermixing kinetics [A.S. Helmy *et al.* 1997, H.S. Djie *et al.* 2004]. This technique was also successfully used to fabricate integrated devices [H.S. Djie *et al.* 2006a]. This process has the advantage to be

based on relatively easily available tools, however, especially in the case of H_2 plasma irradiation, the numerous issues related to the reliability and reproducibility of the process will require further research for this process to be a real solution to photonic devices integration.

3.2.4 Laser induced quantum well intermixing

Laser induced QWI depends strongly on the nature of the laser (CW vs pulse), emission wavelength and the pulse duration. Photons with energy higher than the absorption edge of the semiconductor are absorbed easily and increase the lattice temperature, while photons with smaller energy can only be absorbed at defect sites or through multi-photon processes.

3.2.4.1 Continuous wavelength laser induced QWI

The first example of laser induced disordering goes back to 1986 when Epler *et al*. used an argon ion laser (λ = 488 nm) to intermix an AlGaAs/GaAs superlattice [J.E. Epler *et al.* 1986]. The laser power densities of the order of $2.5\times10^7 / \mathrm{cm}^2$ were used. Intermixing was primarily due to the rapid melting and regrowth of the laser treated material. Covering the heterostructure with Si and Si_3N_4 caps prior to the laser irradiation allowed Si impurities to incorporate in the heterostructures during the irradiation. An annealing step then activated the impurity diffusion, similarly to the IID technique, leading to an impurity induced interdiffusion of the superlattice. The laser spot can be applied on a very localised area. Delimiting the different regions is done either by directly writing on the sample by using a scanning beam or by depositing a reflecting mask defined by lithography. Using the laser induced diffusion, Epler's team reached a 40 nm sharpness between the disordered and as-grown region. Even if scanning electron microscopy showed damage associated with the laser irradiation, low threshold laser diodes were fabricated using Ar^+ laser disordering [J.E. Epler *et al.* 1987, J.E. Epler *et al.* 1988].

A CW Nd:YAG laser (1-20 W/mm^2) was investigated for QWI in InGaAs/InGaAsP heterostructures by McLean *et al*. in 1992. The irradiation time was of the order of 30 minutes. The wavelength of the laser source was chosen so that photons were only absorbed in the barriers and the wells, while at room temperature, the cladding layers are transparent to them (figure 3-15) [C.J. McLean *et al.* 1992]. Laser radiation was absorbed in the quantum well region where relaxation of charge carriers in excess concentration and non-radiative recombination generates heat which activates the intermixing. The deposition of a dielectric cap also limit the surface desorption induced by the laser irradiation [A. McKee *et al.* 1994]. The quantum well intermixing extent is controlled by modifying the irradiation time or the applied power density. Although this technique is "layer composition sensitive" [J.H. Marsh 1993] at room temperature, as the temperature of the heterostructure increases, its bandgap decreases and photon absorption can occur over the whole sample thickness.

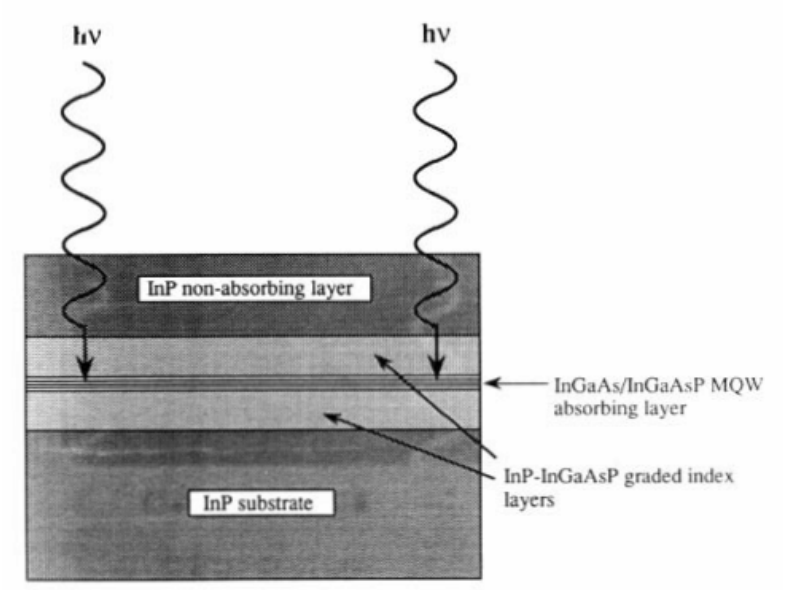

Figure 3-15: Laser absorption in the quantum wells and barriers. The InP cladding layer and the substrate are transparent to the incident light [J.H. Marsh 1993].

Figure 3-16 shows the peak position of photoluminescence emission from an InGaAs/InGaAsP/InP heterostructure sample after Nd:YAG laser irradiation with an enlarged Gaussian beam. The power density used was 0.5 W/mm^2 for 20 s and the wavelength shift covered more than 120 nm. For a moderate irradiation (site #2), the laser annealing repaired part of the structural defects still present after the heterostructure growth, increasing the photoluminescence signal intensity [J.J. Dubowski *et al.* 2002].

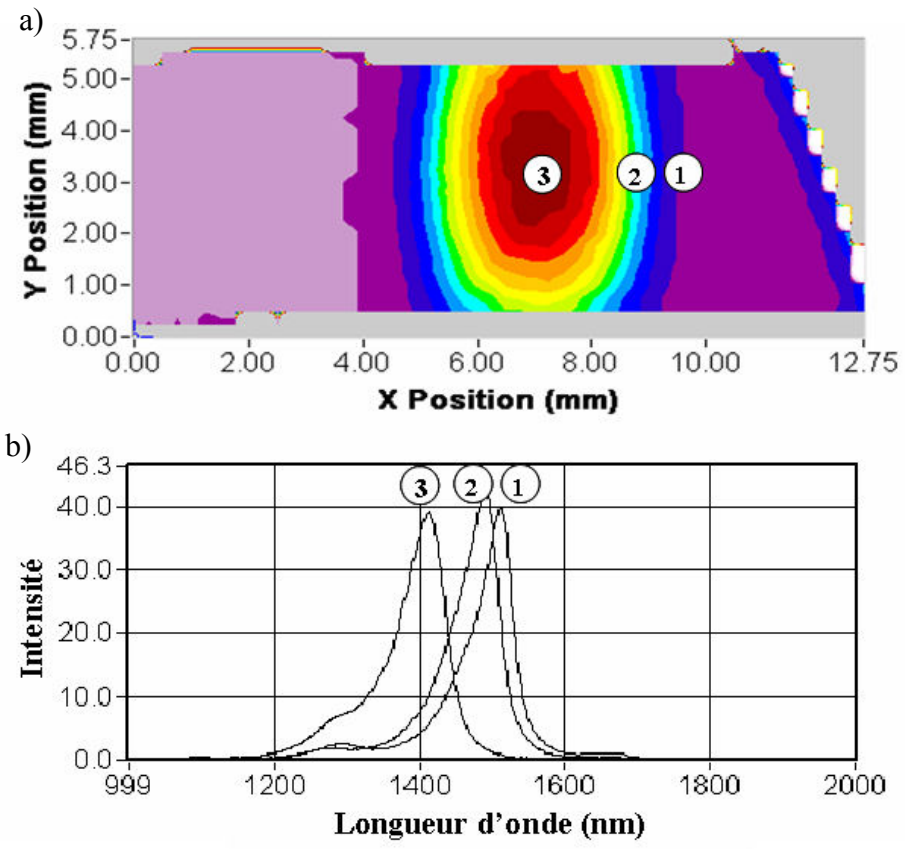

Figure 3-16: a) Photoluminescence mapping of a InGaAs/InGaAsP/InP heterostructure irradiated with an Nd:YAG laser, b) photoluminescence spectra taken on the sample at position 1,2,3 [J.J. Dubowski et al. 2002].

Direct laser writing has been used to heat specific regions of a quantum well heterostructure sample and thus create a multi-bandgap sample [J.J. Dubowski *et al.* 2002].

This technique has the potential to produce intermixed material with excellent optical and electrical properties. However, its spatial selectivity is limited by the heat lateral diffusion inside

the active region and the laser spot size. This technique was also used to fabricate different types of photonic integrated circuits such multi-wavelength laser diode arrays and modulator/laser diode chips [A. McKee *et al.* 1997, J.J. Dubowski *et al.* 2002].

3.2.4.2 Pulsed laser induced disordering

Pulse laser irradiation was investigated to study QWI in heterostructures based on InP [C.J. McLean *et al.* 1995] or GaAs [B.S. Ooi *et al.* 1997]. As in the previous technique, laser light is absorbed is the quantum well. Laser pulses can rapidly heat the crystal lattice. The rapid thermal dilation breaks molecular bonds and alters the crystal lattice. This increases significantly the local concentration of point defects [T.K. Ong *et al.* 2000]. Since the laser pulses don't supply enough energy to activate the interdiffusion, an additional annealing step is needed. This operation can be done in a rapid thermal processor [B.S. Ooi *et al.* 2004] or with a continuous wavelength laser [B.C. Qiu *et al.* 1998a]. In the later case, to prevent the surface desorption of group V atoms, Qiu *et al.* deposited a SiO_2 or Si_xN_y cap on top of the heterostructure. Such cap layer can also enhance (SiO_2) or inhibiting (Si_3N_4) the intermixing process. Spatially resolved photoluminescence measurements on sample partially covered with a patterned reflective gold mask (figure 3-17) demonstrated that the spatial resolution of this technique is of the order of 2.5 μm [B.S. Ooi *et al.* 2004]. Time resolved spectroscopy showed that the carrier lifetime can be reduced down by one order of magnitude after laser irradiation [S.J. Fancey *et al.* 1996]. This technique was used to fabricate multi-wavelength laser diode arrays [B.S. Ooi *et al.* 2004] and electro-absorbing modulators [G. Lullo *et al.* 1994]. It was also used as an in-situ wavelength trimming tool for DFB lasers [T.K. Sudoh *et al.* 1997].

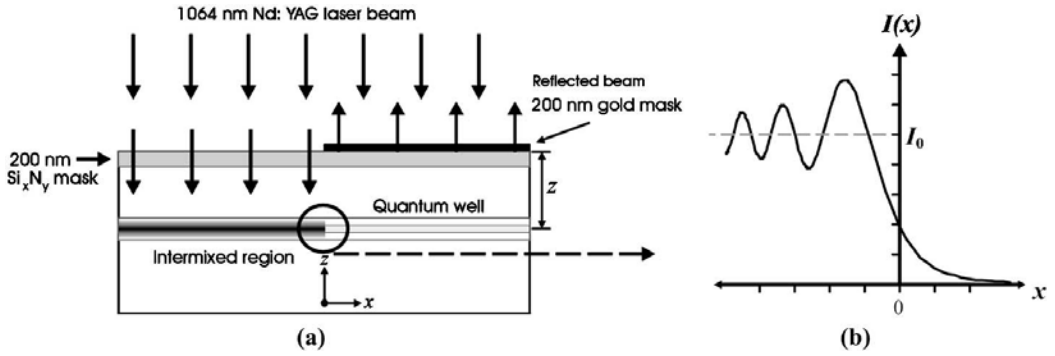

Figure 3-17: a) Laser irradiation through a patterned reflective gold mask, b) intensity plot in the quantum well layer of the diffracted laser beam [B.S. Ooi *et al.* 2004].

The micrometer scale spatial resolution makes both CW and pulsed laser QWI techniques attractive for device fabrication they have the potential to fabricate material suitable for achieving complex integrated photonic devices especially when taking into account the large number of microelectronic processes based on similar laser processing technologies that lead to a high maturity of these systems.

3.2.4.3 Ultra-violet laser induced quantum well intermixing

UV laser interaction with semiconductor surfaces can be carried out without affecting material located deeper than, typically, 10-20 nm. In this way, a layer of an altered material with high concentration of structural defects can be produced, e.g., without inducing residual damage to the active region of the QW wafer. Consequently, the UV laser QWI technique has the potential to fabricate integrated photonic devices with minimally compromised parameters related to laser-induced defects. Excimer lasers, which have already been used in microelectronics (high resolution photolithography, repairing masks, thin film annealing) can also be used to initiate atmosphere-dependent chemical reactions at the semiconductor surface.

In UV laser controlled quantum well intermixing, the surface of the heterostructure is selectively irradiated by UV laser pulses (figure 3-18) to induce the formation of defects or

change the near surface layer chemical stoechiometry [J.J. Dubowski 2003]. Subsequently, the heterostructure follows an annealing step at high temperature for a short period of time (~15 seconds to 120 seconds) to induce QWI. Because UV photons are strongly absorbed by the semiconductor cap layer, it is possible to limit the macroscopic alterations to a relatively thin (sacrificial) layer, which can be removed after the annealing procedure. This makes it possible to eliminate the influence of laser generated residual defects on performance of devices fabricated from the intermixed material [M. Paquette *et al.* 1997].

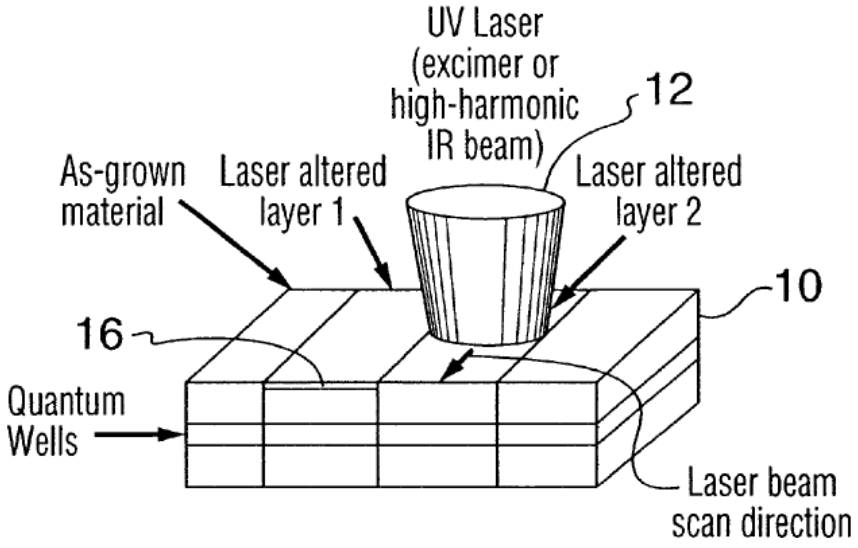

Figure 3-18: UV or excimer laser irradiation of a QW heterostructure allows achieving selective area QWI [J.J. Dubowski 2003].

To demonstrate the potential of this technique, a InP-based quantum well heterostructure was patterned with KrF excimer (λ = 248 nm, Δt = 30 ns) laser pulses for a fluence of about 100 mJ/cm^2 [J.J. Dubowski 2003]. Two exposition sites, defined by a laser mask projection technique were irradiated with 500 and 1000 pulses. The sample was then annealed for 10 seconds at 750°C. The annealing step resulted in a 6 nm blueshift in the untreated area, while the quantum well signal blueshifted of 29 nm and 56 nm in the sites exposed with 500 and 1000 pulses,

respectively. This technique was also recently used to intermixed InGaAs/GaAs quantum dots [H.S. Djie *et al.* 2006b].

Influence of UV irradiation parameters on quantum well intermixing

As it was previously discussed, the depth at which laser can generate defects strongly depends on the energy – or the wavelength – of the incident photons. Figure 3-19 shows absorption coefficients, α, for GaAs and InP as a function of photon energy. For energies exceeding that of the semiconductor bandgap, the absorption coefficient raises rapidly, which results in a shallower absorption depth. However, heat diffusion processes can spread laser-generated defects to depths significantly exceeding those of the absorption length α^{-1}. The sample reflection coefficient (figure 3-20) also affects the processes of defects creation since it affects the transmitted power density.

The interaction of laser pulses with a material also depends on the temporal length of the laser pulses in use. For example, the ablation threshold decreases as the pulse length decreases (figure 3-21). Under ultra-short pulses, thermal conduction is minimal and can be neglected. The interaction volume is then limited by the absorption thickness α^{-1}. The defect generation process is also influenced by the pulse length. While under longer pulses the thermal effects are greatly responsible for expulsing mater out of the target, under ultra-short, it is associated with photomechanical processes [D. Perez *et al.* 2002].

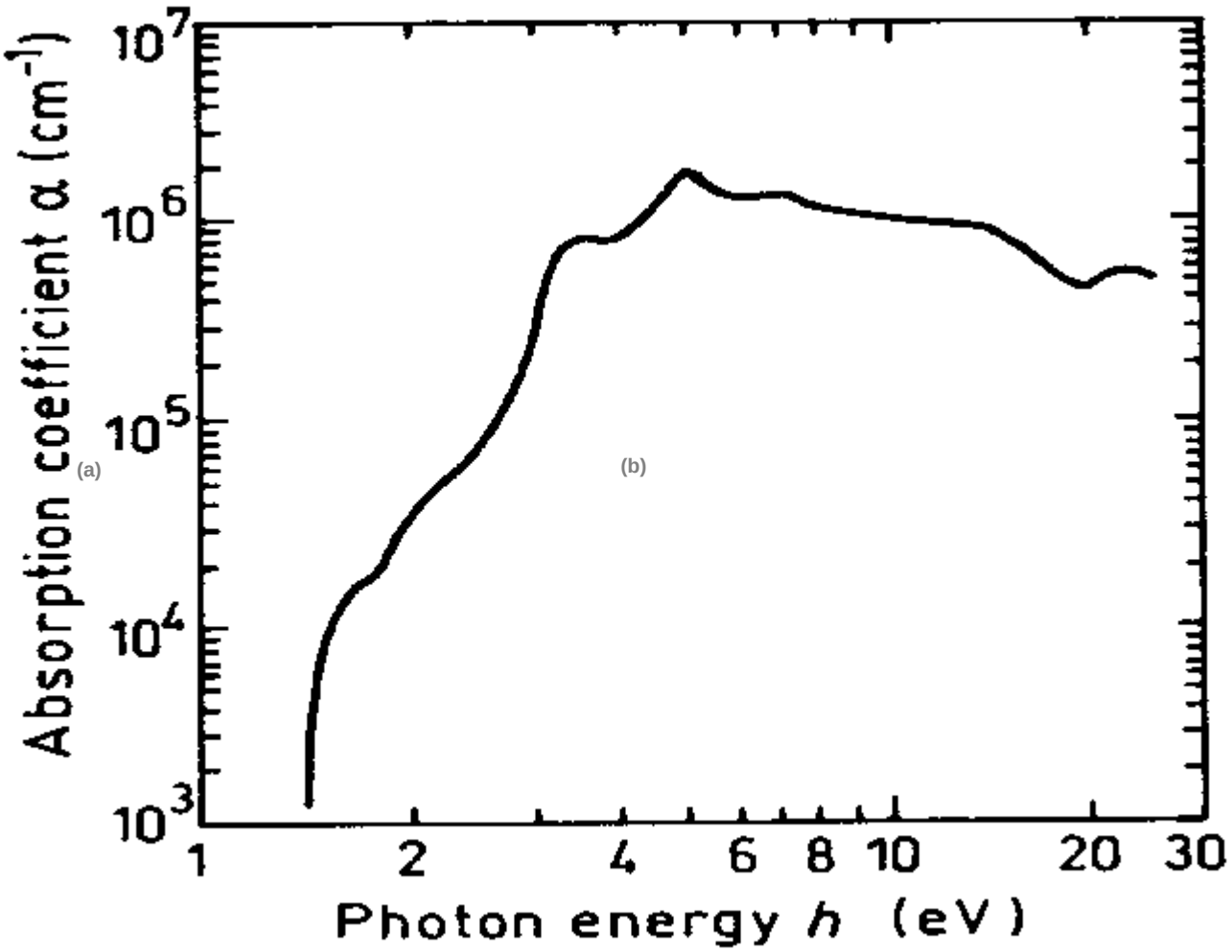
Absorption coefficient α (cm⁻¹)
10⁷
10⁶
10⁵
10⁴
10³
(a)
(b)
1
2
4
6
8
10
20
30
Photon energy h (eV)

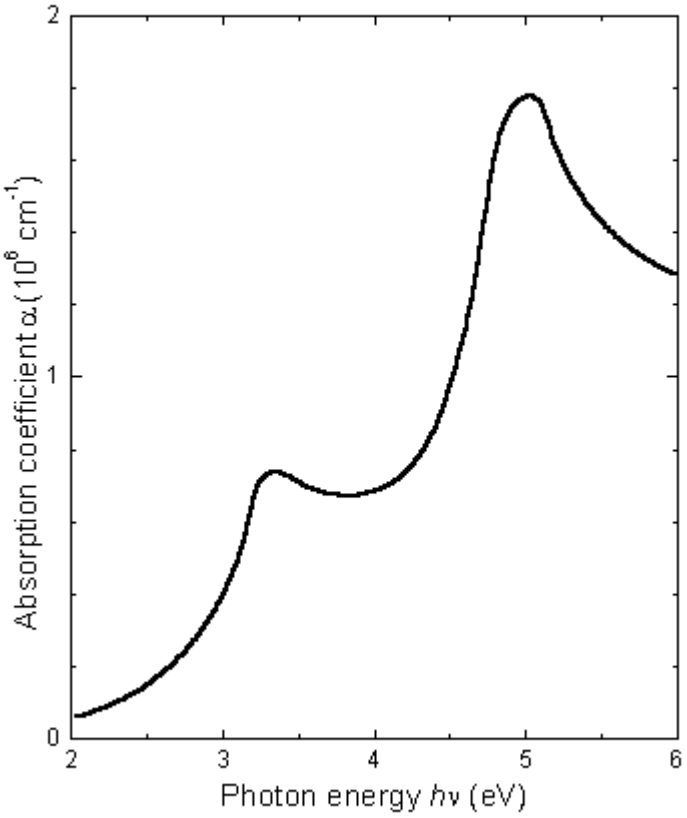

Figure 3-19: Absorption coefficients as a function of the incident photon energy for a) GaAs [H.C. Casey, Jr. *et al.* 1975] and b) InP [D.E. Aspnes *et al.* 1983]

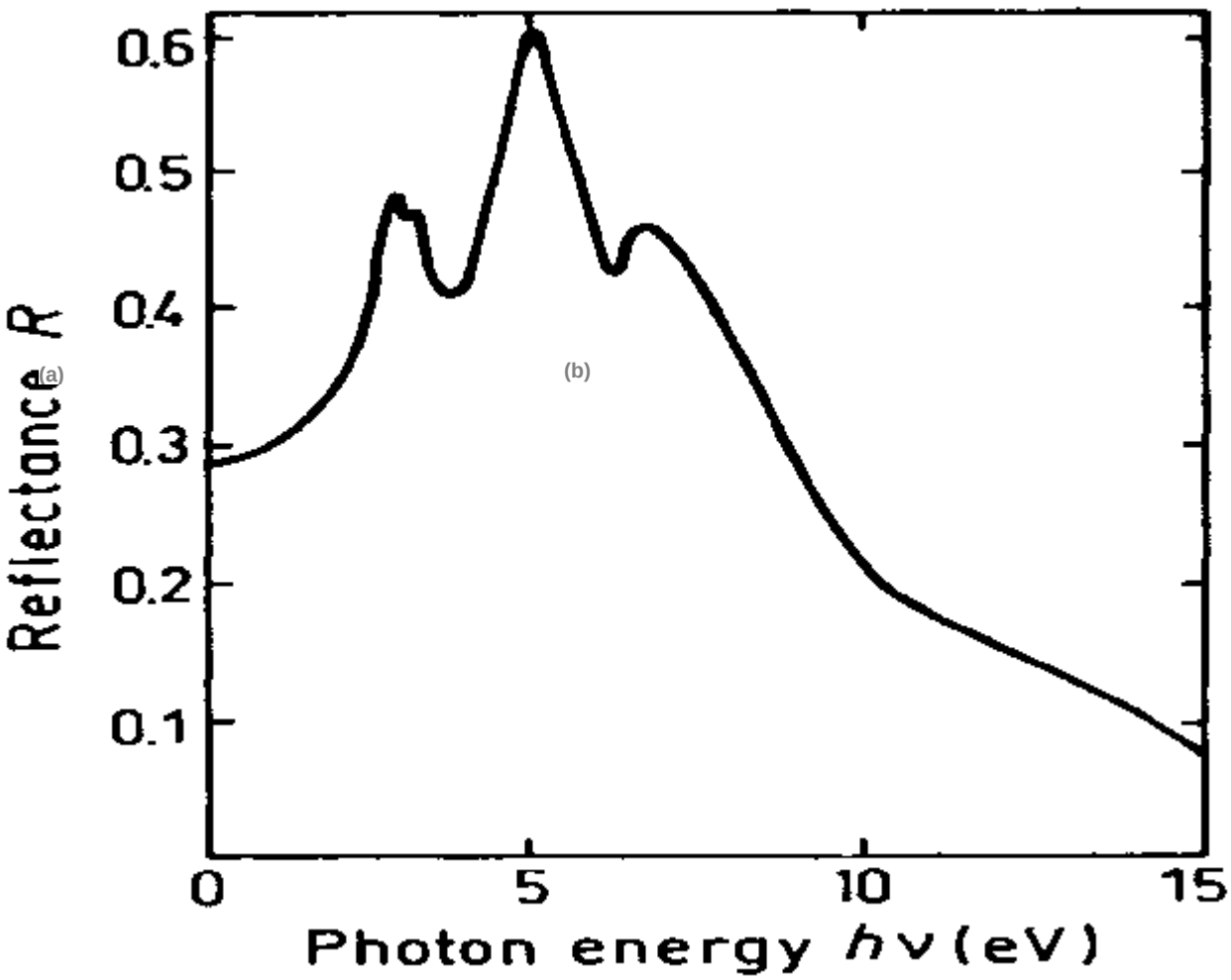
0.6
0.5
0.4
0.3
0.2
0.1
Reflectance R
(a)
(b)
0
5
10
15
Photon energy hν (eV)

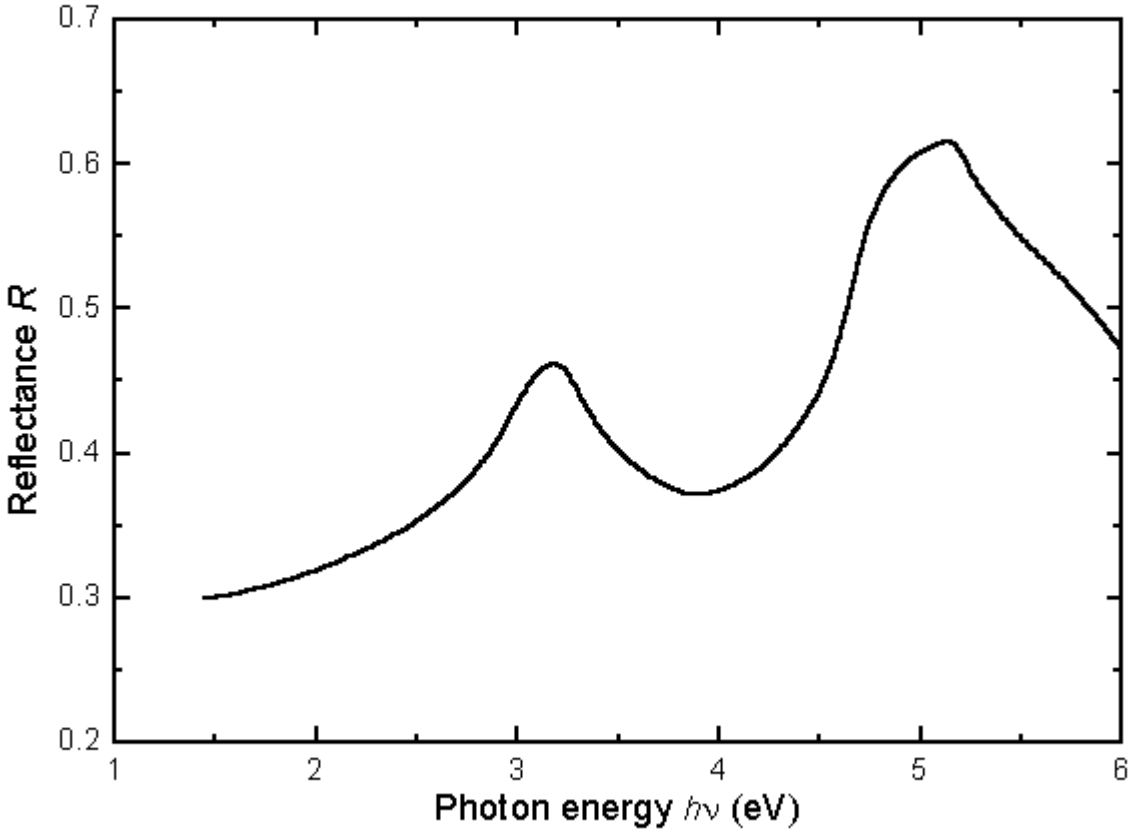

Figure 3-20: Reflection coefficients versus normal incident photons energy for a) GaAs[H.R. Philipp *et al.* 1963] and b) InP[D.E. Aspnes *et al.* 1983]

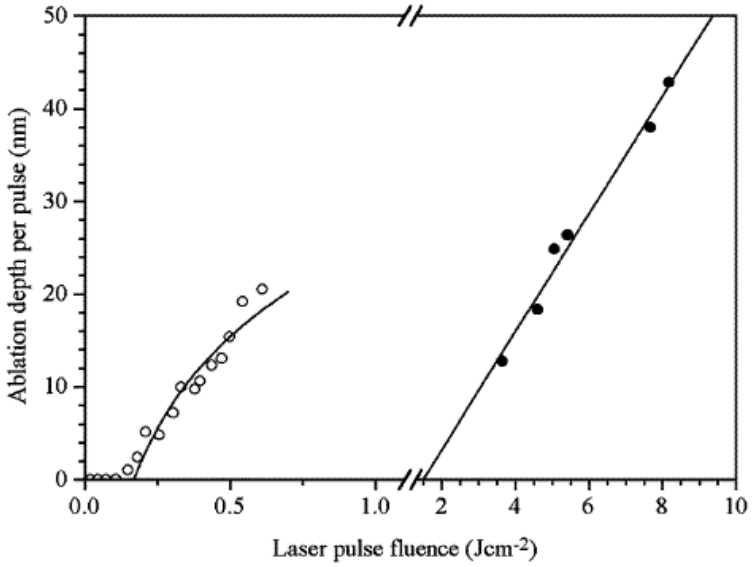

Figure 3-21: Ablation depth of a cupper target as a function of the energy density of KrF (248 nm) laser (short o, 0.5 ps) and long (•, 20 ns) pulses. [S. Amoruso *et al.* 1999]

The laser repetition rate also has an influence on the dynamics of laser mater interaction. During each pulse, the temperature inside the interaction volume increases and reaches its maximum. The heat then diffuses to the substrate. If the time between each pulse is long enough, the surface can return its original temperature. In such case, each pulse is independent. On the opposite, if the period is shorter than the heat diffusion time, heat accumulates as the number of pulse increases and new reactions can be activated. For example, in UV laser enhanced oxidation of GaAs, a change of the surface temperature alters the oxidation dynamics. Rapid pulses would favour in time the preferential formation of a non-stoichiometric gallium oxide while slower ones would generate an oxide with equal proportions of gallium oxide and arsenic oxide.

Because there versatility, UV lasers are a highly attractive tool for post-growth processing of semiconductor wafers. Since the photon penetration depth in the heterostructure depends on the photon wavelength, the altered layer thickness and the defects concentration can be achieved by choosing the laser wavelength and the irradiation dose. Excimer laser can also be used to process relatively large areas in one step, similarly to the area coverage achieved by the excimer-

based photolithography technique. They can generate surface heating, generate near surface defects and alter the surface chemistry [J. Genest *et al.* 2007b]. All theses surfaces treatments can be achieved with a regular projection lithography system which allows direct patterning samples.

The objective of this work is to improve the UV-QWI technique by optimizing the generation of point defects process or by enhancing control on their diffusion toward the QWs. The devices fabricated on the intermixed material should have comparable characteristics to the one fabricated on untreated heterostructure. In the long term, optimizing the bandgap shift as a function of the UV laser exposition should increase the UV-QWI reproducibility and reliability.

3.3 Summary

In this chapter, I described the QWI concept and presented a brief review of different QWI techniques. I discussed the advantages and weaknesses of each technique. I put more importance on techniques based on laser technologies as it plays a major role in this thesis. However, I also put some emphasis of the impurity free vacancies disordering technology since, as with UV laser controlled quantum intermixing, it directs the intermixing by changing the heterostructure surface properties. We can summarise this chapter with the following conclusions:

Quantum well intermixing is a process activated thermally. It changes the shape of a quantum well form a square-like well to a smoother form which raises the position of the discrete energy levels inside the well and changes the material bandgap. The intermixing process is accelerated by the presence of point defects in the well vicinity.

Impurity induced disordering is a well documented and understood technology. However, because it increases the optical losses in the active region, it is unsuitable for passive optoelectronic devices and it increases power consumption in active devices.

Impurity free vacancies disordering is a relatively simple technology to achieve quantum well intermixing. Enhanced and suppressed blueshifts were demonstrated using different capping layers. It is very effective for GaAs-based QW heterostructures, but has demonstrated limited use for InP-based heterostructures. Since defects are introduced at the surface, the spatial resolution of this technology is limited by the lateral diffusion of point defects and depends on the location of the active region below the surface. The quality of dielectric cap is difficult to control and it leads to reproducibility issues.

The “universal damage” technology, or silica sputtering technology, has the advantage of working well on GaAs and on InP based heterostructures because point defects are created by both the sputtering damage and the surface out-diffusion in the dielectric layer. However, it is difficult to control the amount of generated defects; therefore reproducibility becomes a major issue. This technology reduces the material quality.

Ion implantation induced QWI works reasonably well for both GaAs- and on InP-based heterostructures. Models of defect creation are also available for this technology. When ions are implanted, defects can be generated at the desired depth by changing the ion specie or the acceleration energy. However, achieving multi-bandgap wafers require multi-steps implantation or grey tone masking which reproducibility might be an issue. Shallow ion implantation done with a reactive ion etcher or an induced coupled plasma etching system would be an interesting option to implant sample without using an expensive ion implanter. Furthermore, under high

energy acceleration, ion implantation leaves residual damage near the active region which reduces the devices performances.

Since they are absorbed in a very thin volume of the surface layer, UV lasers can be used efficiently to generate QWI promoting defects. The laser can also alter the chemical stoechimetry of the near surface layer so that the altered layer enhances or prevents diffusion of point defects towards the QW region. Combined with surface heating and possibility to alter the surface chemistry, the UV excimer lasers are potentially attractive tools for the fabrication of PICs.

3.4 Bibliography

Adachi, S. (1982) *Material parameters of $In_{1-x}Ga_xAs_yP_{1-y}$ and related binaries*, Journal of Applied Physics, vol. 53, n° 12, 8775-92.

Aimez, V., Beauvais, J., et al. (2002) *Low-energy ion-implantation-induced quantum-well intermixing*, IEEE Journal of Selected Topics in Quantum Electronics, vol. 8, n° 4, 870-879.

Amoruso, S., Bruzzese, R., et al. (1999) *Characterization of laser-ablation plasmas*, Journal of Physics B (Atomic, Molecular and Optical Physics), vol. 32, n° 14, 131-72.

Aspnes, D. E. and Studna, A. A. (1983) *Dielectric functions and optical parameters of Si, Ge, GaP, GaAs, GaSb, InP, InAs, and InSb from 1.5 to 6.0 eV*, Physical Review B, vol. 27, n° 2, 985.

Beauvais, J., Marsh, J. H., et al. (1992) *Suppression of Bandgap Shifts in Gaas/Algaas Quantum-Wells Using Strontium Fluoride Caps*, Electronics Letters, vol. 28, n° 17, 1670-1672.

BenDaniel, D. J. and Duke, C. B. (1966) *Space-Charge Effects on Electron Tunneling*, Physical Review, vol. 152, n° 2, 2104-2107.

Bollet, F., Gillin, W. P., et al. (2003) *On the diffusion of lattice matched InGaAs/InP microstructures*, Journal of Applied Physics, vol. 93, n° 7, 3881-5.

Brice, D. K., Borders, J. A., et al. (1977). *Ion Implantation in semiconductors*, New York, Plenum Publishing Corporation, xiv, 754 p.

Britton, D. T. and Harting, M. (2002) *The influence of strain on point defect dynamics*, Advanced Engineering Materials, vol. 4, n° 8, 629-635.

Casey, H. C., Jr., Sell, D. D., et al. (1975) *Concentration dependence of the absorption coefficient for n- and p - type GaAs between 1.3 and 1.6 eV*, Journal of Applied Physics, vol. 46, n° 1, 250-257.

Charbonneau, S., Koteles, E. S., et al. (1998) *Photonic integrated circuits fabricated using ion implantation*, IEEE Journal of Selected Topics in Quantum Electronics, vol. 4, n° 4, 772-793.

Charbonneau, S., Poole, P. J., et al. (1995) *Quantum-well intermixing for optoelectronic integration using high energy ion implantation*, Journal of Applied Physics, vol. 78, n° 6, 3697-705.

Choi, W. J., Lee, J. I., et al. (1994) *Enhanced disordering of GaAs/AlGaAs multiple quantum well by rapid thermal annealing using plasma enhanced chemical vapour deposited SiN capping layer grown at high RF power condition*, Journal of Materials Science Letters, vol. 13, n° 5, 326-8.

Cohen, R. M. (1997) *Point defects and diffusion in thin films of GaAs*, Materials Science & Engineering: R: Reports, vol. 20, n° 4-5, 167.

Cusumano, P., Ooi, B. S., et al. (1997) *Suppression of quantum well intermixing in GaAs/AlGaAs laser structures using phosphorus-doped SiO₂ encapsulant layer*, Journal of Applied Physics, vol. 81, n° 5, 2445-7.

Deppe, D. G. and Holonyak, N., Jr. (1988) *Atom diffusion and impurity-induced layer disordering in quantum well III-V semiconductor heterostructures*, Journal of Applied Physics, vol. 64, n° 12, 93-113.

Dion, C., Poole, P. J., et al. (2006) *Tuning of the electronic properties of self-assembled InAs/InP(001) quantum dots using grown-in defect mediated intermixing*, Applied Physics Letters, vol. 89, n° 13, 131905-3.

Djie, H. S. and Mei, T. (2006a) *Plasma-induced quantum well intermixing for the universal high-density photonic integration*, Journal of Crystal Growth, vol. 288, n° 1, 49.

Djie, H. S., Mei, T., et al. (2003) *Photoluminescence enhancement by inductively coupled argon plasma exposure for quantum-well intermixing*, Applied Physics Letters, vol. 83, n° 1, 60-2.

Djie, H. S., Mei, T., et al. (2004) *Experimental and theoretical analysis of argon plasma-enhanced quantum-well intermixing*, Quantum Electronics, IEEE Journal of vol. 40, n° 2, 166-174.

Djie, H. S., Ooi, B. S., et al. (2006b) *Quantum dot intermixing using excimer laser irradiation*, Applied Physics Letters, vol. 89, n° 8, 081901.

Dubowski, J. J. (2003) *Laser-induced bandgap shifting for photonic device integration*, U.S. 6,670,644.

Dubowski, J. J., Feng, Y., et al. (2002) *Monolithic multiple wavelength ridge waveguide laser array fabricated by Nd : YAG laser-induced quantum well intermixing*, Journal of Vacuum Science & Technology A, vol. 20, n° 4, 1426-1429.

Elman, B., Koteles, E. S., et al. (1989) *GaAs/AlGaAs quantum-well intermixing using shallow ion implantation and rapid thermal annealing*, Journal of Applied Physics, vol. 66, n° 5, 2104-2107.

Epler, J. E., Burnham, R. D., et al. (1987) *Low threshold buried heterostructure quantum well diode lasers by laser-assisted disordering*, Applied Physics Letters, vol. 50, n° 23, 1637-1639.

Epler, J. E., Burnham, R. D., et al. (1986) *Laser induced disordering of GaAs-AlGaAs superlattice and incorporation of Si impurity*, Applied Physics Letters, vol. 49, n° 21, 1447-1449.

Epler, J. E., Thornton, R. L., et al. (1988) *Very low threshold buried heterostructure quantum well lasers by laser-assisted disordering*, Applied Physics Letters, vol. 52, n° 17, 1371-1373.

Eshelby, J. D. (1951) *The Force on an Elastic Singularity* Philosophical Transactions of the Royal Society of London. Series A, Mathematical and Physical Sciences, vol. 244, n° 877 87-112.

Fancey, S. J., Buller, G. S., et al. (1996) *Time-resolved photoluminescence microscopy of GaInAs/GaInAsP quantum wells intermixed using a pulsed laser technique*, Journal of Applied Physics, vol. 79, n° 12, 9390-9392.

Fu, L., Lever, P., et al. (2003) *Suppression of interdiffusion in InGaAs/GaAs quantum dots using dielectric layer of titanium dioxide*, Applied Physics Letters, vol. 82, n° 16, 2613-2615.

Fu, L., Wong-Leung, J., et al. (2002) *Suppression of interdiffusion in GaAs/AlGaAs quantum-well structure capped with dielectric films by deposition of gallium oxide*, Journal of Applied Physics, vol. 92, n° 7, 3579.

Gareso, P. L., Buda, M., et al. (2004) *Suppression of thermal atomic interdiffusion in C-doped InGaAs/AlGaAs quantum well laser structures using TiO_2 dielectric layers*, Applied Physics Letters, vol. 85, n° 23, 5583-5585.

Genest, J., Dubowski, J. J., et al. (2007) *UV laser controlled quantum well intermixing in InAlGaAs/GaAs heterostructures*, Journal of Physics: Conference Series, vol. 59, n° 1, 605-9.

Guido, L. J., Jackson, G. S., et al. (1987) *Index-Guided $Al_xGa_{1-XA}s$-GaAs Quantum-Well Heterostructure Lasers Fabricated by Vacancy-Enhanced Impurity-Induced Layer*

Disordering from an Internal $(Si_2)_Y(GaAs)_{1-Y}$ Source, Applied Physics Letters, vol. 50, n° 10, 609-611.

Gunawan, O., Ong, T. K., et al. (2000). *A theoretical analysis of quantum well intermixing using the pulsed laser irradiation technique in InGaAs/InGaAsP laser structure*, Beijing, China, Elsevier.

Hamilton, C. J., Hicks, S. E., et al. (1995) *Suppression of Bandgap Shifts in GaAs/AlGaAs Multiquantum Wells Using Hydrogen Plasma Processing*, Electronics Letters, vol. 31, n° 16, 1393-1394.

Haysom, J. E., Aers, G. C., et al. (2000) *Study of quantum well intermixing caused by grown-in defects*, Journal of Applied Physics vol. 88, n° 5, 3090-3092.

Helmy, A. S., Aitchison, J. S., et al. (1997) *The kinetics of intermixing of GaAs/AlGaAs quantum confined heterostructures*, Applied Physics Letters, vol. 71, n° 20, 2998-3000.

Helmy, A. S., Johnson, N. P., et al. (1998) *A study of impurity-free vacancy disordering in GaAs-AlGaAs for improved modeling*, IEEE Journal of Selected Topics in Quantum Electronics, vol. 4, n° 4, 661-8.

Holonyak, N., Jr. (1998) *Impurity-induced layer disordering of quantum-well heterostructures: discovery and prospects*, IEEE Journal of Selected Topics in Quantum Electronics, vol. 4, n° 4, 584-94.

Kaminska, M., Weber, E. R., et al. (1989). *Stoichiometry-related defects in GaAs grown by molecular-beam epitaxy at low temperature*, Bozeman, MT, USA.

Kapon, E., Stoffel, N. G., et al. (1988) *Birefringent channel waveguides defined by impurity-induced superlattice disordering*, Applied Physics Letters, vol. 52, n° 5, 351-3.

Kowalski, O. P., Hamilton, C. J., et al. (1998) *Monolithic integration via a universal damage enhaced quantum-well intermixing technique*, Journal of Selected Topics in Quantum Electronics, vol. 4, n° 4, 636-646.

Lai, R., Pamulapati, J., et al. (1991) *Low-loss, single-mode In0.53Ga0.47As/In0.52Al0.48As/InP optical waveguides fabricated by Zn-induced impurity-induced layer disordering*, Journal of Applied Physics, vol. 70, n° 9, 5136-7.

Laidig, W. D., N. Holonyak, r. J., et al. (1981) *Disorder of an AlAs-GaAs superlattice by impurity diffusion*, Applied Physics Letters, vol. 38, n° 10, 776-778.

Lee, J. W. and Laidig, W. D. (1984) *Diffusion and interdiffusin in Zn-disordered AlAs-GaAs superlattices*, Journal of Electronic Materials, vol. 13, n° 1, 147-165.

Leon, R., Yong, K., et al. (1996) *Effects of interdiffusion on the luminescence of InGaAs/GaAs quantum dots*, Applied Physics Letters, vol. 69, n° 13, 1888-90.

Li, E. H., Ed. (2000). Semiconductor Quantum Wells Intermixing. Optoelectronic Properties of Semiconductors and Superlattices. Amsterdam, Netherlands, Gordon and Breach Science Publishers, 695 p.

Liu, X., Lu, W., et al. (2000) *Wavelength shifting of adjacent quantum wells in V-groove quantum wire structure by selective implantation and annealing*, Journal of Applied Physics, vol. 87, n° 3, 1566-8.

Liu, X. F., Qiu, B. C., et al. (2000) *Control of multiple bandgap shifts in InGaAs-AlInGaAs multiple-quantum-well material using different thicknesses of PECVD SiO₂ protection layers*, IEEE Photonics Technology Letters, vol. 12, n° 9, 1141-3.

Lullo, G., McKee, A., et al. (1994) *Fabrication of electroabsorption optical modulators using laser disordered GaInAs/GaInAsP multiquantum well structures*, Electronics Letters, vol. 30, n° 19, 1623-5.

Marsh, J. H. (1993) *Quantum-Well Intermixing*, Semiconductor Science and Technology, vol. 8, n° 6, 1136-1155.

McDougall, S. D., Kowalski, O. P., et al. (1997) *Extended cavity ridge waveguide lasers operating at 1.5μm using simple damage induced quantum well intermixing process*, Electronics Letters, vol. 33, n° 23, 1957-1958.

McDougall, S. D., Kowalski, O. P., et al. (1998) *Monolithic integration via a universal damage enhanced quantum-well intermixing technique*, IEEE Journal of Selected Topics in Quantum Electronics, vol. 4, n° 4, 636-46.

McKee, A., McLean, C. J., et al. (1994) *High quality wavelength tuned multiquantum well GaInAs/GaInAsP lasers fabricated using photoabsorption induced disordering*, Applied Physics Letters, vol. 65, n° 18, 2263-5.

McKee, A., McLean, C. J., et al. (1997) *Monolithic integration in InGaAs-InGaAsP multiple-quantum-well structures using laser intermixing*, IEEE Journal of Quantum Electronics, vol. 33, n° 1, 45-55.

McLean, C. J., Marsh, J. H., et al. (1992) *Layer selective disordering by photoabsorption-induced thermal diffusion in InGaAs/InP based multiquantum well structures*, Electronics Letters, vol. 28, n° 12, 1117-1119.

McLean, C. J., McKee, A., et al. (1995) *Quantum well intermixing with high selectivity using a pulsed laser technique*, Electronics Letters, vol. 31, n° 15.

Mikhailov, G. M., Bulkin, P. V., et al. (1992) *XPS investigation of the interactive between ECR-excited hydrogen and the native oxide of GaAs (100)*, Vacuum, vol. 43, n° 3, 199-201.

Mitra, S. and Stark, J. P. (1991) *Role of vacancies and implantation defects in GaAs/AlAs*

superlattice intermixing, Journal of Materials Science, vol. 26, n° 24, 6650.

Ng, S. L., Djie, H. S., et al. (2003) *Fabrication of wide-band electro-absorption waveguide modulator arrays using quantum well-intermixing process*, Optics Communications, vol. 226, n° 1-6, 191-7.

Ng, S. L., Lim, H. S., et al. (2002). *Generation of multiple energy bandgaps using a gray mask process and quantum well intermixing*, Nara, Japan, Japan Soc. Appl. Phys.

Ong, T. K., Gunawan, O., et al. (2000) *High-spatial-resolution quantum-well intermixing process in GaInAs/GaInAsP laser structure using pulsed-photoabsorption-induced disordering*, Journal of Applied Physics, vol. 87, n° 6, 2775-9.

Ooi, B. S., Ayling, S. G., et al. (1995a) *Fabrication of Multiple Wavelength Lasers in GaAs-AlGaAs Structures Using a One-Step Spatially Controlled Quantum-Well Intermixing Technique*, IEEE Photonics Technology Letters, vol. 7, n° 9, 944-946.

Ooi, B. S., Bryce, A. C., et al. (1995b) *Integration process for photonic integrated circuits using plasma damage induced layer intermixing*, Electronics Letters, vol. 31, n° 6, 449-51.

Ooi, B. S., Hamilton, C. J., et al. (1997) *Quantum-well intermixing in GaAs-AlGaAs structures using pulsed laser irradiation*, IEEE Photonic Technology Letters, vol. 9, n° 5, 587-589.

Ooi, B. S., Ong, T. K., et al. (2004) *Multiple-wavelength integration in InGaAs-InGaAsP structures using pulsed laser irradiation-induced quantum-well intermixing*, IEEE Journal of Quantum Electronics, vol. 40, n° 5, 481.

Paquette, M., Beauvais, J., et al. (1997) *Blueshifting of InGaAsP/InP laser diodes by low-energy ion implantation*, Applied Physics Letters, vol. 71, n° 26, 3749-51.

Pepin, A., Vieu, C., et al. (1997) *Evidence of stress dependence in SiO_2/Si_3N_4 encapsulation-based layer disordering of GaAs/AlGaAs quantum well heterostructures*, Journal of Vacuum Science & Technology B, vol. 15, n° 1, 142-153.

Perez, D. and Lewis, L. J. (2002) *Ablation of solids under femtosecond laser pulses*, Physical Review Letters, vol. 89, n° 25, 255504-1.

Philipp, H. R. and Ehrenreich, H. (1963) *Optical Properties of Semiconductors*, Physical Review, vol. 129, n° 4, 1550.

Plummer, J. D., Deal, M. D., et al. (2000). *Silicon VLSI Technology : Fundamentals, Practice and Modeling*, Upper Saddle River, NJ, Prentice Hall, 817 p.

Qiu, B. C., Bryce, A. C., et al. (1998a) *Monolithic integration in InGaAs-InGaAsP multiquantum-well structure using laser processing*, IEEE Photonics Technology Letters, vol. 10, n° 6, 769.

Qiu, B. C., Ooi, B. S., et al. (1998b) *Reduced damage reactive ion etching process for fabrication of InGaAsP/InGaAs multiple quantum well ridge waveguide lasers*, Journal of Vacuum Science & Technology B (Microelectronics and Nanometer Structures), vol. 16, n° 4, 1818-22.

Rahman, M., Foad, M. A., et al. (1993). *Defect penetration during the plasma etching of semiconductors*, Boston, MA, USA, Mater. Res. Soc.

Rao, E. V. K., Hamoudi, A., et al. (1995) *New encapsulant source for III-V quantum well disordering*, Applied Physics Letters, vol. 66, n° 4, 472-474.

Robert, F., Bryce, A. C., et al. (2004) *Passive mode locking of InAlGaAs 1.3-µm strained quantum wells extended cavity laser fabricated by quantum-well intermixing*, IEEE Photonics Technology Letters, vol. 16, n° 2, 374-6.

Shimada, N., Fukumoto, Y., et al. (2004) *Monolithic integration of lasers and passive elements using selective QW disordering by rapid thermal annealing with SiO_2 caps of different thicknesses*, Electronics and Communications in Japan (Part II: Electronics), vol. 87, n° 1, 34-42.

Srikrishnan, K. V. (2005) *Smart-cut process for the production of thin semiconductor material films*, US 5882987.

Sudoh, T. K., Kumano, M., et al. (1997) *Wavelength trimming by photoabsorption-included disordering for multiple-wavelength distributed-feedback laser arrays*, IEEE Photonics Technology Letters, vol. 9, n° 7, 887-8.

Tan, T. Y. (1991) *Point defect thermal equilibria in GaAs*, Materials Science & Engineering B (Solid-State Materials for Advanced Technology), vol. B10, n° 3, 227.

Teng, J. H., Dong, J. R., et al. (2001) *Impurity-free intermixing in compressively strained InGaAsP multiple quantum well structures*, Materials Science in Semiconductor Processing, vol. 4, n° 6, 621.

Ying, M., Liu, P., et al. (2003) *Investigation of intermixing induced by sputtering and annealing in multiple quantum well*, Applied Surface Science, vol. 205, n° 182-187.

Yu, J. S., Song, J. D., et al. (2002) *Influence of dielectric deposition parameters on the $In_{0.2}Ga_{0.8}As/GaAs$ quantum well intermixing by impurity-free vacancy disordering*, Journal of Applied Physics, vol. 92, n° 3, 1386-1390.

Yuan, S., Jagadish, C., et al. (1998) *Anodic-oxide-induced intermixing in GaAs-AlGaAs quantum-well and quantum-wire structures*, IEEE Journal of Selected Topics in Quantum Electronics, vol. 4, n° 4, 629-35.

Ziegler, J. F. (1992). *Handbook of ion implantation technology*, Amsterdam ; New York, North-Holland, vii, 700 p.

Chapter 4: Experimental procedures

The first part of this chapter is dedicated to the description of the excimer laser techniques used to investigate the UV-QWI process. In the second section of this chapter, I describe the structure of four heterostructures used in this work. The third part presents the characterisation techniques applied to measure the extent of the intermixing, lateral resolution of the UV-QWI process and to analyse surface properties of the laser irradiated samples.

4.1 Excimer lasers

Excimer laser are the most powerful lasers existing in the UV spectrum. Excimer comes from the expression **exci**ted di**mer** which is a type of molecules formed by the combination of two identical atoms or constituents in their excited state. However, nowadays the term excimer is used by convention since most "excimer" lasers are based on exciplexes (excited complexes) of rare-gas monohalides which exist only in its excited state. The exciplexes are formed from rare-gases such as Ar, Kr or Xe and halides F and Cl [D. Basting *et al.* 2005]. Excimer laser transitions can be used to generate wavelengths between 126 nm (Ar_2) and 660 nm (Xe_2F), however the most commonly employed laser gas mixtures are fluorine (F_2, 157 nm), argon fluoride (ArF, 193 nm), krypton fluoride (KrF, 248 nm), xenon chloride (XeCl, 308 nm) and xenon fluoride (XeF, 351 nm).

The production of the excited excimer molecules is based on a complex plasma reaction which occurs when the gas is submitted to an electrical discharge. The formation of the excited

molecule is dominated by two processes: the ion channel and the neutral channel (figure 4-1). For example, for a KrF laser, both reactions take place in few nanoseconds leaving the excited KrF^* molecule at the minimum of the potential energy curve of the upper state. The KrF^* complex decays after several nanoseconds via the emission of a 248 nm photon and decomposes into Kr and F. The Kr and F components are then available for another excitation cycle. Since the KrF molecule does not exist in its unexcited state, KrF laser and other excimer lasers belong to the four energy levels class of lasers, which means that emission process does not suffer from ground state saturation and thus have a relatively high efficiency. Because of the short life time of the excited exciplexe and the fast loss processes in the cavity, pump power densities exceeding 1 MW/cm^3 are needed to efficiently excite the excimer lasers. Such power densities can only be reached by pulsed systems which prevents excimer lasers from operation in continuous wave mode.

The following expressions describe the detail of the different chemical reactions taking place in a KrF laser. Similar expressions can be use to describe other excimer and exciplexe reactions [D. Basting *et al.* 2005].

Pumping:

$$\begin{aligned} e^- + Kr &\Rightarrow Kr^+ + e^- + e^- && \text{positive inert-gas ion production} \\ e^- + Kr &\Rightarrow Kr^* + e^- && \text{inert-gas metastable production} \\ e^- + F_2 &\Rightarrow F^- + F && \text{negative ion production} \\ Kr^+ + F^- + M &\Rightarrow KrF^* + M && KrF^* \text{ production (ion channel)} \\ Kr^* + F_2 &\Rightarrow KrF^* + F && KrF^* \text{ production (neutral channel)} \end{aligned} \tag{4.1}$$

Stimulated emission:

$$KrF^* + hv \Rightarrow Kr + F + 2hv \ (248nm) \quad \text{laser emission} \tag{4.2}$$

Losses:

$$KrF^* \Rightarrow Kr + F + hv \ (248nm) \quad \text{spontaneous emission} \tag{4.3}$$

$$KrF^* \Rightarrow Kr + F + hv\ (248nm) \quad \text{spontaneous emission} \qquad (4.3)$$

collisional deactivation

collisional deactivation producing Kr_2F

impurity absorption of laser photon

In equations (4.1), (4.2) and (4.3), * stands for the excited state of an atom or a molecule, M is a third body - usually an atom from the buffer gas -, while X represents and impurity in the laser gas.

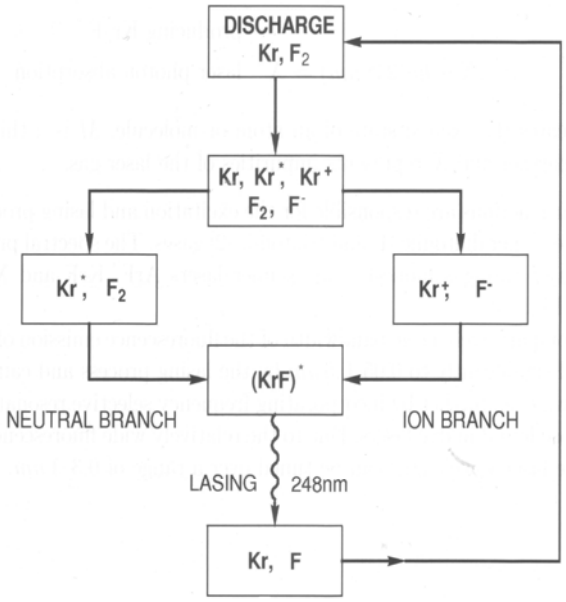

Figure 4-1: Excitation kinetics of the KrF excimer laser [D. Basting *et al.* 2005]

Excimer lasers are the most popular laser system to achieve laser ablation. Since the UV wavelengths are usually absorbed in a shallow region of material near the surface, excimer lasers offer a good control of the ablation depth and of the thickness of the treated layer. The duration of the pulse also allows irradiation peak power up to 10^{10} W/cm^2. Excimer lasers are used in microelectronics industry for photolithography at 248 and 193 nm [V. Pol *et al.* 1987], and

annealing of amorphous silicon for flat panel display applications [P.M. Smith *et al.* 1997]. They have also been used for micromachining and surface patterning [J.H. Brannon 1989, C.J. Hayden 2003], chemical or physical modification [H.M. Phillips *et al.* 1993, E.E. Mayer *et al.* 1999] and for hole drilling in electronic circuit packaging [J.R. Lankard, Sr. *et al.* 1992]. Excimer laser are also used as an excitation source for pulsed laser deposition of high quality material [D.B. Chrisey *et al.* 1994].

4.1.1 KrF laser characteristics

Before studying quantum well intermixing, it is important to understand the behaviour of the tool we are using. The condition of the excimer laser might have huge influence of the intermixing process. Figure 4-2 shows the temporal pulse shape of the KrF laser, before and after the vessel was refilled, for two pulse fluences: 200 mJ/pulse and 600 mJ/pulse. Even though, the deposited energy was the same before and after the refill, the peak power was almost twice higher for the new gas mixture than for the older one. At 600 mJ/pulse, we even observed the saturation in the peak power of the older gas pulse (figure 4-2).

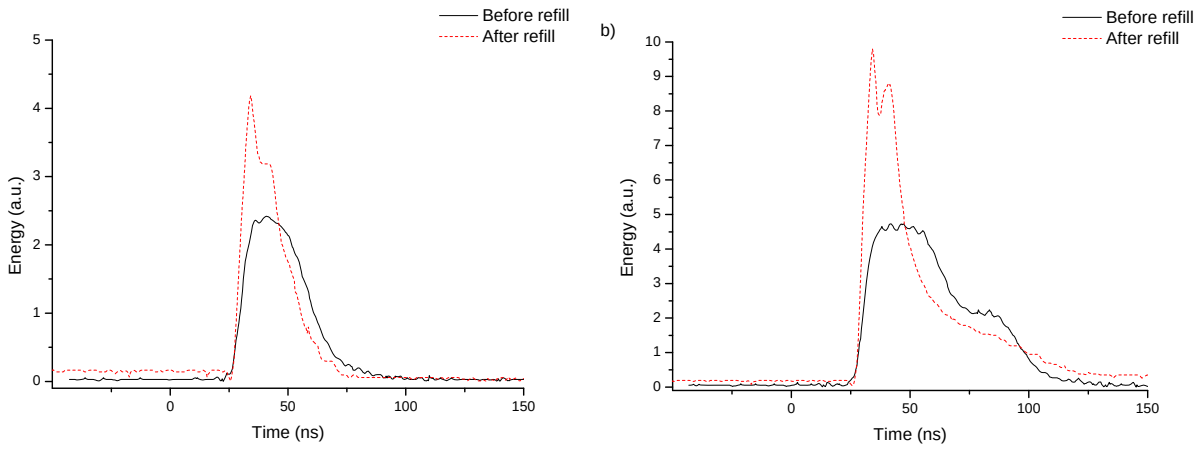

Figure 4-2: KrF laser temporal pulse shape dependence on the gas mixture age for pulse fluences of a) 200 mJ/pulses and b) 600 mJ/pulses

The age of the gas mixture also influences the stability of the energy density between each pulse. While it delivered smaller peak power, for the same pulse energy, an older gas mixture offered higher stability than a newer one (figure 4-3). Moreover, for the new gas mixture as well as for the older one, the laser stability tended to increase as the delivered energy increased. However, in the case of the pulse total energy, older gas mixture demonstrated a draw back of its stability when reaching pulse energy over 400 mJ/pulse. This happened as we observed the formation of a shoulder in the temporal pulse shape of the older mixture laser pulse. The fluctuations of this secondary peak contributed to the overall pulse total energy instability.

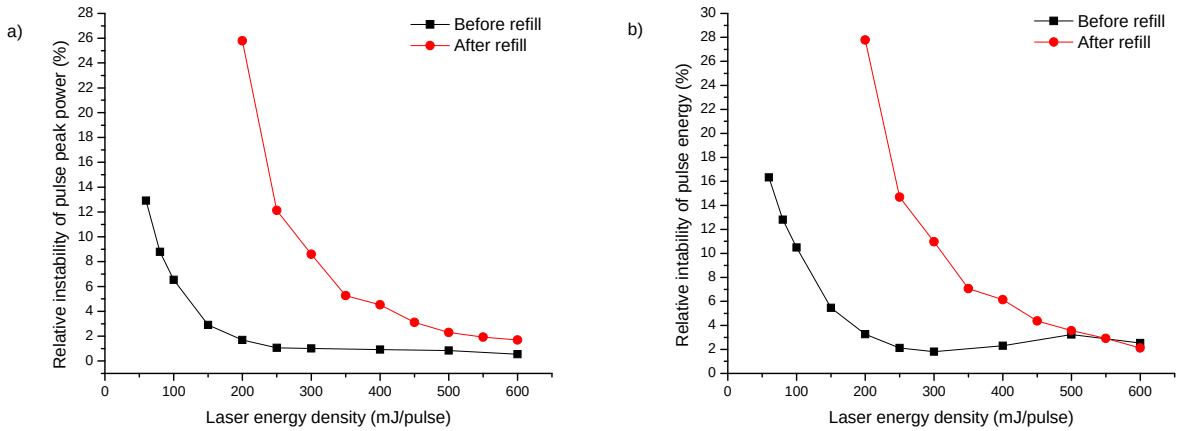

Figure 4-3: KrF laser instability of pulse a) peak power and b) total energy as a function of the pulse energy.

4.1.2 Excimer laser beam homogenization and beam delivery components

The raw beam coming out of an excimer laser is of low coherence and spatially non-uniform (figure 4-4). Furthermore, the spatial non-uniformity can change over time. To avoid the formation of spots of increased intensity (hot spots), it is necessary to provide some means of homogenizing the laser beam. A device comprising arrays of fly-eye microlenses is one of the most efficient homogenizing systems. Typically, it consists of two parallel arrays of cylindrical lenses. The incoming laser beam is first divided into many beamlets by the first array. The

beamlets converge in a focal plan between the two arrays where they form an array of point images. The second array brings back the incoming beamlets to a parallel configuration and then are then all refocused by a collector lens (figure 4-5). The homogenized laser beam is focused in the focal plan of the collector lens and it consists of the sum of all the collected beamlets. Fly-eye beam homogenizers are especially used for mask projection lithography and in micromachining tools.

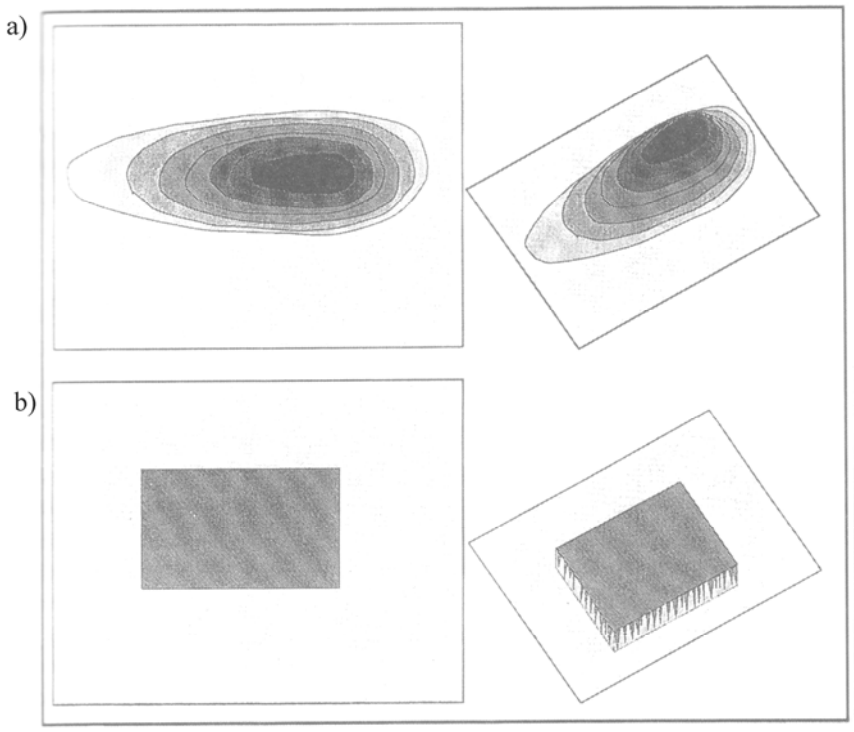

Figure 4-4: Laser beam spatial intensity maps, a) from the exit of the laser aperture and b) after homogenization [H.K. Park *et al.* 1994].

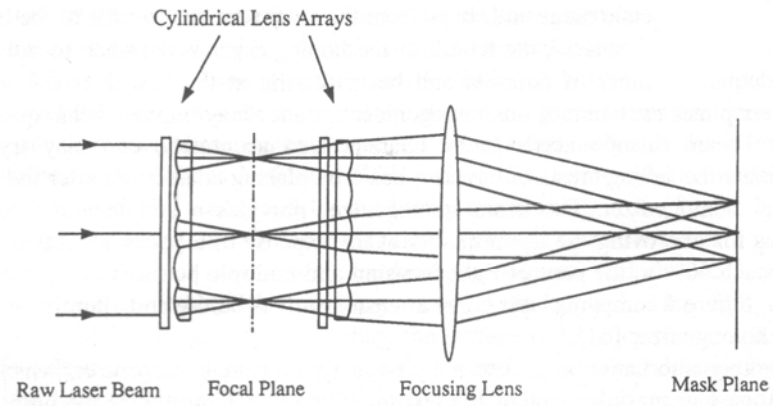

Figure 4-5: Schematic diagram of a fly-eye homogenizer with two cylindrical lenses arrays [X. Zhang *et al.* 1996].

A projection system can be used to shape the homogenized beam and to reduce its size. The mask is placed in the focal plan of the collector lens. Metallic absorption mask can be used, but because UV light is strongly absorbed in metal, those masks are usually quickly damaged by sputtering, melting and/or mechanical deformation. Dielectric masks made on transparent substrate can sustain higher fluences. An example of the projection optics is shown in figure 4-6.

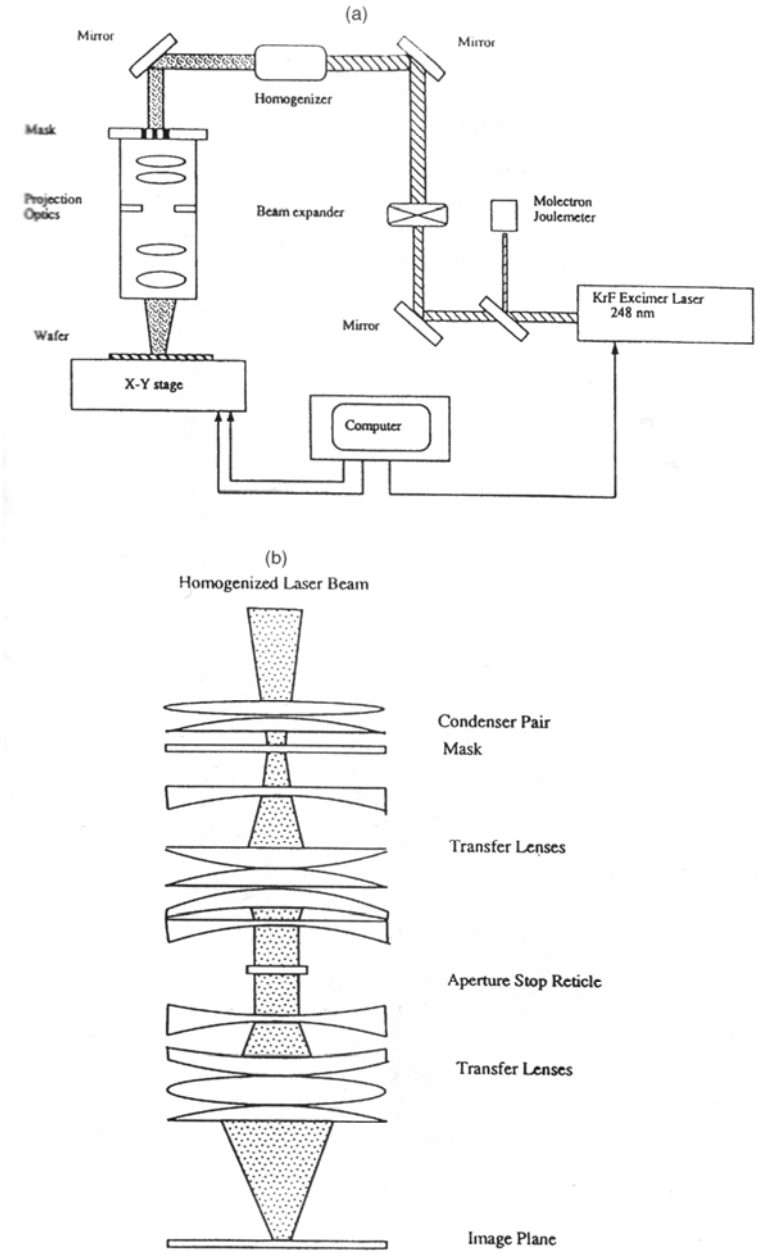

Figure 4-6: a) Schematic of a laser micromachining tool and b) schematic of the projection optics [X. Zhang *et al.* 1996].

4.2 Studied heterostructures

We studied UV laser controlled quantum well intermixing in both GaAs and InP based heterostructures. The wafers QT564 and EW600606 were both GaAs based quantum well heterostructures. Their main difference is the depth of the active region, the doping level in the

contact layer and the different nature of the well layer. The QT564 wafer has two unstrained GaAs quatum wells while the EW600606 wafer has one compressively strained InAlGaAs quantum well.

The M0062 and the C342 heterosturctures were both fabricated on InP substrate. However, the first one has an active region made of five InGaAs quantum wells while the other has three plans of InAs quantum dashes. All of those four heterostructures were design to permit the fabrication of laser diodes.

4.2.1 QT564 AlGaAs/GaAs quantum well heterostructure

The QT564 heterostructure was grown at the University of Glasgow and consisted of two 7.5 nm thick GaAs quantum wells (QWs) separated by a 10.3 nm $Al_{0.43}Ga_{0.57}As$ barriers and buried ~1 μm under the surface. The active region was grown on an n-type Se doped (100) GaAs substrate on which was grown a 100 nm GaAs buffer layer and a 450 nm $Al_{0.43}Ga_{0.57}As$ buffer layers. Both layers were Se doped ($1.7x10^{18}$ cm^3). The structure was terminated with a C doped ($1.8x10^{18}$ cm^{-3}) $Al_{0.43}Ga_{0.57}As$ optical confinement layer, which was 740 nm thick and a Zn-doped ($7x10^{18}$ cm^{-3}) GaAs contact layer, which was 100 nm thick. This heterostructure was designed for lasing operation at 852 nm at room temperature. Figure 4-7 illustrates the QT564 heterostructure.

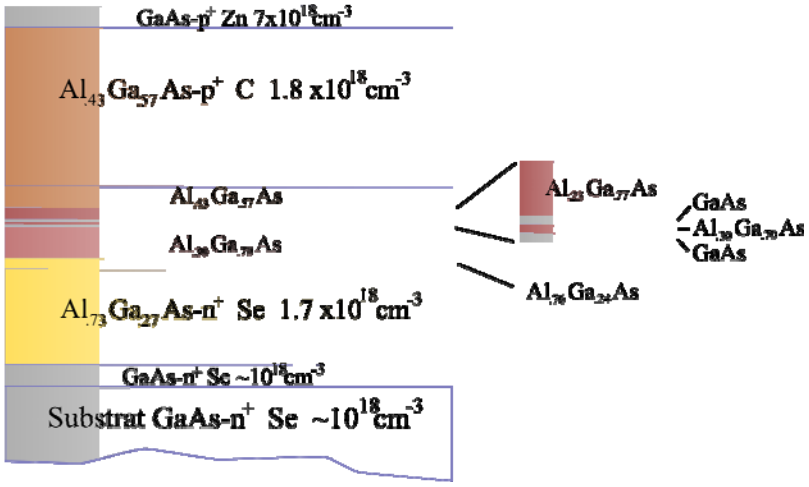

Figure 4-7: Schematic of the QT564 AlGaAs/GaAs quantum well heterostructure.

4.2.2 EW600606 InAlGaAsAlGaAs/GaAs quantum well heterostructure

The EW60060 wafer was designed and grown by EpiWorks. It consists of a single 7 nm $In_{0.1}Al_{0.13}Ga_{0.77}As$ QW which was positioned ~2 µm below the surface. The barriers were made of 400 nm thick AlGaAs graded index structure (GRIN) layers. This structure was grown on an n-type doped GaAs substrate with a Si-doped (10^{18} cm^{-3}) buffer structure composed of a 200 nm GaAs layer and a 200 nm AlGaAs GRIN layer. Two 1500 nm $Al_{0.6}Ga_{0.4}As$ claddings, on each side of the well, assured optical confinement. This QW wafer was designed for lasing operation at 808 nm at room temperature. Figure 4-8 shows an illustration of the EW600606 heterostructure.

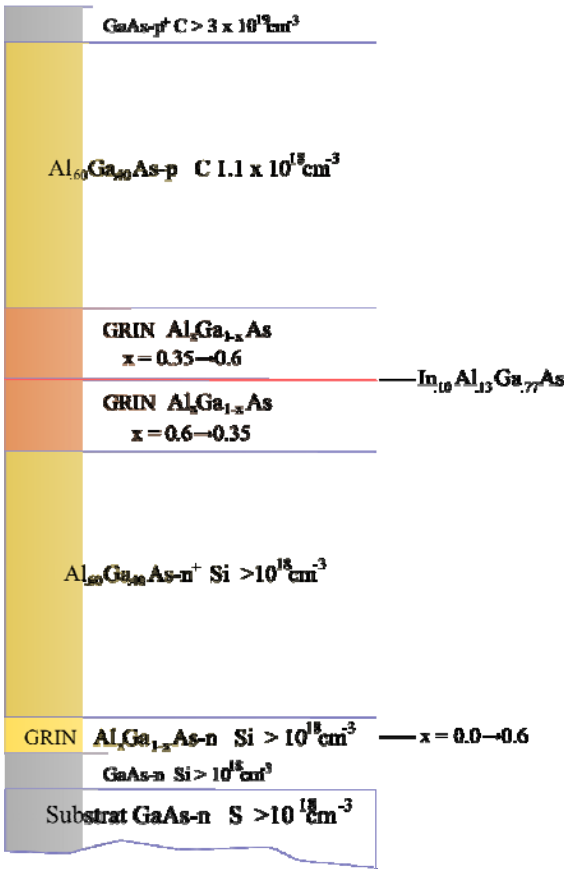

Figure 4-8: Illustration of the EW600606 InAlGaAs/AlGaAs/GaAs quantum well heterostructure.

4.2.3 M0062 InGaAs/InGaAsP/InP quantum well heterostructure

The M0062 wafer was an InGaAs/InGaAsP/InP QW heterostructures grown on a S-doped InP substrate using a Metal-organic Chemical Vapour Deposition (MOCVD) system at the Canadian Photonic Fabrication Center in Ottawa. The active region was grown on a 1400 nm InP and a 130 nm InGaAsP Si-doped buffer layers ($2x10^{18}$ cm^{-3} and $5x10^{17}$ cm^{-3}, respectively) and it comprised five InGaAs quantum wells of 5 nm separated by 12 nm InGaAsP barriers. The top cladding was composed of two Zn-doped layers of InP separated by a 10 nm InGaAsP etch stop layer. The contact layer, 100 nm Zn-doped InGaAs, was separated from the cladding by a second 50 nm thick etch stop and was covered with a 200 nm InP sacrificial layer. The composition of

the QWs was chosen to have material suitable for the fabrication of laser diodes operating at 1.50 µm at room temperature. Other details concerning this heterostructure are given in figure 4-9.

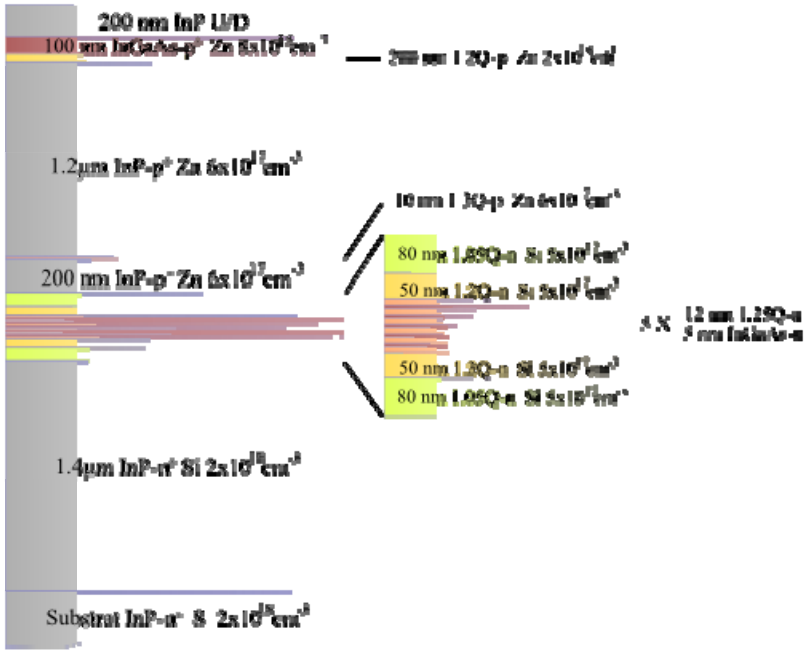

Figure 4-9: Schematic of the M0062 InGaAs/InGaAsP/InP quantum well heterostructure.

4.2.4 C342 InAs/InGaAsP/InP quantum sticks heterostructure

A heterostructure based on InAs quantum sticks (QS) in InGaAsP (1.2µm) with InP spacer on each side was grown by molecular beam epitaxy at the Institut de nanotechnologies de Lyon, France. An InGaAs-p+ contact layer and a 200 nm InP sacrificial layer were grown on top of the spacer. The sticks PL emission is centred at 1470 nm (figure 4-10a), while the FWHM is ~ 78 meV. PL from the quaternary material is right on 1.2 µm. Figure 4-10b) shows the X-ray double diffraction spectra from the sample. From the superposition of the Q 1.2, InGaAs and InP peak, we can conclude that the grown material is lattice matched with the InP substrate. The lattice mismatch was found to be 1.1x10-4 for Q1.2 and 9.9x10-5 for the InGaAs layer. Other details concerning this heterostructure are given in figure 4-11.

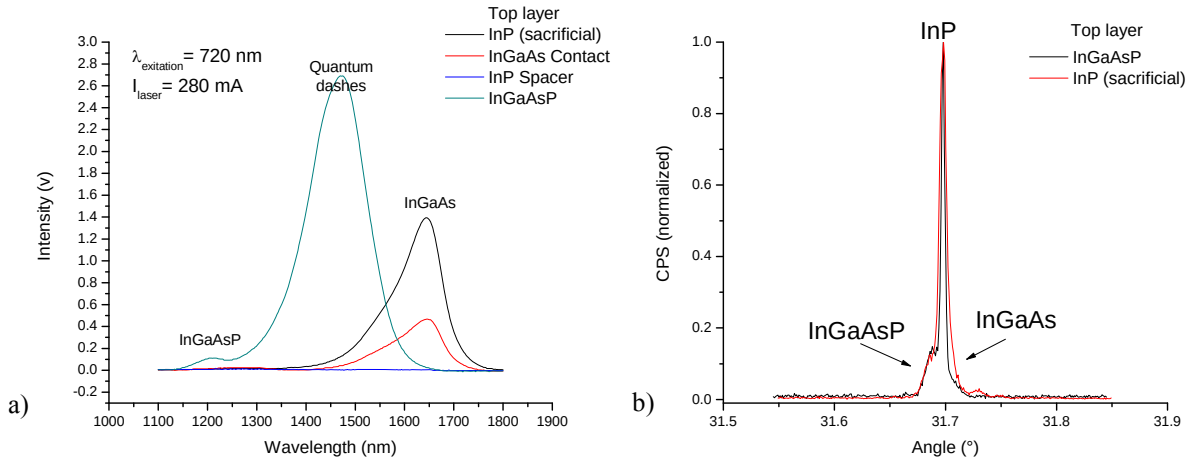

Figure 4-10: a) PL spectra of the InAs QS grown structure after different etching step, b) X-ray diffraction spectra of the full structure and with the capping layers etch down to the Q 1.2 barrier.

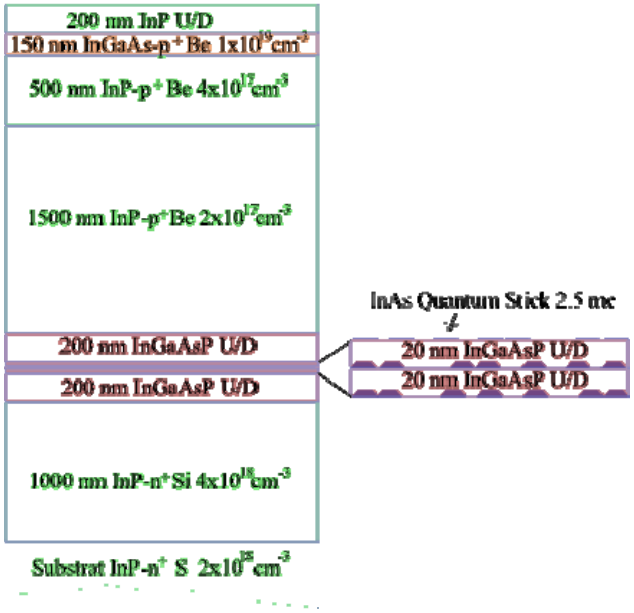

Figure 4-11: Schematic of the C342 InAs/InGaAsP/InP quantum dashes heterostructure.

4.3 Irradiation setup

For this project, I used two different excimer laser irradiation setups. The first one used a krypton-fluoride (KrF) laser and was located at the National Research Council of Canada in Ottawa, in the Institute for Chemical Process and Environmental Technology. The second setup used and argon-fluoride laser and was located in the Laboratoire de semiconducteurs quantiques et nanotechnologies photoniques at the Université de Sherbrooke.

4.3.1 KrF laser setup

The KrF laser (λ = 248 nm) setup a Lambda Physik LPX 300 laser which delivered 22 ns pulses with energy of up to 1.2 J/pulse. The laser beam was shaped with a MicroLas microlens array (fly-eye) beam homogenizer to a 7x7 mm^2 top hat profile. A variable attenuator controlled the incident intensity on the sample. The setup allowed irradiation under different atmosphere (figure 4-12). A fused silica with anti-reflection coating was used as a mirror allowing delivery of the laser beam to the environmental chamber. The setup allowed irradiation in oxygen, nitrogen and ammonia, but a cryogenic trap and a scrubber were also installed for treatments under more reactive gas such as chlorine.

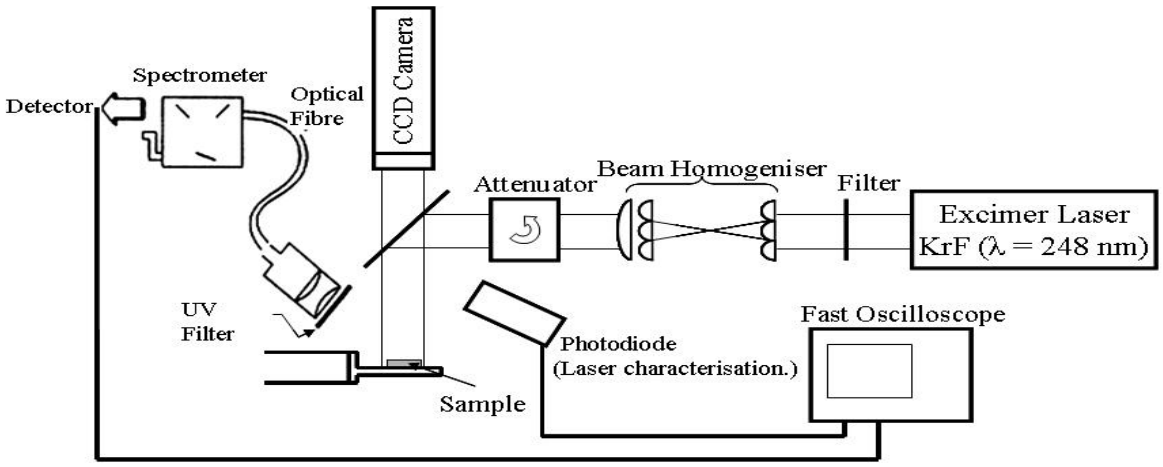

Figure 4-12: Schematic of the KrF irradiation setup.

4.3.1.1 Photoluminescence measurements during laser irradiation

This setup was equipped with a system allowing for the measurements of photoluminescence (PL) from the sample using a set of lenses and an optical fibre. A spectrometer dispersed the light which was detected with a photomultiplier. The laser pulses were analysed by a 1 GHz oscilloscope and recorded by a computer. The KrF laser can be used to 1) alter the surface properties of the irradiated sample and to 2) excite the PL signal. Figure 4-13 shows the UV excited PL of a GaAs sample and of an InAlGaAs/AlGaAs/GaAs heterostructure. The signal noise is due to the KrF laser peak to peak power instability, which was more important

for low fluence irradiation. Figure 4-13 shows a weaker signal from the heterostructure than from a pure GaAs sample. This could be explained by the high concentration of impurities (N_d > 3.19 x 10^{19} cm^{-3}) which act as PL attenuating non-radiative centers.

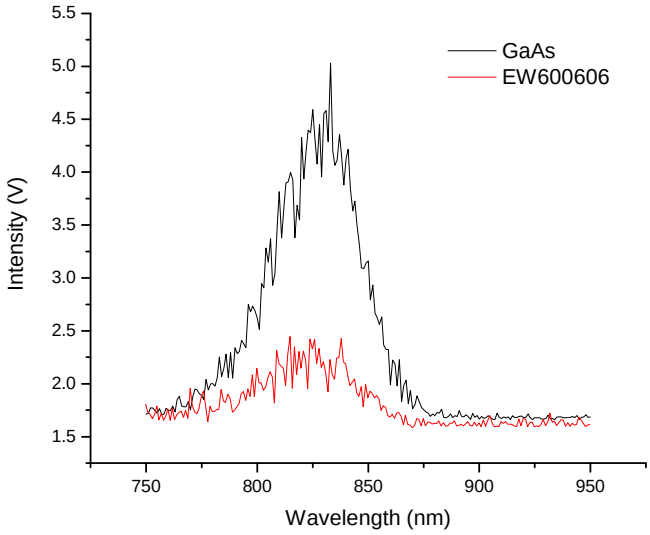

Figure 4-13: Ultraviolet excited photoluminescence of a GaAs sample (black) and of EW600606 sample (red)

The influence of the irradiation on the PL signal intensity is presented in figure 4-14. At low fluences (F < 260 mJ/cm^2), the signal first increase and then decreases as the number of pulse increases, while at high fluences the increase in unnoticeable. We usually attribute variation in the intensity of the photoluminescence signal to generation or the inhibition of non-radiative center at the sample surface [R.R. Chang *et al.* 1987].

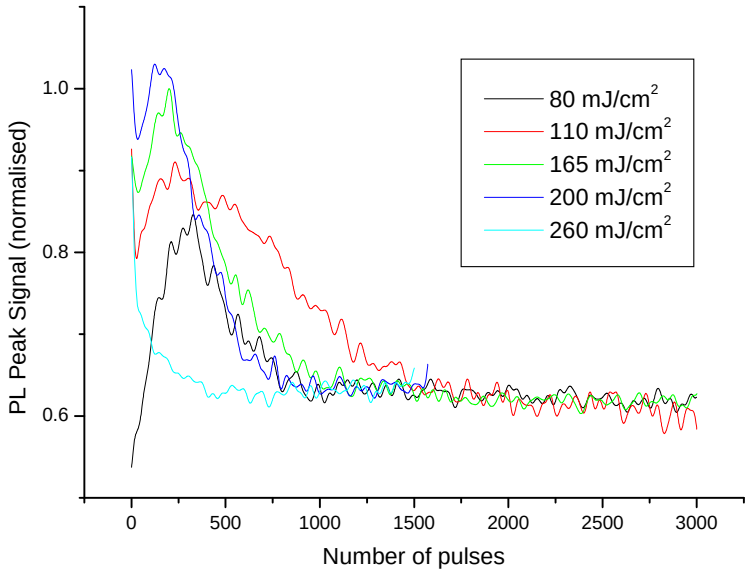

Figure 4-14: UV laser excited PL in InAlGaAs/AlGaAs/GaAs heterostructure samples for different fluences. The photoluminescence signal was measured at a fixed wavelength of 825 nm.

4.3.2 ArF laser setup

The ArF (λ = 193 nm) laser setup used a GSI Lumonics Pulse Master laser which delivered pulses of ~16 ns length with energy up to 200 mJ/pulse. As with the KrF laser, the laser beam was shaped with a micro-lenses array (fly-eye) beam homogenizer to a 13 x18 mm^2 beam having a top hat profile. A variable attenuator controlled the incident beam intensity on the sample. A projection mask was used to shape the beam delivered to the sample surface (figure 4-15). The demagnification ratio of the system was about 2.7Projection optics then reduced the laser beam by a factor of 1/3 and focussed it at the sample site. Position of the sample was controlled with a lateral resolution of 10 µm using an x-y-z-theta mechanical stage. Two inspection cameras were used to monitor macroscopic changes of the surface that were induced with the laser. A PL spectroscopy system was also available for this setup.

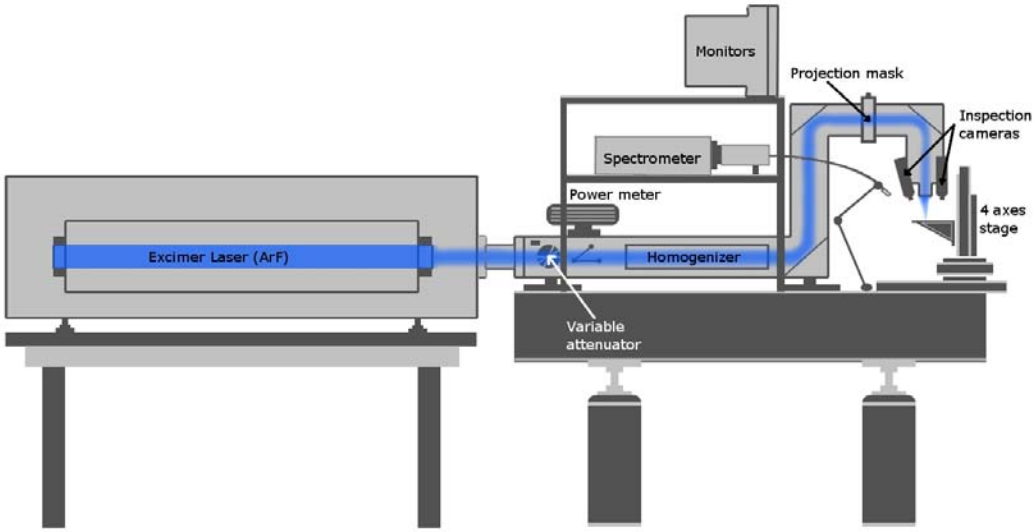

Figure 4-15: Schematic of the ArF irradiation setup.

4.4 Characterization techniques

In this section, I describe the characterisation techniques used during my work. The principal technique used was photoluminescence (PL). It measures the intensity and energy of radiative transition. It can thus characterise the extent of bandgap shift and gives a qualitative idea of the material quality. Cathodoluminescence is a similar technique which employs electrons as a source of excitation. It offers a better lateral resolution than photoluminescence. Profilometry and x-ray photo-electron spectroscopy (XPS) were applied to characterise the sample surface after laser irradiation. Profilometry measures change in surface morphology while XPS analyses the surface chemistry.

4.4.1 Photoluminescence

Photoluminescence is a phenomenon of emission of light by a material exposed to the radiation form a light of specific wavelength (energy of photons). It requires that light source to excite electrons from a base to an excited state of the material..

More specifically, in the case of a direct bandgap semiconductor, we usually choose an excitation source with photons energy higher than the material bandgap. The electrons are excited from the valence band to the conduction band. The electrons relax to the bottom of the conduction band through phonon emission. The recombination of the electrons with holes at the top of the valence band results in the emission of photons with a wavelength corresponding to the energy of the semiconductor bandgap. In addition to interband transition, photoluminescence can probe transitions between impurities levels, interband traps, defects and bound quasi-particles [J.I. Pankove 1975b]. Theses transitions are especially visible at low temperature.

The intensity of the PL signal also offers qualitative information on the quality of the studied material. For example, weaker signal is usually attributed to a high density of surface states [R.R. Chang *et al.* 1987]. Other non-radiative processes associated with the presence of defects are also responsible for quenching the photoluminescence signal. The full width at half-maximum of the PL signal is often considered as an indicator of the quality of the studied sample. As suggest the Heisenberg uncertainty principle (see equation (4.4)), a broadening in of the photoluminescence peak is associated with shorter carriers lifetime. This broadening (shortening of the lifetime) can be the results of a change in the electronic confinement [F. Bollet *et al.* 2003], the generation of trapping defects or the relaxation of strain [A.S.W. Lee *et al.* 1999].

$$\Delta E \Delta t \gtrsim \frac{\hbar}{2} \tag{4.4}$$

Figure 4-16 shows a schematic of a standard PL setup. The sample is placed on a copper cold finger inside a cryostat with an optical window. The cold finger is connected to a close circuit of refrigerated helium. The helium is compressed and brought in contact with the cold finger. With this system, we are able to bring the sample temperature down to 18 K. A resistive

heater can be used to raise the temperature. To prevent the contamination of the sample surface and to maintain the thermal insulation, the cryostat chamber is pumped by a mechanical pump.

The excitation is provided by frequency doubled Nd:YAG laser (λ = 532 nm). The laser beam is mechanically chopped at 400 Hz to allow synchronic detection of the signal. The laser beam illuminates the sample inside the cryostat through the window. The luminescence form the sample is collected by a large lens (A) and focused at the entrance of the monochromator by a second lens (B). A 1200 lines/mm grating, inside the monochromator, disperses the PL signal. A photomultiplier transforms the optical signal that is filtered and pre-amplified. The signal is measured using a lock-in amplifier technique.

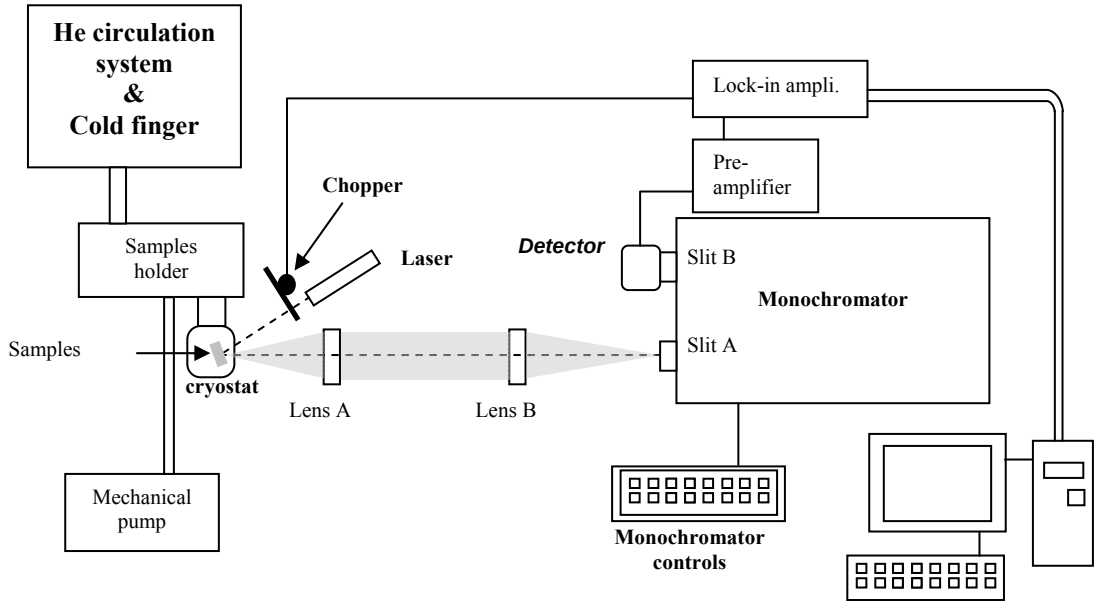

Figure 4-16: Schematic of the photoluminescence setup.

4.4.2 Cathodoluminescence

Cathodoluminescence (CL) is a phenomenon of luminescence of a material exposed to a beam of electrons. The most known example of CL is realized with a cathode ray irradiating a tube display. In a semiconductor, CL occurs when highly energetic electrons irradiate the

material in vacuum and induce transition of electrons from the valence to the conduction band. When an electron and a hole recombine, there is a probability that a photon is emitted. This probability and the energy of emitted photon depend on the semiconductor band structure and on the presence of impurities and other defects in semiconductor.

CL is a spectrometry technique used in material science, similarly to PL, although it is more difficult to work with due to the vacuum level required. An electron beam is focused on the sample and excites an interaction volume which emits light as it relaxes itself [B.G. Yacobi *et al.* 1990]. An electron gun is used as an excitation source. The light is collected and separated by a monochromator. The signal is then measured by a photodetector. Scanning the beam in the X-Y plane allows mapping of the optical response of a whole region.

The primary advantage of this technique is the ability to resolve features down to 20 nanometers. The spatial resolution of CL is related to the probe size of the electron beam which is of the order of a nanometer. However, a highly energetic electron beam will get deep inside a structure and will diffuse in a volume bigger than the beam probe size. Figure 4-17 shows a schematic of the interaction volume in an unspecified material and the lateral diffusion of electrons. The resolution is then limited by the primary electrons diffusion length R_e, which increases with the acceleration energy, and the diffusion length of the minority charge carriers L_d. Both diffusion lengths depend on the studied semiconductor. We can express the cathodoluminescence "resolution length" by $d_{CL} = 2\sqrt{R_e^2 + L_d^2}$, which corresponds to the sum of two Gaussian distributions. Even when considering theses limitations, cathodoluminescence is still one of the best technique to observe small luminescent feature and thus to assay the lateral resolution of quantum well intermixing processes.

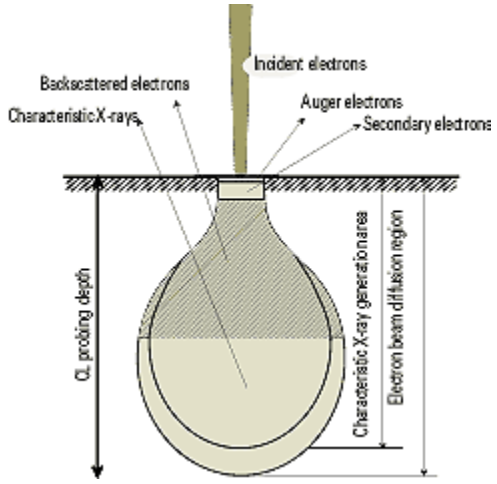

Figure 4-17: Origin of the different signals resulting from the interaction of the electrons beam with the sample and signal detection depth [M. Takakura *et al.* 2001].

As PL, CL is very efficient to probe direct bandgap semiconductors, but it can also be used to examine the weak amount of light emitted by indirect bandgap semiconductors like silicon and germanium. For example, because the luminescence in silicon containing dislocations is different from the one from the perfect crystal, cathodoluminescence is used in the microelectronic industry to map defects in integrated circuits [S. Ostapenko *et al.* 2004].

In our case, cathodoluminescence was performed in a LEO Zeiss Supra 55VP scanning electron microscope. The light emitted from the sample was collected by a semi-parabolic mirror placed right on top of the sample. The distance between the mirror and the sample were established so the sample sat in the focal plan of the mirror. The collected light was directed toward the monochromator through a waveguide. A lens focused the signal on the entrance slit of the monochromator. This setup disposes of a displaceable mirror which allows the light to pass directly to the detector without being dispersed by the 1200lines/mm grating inside the monochromator. It is then possible to measure the integrated emission from the sample. The

signal was measured by a photomultiplier tube cooled down by carbon dioxide snow. The signal was acquired by a photon counting system. Figure 4-18 shows a photograph of the cathodoluminescence setup used.

Figure 4-18: Photograph of the chatodoluminescence setup.

4.4.3 Profilometry

Profilometry measures small variation in the vertical direction. A contact profilometer scans a stylus over a sample. Small surface variation causes the stylus to move up or down which is transformed to an analog signal by an accelerometer. Contact profilometer can usually measure vertical features from 5 nm to few tens of micrometers. The lateral resolution, however, is limited by the stylus size (~ 5µm to 25µm).

In our case, profilometry was performed with a Tencor P-1 profilometer with a 5 μm stylus. The system vertical resolution is 0.1 nm or 2.5 nm depending on the vertical range (13 μm or 200 μm) while the horizontal range is 200 mm.

4.4.4 X-ray photo-electron spectroscopy

X-ray photo-electron spectroscopy (XPS) is a quantitative spectroscopic technique that measures the chemical composition of a material. This technique uses an X-rays beam to knock out core electrons from the sample constituent atoms. Figure 4-19 illustrate the physics concepts behind XPS. By measuring kinetic energy E_{KE} of the expulsed electrons, we can determine the electron binding energy E_B as a function of the X-ray photon energy E_{ph} and the electron spectrometer work function ϕ:

$$E_B = E_{ph} - E_{KE} - \phi . \tag{4.5}$$

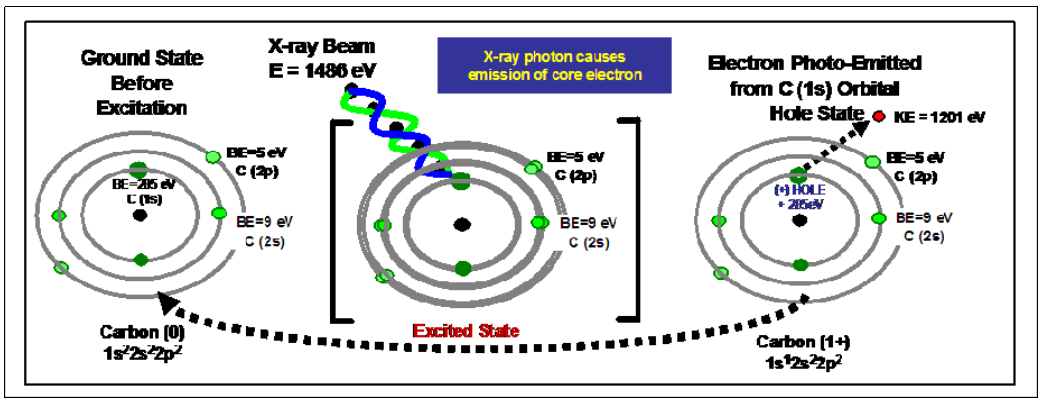

Figure 4-19: Illustration of the XPS concept.[2]

Usually, XPS spectra are shown as a graph of the electron count as a function on the electron binding energy. Because each element produces a characteristic footprint of XPS peaks, binding energies are analysed to indentify the atomic composition of the sample. The peaks correspond to the electronic orbitals of the atoms (1s, 2s, 2p, 3s, 3p, etc) and, because of the

[2] This image is under the terms of the GNU Free Documentation License version 1.2

change in the electrons binding energy, the position of the peaks varies when the atom is bound to another one of a different nature. The number of detected electrons for each peak is directly related to the density of the related atom in the interaction volume. By normalizing the count by a known relative sensitivity factor, it is possible to establish the relative ratio of each atom and thus, determine the chemical composition of the studied compound.

Electrons have a relatively short escape length. Even though the X-ray photons penetrate few micrometers inside the material, only the electrons generated within a 10 nanometers thick layer can escape for the material. In other words, XPS is a technique which is quite sensitive to the surface condition. The presence of a surface native oxide or of surface contamination will certainly affect the results.

4.4.4.1 Thickness measurements of capping layer measurement

XPS has been used to estimate the thickness of a capping layer. For a given element, if the XPS spectrum shows both the bulk material and the capping layer peaks, the top layer thickness can be obtained using the following equation [T.A. Carlson *et al.* 1972, C.F. Yu *et al.* 1986]:

$$d_{tf} = \alpha_{tf} \sin\theta \ln\left(\frac{I_{tf}}{I_{sub}}\frac{D_{sub}}{D_{tf}}\frac{\alpha_{sub}}{\alpha_{tf}}+1\right), \qquad (4.6)$$

where the D_{sub}/D_{tf} is the density ratio between the substrate and the film, while I_{tf}/I_{sub} is the photoelectron intensity ratio, α_{tf} and α_{sub} are the electron mean escape depths in the thin film and in the substrate, and θ is the photoelectrons exit angle relative to the surface.

4.5 Summary

In this chapter, I discussed experimental methods used to carry out and study the UV laser controlled QWI process. I described the general concept of the UV-QWI technology and

discussed the influence of irradiation conditions on the defects generation process (this should be covered more in detail). I also illustrated the UV laser irradiation setups, describing the role and working principles of the excimer laser and the beam delivery system.

UV laser controlled quantum well intermixing uses UV photons to induce defects generation or to alter the chemistry of the near surface region. It is possible to limit the macroscopic alterations to a sacrificial layer which can be removed after the annealing procedure limiting the importance of residual defects on devices fabricated on the intermixed areas. Because of the dependence of the material absorption and reflection coefficient on the laser wavelength, at the same fluence, the type of excimer laser used during the irradiation influences the deposited energy and the interaction volume. Since the beam coming out of an excimer laser is spatially non-uniform, it is important to homogenize it with an array of lenses. The homogenized beam can then be use to pattern a sample.

The four studied heterostructures were also described: two quantum well heterostructures are based on a GaAs substrate, one of the heterostructure fabricated on InP has an active region made of InGaAs quantum wells while the other has three plans of InAs quantum sticks. The four heterostructures were design to permit the fabrication of laser diodes.

The characterisation techniques applied to measure the extent of the intermixing and to analysis the laser treated surfaces were also presented. Photoluminescence and cathodoluminescence are used to measure the blueshift extent. The laser influence on the treated surface morphology and chemistry is analysed by stylus profilometry and x-ray photoemission spectroscopy respectively.

4.6 Bibliography

Basting, D. and Marowsky, G., Eds. (2005). Excimer laser technology. Berlin, Springer/Praxis, 433 p.

Bollet, F., Gillin, W. P., et al. (2003) *On the diffusion of lattice matched InGaAs/InP microstructures*, Journal of Applied Physics, vol. 93, n° 7, 3881-5.

Brannon, J. H. (1989) *Micropatterning of surfaces by excimer laser projection*, Journal of Vacuum Science & Technology B (Microelectronics Processing and Phenomena), vol. 7, n° 5, 1064-71.

Carlson, T. A. and McGuire, G. E. (1972) *Study of the x-ray photoelectron spectrum of tungsten--tungsten oxide as a function of thickness of the surface oxide layer*, Journal of Electron Spectroscopy and Related Phenomena, vol. 1, n° 2, 161.

Chang, R. R., Iyer, R., et al. (1987) *Surface characterization of InP using photoluminescence*, Journal of Applied Physics, vol. 61, n° 5, 1995-2004.

Chrisey, D. B. and Hubler, G. K., Eds. (1994). Pulsed Laser Deposition of Thin Films, Wiley-Interscience, p.

Hayden, C. J. (2003) *Three-dimensional excimer laser micromachining using greyscale masks*, Journal of Micromechanics and Microengineering, vol. 13, n° 5, 599-603.

Lankard, J. R., Sr. and Wolbold, G. (1992) *Excimer laser ablation of polyimide in a manufacturing facility*, Applied Physics A (Solids and Surfaces), vol. A54, n° 4, 355-9.

Lee, A. S. W., Li, E. H., et al. (1999) *Vacancy-enhanced intermixing in highly strained InGaAs/GaAs multiple quantum well photodetector*, Journal of Applied Physics, vol. 86, n° 6, 3402-3407.

Mayer, E. E., Gillett, D. A., et al. (1999) *Fiber Bragg grating writing by interferometric or phase-mask methods using high-power excimer lasers*, Fiber and Integrated Optics, vol. 18, n° 3, 189-98.

Ostapenko, S. and Romero, M. (2004). *Defect mapping in full-size multi-crystalline Si wafers*, Batz-sur-Mer, France, EDP Sciences.

Pankove, J. I. (1975). *Optical processes in semiconductors*, New York, Dover Publications, 422 p.

Park, H. K., Grigoropoulos, C. P., et al. (1994) *A practical excimer laser-based cleaning tool for removal of surface contaminants*, IEEE Transactions on Components, Packaging, and Manufacturing Technology, Part A, vol. 17, n° 4, 631-43.

Phillips, H. M., Wahl, S., et al. (1993) *Submicron electrically conducting wires produced in polyimide by ultraviolet laser irradiation*, Applied Physics Letters, vol. 62, n° 20, 2572-4.

Pol, V., Bennewitz, J. H., et al. (1987) *Excimer laser based lithography: a deep-ultraviolet wafer stepper for VLSI processing*, Optical Engineering, vol. 26, n° 4, 311-18.

Smith, P. M., Carey, P. G., et al. (1997) *Excimer laser crystallization and doping of silicon films on plastic substrates*, Applied Physics Letters, vol. 70, n° 3, 342-4.

Takakura, M., Notoya, S., et al. (2001) "Application of Cathodoluminescence to EPMA." JEOL News **35**,

Yacobi, B. G. and Holt, D. B. (1990). *Cathodoluminescence microscopy of inorganic solids*, New York, Plenum Press, ix, 292 p.

Yu, C. F., Podlesnik, D. V., et al. (1986) *Ultraviolet-Light-Enhanced Oxidation of Gallium-Arsenide Surfaces Studied by X-Ray Photoelectron and Auger-Electron Spectroscopy*, Chemical Physics Letters, vol. 130, n° 4, 301-306.

Zhang, X., Grigoropoulos, C. P., et al. (1996) *Excimer laser projection micromachining of polyimide thin films annealed at different temperatures*, IEEE Transactions on Components, Packaging & Manufacturing Technology, Part C (Manufacturing), vol. 19, n° 3, 201-13.

Chapter 5: UV laser irradiation quantum well intermixing in GaAs-based heterostructures

This chapter presents the results of UV-excimer-laser-induced quantum well intermixing in AlGaAs/GaAs (QT564, see figure 4-7, page107 for details) and InGaAlGaAs/AlGaAs/GaAs (EW600606, see figure 4-8 on page 108 for details) laser diodes heterostructures. In the first part, I discuss the results of RTA that allowed determining thermal stability of the investigated microstructures.

The second part of the chapter discusses the results of suppressed intermixing in these microstructures, as presented in a journal article titled "Suppressed intermixing in InAlGaAs/AlGaAs/GaAs and AlGaAs/GaAs quantum well heterostructures irradiated with a KrF excimer laser", *Applied Physics A: Materials Science & Processing*, vol. 89, no. 2, pages 423 to 426, published in November 2007 [J. Genest *et al.* 2007a].

5.1 Preliminary study of interdiffusion properties

Tests were performed to establish the thermal stability of both heterostructures. We first cleaved a series of samples from each heterostructures wafers. The samples were solvent cleaned in beakers with Opticlear, acetone and isopropyl alcohol and dried with nitrogen. We then annealed each sample in a rapid thermal processor for temperature ranging from 850°C to 925°C during 30s. The annealing was done in a forming gas atmosphere (90% N_2 and 10% H_2) to prevent oxidation of the samples from residual adsorbed water vapor or oxygen. The

interdiffusion extent was measured by low temperature (20 K) photoluminescence where we used a doubled Nd:YAG laser (532 nm) as excitation source.

5.1.1 Thermal stability of the QT564 heterostructure

Figure 5-1 shows normalized low-temperature (20 K) PL spectra obtained from a reference and the annealed samples. The spectra show two peaks. The large asymmetric one, centered around 823 nm, corresponds to the bulk GaAs. The significantly narrower peak, located at 798 nm for the reference sample, is related to the QWs emission. The QW peak remained almost unchanged following the RTA treatment at 850°C. However, its relative intensity increased by 30 %, suggesting that some as-grown defects get annealed-out during the high temperature treatment. At higher temperature, we observed an increased in the sample out-gassing resulting in the presence of a denser haze at its surface. This was accompanied with a decrease of the PL relative intensity due to the presence of absorption centers in the heterostructure top layers. For temperatures higher than 850°C, the QWs emission peak split itself in two: a first peak moved toward the shorter wavelengths as the annealing temperature increased while the second one remained at 798 nm. This splitting of the QWs peak implies that QWI was limited to specific regions in each sample. Furthermore, since this was observable in all the samples, it suggests that only one of the two wells went through the QWI process which could be related to the presence of an undesired stressed layer between the two wells.

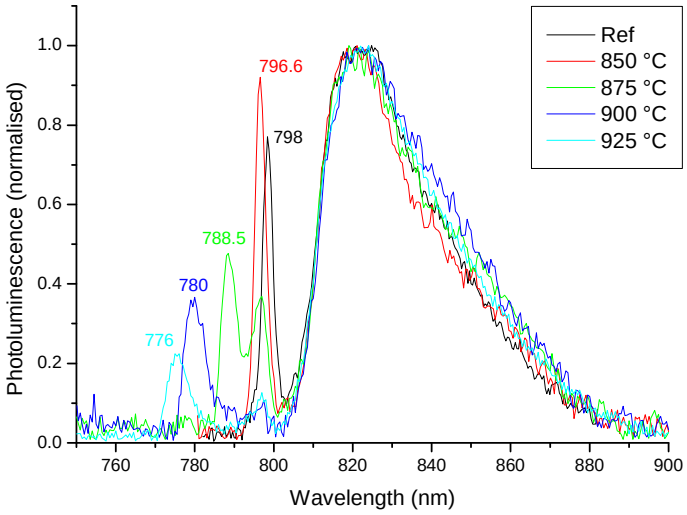

Figure 5-1: Low temperature photoluminescence spectra for QT564 samples annealed at temperature ranging from 850°C to 925°C for 30 s.

5.1.2 Thermal stability of the EW600606 heterostructure

Figure 5-2 shows low-temperature (20 K) normalized PL spectra obtained from a reference and the annealed samples of the EW600606 structure. The QW position for the reference sample was located at 754 nm, while after an annealing at 910°C for 30 seconds the QW peak was located at 705 nm.

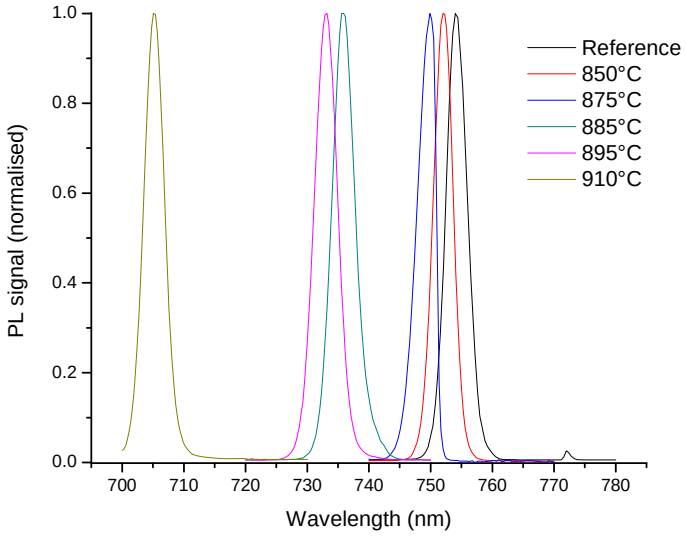

Figure 5-2: Low temperature photoluminescence spectra for EW600606 samples annealed at temperature ranging from 850°C to 925°C for 30 s.

A finite element model developed on the commercial software FemLab were used to simulate interdiffusion in the EW600606 heterostructure. The model considered equal diffusion rate of all group III atoms. For different diffusion length $L_D = \sqrt{D_{III}\Delta t}$, where D_{III} is the group III atoms diffusion coefficient and Δt is the diffusion time, the calculation determined the intermixed concentration and energy bands profiles. We then solved the Schrödinger equation in the intermixed conduction band and valence band potential wells to determine the energy levels for the electrons and holes. The energy E of the transition was determined by:

$$E = E_g + E_{n1} + E_{hh1} \tag{5.1}$$

where E_g is the bandgap of the intermixed well while E_{n1} and E_{hh1} are the fundamental energy levels for electrons in the conduction band and heavy holes in the valence band respectively. We then calculated the resulting wavelength λ:

$$\lambda = \frac{hc}{E}, \tag{5.2}$$

where h is Planck constant and c is the speed of light in vacuum. Figure 5-3 shows the calculated energy shift or photoluminescence blueshift due to the intermixing in the EW600606 heterostructure.

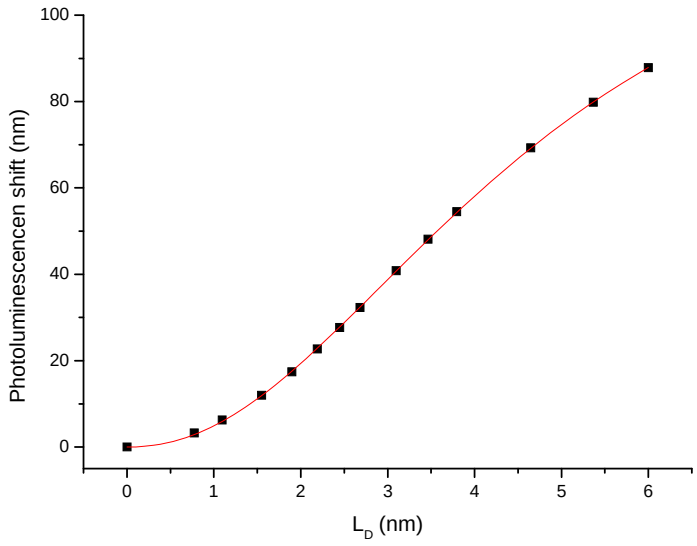

Figure 5-3: Simulation of a photoluminescence shift in InAlGaAs/AlGaAs quantum well for different group III atoms diffusion length.

Applying the relation between the photoluminescence shift and the diffusion length to the thermal stability measurements on the EW600606 heterostructure, we calculated the group III interdiffusion coefficient D_{III} as a function of the temperature, as shown in figure 5-4. From this, we extracted an activation energy E_A and diffusion coefficient D_0 to be 5.03 eV and 10^6 cm^2/s, respectively. A great variation of activation energy ranging from ~0.32 eV to ~6.2 eV for AlGaAs/GaAs heterostructures and ~1.5 eV to ~9 eV for InGaAs/GaAs heterostructures was obtained in similar studies [E.H. Li 2000]. D_0 values ranging from ~10^{-11} to ~10^{10} cm^2/s were also observed. Although, the non-equilibrium concentration of point defects, the doping and the annealing environment (Ga or As rich) influence the diffusion coefficient in GaAs-based

heterostructure [R.M. Cohen 1997], such broad ranges of activation energy E_A and diffusion coefficient D_0 is not perfectly understood [E.H. Li 2000].

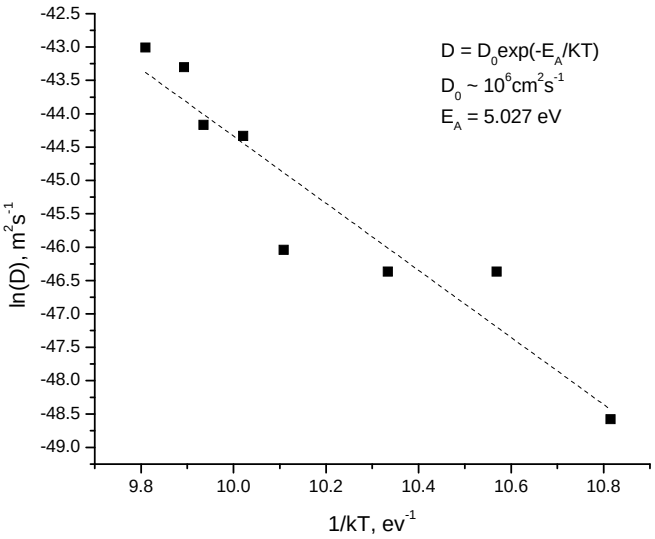

Figure 5-4: Intermixing coefficient D versus $1/k_BT$ for EW600606 samples annealed at different temperatures for 30 s.

5.2 Suppressed intermixing in InAlGaAs/AlGaAs/GaAs and AlGaAs/GaAs quantum well heterostructures irradiated with a KrF excimer laser

J Genest, J J Dubowski[3], V Aimez

Centre de recherche en Nanofabrication et Nanocaractériasation (CRN2), Département de Génie Électrique et Génie Informatique, Université de Sherbrooke, Sherbrooke, Québec, J1K 2R1, Canada

5.2.1 Abstract

The influence of gallium arsenide surface modification induced by irradiation with a KrF excimer laser on the magnitude of the quantum well (QW) intermixing effect has been

✉ Fax: (819) 821-7937, E-mail: Jan.J.Dubowski@USherbrooke.ca
[3] Canada Research Chair in Quantum Semiconductors

investigated in InAlGaAs-AlGaAs-GaAs QW heterostructures. The irradiation in an air environment with laser pulses of fluences between 60 and 100 mJ/cm^2 has resulted in the formation of a gallium oxide-rich film at the surface. Following the annealing at 900°C, an up to 35 nm suppression of the band gap blue shift was observed in all the laser irradiated samples when compared to the non-irradiated samples. The origin of suppression has been discussed in terms of stress controlled diffusion.

5.2.2 Introduction

Over the last twenty years, selected area post-growth modification of the quantum well (QW) bandgap structure through the interdiffusion process known as quantum well intermixing (QWI) has been the subject of numerous investigations [J.H. Marsh 1993, E.H. Li 2000]. In AlGaAs/GaAs QW heterostructures, intermixing Al and Ga atoms at the well-barrier interface results in an increase of the effective band gap energy. This is accompanied by changes in the electronic confinement as well as the refractive index of the intermixed layer [L.J. Guido *et al.* 1987]. The thermally activated QWI process can be modified by the controlled introduction of impurities and defects to the QW material. For example, gallium vacancies (V_{Ga}) are known to enhance QWI in AlGaAs/GaAs [S. Mitra *et al.* 1991]. Since this process could be induced in selected areas of a QW wafer, the QWI approach has been attractive for the fabrication of monolithically integrated optoelectronic devices [E.H. Li 2000].

The most frequently investigated methods of QWI include impurity induced intermixing [L.J. Guido *et al.* 1987], impurity-free vacancy diffusion [J.H. Teng *et al.* 2001] and QWI induced by ion implantation [S. Charbonneau *et al.* 1998, V. Aimez *et al.* 2002]. QWI has also been achieved by selective area coating of QW wafers with different oxides, nitrides and fluorides fabricated by conventional thin film deposition techniques. Both enhanced [A.S. Helmy

et al. 1998] and reduced [J. Beauvais *et al.* 1992] intermixing has been observed depending on the physical and chemical properties of coating layers. Different lasers have also been investigated for intermixing of different III-V QW systems [J.J. Dubowski *et al.* 2002, B.S. Ooi *et al.* 2004]. Continuous wave (CW) and pulsed Nd:YAG lasers were found to induce significant interdiffusion in InGaAsP/InGaAs/InP quantum well heterostuctures [J.J. Dubowski *et al.* 2002] and InAs/GaAs quantum dots [J.J. Dubowski *et al.* 2000]. Among the numerous QWI techniques, UV excimer laser controlled QWI (UV-QWI) has been proposed as a new approach potentially addressing limitations of other QWI techniques related to the control of the process, its reproducibility and spatial resolution [J.J. Dubowski 2003]. In addition to the enhanced intermixing in InGaAs/InGaAsP QWs heterostructures [J.J. Dubowski 2003] by UV-QWI, we have recently reported that the UV-QWI process can also lead to the suppression of intermixing [J. Genest *et al.* 2004]. We have shown that the short wavelength of the surface modifying radiation and the relatively shallow location of the QW allow suppression of QWI with a spatial resolution of as high as 1 μm [J. Genest *et al.* 2007b]. In this paper we discuss the mechanism of excimer laser-induced suppression of the QWI process in InAlGaAs/AlGaAs/GaAs and AlGaAs/GaAs QW heterostructures.

5.2.3 Experimental details

Two laser diodes heterostructures grown by molecular beam epitaxy were used for this study. The first one (Q1) consisted of two 7.5 nm thick GaAs quantum wells (QWs) separated by a 10.3 nm $Al_{0.43}Ga_{0.57}As$ barriers and buried 1 μm under the surface. The active region was grown on an n-type Se doped (100) GaAs substrate with a 100 nm GaAs and a 100 nm $Al_{0.43}Ga_{0.57}As$ buffer layers. Both layers were Se doped ($1.7x10^{18}$ cm^3). The structure was terminated with a C doped ($1.8x10^{18}$ cm^{-3}) $Al_{0.43}Ga_{0.57}As$ optical confinement layer, which was

740 nm thick and a Zn-doped ($7x10^{18}$ cm^{-3}) GaAs capping layer, which was 100 nm thick. This heterostructure was designed for lasing operation at 852 nm at room temperature.

The second heterostructure (Q2) was composed of a single 7 nm $In_{0.1}A_{0.13}Ga_{0.77}As$ QW. The barriers were made of 400 nm thick AlGaAs graded index structure (GRIN) layers. The QW was positioned 2 μm below the wafer surface. This structure was grown on an n-type Si doped GaAs substrate with a C-doped (10^{18} cm^{-3}) buffer structure composed of a 200 nm GaAs layer and a 200 nm AlGaAs GRIN layer. Two 1500 nm $Al_{0.6}Ga_{0.4}As$ claddings, on each side of the well, assured optical confinement. This QW wafer was designed for lasing operation at 808 nm at room temperature.

Samples of 5 mm x 5 mm were cleaved from both wafers and solvent cleaned using a standard cleaning procedure. They were then irradiated with a KrF excimer laser operating at 248 nm at a pulse repetition rate of 3 Hz. The laser beam was shaped with a fly-eye array beam homogenizer to form a 7 mm x 7 mm top-hat profile. Samples were irradiated with 1000 pulses of fluences varying from 50 to 100 mJ/cm^2. The maximum surface temperature induced with a 100 mJ/cm^2 pulse has been estimated to be 250°C. The air environment of the current experiment and multi-pulse irradiation are expected to lead to a significant deviation of the GaAs surface from stoichiometric conditions. Following the laser irradiation, all samples were annealed in a rapid thermal annealer (RTA) at 900°C. The RTA treatment consists of a 15 second ramping from room temperature to the annealing temperature and a 30 second anneal at a set temperature. The annealing was carried out in a forming gas atmosphere (N_2 90% and H_2 10%) while cooling was done under nitrogen to prevent oxidation.

Low temperature (20K) photoluminescence (PL) was used to characterize the samples. A frequency doubled Nd:YAG laser (λ = 532 nm) was used to excite the sample while the PL signal was dispersed by a monochromator and detected by a photomultiplier. X-ray photoelectron spectroscopy (XPS) measurements were carried out with a Kratos HS system and a monochromatic Aluminium K_α x-ray source. The atomic concentration of Ga, As and O were measured by analysing the Ga 3d, As 3d and O 1s photoelectron spectra. The thickness of the GaAs oxide layer (mostly composed of Ga_2O_3 and As_2O_3), d_{ox}, was estimated using the intensity ratio of the oxides and substrate. It was assumed that the oxide is a homogeneous mix of Ga_2O_3 and As_2O_3. For a given element, if the XPS spectrum shows both the oxide and the GaAs cap layer peaks, the oxide thickness can be obtained using the following equation [C.F. Yu *et al.* 1986]:

$$d_{ox} = \alpha_{ox} \sin\theta \ln\left(\frac{I_{ox}}{I_{sub}}\frac{D_{sub}}{D_{ox}}\frac{\alpha_{sub}}{\alpha_{ox}} + 1\right), \qquad (5.3)$$

where the D_{sub}/D_{ox} is the density ratio between the substrate and the oxide while I_{ox}/I_{sub} is the photoelectron intensity ratio, α_{ox} and α_{sub} are the electron mean escape depths in the oxide and in the substrate, and θ is the photoelectrons exit angle relative to the surface. The electron mean escape depths in GaAs and in the oxide have been calculated using the Cumpson and Seah [P.J. Cumpson *et al.* 1997] model for the Ga 3d peak. These values are 2.6 and 2.0 nm in GaAs and in Ga_2O_3, respectively, while it is 2.5 nm for As 3d in both As_2O_3 and the substrate [C.F. Yu *et al.* 1986].

5.2.4 Results and discussion

Figure 5-5 shows the dependence of the blue shift amplitude as a function of the laser fluence for four samples from the Q1 wafer (square symbols) and five samples from the Q2 wafer

(circle symbols) following laser irradiation and RTA. The results for RTA only (non-irradiated) samples indicate that the bandgap of the InAlGaAs/AlGaAs/GaAs and AlGaAs/GaAs quantum well structures was thermal shifted by 104 and 48 meV (43 and 27 nm), respectively. This compares with the shift reduce to only 15 and 9 meV (7 and 5 nm) for the same QW microstructures that were irradiated with 1000 pulses at 100 and 88 mJ/cm^2, respectively. These results confirm the role of the physical and chemical properties of the surface in controlling the amplitude of the intermixing mechanism that has been observed earlier [C.J. Hamilton *et al.* 1995, J.J. Dubowski 2003]. We argue that the oxide layer fabricated at the surface influences the interdiffusion through the locally induced thermal stress. For example, it has been demonstrated that deposition of Si_3N_4 on SiO_2 coated GaAs QW structure creates tensile stress which prevents SiO_2-enhanced V_{Ga} diffusion toward the quantum wells [A. Pepin *et al.* 1997].

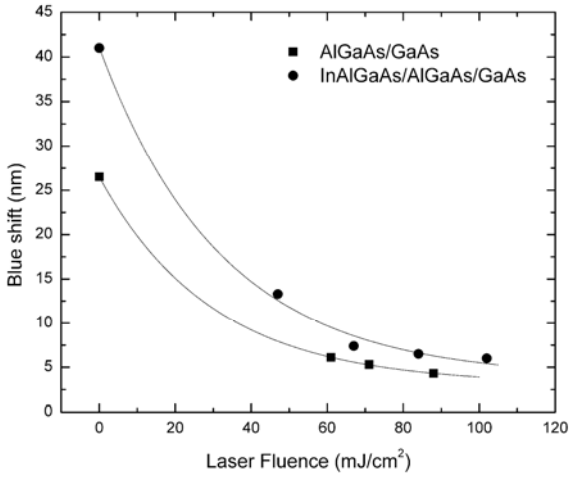

Figure 5-5: Dependence of the amplitude of blue shift in as-grown and 1000 pulse laser irradiated AlGaAs/GaAs (squares) and InAlGaAs/AlGaAs/GaAs (circles) samples following their RTA at 900°C for 30 s.

Figure 5-6 shows a dependence of the QW PL intensity for the processed samples following annealing. For Q1, an up to 260% PL intensity enhancement has been observed for the 88 mJ/cm^2 irradiated sample. For Q2, a 50% enhancement has been observed for the 84 mJ/cm^2 irradiated sample. This has been reduced to the initial level of the PL signal following the

irradiation at 108 mJ/cm^2; processing with such laser fluence leads to microscopic surface damage that could explain this signal reduction. An enhancement of the PL signal has been reported previously for InGaAs/InGaAsP heterostructures processed with an XeCl (λ = 308 nm) excimer laser in air [J.J. Dubowski *et al.* 1999]. This result has been attributed to the formation of a thin Ga_xO_y layer on the surface of InGaAs.

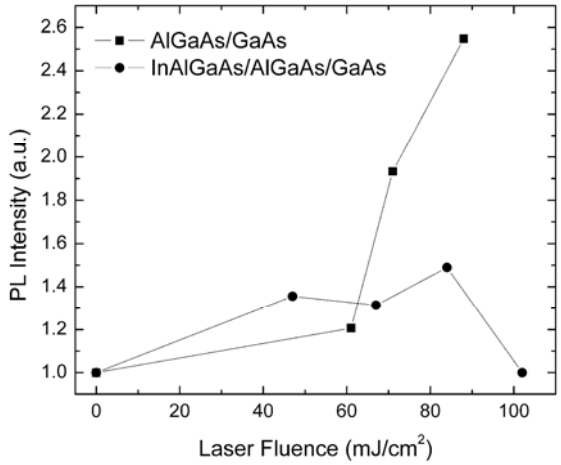

Figure 5-6: Intensity of the QW photoluminescence signal from AlGaAs/GaAs (squares) and InAlGaAs/AlGaAs/GaAs (circles) samples irradiated with pulses of different laser fluence and after RTA at 900$°C for 30 s

Relative near-surface atomic concentration of Ga and As in as-grown and two laser irradiated samples (Q2) was estimated using XPS measurements as illustrated in figure 5-7. It shows a significant reduction of the GaAs-related Ga peak, which is accompanied by the growth of the Ga peak originating from Ga_2O_3. The non-stoichiometric ratio of arsenic oxides and gallium oxide and the presence of elemental arsenic in laser treated samples is due to transformation of As_2O_3 in Ga_2O_3 which can be described by the following formula:

$$2\ GaAs + As_2O_3 \rightarrow Ga_2O_3 + 4\ As\ . \qquad (5.4)$$

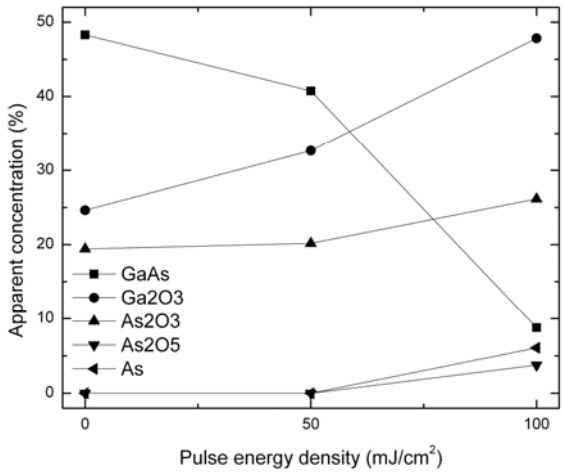

Figure 5-7: Atomic concentrations of Ga and As XPS peaks related to GaAs (■), Ga_2O_3 (●), As_2O_3 (●), As_2O_3 (▲), As_2O_5 (▼) and As (◄) in as-grown and laser-irradiated (no RTA) InAlGaAs/AlGaAs/GaAs samples.

The presence of native GaAs oxides is observed in the as-grown sample. All laser treated samples, however, showed a reduction in the overall arsenic concentration. This is due to fact that As, As_2 and As_4 have a higher vapour pressure than Ga and, thus, the As atoms are relatively easily desorbed from the substrate. The laser treated samples also show an increase in the overall oxygen concentration which can be related to the enhanced GaAs oxidation induced by UV laser irradiation in air [C.F. Yu *et al.* 1986].

XPS results revealed that laser irradiation of GaAs induced the growth of gallium rich oxide on the sample surface. From XPS data, the calculated overall thickness of the oxide (Ga_2O_3 + As_2O_3) layer formed at the surface of a 1000-pulses irradiated Q2 sample was calculated using equation (5.3) and results are plotted in figure 5-8 as a function of the laser fluence. It can be seen that a 5.5 nm thick oxide layer has been formed following the irradiation at 100 mJ/cm^2. Energy dispersive X-ray spectroscopy results on Q1 show a qualitatively similar increase of oxygen concentration after laser treatment.

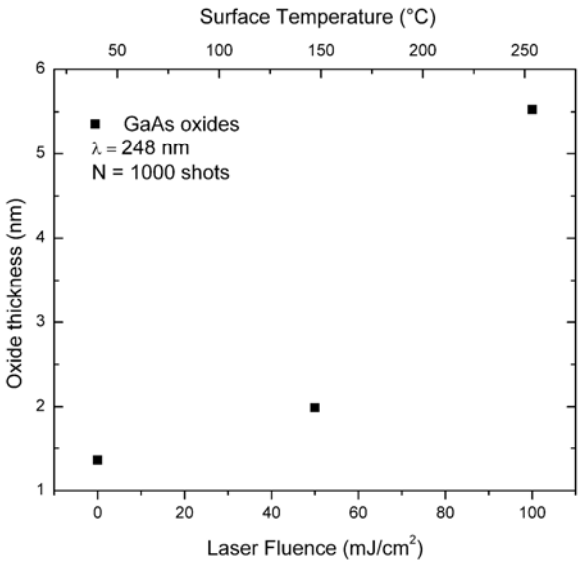

Figure 5-8: Overall calculated oxide thickness (Ga_2O_3 and As_2O_3) on the surface of GaAs irradiated with a KrF laser in an air environment. Calculated surface temperatures induced with the laser are indicated on the top axis of this figure.

We argue that the laser-induced formation of the oxide layer is responsible for the reduced amplitude of the QWI effect. This is in agreement with the results reported earlier showing that due to the greater thermal expansion coefficient of gallium oxide ($7.3x10^{-6}$ K^{-1}) than that of GaAs ($5.73x10^{-6}$ K^{-1}), the presence of gallium oxide will induce an interdiffusion-reducing stress in annealed GaAs [L. Fu *et al.* 2002a]. Of particular interest is that the substrate/oxide interface fabricated by the irradiation with the excimer laser likely contains fewer relaxation sites, as the investigated oxide has been naturally grown instead of being physically deposited. This could explain the high efficiency of a 5 nm thick film, predominantly composed of gallium oxide, in suppressing the intermixing that led to a reduction of bandgap shift by 80.7 meV (35 nm) in comparison to the as-grown and annealed Q2 samples. Interestingly, for the same type of structure and similar annealing conditions, ~40 meV and ~29 meV suppressions have been reported using 150 nm thick TiO_2 coating [P.L. Gareso *et al.* 2004] and 90 nm of Ga_xO_y on 200 nm of SiO_2 bilayer coating [L. Fu *et al.* 2002a], respectively.

5.2.5 Conclusions

We have investigated the influence of a KrF excimer laser generated layer of an oxide material at the surface of GaAs on the quantum well intermixing process in AlGaAs/GaAs and in InAlGaAs/AlGaAs/GaAs QW heterostructures. XPS measurements showed that the irradiation with a laser delivering pulses of 60 to 100 mJ/cm^2 in air environment leads to the formation of a predominantly gallium oxide rich layer. Rapid thermal annealing of such samples has resulted in an up to 35 nm retardation of the bandgap shifting amplitude in comparison to the non-irradiated samples. We argue that the mechanism responsible for this behaviour is the reduced intermixing due to the Ga_2O_3-induced tensile stress in the investigated QW microstructures. The ability to fabricate gallium oxide rich regions on a wafer irradiated with an excimer laser, e.g., by a laser projection lithography technique, has the potential application for the simplified fabrication of multi-bandgap QW wafers when compared to conventional QWI techniques involving selective area ion-implantation or oxide deposition. In addition, this new excimer-laser-based process for suppressed bandgap shifting can be used in conjunction with other QWI approaches to create high-contrast zones in multi-bandgap structures.

5.2.6 Acknowledgment

This research has been supported in part by the Natural Science and Engineering Research Council of Canada. The help provided by Mike Post of the National Research Council Canada and Sonia Blais of the IMSI at the Université de Sherbrooke is greatly appreciated. Jonathan Genest acknowledges the NRC Canada Graduate Student Scholarship Supplement award.

5.3 References

Aimez, V., Beauvais, J., et al. (2002) *Low-energy ion-implantation-induced quantum-well intermixing*, IEEE Journal of Selected Topics in Quantum Electronics, vol. 8, n° 4, 870-879.

Beauvais, J., Marsh, J. H., et al. (1992) *Suppression of Bandgap Shifts in Gaas/Algaas Quantum-Wells Using Strontium Fluoride Caps*, Electronics Letters, vol. 28, n° 17, 1670-1672.

Charbonneau, S., Koteles, E. S., et al. (1998) *Photonic integrated circuits fabricated using ion implantation*, IEEE Journal of Selected Topics in Quantum Electronics, vol. 4, n° 4, 772-793.

Cohen, R. M. (1997) *Point defects and diffusion in thin films of GaAs*, Materials Science & Engineering: R: Reports, vol. 20, n° 4-5, 167.

Cumpson, P. J. and Seah, M. P. (1997) *Elastic Scattering Corrections in AES and XPS. II. Estimating Attenuation Lengths and Conditions Required for their Valid Use in Overlayer/Substrate Experiments*, Surface and Interface Analysis, vol. 25, n° 6, 430-446.

Dubowski, J. J. (2003) *Laser-induced bandgap shifting for photonic device integration*, U.S. 6,670,644.

Dubowski, J. J., Allen, C. N., et al. (2000) *Laser-induced InAs/GaAs quantum dot intermixing*, Applied Physics Letters, vol. 77, n° 22, 3583.

Dubowski, J. J., Feng, Y., et al. (2002) *Monolithic multiple wavelength ridge waveguide laser array fabricated by Nd : YAG laser-induced quantum well intermixing*, Journal of Vacuum Science & Technology A, vol. 20, n° 4, 1426-1429.

Dubowski, J. J., Poole, P. J., et al. (1999) *Enhanced quantum-well photoluminescence in InGaAs/InGaAsP heterostructures following excimer-laser-assisted surface processing*, Applied Physics A: Materials Science & Processing, vol. 69, n° 7, S299.

Fu, L., Heijden, R. W. V. D., et al. (2002) *Study of intermixing in a GaAs/AlGaAs quantum-well structure using doped spin-on silica layers*, Applied Physics Letters, vol. 80, n° 7, 1171.

Gareso, P. L., Buda, M., et al. (2004) *Suppression of thermal atomic interdiffusion in C-doped InGaAs/AlGaAs quantum well laser structures using TiO_2 dielectric layers*, Applied Physics Letters, vol. 85, n° 23, 5583-5585.

Genest, J., Dubowski, J. J., et al. (2004) *UV Laser Induced Quantum Well Intermixing of III-V Heterostructures*, Proc. SPIE, vol. 5451, n° 550.

Genest, J., Dubowski, J. J., et al. (2007a) *Suppressed intermixing in InAlGaAs/ AlGaAs/GaAs and AlGaAs/GaAs quantum well heterostructures irradiated with a KrF excimer laser*, Applied Physics A: Materials Science & Processing, vol. 89, n° 2, 423-426.

Genest, J., Dubowski, J. J., et al. (2007b) *UV laser controlled quantum well intermixing in InAlGaAs/GaAs heterostructures*, Journal of Physics: Conference Series, vol. 59, n° 1, 605-9.

Guido, L. J., Jackson, G. S., et al. (1987) *Index-Guided $Al_xGa_{1-X}As$-GaAs Quantum-Well Heterostructure Lasers Fabricated by Vacancy-Enhanced Impurity-Induced Layer Disordering from an Internal $(Si_2)_Y(GaAs)_{1-Y}$ Source*, Applied Physics Letters, vol. 50, n° 10, 609-611.

Hamilton, C. J., Hicks, S. E., et al. (1995) *Suppression of Bandgap Shifts in GaAs/AlGaAs Multiquantum Wells Using Hydrogen Plasma Processing*, Electronics Letters, vol. 31, n° 16, 1393-1394.

Helmy, A. S., Johnson, N. P., et al. (1998) *A study of impurity-free vacancy disordering in GaAs-AlGaAs for improved modeling*, IEEE Journal of Selected Topics in Quantum Electronics, vol. 4, n° 4, 661-8.

Li, E. H., Ed. (2000). Semiconductor Quantum Wells Intermixing. Optoelectronic Properties of Semiconductors and Superlattices. Amsterdam, Netherlands, Gordon and Breach Science Publishers, 695 p.

Marsh, J. H. (1993) *Quantum-Well Intermixing*, Semiconductor Science and Technology, vol. 8, n° 6, 1136-1155.

Mitra, S. and Stark, J. P. (1991) *Role of vacancies and implantation defects in GaAs/AlAs superlattice intermixing*, Journal of Materials Science, vol. 26, n° 24, 6650.

Ooi, B. S., Ong, T. K., et al. (2004) *Multiple-wavelength integration in InGaAs-InGaAsP structures using pulsed laser irradiation-induced quantum-well intermixing*, IEEE Journal of Quantum Electronics, vol. 40, n° 5, 481.

Pepin, A., Vieu, C., et al. (1997) *Evidence of stress dependence in SiO_2/Si_3N_4 encapsulation-based layer disordering of GaAs/AlGaAs quantum well heterostructures*, Journal of Vacuum Science & Technology B, vol. 15, n° 1, 142-153.

Teng, J. H., Dong, J. R., et al. (2001) *Impurity-free intermixing in compressively strained InGaAsP multiple quantum well structures*, Materials Science in Semiconductor Processing, vol. 4, n° 6, 621.

Yu, C. F., Podlesnik, D. V., et al. (1986) *Ultraviolet-Light-Enhanced Oxidation of Gallium-Arsenide Surfaces Studied by X-Ray Photoelectron and Auger-Electron Spectroscopy*, Chemical Physics Letters, vol. 130, n° 4, 301-306.

Chapter 6: Lateral resolution of the UV laser induced quantum well intermixing suppression in GaAs-based heterostructures

High contrast bandgap engineering is an important characteristic for industrially viable integration technology. For this reason, knowing the lateral resolution of a quantum well intermixing technique is necessary to establish the potential of this technique to manufacture monolithically integrated photonic circuits. As shown in the previous chapter, UV laser irradiation can be used to prevent intermixing in GaAs-based heterostructure. In this chapter, I determine the lateral resolution of the UV laser suppression of quantum well intermixing technique in both studied GaAs-based quantum well heterostructure. The analysis was done on two samples on which a SiO_2 mask was patterned. The SiO_2 prevent the oxidation of the GaAs under the UV irradiation. As we have seen in the previous chapter, the grown gallium oxide inhibits the interdiffusion process. The resolution of the technique is analysed by photoluminescence mapping and by cathololuminescence.

The first section of this chapter presents simulations of cathodoluminescence in the QT564 heterostructure. Scenarios with the presence and the absence of the oxide mask are treated. This section also discusses the resolution of the cathodoluminescence technique at the chosen acceleration energy.

The second part of this chapter consists of a journal article titled “UV laser controlled quantum well intermixing in InAlGaAs/GaAs heterostructures”. Published in the *Journal of*

Physics: Conference Series, vol. 59, no. 1 at pages 605-609. It presents the lateral resolution study.

6.1 Cathodoluminescence simulation

The cathodoluminescence simulations were done with CASINO [D. Drouin *et al.* 2007]. This Monte-Carlo calculation program calculates the trajectories of electron inside a given material. The QT564 (details in figure 4-7 at page 107) heterostructure was inputted as the target material. The acceleration energy used was 20 keV.

6.1.1 Cathodoluminescence in the QT564 heterostructure

Figure 6-1 shows the simulated electron-mater interaction volume in the QT564 heterostructure from the iso-energy curves. The diffusion of the 10 nm electron probe is illustrated. We observe that less than 20% of the electrons penetrate the active region. Hopefully, because charge carrier can diffuse over a few micrometers, the carriers generated in the layers on top of the active region can reach the active region before recombining. Because of the potential well, carriers diffusing in the quantum well get trapped there and will relax themselves through radiative recombination. However the carrier diffusion also limits the cathodoluminescence resolution: they diffuse in all three directions and expend the interaction volume.

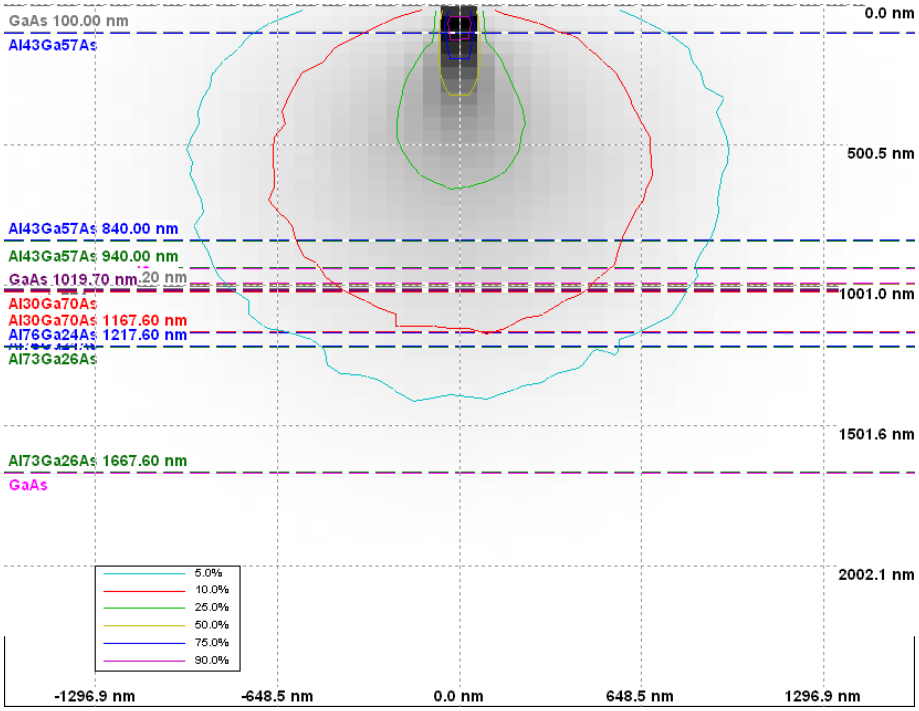

Figure 6-1: CASINO[D. Drouin *et al.* 2007] simulation of the interaction volume in the QT564 quantum well heterostructure.

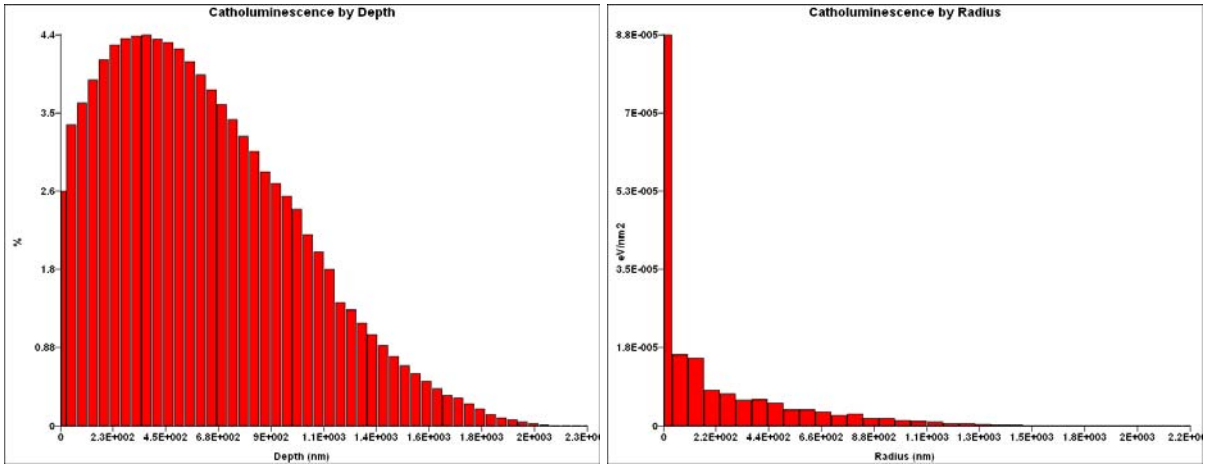

Figure 6-2: Simulation of the origin of the cathodoluminescence a) as a function of the depth and b) as a function of the radius from the center of the electron beam

6.1.2 Cathodoluminescence through the oxide mask

Because they lose energy in the oxide mask, the number of electron reaching the active region is smaller than in bare sample. The cathodoluminescence intensity from the well will then be smaller.

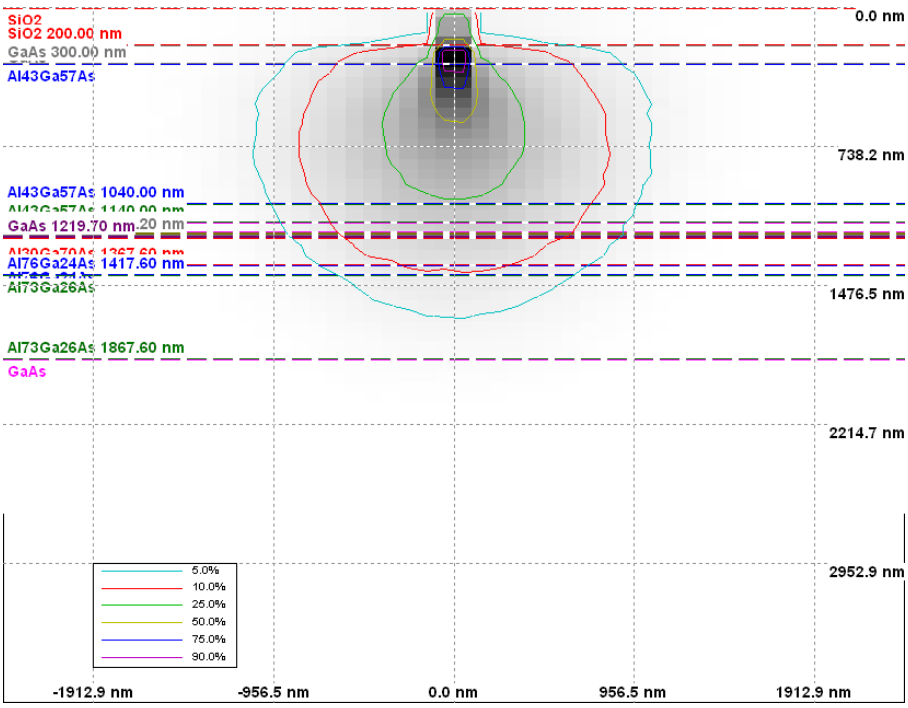

Figure 6-3: CASINO simulation of the interaction volume in the QT564 quantum well heterostructure capped with 200 nm of SiO_2.

6.2 UV laser controlled quantum well intermixing in InAlGaAs/GaAs heterostructures

J Genest[1], J J Dubowski[1], V Aimez[1], N Pauc[1], D Drouin[1] and M Post[2]

[1] Regroupement québécois sur les matériaux de pointe (RQMP), Département de génie électrique et génie informatique, Université de Sherbrooke, Sherbrooke, Québec J1K 2R1, Canada

[2] Institute for Chemical Process and Environmental Technology National Research Council of Canada, Ottawa, Ontario K1A 0R6, Canada

Jonathan.Genest@USherbrook.ca

6.2.1 Abstract.

The influence of surface irradiation of GaAs with a KrF excimer laser on the magnitude of the quantum well intermixing (QWI) effect has been investigated on GaAs/AlGaAs and GaAs/AlGaAs/InAlGaAs QWs heterostructures. The selective area irradiation through a SiO_x mask was carried out in an atmospheric environment. Following the 1000 pulses irradiation at 100 mJ/cm^2, the samples were annealed in a rapid thermal annealing furnace at 900 ºC. Photoluminescence mapping and cathodoluminescence measurements show that significant laser-induced suppression of the QWI process can be achieved with lateral resolution of the order of 1 μm.

6.2.2 Introduction

GaAs and InP based heterostructures are the material of choice for the fabrication of active photonic devices. However, the fabrication of photonic integrated circuits (PICs) requires the simultaneous integration of multiple bandgap structures within a single chip. In order to produce cost-effective PICs, selective area bandgap control of the heterostructure is of primary importance. Quantum Well Intermixing (QWI) is a leading post-growth approach to fabricate monolithic chips with areas of different bandgaps [E.H. Li 1998]. Among the numerous QWI techniques, UV-Laser controlled QWI is a new approach which has the potential to overcome common QWI techniques limitations primarily related to the control of the process.

The most frequently investigated methods of QWI include impurity induced intermixing [L.J. Guido *et al.* 1987], impurity-free vacancy diffusion [J.H. Teng *et al.* 2001] and QWI induced by ion implantation [S. Charbonneau *et al.* 1998, V. Aimez *et al.* 2002]. QWI has also been achieved by selective area coating of QW wafers with different oxides, nitrides and fluorides fabricated by conventional thin film deposition techniques [J.S. Yu *et al.* 2002]. Both

enhanced [N. Shimada *et al.* 2004] and reduced [J. Beauvais *et al.* 1992] intermixing has been observed depending on the physical and chemical properties of coating layers.

In this work, a KrF excimer laser has been used to suppress the intermixing in selected areas in GaAs/AlGaAs and GaAs/AlGaAs/InAlGaAs QWs heterostructures. Lateral resolution of this technique has also been investigated using photoluminescence (PL) mapping and cathodo-luminescence (CL).

6.2.3 Experiment

6.2.3.1 QW wafers description

Two different QW structures were used for this work. The first one (Q1) consisted of two 7.5 nm thick GaAs quantum wells (QWs) separated by AlGaAs barriers. This structure was grown by molecular beam epitaxy on a n-type doped (100) GaAs substrate. It was designed for lasing operation at 852 nm at room temperature. Details of the structure are shown in table 6-1. The second heterostructure (Q2) was composed of a single 7 nm $In_{0.1}Al_{0.13}Ga_{0.77}As$ QW. The barriers were made of AlGaAs GRIN layers. The second structure was also grown on a n-type GaAs substrate. This QW wafer was designed for lasing operation at 808 nm at room temperature. The table 6-2 shows Q2 specific details.

Table 6-1: Q1 layers composition and thickness

Composition	Width (nm)	Doping (cm^{-3})	Dopant
GaAs-p	100	$7x10^{18}$	Zn
$Al_{.43}Ga_{.57}As$-p	740	$1.8x10^{18}$	C
$Al_{.43}Ga_{.57}As$	100		UD
$Al_{.23}Ga_{.77}As$	54.4		UD
GaAs (QW)	7.5		UD
$Al_{.23}Ga_{.77}As$	10.3		UD
GaAs (QW)	7.5		UD
$Al_{.30}Ga_{.70}As$	147.9		UD
$Al_{.76}Ga_{.24}As$	50		UD
$Al_{.73}Ga_{.27}As$-n	45	$1.7x10^{18}$	Se
GaAs-n	100	$1.7x10^{18}$	Se
GaAs-n	substrate		Se

Table 6-2: Q2 layers composition and thickness

Composition	Mole fraction	Width (nm)	Doping (cm^{-3})	Dopant
GaAs-p^+		200	3×10^{19}	C
$Al_xGa_{1-x}As$	$x = 0.6$	1500	1.1×10^{18}	C
$Al_xGa_{1-x}As$ (GRIN)	$x = 0.35 \rightarrow 0.6$	400	U/D	
$In_xAl_yGa_{1-x-y}As$ (QW)	$x = 0.1$; $y = 0.13$	7	U/D	
$Al_xGa_{1-x}As$ (GRIN)	$x = 0.6 \rightarrow 0.35$	400	U/D	
$Al_xGa_{1-x}As$	$x = 0.6$	1500	10^{18}	Si
$Al_xGa_{1-x}As$ (GRIN)	$x = 0.0 \rightarrow 0.6$	200	10^{18}	Si
GaAs-n		200	10^{18}	Si
GaAs-n		Subst.		

6.2.3.2 Samples processing

Samples from both wafers were first cleaved and cleaned. A 200 nm thick silicon oxide was then deposited by the PECVD technique. Conventional photolithography and chemical etching were used to form patterned stripes and to process openings with widths changing from 200 μm down to 5 μm. Samples were then irradiated with a KrF excimer laser operating at 248 nm and delivering 22 ns long pulses at the rate of 3 Hz. The laser beam was shaped with a MicroLas microlens array (fly-eye) beam homogenizer [H.J. Kahlert *et al.* 1993, E.C. Harvey *et al.* 1997] to form a top-hat profile. This is done by averaging the localized intensity variations. All individual beamlets coming from the microlens array overlap in the focal plan.

The exposed area was 7 mm x 7 mm. Samples were irradiated in an atmospheric environment with 1000 pulses, each delivering a fluence of 100 mJ/cm^2.

Following the laser irradiation, the samples went through a Rapid Thermal Annealing (RTA) step at 900°C. The RTA treatment consists of a 15 second ramping from room temperature to the annealing temperature and a 30 second anneal at a set temperature. The annealing was carried out in a hydrogen and nitrogen atmosphere while cooling was done under nitrogen.

6.2.3.3 Characterization

Photoluminescence (PL) mapping and Cathodoluminescence (CL) were used to characterize the modified bandgap energy and the lateral resolution of the UV laser controlled QWI technique. The PL mapping experiments were carried out at room temperature with a Philips PLM150 mapping system. A frequency doubled Nd:YAG laser (λ = 532 nm) was used to excite the sample while the luminescence was dispersed by a monochromator and detected by an InGaAs photodiode array. The lateral resolution of this system was about 10 μm.

The CL experiments were performed with a LEO-55VP scanning electron microscope (SEM) under high vacuum. Both CL imaging and spectroscopy were achieved with a photomultiplier tube (PMT) that was used to detect the luminescence dispersed by a GATAN 300 mm monochromator. We acquired monochromatic CL images in the fixed CL Wavelength Imaging mode (CLWI) to achieve spatial mapping of the QW emission.

6.2.4 Results and Discussion

6.2.4.1 PL mapping

Figure 6-4 shows the room temperature PL map of sample Q1 after KrF laser irradiation and annealing. We have previously demonstrated that the similar treatment of this material could reduce the blue shift of its bandgap by 22 nm in comparison to the non-treated material [J. Genest *et al.* 2004]. Here, the PL mapping shows a similar shift contrast of 20 nm between the masked and unmasked area. As shown in figure 6-5a), this contrast is not affected by the width of the openings. Note that a 5 µm line is difficult to resolve due to the limited lateral resolution of the experimental setup. Thus, we can conclude that the UV laser controlled QWI intermixing on this type of material is better than 10 µm.

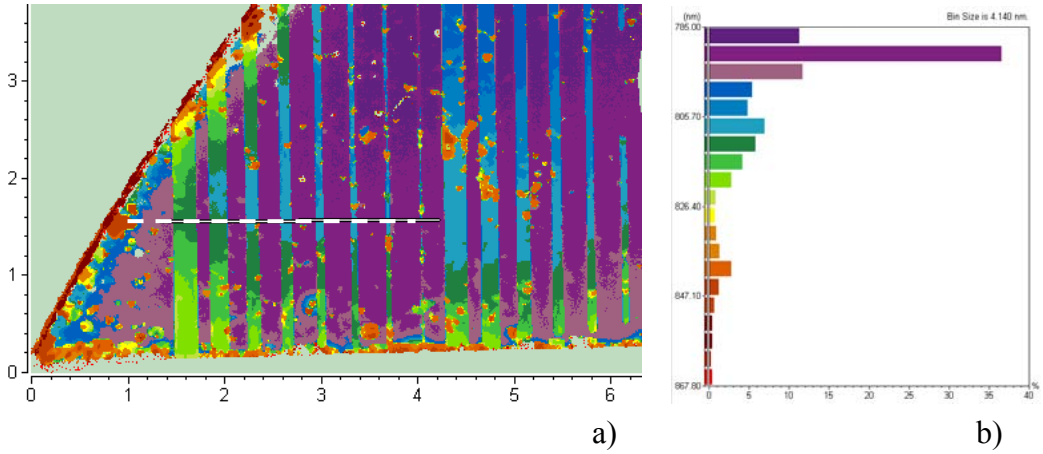

a) b)

Figure 6-4a) Room temperature PL mapping from sample Q1 after laser treatment and annealing. The dash line represents the position of the line scan. b) Wavelength histogram and legend.

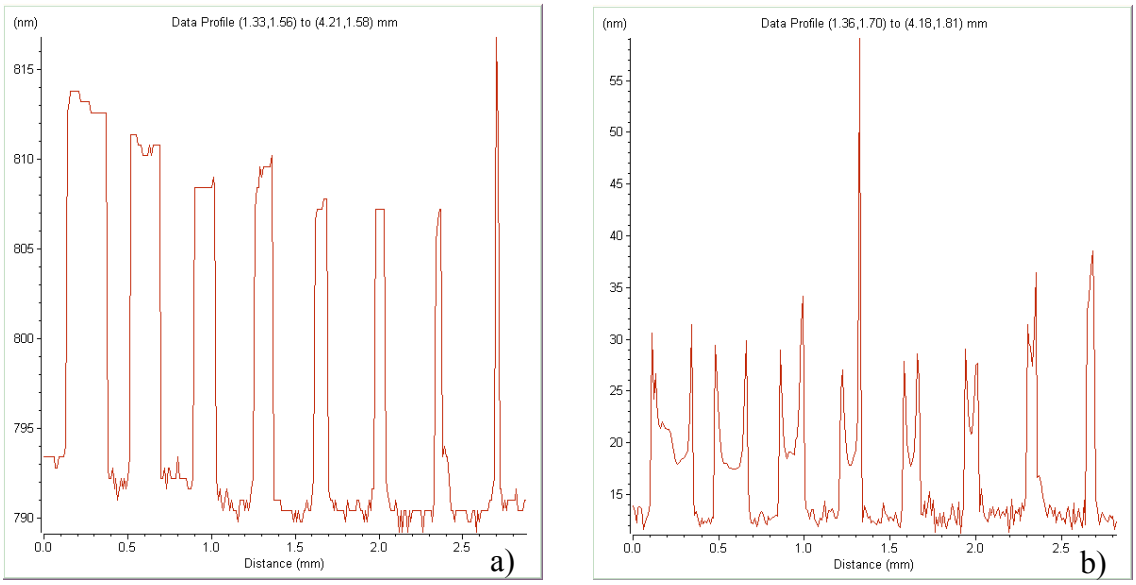

Figure 6-5: Linescan from PL map of Q1. a) PL peak position b) PL FWHM

Figure 6-5b) shows that the PL peak full width at half maximum (FWHM) increases from 12 to 18 nm for the masked and unmasked region, respectively. Such broadening of the QW PL peak is usually attributed to the presence of defects in the QW vicinity [J.H. Marsh 1993], or to the development of stress in the active layer region [A.S.W. Lee *et al.* 1999]. Since defects diffusion in the QWs region is commonly known to enhance the intermixing process and thus to increase the recombination energy, we can associate the increase of the FWHM in the less blueshifted regions to the stress induced in the structure. Note that the edge effect on the line scan is caused by the superposition of signals from each side of the interface.

6.2.4.2 Cathodoluminescence

Since the active layers in Q2 are buried deeply under the structure surface and since the top layers are heavily doped, the room temperature PL signal from this wafer was below the detection limit of our PL setup. Low temperature (5K) CL was used to characterize the UV laser effect in the 5 µm width opening. Figure 6-6 shows the CL spectra from the masked and

unmasked areas. The unmasked area spectrum exhibits two recombination peaks instead of one. Since the spatial origins of those two peaks are distinct (see figure 6-7a and b), this phenomenon is likely related to a diffraction effect. The diffraction effect could also explain the smaller QWI suppression (10 nm) in the edge area of the unmasked region compared to the 22 nm suppression in its center. This suggests the possibility of using phase shift masks for high resolution bandgap shifting.

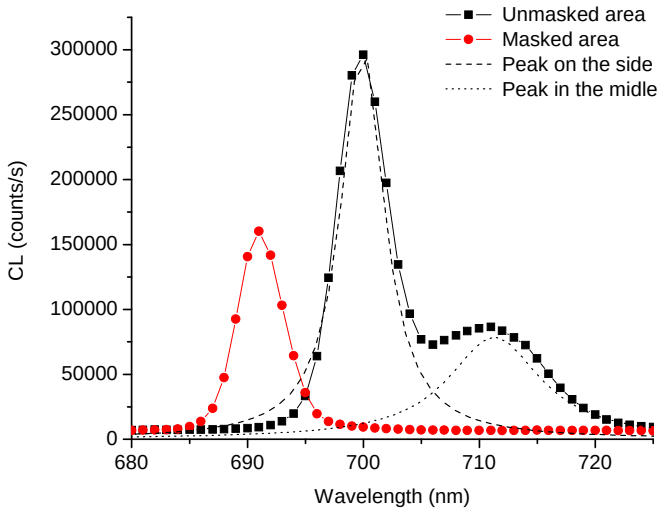

Figure 6-6: Low temperature CL spectra for the masked and unmasked area.

Figure 6-7 shows low-temperature CL wavelength images collected at 700, 712 and 690 nm. It can be seen that the transition between the masked and unmasked regions is approximately 1 μm wide. Given that this value is limited by the lateral width of the electron-matter interaction volume, which for the investigated heterostructure and at 20 kV is about 1 μm, we argue that the resolution of the UV laser controlled QWI intermixing process on this type of material is 1 μm or better. However, CL signals coming from the laser exposed area also demonstrate an increase in

their FWHM. It increases from 3.9 nm under the mask to 4.5 for the edge region to 9.7 nm for the less blueshifted area. These results are consistent with the stress driven explanation of the thermal shift.

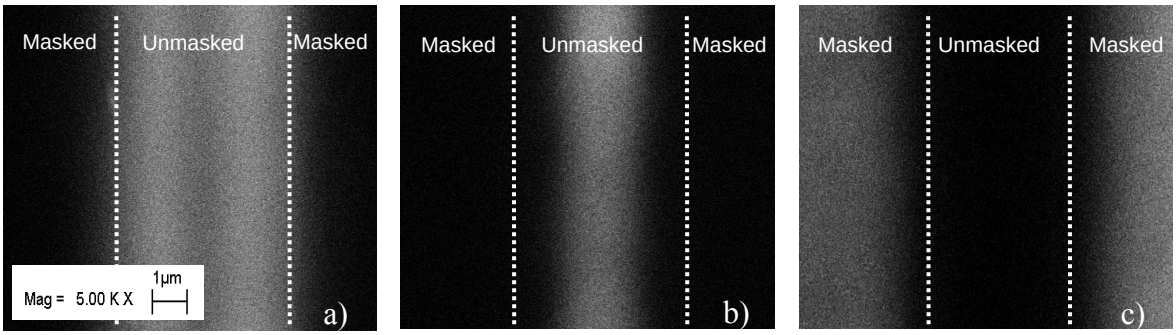

Figure 6-7: Low temperature CL wavelength images at a) 700 nm, b) 712 nm and c) 690 nm. The white dashed lines show the frontier between the masked and unmasked regions.

6.3 Summary

It is demonstrated that KrF laser irradiation followed by RTA is an effective technique to suppress quantum well intermixing in GaAs/AlGaAs and GaAs/AlGaAs/InAlGaAs QWs heterostructures. The lateral resolution of this UV-Laser QWI technique has been evaluated to be about 1 μm or better.

This new process has the potential for the fabrication of multi-bandgap QW wafers processed with an excimer laser in a similar manner as the excimer-based photolithography for microelectronics. Alternatively, the ability to suppress the thermal shift using the excimer laser irradiation can be used in conjunction with other QWI approaches to create zones of materials with increased bandgap contrast and better control.

6.4 References

Aimez, V., Beauvais, J., et al. (2002) *Low-energy ion-implantation-induced quantum-well intermixing*, IEEE Journal of Selected Topics in Quantum Electronics, vol. 8, n° 4, 870-879.

Beauvais, J., Marsh, J. H., et al. (1992) *Suppression of Bandgap Shifts in Gaas/Algaas Quantum-Wells Using Strontium Fluoride Caps*, Electronics Letters, vol. 28, n° 17, 1670-1672.

Charbonneau, S., Koteles, E. S., et al. (1998) *Photonic integrated circuits fabricated using ion implantation*, IEEE Journal of Selected Topics in Quantum Electronics, vol. 4, n° 4, 772-793.

Drouin, D., Couture, A. R., et al. (2007) *CASINO V2.42 - A Fast and Easy-to-use Modeling Tool for Scanning Electron Microscopy and Microanalysis Users*, Scanning, vol. 29, n° 3, 92-101.

Genest, J., Dubowski, J. J., et al. (2004) *UV Laser Induced Quantum Well Intermixing of III-V Heterostructures*, Proc. SPIE, vol. 5451, n° 550.

Guido, L. J., Jackson, G. S., et al. (1987) *Index-Guided $Al_xGa_{1-XA}s$-GaAs Quantum-Well Heterostructure Lasers Fabricated by Vacancy-Enhanced Impurity-Induced Layer Disordering from an Internal $(Si_2)_Y(GaAs)_{1-Y}$ Source*, Applied Physics Letters, vol. 50, n° 10, 609-611.

Harvey, E. C. and Rumsby, P. T. (1997). *Fabrication techniques and their application to produce novel micromachined structures and devices using excimer laser projection*. Micromachining and Microfabrication Process Technology III, SPIE.

Kahlert, H. J., Sarbach, U., et al. (1993). *Excimer laser illumination and imaging optics for controlled microstructure generation*, Boston, MA, USA.

Lee, A. S. W., Li, E. H., et al. (1999) *Vacancy-enhanced intermixing in highly strained InGaAs/GaAs multiple quantum well photodetector*, Journal of Applied Physics, vol. 86, n° 6, 3402-3407.

Li, E. H., Ed. (1998). Selected Papers on Quantum Well Intermixing for Photonics. SPIE milestones series. Bellingham, WA, SPIE, 622 p.

Marsh, J. H. (1993) *Quantum-Well Intermixing*, Semiconductor Science and Technology, vol. 8, n° 6, 1136-1155.

Shimada, N., Fukumoto, Y., et al. (2004) *Monolithic integration of lasers and passive elements using selective QW disordering by rapid thermal annealing with SiO_2 caps of different thicknesses*, Electronics and Communications in Japan (Part II: Electronics), vol. 87, n° 1, 34-42.

Teng, J. H., Dong, J. R., et al. (2001) *Impurity-free intermixing in compressively strained InGaAsP multiple quantum well structures*, Materials Science in Semiconductor Processing, vol. 4, n° 6, 621.

Yu, J. S., Song, J. D., et al. (2002) *Influence of dielectric deposition parameters on the $In_{0.2}Ga_{0.8}As/GaAs$ quantum well intermixing by impurity-free vacancy disordering*, Journal of Applied Physics, vol. 92, n° 3, 1386-1390.

Chapter 7: ArF laser-based quantum well intermixing in InGaAs/InGaAsP heterostructures

Jonathan Genest, Romain Béal, Vincent Aimez, and Jan J. Dubowski[4a)]

Department of Electrical and Computer Engineering, Center of Excellence for Information Engineering, Université de Sherbrooke, Sherbrooke, Québec J1K 2R1, Canada

7.1 Abstract

Radiation from a 193 nm ArF excimer laser was investigated as a means to modify surface properties of InGaAs/InGaAsP quantum well heterostructures and introduce defects required to enhance intermixing during the annealing process. A top 200 nm thick sacrificial layer of InP served as a reservoir for laser generated defects. The irradiation with up to 90 pulses of fluence ranging from 65 to 150 mJ/cm^2 allowed to generate an array of 1.2 mm x 1mm sites of quantum well intermixed material, with bandgap energy net blue-shifted up to 107 nm. We discuss the mechanism and advantages of this approach for post-growth wafer level fabrication of multi-bandgap quantum well material.

[4] Electronic mail: jan.j.dubowski@usherbrooke.ca

Monolithically integrated photonic devices require GaAs- or InP-based wafers with multi-bandgap structures, the fabrication of which has continuously challenged epitaxial films growers. In an attempt to overcome some of the problems related to the epitaxial growth of such wafers, the post-growth processing quantum well intermixing (QWI) technique has been studied intensively because it changes the confinement profile of a semiconductor heterostructures [J.H. Marsh 1993, E.H. Li 2000]. QWI is based on site-selected introduction of impurities or point defects. During a subsequent annealing step, the introduced defects or impurities diffuses toward the quantum well (QW)-barrier region where they increase the rate of the intermixing process. Typically, this is achieved by direct doping [L.J. Guido *et al.* 1987], ion implantation [S. Charbonneau *et al.* 1998, V. Aimez *et al.* 2002] or by diffusion of surface atoms into a thin layer of film deposited on top of the QW microstructure [J.S. Yu *et al.* 2002, N. Shimada *et al.* 2004]. However, conventional QWI techniques lack the reproducibility and the reliability required for industrial fabrication of complex multibandgap wafers and a suitable in-situ monitoring technique has yet to be developed. Excimer lasers are potentially attractive for QWI as they can be used to pattern wafers in numerous sites with different doses of radiation required for point defect generation. Consequently, a multi-bandgap wafer can be produced in a single rapid thermal annealing (RTA) step [J.J. Dubowski 2003]. In addition to the expected enhancement of the intermixing process, we have recently demonstrated that KrF (248 nm) laser irradiation of GaAs based QW heterostructures could also inhibit QWI [J. Genest *et al.* 2007b]. Clearly, the nature and role of excimer laser induced defects and formation of the surface alternate layer in the QWI process requires detailed studies. The attractiveness of this approach stems from the fact that the

use of excimer lasers for doping and annealing of large surfaces has already been demonstrated in an industrial environment. Here, we report on the results of ArF excimer induced QWI in InGaAs/InGaAsP QW heterostructures. We investigate the role and mechanisms of laser created defects in a sacrificial layer of InP in the QWI process.

The investigated InGaAs/InGaAsP/InP QW heterostructure was grown by a metalorganic chemical vapour deposition technique on an S-doped InP substrate. It consists of 5 InGaAs quantum wells with composition chosen to have material suitable for the fabrication of laser diodes operating at 1.50 μm at room temperature. The 5 nm thick quantum wells are separated by 12 nm thick InGaAsP barriers. The active region was grown on a 1.4 μm thick buffer layer of n-type (Si, $2x10^{18}$ cm^{-3}) InP and a 130 nm thick n-type (Si, $5x10^{17}$ cm^{-3}) InGaAsP. The top cladding was composed of two Zn-doped layers of InP, 200 and 1200 nm thick, separated by a 10 nm InGaAsP etch stop layer. The contact layer, 100 nm Zn-doped InGaAs, was separated from the cladding by a second etch stop layer (50 nm) and was covered with a 200 nm thick sacrificial layer of undoped InP. Since bonds strength in InP is lower than in InGaAs [C. Carmody *et al.* 2003] we expect the generation of a high concentration of point defects with relatively low laser fluences in the sacrificial layer. Furthermore, this layer can be selectively etched away after annealing, leaving undamaged InGaAs surface for the fabrication of photonic device on the intermixed material [V. Aimez *et al.* 2002].

We used an ArF excimer laser (λ = 193 nm) which delivered 15 ns pulses of fluence in the range of 68 - 150 mJ/cm^2. The laser beam was homogenized with a double micro-lens fly-eye-array and used to project an image of a rectangular mask on the sample surface. With a computer controlled X-Y-Z positioning of the sample, the setup allowed for the processing of the same sample at

numerous sites, each measuring approximately 1.2 mm x 1.0 mm. The irradiation was carried out in an ambient air environment.

Following the irradiation, the samples were annealed in a RTA furnace under nitrogen atmosphere at 725°C for 2 minutes. Since numerous sites of the same sample could be processed with the laser, the annealing conditions were nominally the same for different sites.

Room temperature photoluminescence (PL) measurements were carried out with a commercial mapper (Philips PLM-150) using an Nd:YAG laser (λ = 1064 nm) as an excitation source and an InGaAs array detector. The composition of the laser modified surface of InP was investigated with an X-ray photoelectron spectroscopy (XPS, Kratos HS system) using a monochromatic Aluminium K_α X-ray source.

Figure 7-1 shows a PL map of the sample that was irradiated with the ArF laser delivering pulses at 95 and 150 mJ/cm^2. The RTA treatment has resulted in the formation of an array of clearly distinguishable sites of different bandgap material. The upper and lower numbers shown for each site indicate pulse number and amplitude of the blue shift, respectively. For example, it can be seen that the 50-pulse-irradiation at 95 mJ/cm^2 achieves a blueshift of 107 nm (shift from 1523 to 1416 nm). For most of the irradiated sites, the sample shows a reasonable lateral uniformity of the PL emission wavelength, with the standard deviation about 2 nm. Previously investigated irradiation of a similar InGaAs/InGaAsP QW heterostructure with 100 mJ/cm^2 pulses delivered by a KrF excimer (248 nm) has demonstrated 50 and 25 nm blue shifts achieved with 1000 and 500 pulses, respectively [J.J. Dubowski 2003]. The dynamics of the current approach are much stronger and, as it is discussed further in this communication, we could observe significantly greater blueshifts achieved with less than the 100-pulse irradiation.

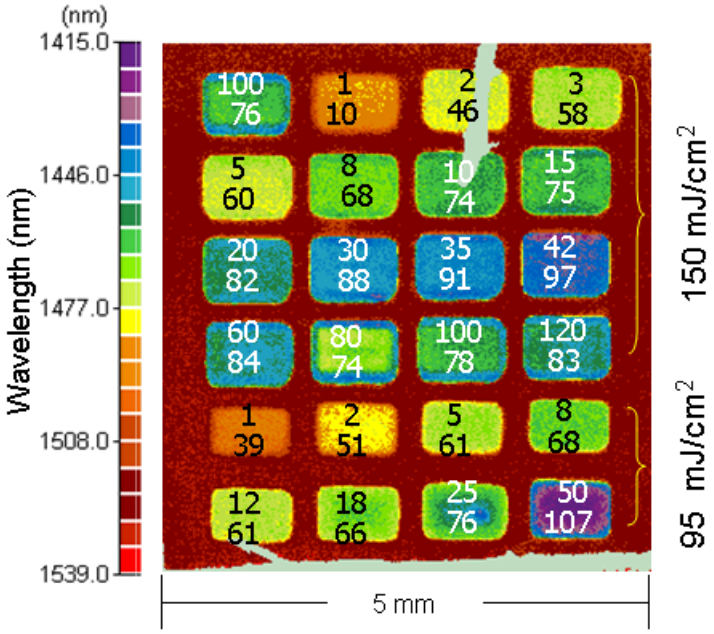

Figure 7-1: Room temperature photoluminescence map of an ArF laser patterned InGaAs/InGaAsP/InP quantum well heterostructure following the annealing at 725°C for 120 seconds. For each site, the upper and lower numbers correspond to the number of laser pulses and blueshift amplitude, respectively.

The formation of a laser generated altered layer, primarily consisting of In_xO_y, has been observed by XPS measurements. Figure 7-2 shows a series of In $3d_{5/2}$ XPS spectra taken from sites on the sacrificial layer that were irradiated at 70 mJ/cm^2 with 10, 50 and 150 pulses. A comparison with the as-grown InP surface clearly indicates the formation of an In_xO_y layer. We have observed that for 90 mJ/cm^2 and N > 50 pulses the oxide layer was thick enough to mask entirely the XPS signal form the bulk InP layer. This indicates that the thickness of the laser created altered layer was at least three time larger than the electron attenuation length in InP, i.e., ~ 2 nm at 1 keV [I.A. Babalola *et al.* 1984], which is comparable to the absorption depth of the 193 nm radiation in InP (α_{ArF} = 1.3 x10^6 cm^{-1}) [1991]. The XPS results have also indicated an increase of the In/P signal with the number of irradiating pulses. The photo-enhanced reaction with the air environment and photoinduced desorption [G.M. Davis *et al.* 1988] are likely

mechanisms responsible for the creation of an altered layer of material, at least for modest laser fluences (< 90 mJ/cm^2). Current results are consistent with the previously reported formation of a group III-oxide layer on the surface of excimer laser irradiated III-V semiconductors [J.J. Dubowski *et al.* 1999]. Also, the formation of a 5.5 nm thick layer of Ga_2O_3 + As_2O_3 was reported on the surface of GaAs irradiated with 1000 pulses of a KrF excimer delivering 100 mJ/cm^2 per pulse [J. Genest *et al.* 2007a].

Figure 7-2: In $3d_{5/2}$ XPS spectra of the reference InP sample and ArF laser exposed sites for N = 10, 50 and 150 pulses at 70 mJ/cm^2.

Figure 7-3 shows the net blue shift dependence on the number of ArF laser pulses and different pulse fluence observed for the investigated InGaAs/InGaAsP QW microstructure. It can be seen that the blue shift amplitude for 68, 75 and 90 mJ/cm^2 increases systematically with increasing pulse number and, with the exception of the 150 mJ/cm^2 data, it has a tendency to saturate at about 100 nm. This suggests that the concentration of defects available for the enhanced intermixing saturates with the increasing dose of laser radiation. The saturation could

be attributed to the formation of defect clusters which act as traps for point defects, preventing them from diffusing toward the active region and participating in the intermixing process [S. Charbonneau *et al.* 1998]. Additionally, a reduced efficiency of defect formation could take place due to laser-based formation of an In-rich surface [J.J. Dubowski *et al.* 1996]. The results for 90 mJ/cm^2 ($0 < N \leq 25$) and 150 mJ/cm^2 ($0 < N \leq 5$) observed in figure 7-2 seem to confirm this result. We link the saturation of the blue shift amplitudes at 70 nm, observed for 90 mJ/cm^2, and 50 nm, observed for 150 mJ/cm^2, with the appearance of a 'metallic' surface that leads to an increased reflection of the laser beam. The formation of such a surface prevents further development of the alternate layer. However, continuous irradiation in an air environment is also expected to lead to the oxidation of indium and the formation of a thick layer of In_xO_y, as confirmed by our XPS measurements. The reduced amplitude of the blue shift observed for 150 mJ/cm^2 is likely related to the reduced 'reservoir' of laser created defects. Profilometry measurements (not shown) have indicated that material ablation takes place for high irradiation doses. At 150 mJ/cm^2, more than 140 nm of the sacrificial layer was removed with 500 pulses. Following such treatment, we have observed that the blue shift amplitude was reduced by 50 % in comparison to its maximum value. For the case reported in figure 7-2, approximately 14 nm of InP was removed with 50 pulses, and the maximum blueshift amplitude diminished to 90 nm. Thus, our results suggest that the laser irradiation of the InP surface leads to metallisation, oxidation and a slow removal of the oxidized film.

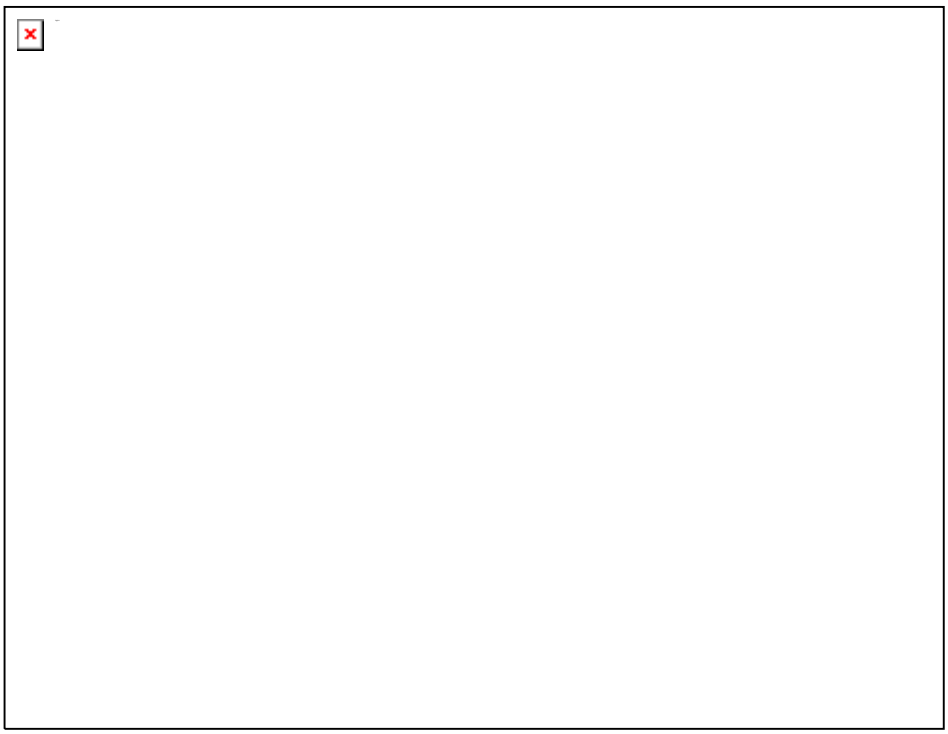

Figure 7-3: Dependence of the net blue shift amplitude on the number of ArF pulses delivered at 68, 75, 90 and 150 mJ/cm2. Solid lines correspond to the theoretically calculated dependences described by Eq. 1. The last two data points at 150 mJ/cm2 were not considered in the fitting procedure.

Using a finite element model of the heterostructure, we were able to extract the intermixing coefficient from the photoluminescence blueshift. The properties of quaternary materials $In_xGa_{1-x}As_yP_{1-y}$ were extracted using Mei's interpolation technique [T. Mei 2007] assuming they were lattice matched on InP. We also assumed the conservation of the lattice matching in the intermixed material so that x = 1 - 0.47y. This assures a maximum 0.032% strain with the InP substrate [S. Adachi 1982]. Therefore, we can express the QWI process with a single intermixing coefficient, D_{III}. For different diffusion lengths $L_{d_{III}} = \sqrt{D_{III}\Delta t}$, where Δt is the diffusion time, the calculation determined the intermixed concentration and energy bands profiles. We solved, for both types of charge carriers, the Schrödinger equation inside the intermixed well to calculate the confined energy levels. The RTA experiments carried out for the as-grown material yielded the intrinsic diffusion coefficient, D_0, equal to $2.1 \pm 0.8 \times 10^{-17}\,cm^2/s$.

This value is almost 50% smaller than $D_0 = 3.7 \times 10^{-17}\,\mathrm{cm}^2/\mathrm{s}$ observed for a similar material system [O. Gunawan *et al.* 2000], which suggests a thermally more stable microstructure investigated in this communication. We describe the intermixing process by a phenomenological model of the radiation-assisted diffusion [H.S. Djie *et al.* 2006b]. In such a case, the intermixing coefficient, D_{III}, is enhanced by the presence of laser created point defects in the QW vicinity, and it can be described by the following formula:

$$D_{III} = D_0 + \sum_{i=1}^{M} D_i \left(1 - e^{-k_i\left(N - N_{th_i}\right)}\right), \text{ with } N > N_{th_1}, \qquad (7.1)$$

where D_i is the defect-enhanced intermixing coefficient, k_i is the pulse dependent rate of defect generation and N and N_{thi} are the total and incubation number of pulses, respectively. Experimental data shown in figure 7-3 have been described reasonably well with solid and dotted lines representing a difference between the total and intrinsic intermixing coefficients ($D_{III} - D_0$). It can also be seen that for 90 and 150 mJ/cm^2 no threshold for initiation of the blue shift was observed ($N_{thi} = 0$). However, 4 and 5 pulses were required to initiate blueshifting for fluences of 68 and 75 mJ/cm^2, respectively. The maximum value of the total intermixing coefficient has been determined to be $D_{\max} = 3.4 \pm 0.4 \times 10^{-16}\,\mathrm{cm}^2/\mathrm{s}$. This value is almost 7 times smaller than $D_{tot} = 2.3 \pm 0.4 \times 10^{-15}\,\mathrm{cm}^2/\mathrm{s}$ that was observed for a similar material system irradiated with a Q-switch Nd:YAG laser [O. Gunawan *et al.* 2000]. This difference could be related to the increased thermal stability of our material. The fast dynamics of defect generation with the 193 nm excimer, however, is clearly demonstrated in figure 7-3. It takes less than 100 pulses to saturate the blueshift amplitude, while it required more than 2000 pulses and significantly greater pulse fluences to achieve the blueshift saturation in a similar QW microstructure irradiated with a pulse Nd:YAG laser [O. Gunawan *et al.* 2000]. The corresponding defect generation coefficients for the first regime (k_1) are 0.01, 0.02, 0.35 and 0.39 for 68, 75, 90 and 150 mJ/cm^2, respectively.

For 90 and 150 mJ/cm^2, k_2 values are 0.08 and 0.11, respectively. A reduced maximum value of the total intermixing coefficient $D_{\max} = 1.92 \pm 0.02 \times 10^{-16}\,\mathrm{cm}^2/\mathrm{s}$ that was obtained for 150 mJ/cm^2, is likely related to the partial removal of the sacrificial layer. In comparison to the pulsed Nd:YAG laser experiments [O. Gunawan *et al.* 2000], our results showed drastically increased rates of defect formation. Thus, the results presented here suggest that a short-wavelength excimer laser irradiation has the potential to offer a highly efficient method of QWI.

In summary, we have investigated a 193-nm ArF excimer laser defect formation in the sacrificial layer of InP, deposited on top of InGaAs/InGaAsP quantum well heterostructures, as a means to enhance the quantum well intermixing process. The net blue shifts, up to 100 nm, have been observed for irradiation with laser pulse fluences not exceeding 90 mJ/cm^2. For higher fluences, metallization and a partial ablation of the sacrificial layer takes place. This results in a smaller concentration of defects available for the intermixing process and, consequently, leads to the two-step saturation observed in the blueshift amplitude. The quantitative description of the mechanisms involved in this ArF laser induced QWI process still requires detailed analysis, however our results have already indicated the control level of the QWI process and flexibility in the fabrication of multibandgap QW wafers that cannot be matched by other known QWI techniques.

The authors wish to acknowledge useful discussions with Alex Voznyy. This work was supported by the Natural Science Engineering Research Council of Canada and NanoQuébec. JJD is a Canada Research Chair in Quantum Semiconductors.

7.2 References

Adachi, S. (1982) *Material parameters of $In_{1-x}Ga_xAs_yP_{1-y}$ and related binaries*, Journal of Applied Physics, vol. 53, n° 12, 8775-92.

Aimez, V., Beauvais, J., et al. (2002) *Low-energy ion-implantation-induced quantum-well intermixing*, IEEE Journal of Selected Topics in Quantum Electronics, vol. 8, n° 4, 870-879.

Anonymous (1991). *Properties of indium phosphide*, London ; New York, INSPEC, 495 p.

Babalola, I. A., Petro, W. G., et al. (1984) *The Ag-InP(110) interface: Photoemission studies of interfacial reactions and Schottky-barrier formation*, Physical Review B, vol. 29, n° 12, 6614.

Carmody, C., Tan, H. H., et al. (2003) *Influence of cap layer on implantation induced interdiffusion in InP/InGaAs quantum wells*, Journal of Applied Physics, vol. 93, n° 8, 4468-70.

Charbonneau, S., Koteles, E. S., et al. (1998) *Photonic integrated circuits fabricated using ion implantation*, IEEE Journal of Selected Topics in Quantum Electronics, vol. 4, n° 4, 772-793.

Davis, G. M., Thomas, D. W., et al. (1988) *Excimer laser direct etching of GaAs*, Journal of Physics D: Applied Physics, vol. n° 5, 683.

Djie, H. S., Ooi, B. S., et al. (2006) *Quantum dot intermixing using excimer laser irradiation*, Applied Physics Letters, vol. 89, n° 8, 081901.

Dubowski, J. J. (2003) *Laser-induced bandgap shifting for photonic device integration*, U.S. 6,670,644.

Dubowski, J. J., Julier, M., et al. (1996). *Laser-assisted dry etching ablation for microstructuring of III-V semiconductors*, Boston, MA, USA, Mater. Res. Soc. Proc.

Dubowski, J. J., Poole, P. J., et al. (1999) *Enhanced quantum-well photoluminescence in InGaAs/InGaAsP heterostructures following excimer-laser-assisted surface processing*, Applied Physics A: Materials Science & Processing, vol. 69, n° 7, S299.

Genest, J., Dubowski, J. J., et al. (2007a) *Suppressed intermixing in InAlGaAs/ AlGaAs/GaAs and AlGaAs/GaAs quantum well heterostructures irradiated with a KrF excimer laser*, Applied Physics A: Materials Science & Processing, vol. 89, n° 2, 423-426.

Genest, J., Dubowski, J. J., et al. (2007b) *UV laser controlled quantum well intermixing in InAlGaAs/GaAs heterostructures*, Journal of Physics: Conference Series, vol. 59, n° 1, 605-9.

Guido, L. J., Jackson, G. S., et al. (1987) *Index-Guided $Al_xGa_{1-XA}s$-GaAs Quantum-Well Heterostructure Lasers Fabricated by Vacancy-Enhanced Impurity-Induced Layer Disordering from an Internal $(Si_2)_Y(GaAs)_{1-Y}$ Source*, Applied Physics Letters, vol. 50, n° 10, 609-611.

Gunawan, O., Ong, T. K., et al. (2000). *A theoretical analysis of quantum well intermixing using the pulsed laser irradiation technique in InGaAs/InGaAsP laser structure*, Beijing, China, Elsevier.

Li, E. H., Ed. (2000). Semiconductor Quantum Wells Intermixing. Optoelectronic Properties of Semiconductors and Superlattices. Amsterdam, Netherlands, Gordon and Breach Science Publishers, 695 p.

Marsh, J. H. (1993) *Quantum-Well Intermixing*, Semiconductor Science and Technology, vol. 8, n° 6, 1136-1155.

Mei, T. (2007) *Interpolation of quaternary III-V alloy parameters with surface bowing estimations*, Journal of Applied Physics, vol. 101, n° 1, 013520-6.

Shimada, N., Fukumoto, Y., et al. (2004) *Monolithic integration of lasers and passive elements using selective QW disordering by rapid thermal annealing with SiO_2 caps of different thicknesses*, Electronics and Communications in Japan (Part II: Electronics), vol. 87, n° 1, 34-42.

Yu, J. S., Song, J. D., et al. (2002) *Influence of dielectric deposition parameters on the $In_{0.2}Ga_{0.8}As/GaAs$ quantum well intermixing by impurity-free vacancy disordering*, Journal of Applied Physics, vol. 92, n° 3, 1386-1390.

Chapter 8: UV-QWI under particular irradiation conditions and applications

This chapter discusses the effect of irradiation conditions on UV-QWI and demonstrates the applicability of UV-QWI for the fabrication of high quality intermixed optoelectronic devices. The first part of this chapter presents the influence of the environment in which the UV laser irradiation is carried out. The effect of physisorbed water vapour on GaAs photo-enhanced oxidation is described, as well as is its effect on the quantum well intermixing. The second part presents recent advances on enhanced quantum well intermixing in InP based heterostructures achieved by excimer laser irradiation. The different effects between ArF and KrF laser irradiation, the influence of the nature of the surface layer and the effect of ion implantation prior to the irradiation are discussed. The characteristics of laser diodes fabricated from the irradiated material are also presented. Finally, in the third section, I present the effect of ArF laser irradiation on quantum dot intermixing in the InAs/InP system.

UV laser irradiation of GaAs in different atmospheres

One of the main advantages of UV laser is that it can activate chemical reactions at the surface of a sample. Depending on the environment in which a sample is irradiated, the UV light can favour the etching of a specific compound or atomic specie; it can also alter the chemistry of the surface and grow a thin layer of a different material. In chapters 5 and 6, I have demonstrated that exposing GaAs based heterostructure to KrF laser pulses in air environment induces the formation or a gallium rich oxide layer and suppress quantum intermixing. However, the process by which the UV photons enhance the GaAs oxidation was not identified. We hypothesised, as

Yu suggested [C.F. Yu *et al.* 1987], that the process was mainly governed by the interaction of physisorbed water vapour on the GaAs surface with photo-excited charge carriers.

To test this and to assess the influence of a neutral environment on the sample surface chemistry, we irradiated InAlGaAs/AlGaAs/GaAs samples in a controlled environment chamber with KrF (248 nm) pulses. We pumped the chamber to reach a pressure of 0.01 mbar before injecting the reactive or neutral gas. After a pressure of 1013 mbar was attained, we fired up the laser for 1000 pulses at 100 mJ/cm^2. The irradiations were done under air, vacuum, nitrogen, oxygen and ammonia while a sample was irradiated under a film of deionized water. We then studied the surface chemistry with x-ray photoelectron spectroscopy (XPS) with a monochromatic aluminium K_α x-ray source. The atomic concentration of Ga, As and O were measured by analysing the Ga 3d, As 3d and O 1s photoelectron spectra. We also looked for trace of nitridation in the sample irradiated in ammonia.

8.1.1 Photoenhanced oxidation under different atmospheres

After irradiation, all samples showed an unaltered mirror like surface except the sample irradiated in deionized water which showed a more brownish coloration. XPS results obtain on GaAs quantum heterostructures supports that the UV laser enhanced oxidation is governed by H_2O instead of O_2. Samples irradiated in controlled environment (vacuum, N_2, O_2 and NH_3) all show a similar GaAs oxidation (figure 8-1a-b). On the other hand samples irradiated in air show a huge increase of their oxygen concentration. Samples irradiated in water show an even higher oxidation than in air: the Ga 3d peak bond to As is invisible while the oxide peak is too broad to be able to identify the oxide nature (figure 8-2). Laser induced surface temperature also seems to be high enough to allow the decomposition of all the As_2O_5 in As_2O_3 and O_2 at temperatures higher than 315°C. The temperature increase also favours the transformation of As_2O_3 in Ga_2O_3

and amorphous As (figure 8-1b) as described in equation (8.1) [C.D. Thurmond *et al.* 1980]. No nitridation was observed on the sample irradiated in nitrogen.

$$2\ GaAs + As_2O_3 = G_2O_3 + 4\ As \qquad (8.1)$$

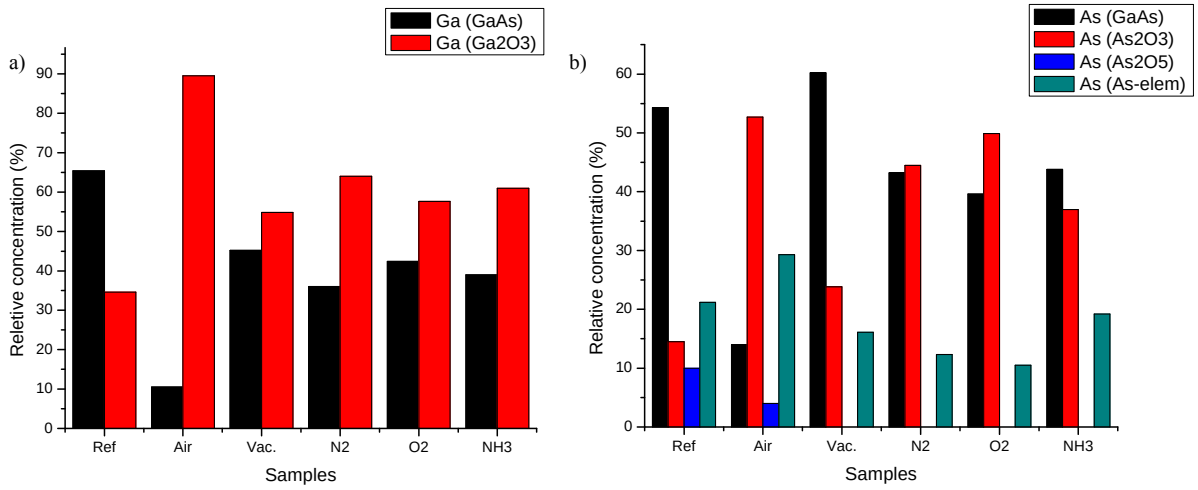

Figure 8-1: **XPS results on GaAs samples a) Ga 3d intensities and b) As 3d intensities after KrF irradiation in different atmosphere.**

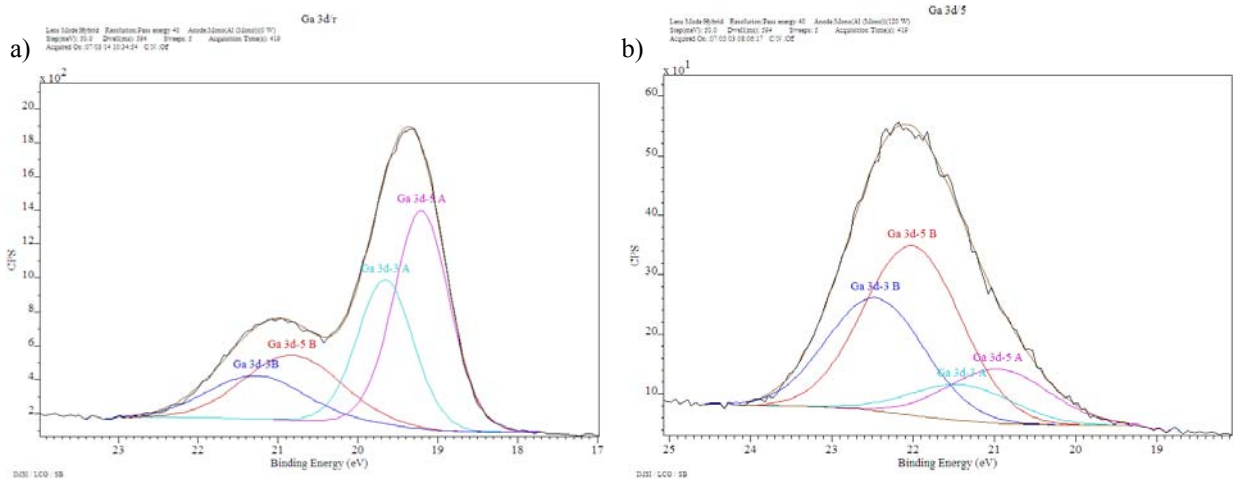

Figure 8-2: XPS spectra for a) reference GaAs and b) GaAs irradiated with KrF pulses in deionized water

8.1.2 Influence of irradiation under neutral atmospheres on the intermixing extent

We also tested the effect of the processing gas on the quantum well extent. As described earlier, we exposed InAlGaAs/AlGaAs/GaAs samples to KrF laser pulses under relative vacuum

(p < 1x10^{-2} mbar) and nitrogen (p ~ 1013 mbar) atmospheres. We then annealed the irradiated samples and an untreated sample in a rapid thermal processor for 60 s at 900°C. We used low temperature (20K) photoluminescence (PL) to characterize the intermixing extent. A frequency doubled Nd:YAG laser (λ = 532 nm) was used to excite the samples while the PL signal was dispersed by a monochromator and detected by a photomultiplier. Figure 8-3 presents the PL spectra for the different irradiation conditions.

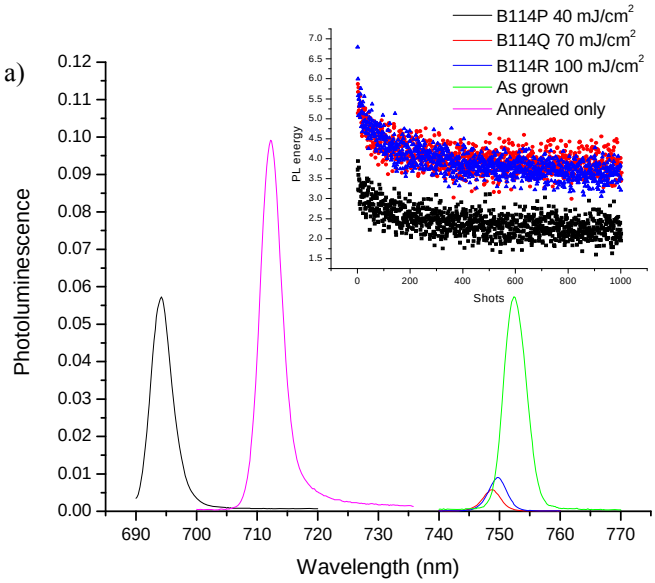

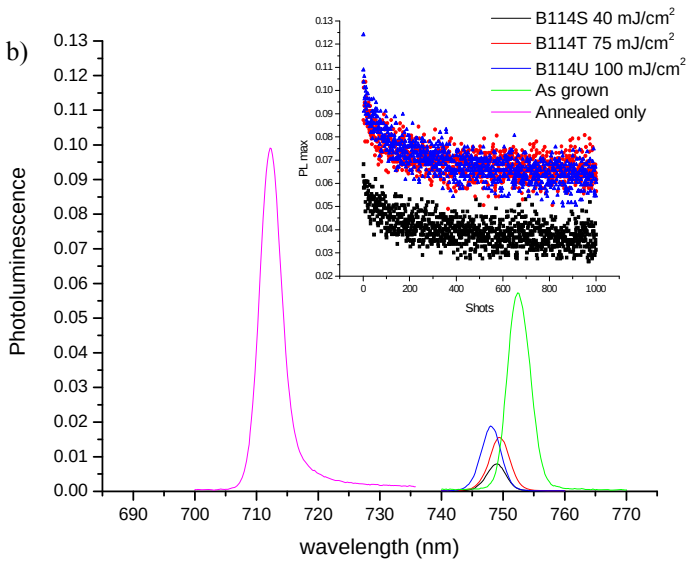

Figure 8-3: Low temperature (20 K) photoluminescence spectra of EW600606 samples irradiated with KrF laser pulses in a) vacuum and b) nitrogen environment. The insets are the UV excited photoluminescence intensities as a function of the number of pulse.

Compared to the reference sample, the annealed-only sample demonstrated a 40 nm blueshift and an almost two fold increase of the photoluminescence signal (figure 8-3). Under vacuum, only the sample irradiated with a fluence of 40 mJ/cm^2 showed a significant blueshit (58 nm). The samples exposed to higher fluences demonstrated a blueshift extent inferior to 5 nm while the photoluminescence intensity was reduced of an order of magnitude (figure 8-3a). From all the samples irradiated in nitrogen, none showed any significant blueshift. Again the blueshift extent was inferior to 5 nm (figure 8-3b). The photoluminescence intensity from theses samples dropped by 66% for the sample exposed to a fluence of 100 mJ/cm^2 to 85% for one irradiated at 40 mJ/cm^2. In contrast with the samples irradiated in air environment (chapter 4), the UV excited photoluminescence signal didn't show any increase as the number of pulse increase. The insets in figure 8-3 illustrates that it only decreased following an exponential decay form.

As mentioned in the previous section, XPS results from samples irradiated in vacuum, nitrogen, oxygen and ammonia all showed similar enhanced oxidation. Although the oxidation

level is smaller than for irradiation in air, the oxide layer might be thick enough to prevent point defects generated in the surface vicinity to diffuse and to generate the intermixing. The photo-enhanced oxidation due the remaining physisorbed water vapour can explain the suppression of quantum well intermixing. For both irradiation environments, the intermixing suppression is comparable to the one obtained in air environment. The resulting ~5 nm of blueshift is then probably caused by the in-grown point defects located far from the surface and which diffuse during the annealing.

However, the presence of the GaAs oxide grown under UV laser irradiation cannot explain the enhanced blueshift obtained in vacuum under 40 mJ/cm^2 laser irradiation. It also cannot explain the photoluminescence signal quenching for higher fluences. Under vacuum or neutral gas, UV photons cannot activate any chemical reaction at the sample surface. All the energy is then transferred in desorption processes, which under small extent generates new point defects but can induce surface damage under large extent. This explains the enhanced blueshift observed for the sample irradiated in vacuum at 40 mJ/cm^2. The induced surface damage explains the photoluminescence signal quenching for higher fluences: the damage sites act as trap center for the excited charge carrier and of as absorption sites for the emitted photoluminescence [I.H. Campbell *et al.* 1990]. It can also participate to the suppression of quantum well intermixing by trapping mobile point defects and preventing their diffusion toward the active region.

8.2 Advancements on UV laser controlled quantum well intermixing in InP based heterostructures

In chapter 7, we have seen that patterned ArF laser irradiation is an efficient tool to fabricate multi-bandgap samples in InP-based laser heterostructure. To better understand the UV laser controlled quantum well intermixing in this type of heterostructure and in a goal to optimize

the technique, we irradiated M0062 samples (heterostructure details in figure 4-9, page 109) under different laser conditions and different top layers. We also fabricated laser diodes from the intermixed material to study its potential to manufacture monolithic photonic integrated circuits.

8.2.1 Comparison between KrF and ArF laser irradiations

As described in chapter 3, one of the most important irradiation parameters is the laser wavelength. Not only does it changes how the charge carriers are excited [D.V. Podlesnik *et al.* 1986], but it also drastically changes the reflection coefficient [D.E. Aspnes *et al.* 1983] and the photon absorption length [H.R. Philipp *et al.* 1963] in the heterostructure. Because of all theses variation, we expect be huge differences between KrF laser and ArF laser controlled quantum well intermixing. One of the two lasers must also be more efficient to generate new point defects and therefore enhance the quantum well intermixing in InP based heterostructure.

To investigate this scenario, we irradiated M0062 samples directly in air environment with KrF (λ = 248 nm, pulse length τ = 25 ns) and ArF (λ = 193 mm, pulse length τ = 15 ns) for fluences F varying between 50 mJ/cm^2 and 200 mJ/cm^2 and number of pulses up to 2000. Because we used two different setups, samples irradiated with KrF laser were exposed over their whole surface while those irradiated with ArF were exposed in multiple areas of 1.2 X 1 mm^2. The estimate absorption depth at those wavelengths are comparable, ~5nm and ~8 nm in InP, for KrF and ArF laser respectively (α_{KrF} = 2 x10^6 cm^{-1}, α_{ArF} = 1.3 x10^6 cm^{-1}). All optical properties of InP under 193 nm photons were extrapolated from Aspnes measurements [D.E. Aspnes *et al.* 1983]. Under these irradiations conditions, we expect the surface to show an altered morphology and chemistry due to the photoinduced desorption and reaction with the air environment [G.M. Davis *et al.* 1988].

The samples were subsequently annealed in a rapid thermal processor under nitrogen atmosphere at 725°C for 2 minutes. An unirradiated sample was also annealed to measure the extent of thermal shift. Room temperature photoluminescence mapping (PL) was carried out with a Nd:YAG laser (λ = 1064 nm) for excitation while PL signal was dispersed by a monochromator and collected by an InGaAs array detector. We used the same model as described in chapter 5 to calculate the interdiffusion coefficient from photoluminescence shift.

Samples irradiated with KrF laser at fluences lower than 140 mJ/cm^2 didn't show an increase in the interdiffusion coefficient compare to the annealed only sample (figure 8-4a). In addition to the two regimes that we have indentified for ArF irradiation, generation and suppression, we identified a third one, incubation, which occurs for low number of pulses prior to the generation regime and where no change in the interdiffusion coefficient was observable. The maximum photoluminescence shift attained was 127 nm and it was obtained for 500 pulses at 190 mJ/cm^2. As a comparison tool, figure 8-4b shows the ArF induced changes in the interdiffusion coefficient presented in chapter 7.

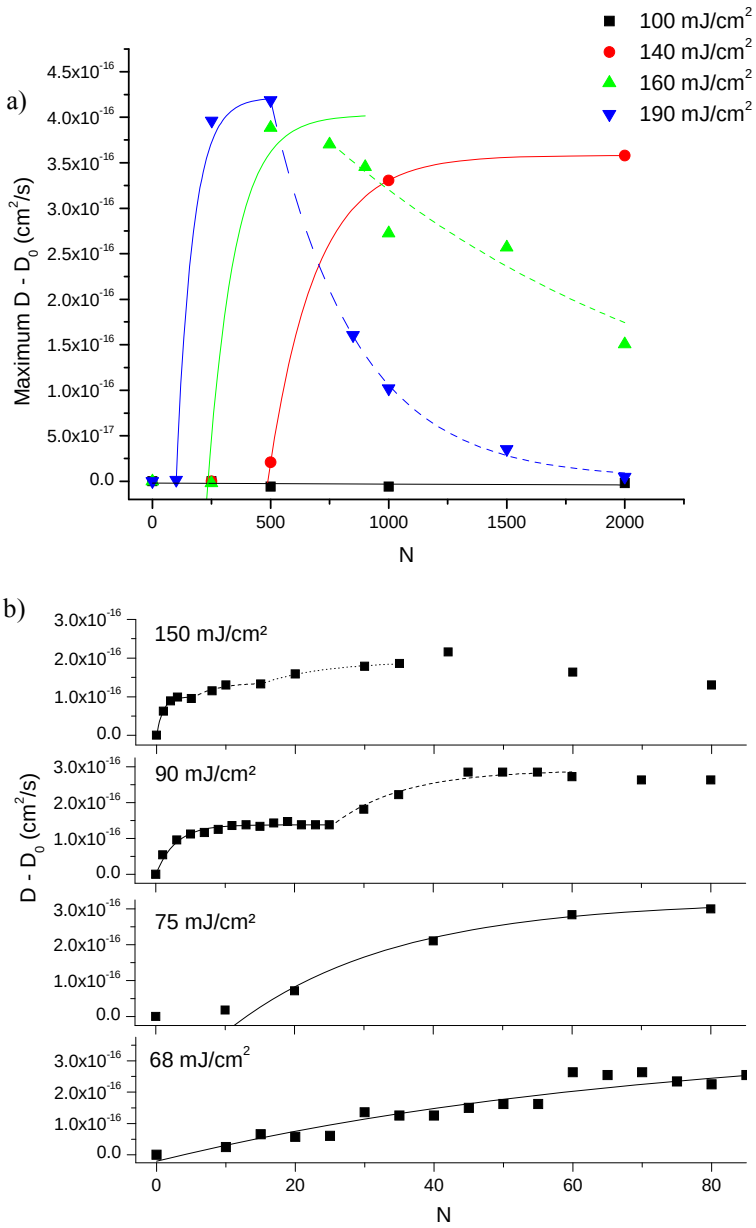

Figure 8-4: Dependence of interdiffusion coefficient amplitude for a)KrF and b) ArF irradiated InGaAs/InGaAsP/InP quantum well heterostructures at four different fluences and after their RTA at 725°C for 120 seconds. The full curves correspond to the phenomenological model.

We used same phenomenological model to describe the point defect generation process observed in M0062 samples irradiated with KrF laser pulses:

$$D = D_0 + \sum_{i=1}^{M} D_i \left(1 - e^{-k_i\left(N - N_{th_i}\right)}\right), \text{ with } N > N_{th_0}, \tag{8.2}$$

where D_0 is the intrinsic diffusion coefficient obtained from the only annealed sample, D_i is the diffusion component due to the generated defects, k_i is the defect generation rate and is dependant of the laser fluence and N and N_{thi} are the number of pulses and the incubation threshold respectively. Because we only observed a single generation process for KrF irradiation, $M = 1$ and equation (8.2) becomes:

$$D = D_0 + D\left(1 - e^{-k(N - N_{th})}\right), \text{ with } N > N_{th}. \tag{8.3}$$

Figure 8-5 compares the defects generation rate k evolution for ArF and KrF irradiation. For both lasers, it follows a linear relationship with the fluence. The generation rate is two orders of magnitude higher for ArF laser than for the KrF laser. The smaller energy required to achieve blueshift can be associated with the smaller normal incidence reflection coefficient of InP at 193 nm, $R_{193} = 0.37$, than at 248, $R_{248} = 0.61$ [D.E. Aspnes *et al.* 1983], but it cannot be held responsible itself for this difference. It is also probable that the required energy to break an InP bond, which is of the order of 6.7 eV [W. Hayes *et al.* 2004], corresponds to the energy of a single ArF photon, but of two KrF photons.

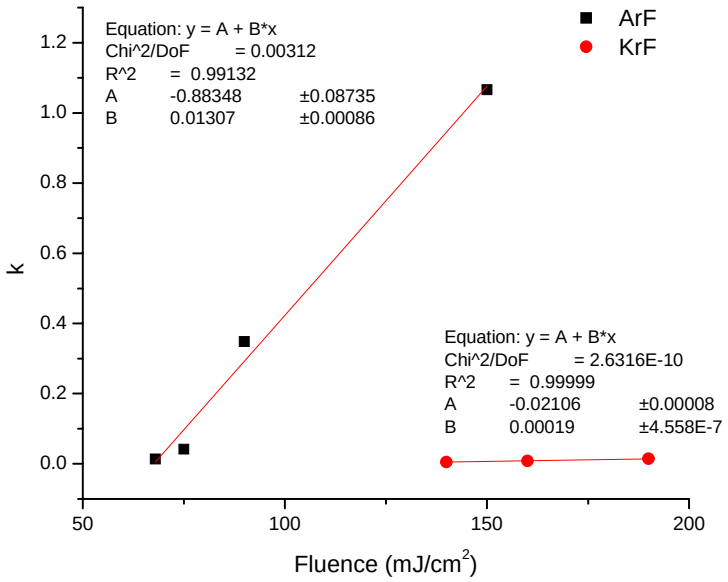

Figure 8-5: Defects generation rates for the first defect creation process of ArF and for KrF irradiations.

All KrF irradiated blueshifted samples demonstrated the presence of hot spots where blueshift increases, suppression and surface ablation would happen at faster rate (figure 8-6). Since this effect is not reproducible from one sample to another, it cannot be related to laser beam non uniformity. In contrast, ArF irradiated samples demonstrated a higher surface uniformity; the appearance of hot spot was observed very rarely and never at fluences higher than 75 mJ/cm^2.

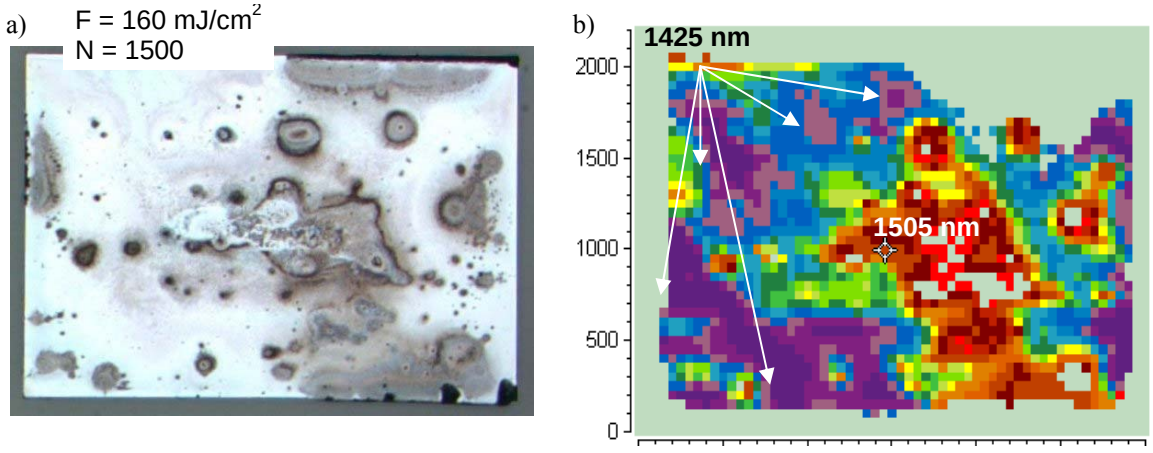

Figure 8-6: a) Photograph and b) photoluminescence mapping of a KrF irradiated and annealed M0062 sample. The presence of hot spots is clearly visible on both pictures.

KrF laser absorption in InP seems to be more affected by surface scattering due to deposited particles or surface defects and therefore more subject to form hot spots. In contrast, ArF laser treated samples showed high lateral uniformity; the standard deviation was about 2 nm in an irradiated area. However, at high number of shots the ablation debris on the edges of the irradiated sites reduces the laser absorption in this region resulting in a different interdiffusion rate on the edge than in the center [D. Basting *et al.* 2005]. Excimer lasers have been used in numerous applications as tool to clean surfaces of materials. ArF is a more likely efficient cleaning tool on InP surface than KrF laser which would explain the difference in lateral uniformity.

8.2.2 ArF controlled quantum well intermixing reproducibility

Up to now, one of the key issues for quantum well intermixing have been lack of reproducibility [M. Buda *et al.* 2002]. To test the reproducibility of the ArF enhanced quantum well intermixing technique, we irradiated a single M0062-2 ~5x5 mm^2 sample with an ArF laser at a fluence of 100 mJ/cm^2 for 5, 10 and 25 pulses. The irradiation was done over four different sites using the same parameters. The sample was then annealed at 725°C for 120 seconds. Because all irradiation sites were on the same sample, we assumed that the annealing conditions variation from site to site could be neglected.

Table 8-1 shows the evolution of the shift reproducibility for the three different numbers of pulses. The relative standard deviation measured went down from 4.5 % after 5 pulses to 0.7% after 25 pulses. The best standard deviation, 0.9, was achieved for 25 pulses. In the latter case, we obtained a 124.8 nm blueshift. Because the laser fluctuations average themselves over large number of pulses, the shift reproducibility increases as the number of pulses increases. This is due to the laser intensity fluctuation form pulse to pulse which has been measured to 10-15 %. To

our knowledge, no exhaustive studies were published on QWI reproducibility in InP-based materials. The general consensus is that most QWI techniques have poor reproducibility, especially from run to run experiments and that it depends a lot on the studied heterostructure.

Table 8-1 : Statistics for different number of pulses

	5	10	25
Median (nm)	1437.9	1432.3	1415.2
Average (nm)	1437.1	1433.7	1415.1
Shift (nm)	102.1	107.7	124.8
Stand. Dev. (nm)	4.6	3.3	0.9
Rel. Dev.	4.5%	3.1%	0.7%

8.2.3 Influence of the top layer during ArF irradiation

As the most exposed layer of a heterostructure, the top layer composition has a huge influence on the fabrication process. As seen in chapter 2, the laser-mater interaction volume depends on the absorption coefficient of the top material and the deposited energy depends partly of its reflection coefficient. However, these parameters are not the only ones which influence QWI. The bond energy, amorphization threshold and doping levels influence the defect generation mechanism and the intermixing saturation [O. Gunawan *et al.* 2000, M. Chicoine *et al.* 2003].

8.2.3.1 InGaAs contact layer

To test the influence of the replacement of the InP sacrificial top layer with the InGaAs contact layer, we chemically etch away the InP sacrificial layer by dipping a M0062 sample (details in figure 4-9, page 109) in a H_3PO_4:HCl (1:1) solution for 10 second. The sample was then rinsed in de-ionized water and dried with nitrogen. We then irradiated the sample in 15 sites at fluences ranging from 95 to 145 mJ/cm^2 and for number of pulses going from 10 to 100. We annealed the sample at 725°C for 120 seconds and measure the blueshift by room temperature

photoluminescence mapping. A frequency doubled Nd:YAG laser (λ = 532 nm) was used to excite the samples.

The first information obtained from the photoluminescence map was the non-uniformity of the blueshift in the regions not exposed to the laser (figure 8-7). The amount of thermal shift was also higher than 25 nm. Interestingly, irradiation for small number of pulses induced less blueshift than in the untreated areas. The highest blueshift value (110 nm) was attained at 145 mJ/cm^2 for the highest number of pulses. Moreover the lateral uniformity was lower than for the irradiation in InP which was even lower for 95 and 127 mJ/cm^2 fluences.

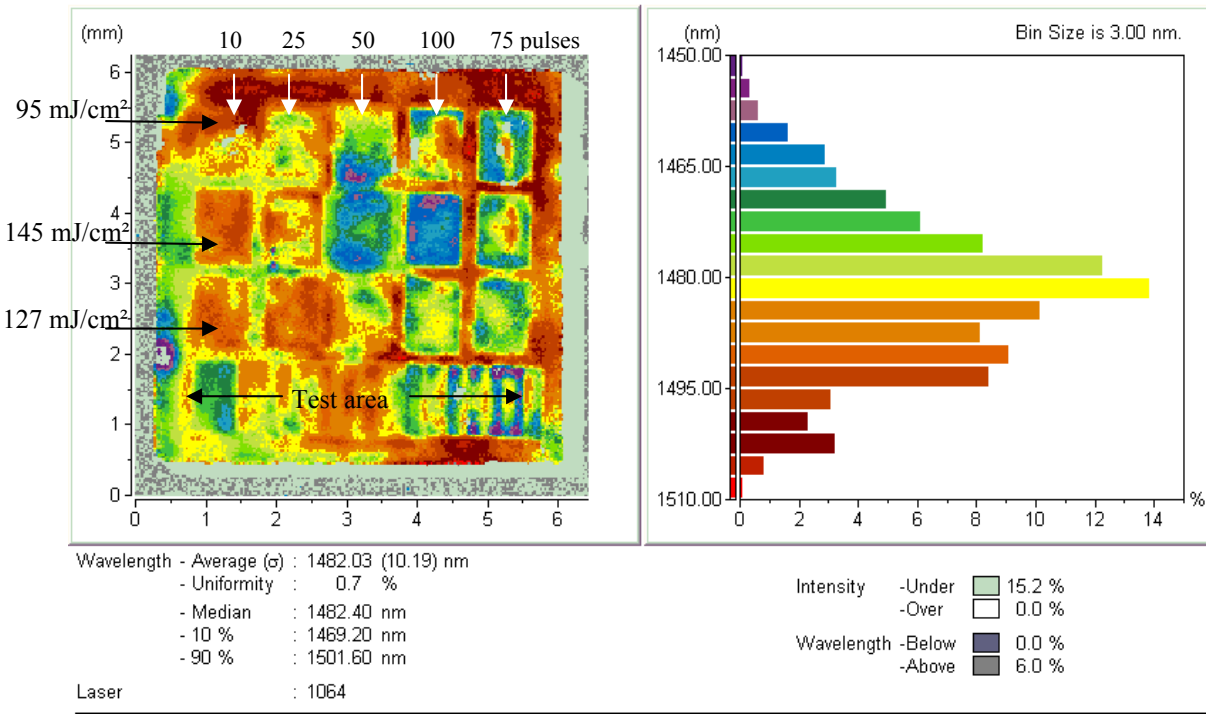

Figure 8-7: Photoluminescence mapping of a M0062 sample on witch the sacrificial layer was removed prior to the irradiation and annealing.

We suspect that the high blueshift value for the unexposed regions and the overall lateral non-uniformity is due to the poor surface quality obtained by the etching solution. Even though this solution is known to be selective on InGaAs, a few monolayers of the contact layer might

have been etched by the solution which would result in the creation of surface point defects. Furthermore, the poor quality surface can scatter the laser light more efficiently and favor the formation of hot spots which would increase the lateral non-uniformity.

Although very little is known about the influence of the nature of the heterostructure top layer in UV laser quantum well intermixing, its effect on ion implantation induced intermixing is known. Carmody *et al* have studied its effect on the extent of quantum well intermixing [C. Carmody *et al.* 2003]. They demonstrated that for the same ion dose and acceleration energy, the blueshift was higher in the sample covered with InP compare to those covered with InGaAs. However, in the latter case, the blueshift behavior showed very little dependence on the implantation temperature, while implantation in InP at room temperature demonstrated rapid blueshift saturation and reduction as the dose increased. The In-P bond strength was measured as 198 kJ/mol, while the In-As and Ga-As bond strength are 201 and 210 kJ/mol [C. Carmody *et al.* 2003]. For Se^{+} implantation at room temperature, the amorphization doses of InP, InAs and GaAs were measured to $1.8x10^{13}$, $7x10^{13}$ and $32x10^{13}$ cm^{-2} respectively [W. Wesch *et al.* 1989].

A parallel explanation can be drawn for the ArF laser irradiation of InP and InGaAs. Because of the higher bond strength in InGaAs, the point defects generation rate is slower than in InP for an identical fluence. With InGaAs, there shouldn't be any blueshift saturation and suppression due to the amorphization of the top layer. This should allow us to reach higher values of blueshift. However, because of the similarities of InGaAs and GaAs, irradiation in air environment might favor the growth of an InGaAs oxide which could suppress the intermixing just like in GaAs based heterostructure. The intermixing suppression observed at high fluence and small number of pulses supports this interpretation.

8.2.3.2 Phosphorus implanted InP

We also studied the effect of combined implantation and laser irradiation in InP based heterostructure. To do so, we first implanted a M0062 sample with P^+ ions with an acceleration energy of 350 keV and a dose of $5x10^{14}$ cm^{-2}. During the implantation, the sample was kept at 200°C. We then irradiated the sample with ArF pulses at 100 and 137 mJ/cm^2 for number of pulses going from 1 to 2000. We then annealed the sample in a rapid thermal processor for 2 minutes à 725°C.

The implantation leaded to a 65 nm total blueshift while all the irradiated sites showed a smaller blueshift value (figure 8-8). The maximum suppression achieved was 30 nm for the site exposed to 2000 pulse at 137 mJ/cm^2. This suppression was also accompanied with the growth of a relatively thick altered layer, up to 200 nm, in each irradiation site (not shown).

Figure 8-8 shows than the laser irradiation never added its intermixing enhancing effect to the ion implantation one. We suspect the laser pulse to only contribute to the amorphization of already damaged InP. In such case, each laser pulse creates new traps for point defects located near the surface. The InP amorphization would also support the change of the surface morphology.

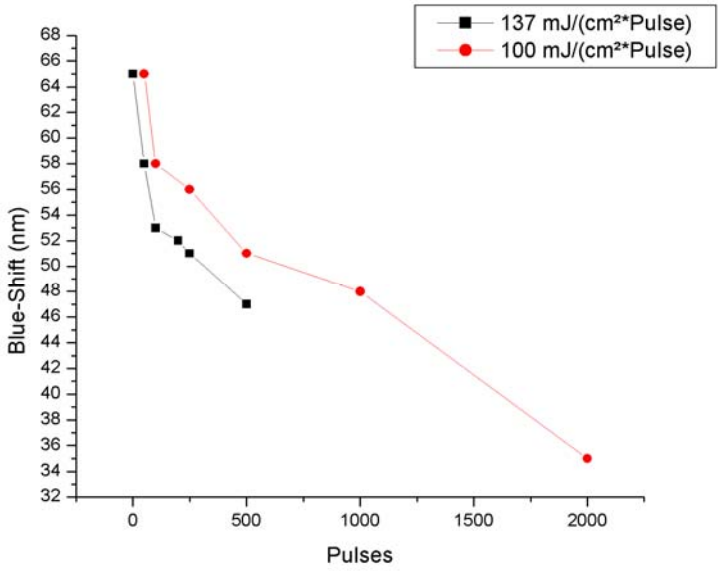

Figure 8-8: Blueshift inhibition in P+ implanted and ArF laser irradiated M0062 sample.

8.2.4 Laser diodes fabricated from intermixed material

Because the UV controlled quantum well intermixing addresses the integration of optoelectronic devices field, it is imperative to test the quality of the intermixed material for the fabrication of functioning devices. To address this, we prepared three M0062 samples, we irradiated half of the surface of a first one with 100 ArF pulses and left the second half untreated. We patterned the second sample on multiple sites by exposing them to various numbers of pulses (1-100). All irradiation were done at a fluence of 150 mJ/cm^2. The third sample was kept as a reference. We then annealed the two first samples (725°C, 120 s) and removed the InP sacrificial layer in an etching solution (H_3PO_4:HCl (1:1), 20 seconds) on the three samples. Table 8-2 describes the fabrication details for the laser diodes. We measured the total emission versus the injected current (L-I) and the emission spectrum above lasing threshold of the fabricated diodes. Figure 8-9 shows the laser diode test setup. A laser diode current source controlled the injected current. The L-I characteristic were taken by directly shining the laser diodes into a germanium

detector while the spectrum measurement were achieved by injecting the laser signal into an optical fiber connected to an optical spectrum analyzer.

Table 8-2: Description of the laser diodes fabrication steps.

Step	Description
1	PECVD[5] deposition of a 200 nm thick SiO_2 layer
2	Spin coating of Shipley 1813 photo-resist
3	Photolithography of 20 µm width injection lines
4	SiO_2 etch in a buffered oxide etchant solution
5	Electron beam evaporation of the front side contact layer: Cr (15 nm), Ti (30 nm), Pd (30 nm) and Au (100 nm)
6	Mechanical thinning and polishing of the samples back sides (t < 150 µm)
7	Electron beam evaporation of the back side contact layer: Au (14 nm), Ge (14 nm), Au (14 nm), Ni (11 nm) and Au (200 nm)
8	Alloy annealing (400°C, 60 seconds)
9	Laser diodes cleave and separation

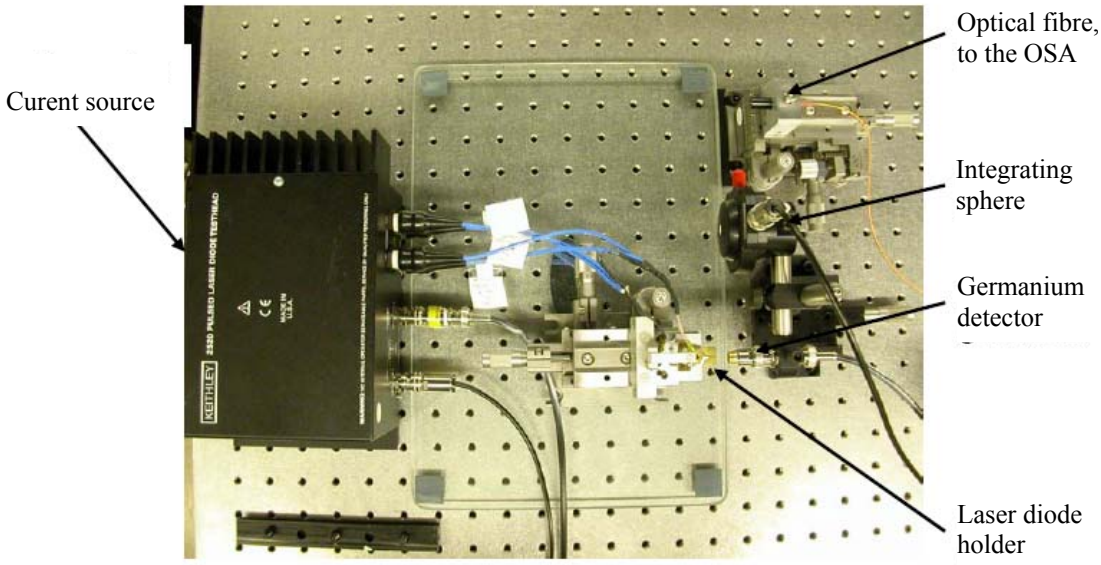

Figure 8-9: Laser diode test setup

The L-I characteristics from the reference and the annealed-only laser diodes demonstrated the same current threshold and the same quantum efficiency. The UV laser treated diodes demonstrated a lower current threshold and similar quantum efficiency than the reference diode (figure 8-10). However, when we raised the current well above the current threshold, the

[5] PECVD: Plasma enhanced chemical vapour deposition

quantum efficiency of intermixed laser diode dropped significantly well below the reference one. The spectrum of the laser diodes shifted toward high energy with the increasing number of pulses. We measured a minimal 15 nm thermal shift between the reference and annealed-only laser diodes while the maximum shift obtained was 120 nm (figure 8-11).

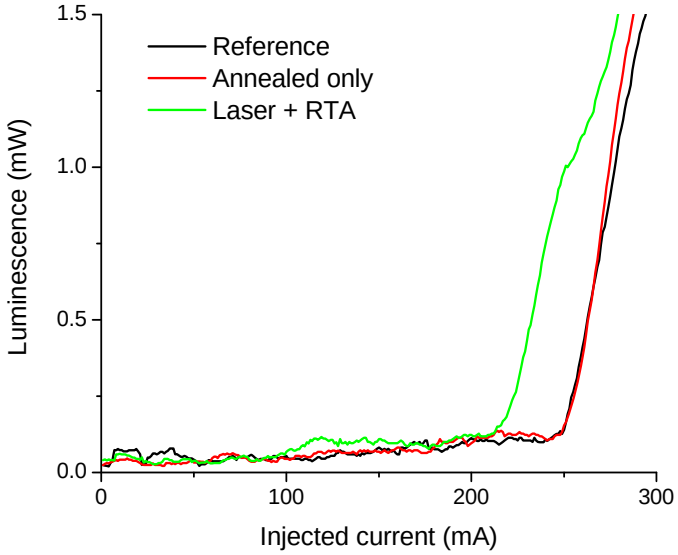

Figure 8-10: L-I characteristics of reference, annealed-only and intermixed laser diodes.

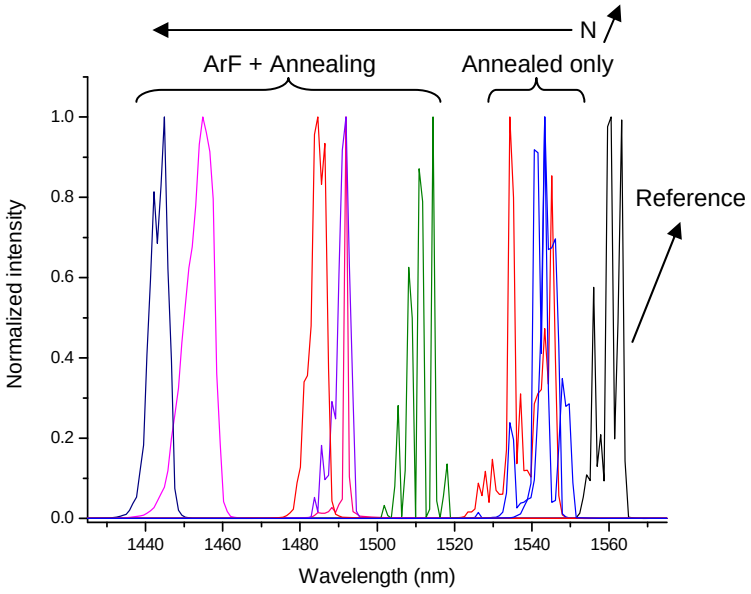

Figure 8-11: UV laser intermixed laser diodes spectra.

The lower current threshold obtained for the intermixed laser diodes demonstrates that UV laser irradiation doesn't generate new charge carriers traps or photon absorption sites near the active region. The quality of the intermixed material is comparable to the one of the reference. The spectra from the intermixed laser diodes also show that by varying the number of pulses, it is possible to cover an important range of emission wavelengths from 1440 to 1560 nm.

8.3 InAs quantum stick intermixing results

Because of their distribution in size and composition, self-assembled InAs quantum sticks (QS) grown of InP substrates emit over broad range of wavelengths around 1.5μm. This makes such material very attractive for biological imaging systems [P.H. Tomlins *et al.* 2005]. InAs/InP quantum sticks could be either used as the gain medium in a tuneable lasers [G. Ortner *et al.* 2006] or as material on which the superluminescent diode could be fabricated [A.W. Sainter *et al.* 2004]. However, despite the intrinsic characteristics of quantum sticks, a broader emission spectrum would allow imaging with a higher resolution and larger tuneability. As in quantum well heterostructures, this can be achieved by selectively tuning the bandgap of the quantum stick heterostructure so that different regions emit at different wavelengths. Here, we propose to achieve a significant blueshift in an InAs/InGaAsP/InP quantum stick laser diode heterostucture by applying the same technique that we have previously applied to the InP-based heterostructure.

We tested this by irradiating in air environment a C342, a complete laser structure, sample (description available in figure 4-11, page 110) for fluences ranging from 68 to 82 mJ/cm^2 and for number of pulses going from 1 to 50. We then annealed the sample at 725°C for 120 seconds and measure the blueshift extent by room temperature photoluminescence mapping.

After laser irradiation, we observed a weak red-shift (~1 nm) in the irradiation sites (figure 8-12). We measured a thermal blueshift of 25 nm while the maximum blueshift (thermal + UV enhanced) is of 50 nm (figure 8-13) after annealing.

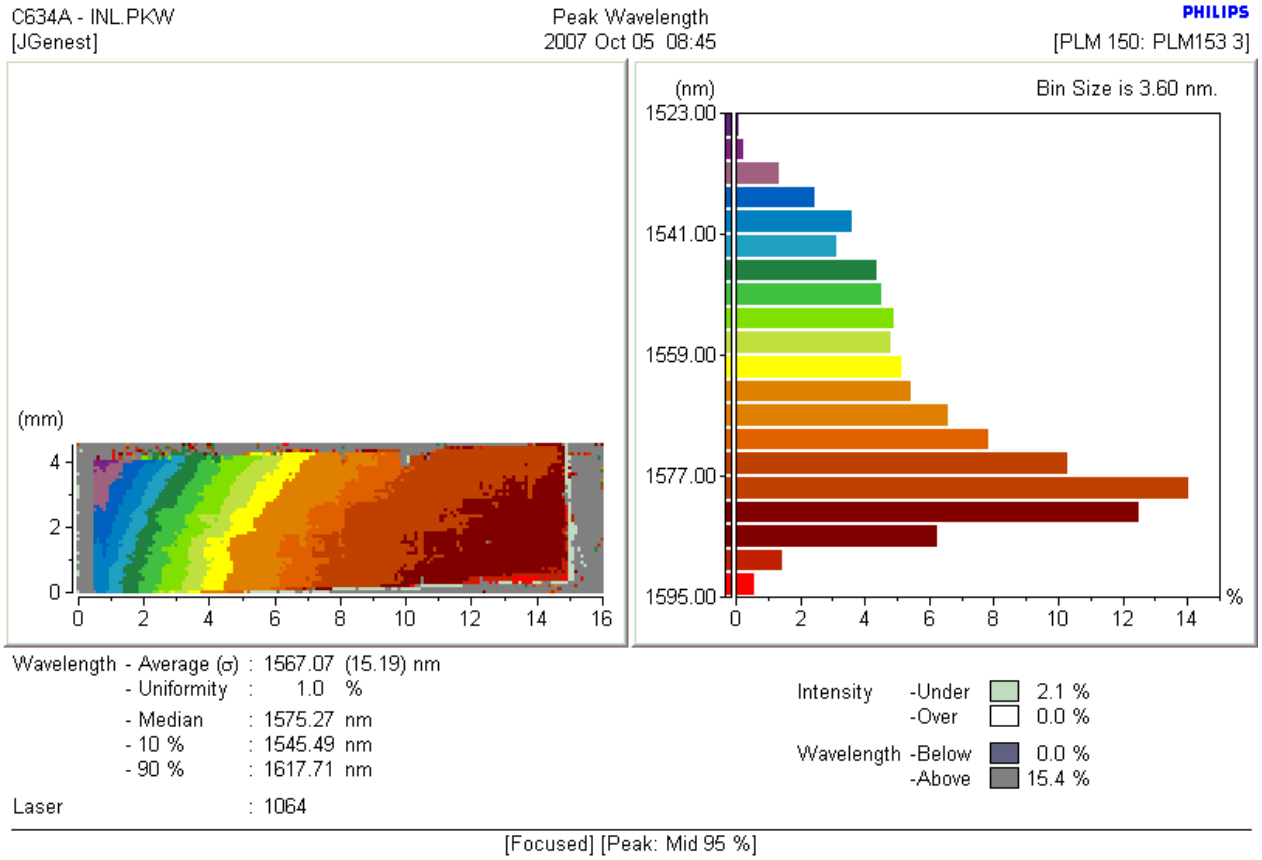

Figure 8-12: Photoluminescence mapping of a InAs/InGaAsP/InP quantum stick sample after UV laser irradiation.

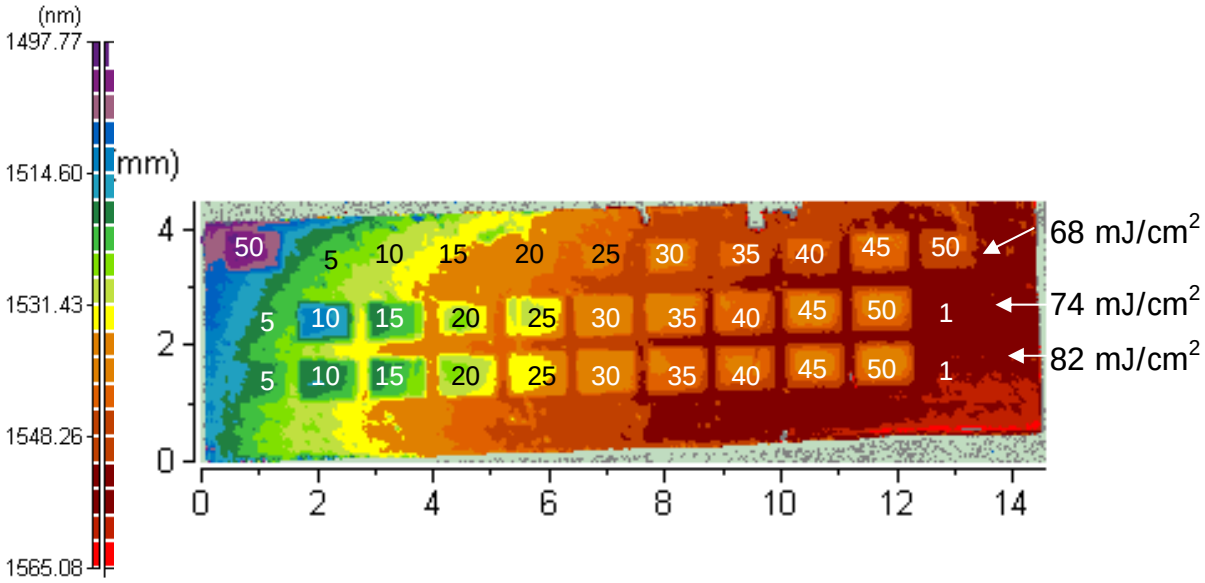

Figure 8-13: Photoluminescence mapping after irradiation and annealing.

We attribute the small redshift after irradiation to the stress generated by the laser assisted oxidation of the sacrificial and the contact layers. The maximum blueshift attained, 50 nm, is relatively small compared to the blueshift obtained in similar, but undoped QS structures: 350 nm obtained by ion implantation [B. Salem *et al.* 2005], ~360 nm reached with a grown defect layer [C. Dion *et al.* 2006] and ~450 nm obtained with SiO_2 dielectric capping [C.K. Chia *et al.* 2005]. It is important to note that in all these cases, the heterostructures were undoped and that the QS layers were whether located less than 120 nm for the surface or right under a layer rich in point defects. Also, the two latter studies were done with whether long annealing time (300s) or at very high temperature for this material system (900°C). QS intermixing in a laser structure was performed by Djie *et al.* using for InAs QS (λ_{QS} ~ 1550 nm) layers embedded in InAlGaAs QWs grown on an InP substrate. They capped their samples with SiO_2 and Si_3N_4 before annealing they them for 120 s at 800°C. The maximum blueshift achieved was ~150 nm [H.S. Djie *et al.* 2007].

A more comparable technique was used by Djie *et al*. in laser structures to intermix InAs quantum dots (λ ~ 775 nm) on an GaAs substrate. They deposited either SiO_2 or Si_3N_4 cap layers on their samples by PECVD and irradiated them with KrF excimer laser pulses for fluences ranging from 200 to 480 mJ/cm^2 and number of pulses up to 150. After an annealing at 750°C for 120 seconds, they observed a maximum blueshift of ~200 nm for a very shallow (40 nm) stack of QD layers [H.S. Djie *et al.* 2006b]. For QDs embedded 1.7µm under the heterostructure surface, the maximum shift achieved was ~32 nm for 100 pluses at 480 mJ/cm^2 and annealing at 700°C for 120 seconds. Although they were achieved with fluences more than four times higher, these latter results are more comparable to ours. As figure 8-14 illustrates, in contrast with Djie's results, we cannot observe blueshift saturation, it is reasonable to think that we can achieve greater blueshift with a more optimized process.

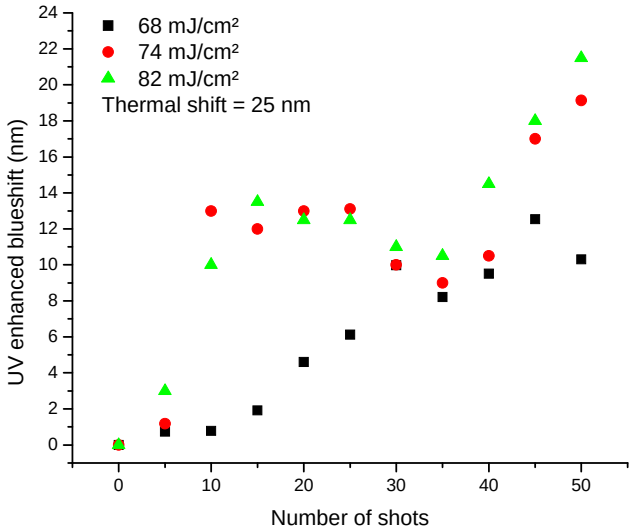

Figure 8-14: Photoluminescence shift associated with UV laser irradiation laser.

8.4 Summary

This chapter describes the UV-QWI technique in non standard conditions. They contribute to a better understanding of the UV laser controlled quantum well intermixing

technique and explore the application of UV laser technology to quantum dot intermixing. We can summarize the concluding remarks as follow:

KrF laser irradiation of GaAs different atmospheres has demonstrated that physisorbed water vapour has a huge influence on the photoenhanced oxidation. Because the availability of water vapours in air, irradiation in this environment leads to the formation of a thicker oxide. Except for the sample irradiated in vacuum with a fluence of 40 mJ/cm^2 for 1000 pulses, which showed a significant blueshit (58 nm), KrF irradiation of GaAs-based quantum well heterostructures in vacuum and nitrogen environments resulted in the suppression of quantum well intermixing and quenching of the photoluminescence intensity. We attribute this behaviour to the combined effects of laser photo-enhanced oxidation due the remaining physisorbed water vapour on the sample surface and of the accumulation of laser induced surface damage. Further tests are needed to discriminate the two phenomena. Annealing the sample at ~ 125°C under nitrogen for few minutes should remove the adsorbed water vapour and should prevent photo-enhanced oxidation. It would also be interesting to study KrF irradiation in vacuum for fluences lower than 40 mJ/cm^2 over a broad range of pulses number. We suspect that under theses conditions it would be possible the enhance quantum well intermixing in GaAs-based heterostructures.

In InP-based heterostructure, KrF and ArF irradiation in environments both enhanced the intermixing process. However, in addition to its smaller defects generation rates, KrF irradiated blueshifted samples were characterized by the formation of hot spots where blueshift increase, suppression and surface ablation would happen at faster rate than elsewhere. This led to non-uniform shift over the sample area. Because of this, we believe that ArF laser is a better candidate to achieve reproducible and spatially uniform multi bandgap material InP based heterostructures.

The nature and condition of the cap layer plays a significant role on the intermixing extent. Because of the higher bond strength in InGaAs, the point defects generation rate in the contact is smaller than in the InP sacrificial layer for an identical fluence of ArF irradiation. Furthermore, the irradiation of an ion implanted InP sacrificial layer reduced the ion implantation enhanced intermixing. We attribute this effect to the laser pulse which mainly contributes to the amorphization of already damaged InP.

We also fabricated laser diodes on the intermixed InGaAs/InGaAsP/InP quantum well samples. The irradiation conditions were chosen to cover broad range of emission wavelength. The current threshold from the intermixed diodes was similar and sometimes smaller than the reference's. We can then conclude that the quality of the intermixed material quality is comparable to the quality of the reference. We have also shown that, for a given fluence, by varying the number of pulses, it is possible to cover an important range of emission wavelengths from 1440 to 1560 nm.

Finally, we have demonstrated the potential of a technology based on UV laser to achieve quantum dot intermixing in InAs/InP quantum sticks embedded in a laser heterostructure. We have blueshifted the sticks to en extent of 50 nm. This is relatively small compare to other documented results, however, as saturation was not observed, it is reasonable to think that we can achieve greater blueshift with a more optimized process. Irradiation under higher fluences and number of pulses would certainly further enhance the quantum dot intermixing.

8.5 References

Aspnes, D. E. and Studna, A. A. (1983) *Dielectric functions and optical parameters of Si, Ge, GaP, GaAs, GaSb, InP, InAs, and InSb from 1.5 to 6.0 eV*, Physical Review B, vol. 27, n° 2, 985.

Basting, D. and Marowsky, G., Eds. (2005). Excimer laser technology. Berlin, Springer/Praxis, 433 p.

Buda, M., Deenapanray, P. N. K., et al. (2002). *Quantum well intermixing for optoelectronic device integration*, Nis, Yugoslavia, IEEE.

Campbell, I. H. and Fauchet, P. M. (1990) *cw laser irradiation on GaAs: arsenic formation and photoluminescence degradation*, Applied Physics Letters, vol. 57, n° 1, 10-12.

Carmody, C., Tan, H. H., et al. (2003) *Influence of cap layer on implantation induced interdiffusion in InP/InGaAs quantum wells*, Journal of Applied Physics, vol. 93, n° 8, 4468-70.

Chia, C. K., Chua, S. J., et al. (2005) *Group-V intermixing in InAs/InP quantum dots*, Applied Physics Letters, vol. 86, n° 5, 051905-3.

Chicoine, M., Francois, A., et al. (2003) *Effects of damage accumulation on quantum well intermixing by low-energy ion implantation in photonic devices*, SPIE proceeding, vol. 5260, n° 423-431.

Davis, G. M., Thomas, D. W., et al. (1988) *Excimer laser direct etching of GaAs*, Journal of Physics D: Applied Physics, vol. n° 5, 683.

Dion, C., Poole, P. J., et al. (2006) *Tuning of the electronic properties of self-assembled InAs/InP(001) quantum dots using grown-in defect mediated intermixing*, Applied Physics Letters, vol. 89, n° 13, 131905-3.

Djie, H. S., Ooi, B. S., et al. (2006) *Quantum dot intermixing using excimer laser irradiation*, Applied Physics Letters, vol. 89, n° 8, 081901.

Djie, H. S., Wang, Y., et al. (2007) *Wavelength tuning of InAs/InAlGaAs quantum-dash-in-well laser using postgrowth intermixing*, Electronics Letters, vol. 43, n° 1, 33-5.

Gunawan, O., Ong, T. K., et al. (2000). *A theoretical analysis of quantum well intermixing using the pulsed laser irradiation technique in InGaAs/InGaAsP laser structure*, Beijing, China, Elsevier.

Hayes, W. and Stoneham, A. M. (2004). *Defects and defect processes in nonmetallic solids*, Mineola, N.Y., Dover edition, 472 p.

Ortner, G., Allen, C. N., et al. (2006) *External cavity InAs/InP quantum dot laser with a tuning range of 166 nm*, Applied Physics Letters, vol. 88, n° 12, 121119-1.

Philipp, H. R. and Ehrenreich, H. (1963) *Optical Properties of Semiconductors*, Physical Review, vol. 129, n° 4, 1550.

Podlesnik, D. V., Gilgen, H. H., et al. (1986) *Interaction of Deep-Ultraviolet Laser-Light with GaAs-Surfaces in Aqueous-Solutions*, Journal of the Optical Society of America B-Optical Physics, vol. 3, n° 5, 775-784.

Sainter, A. W., King, T. A., et al. (2004) *Effect of target biological tissue and choice of light source on penetration depth and resolution in optical coherence tomography*, Journal of Biomedical Optics, vol. 9, n° 1, 193-9.

Salem, B., Aimez, V., et al. (2005) *Band gap tuning of InAs/InP quantum sticks using low-energy ion-implantation-induced intermixing*, Applied Physics Letters, vol. 87, n° 24, 241115-1.

Thurmond, C. D., Schwartz, G. P., et al. (1980) *GaAs oxidation and the Ga-As-O equilibrium phase diagram*, Journal of the Electrochemical Society, vol. 127, n° 6, 1366-71.

Tomlins, P. H. and Wang, R. K. (2005) *Theory, developments and applications of optical coherence tomography*, Journal of Physics D (Applied Physics), vol. 38, n° 15, 2519-35.

Wesch, W., Wendler, E., et al. (1989) *Defect production during ion implantation of various $A_{III}B_V$ semiconductors*, Journal of Applied Physics, vol. 65, n° 2, 519-26.

Yu, C. F., Schmidt, M. T., et al. (1987) *Wavelength Dependence of Optically Induced Oxidation of GaAs(100)*, Journal of Vacuum Science & Technology B, vol. 5, n° 4, 1087-1091.

Chapter 9: Conclusions and perspectives

The work presented in this thesis was aimed at the study and development of a UV laser controlled quantum well intermixing technology for GaAs and InP based heterostructures. Through this research, we have studied its dynamics and evaluated the potential of this technology to manufacture multi-bandgap wafers suitable to fabricate monolithically integrated photonic circuits in quantum wells but also in quantum sticks. However, this work has also highlighted questions and gaps which would need to be addressed in future work. This chapter presents a review of the major findings of this work and some indications for future work and perspectives.

9.1 Conclusions

In this work, we developed a UV laser quantum well/dot intermixing technology to fabricated multi-bandgap materials in AlGaAs/GaAs, InAlGaAs/AlGaAs/GaAs and InGaAs/InGaAsP/InP quantum well laser heterostructures and in InAs/InGaAsP/InP quantum sticks laser heterostructures. For photonic devices to play a more substantial role in the telecommunication market, new photonics technologies need to demonstrate real increase in functionalities which can only be accomplished by developing a reliable and efficient integration technology that can support reduction of circuit size and fabrication costs. Among the different integration approaches for photonic devices, quantum well intermixing technologies are attractive because of their numerous advantages: they are simpler to implement and cheaper than regular etching and regrowth steps, they usually require equipment compatible with microfabrication

technologies and can locally modulated an heterostructure bandgap over broad energy range with few interface defects between the different bandgap regions. However, these technologies are seldom used in the industry. This is mainly due to the lack of reliability and reproducibility of most quantum well technologies for achieving a desire blueshift. Furthermore, most quantum well intermixing technologies are based on the introduction of an extra concentration of point defects into the heterostructure. Such defects can reduce the quality of the intermixed material and affect the optical and electrical performances of devices.

It this work, we have demonstrated that UV laser quantum well intermixing was applicable to control the bandgap in GaAs and InP based laser heterostructures. In GaAs heterostructures, KrF laser irradiation in air environment enhances the surface oxidation which forms a surface stressor mainly composed of Ga_2O_3. During the annealing step, since the thermal expansion coefficient of the oxide is higher than the one of the GaAs, this stressor puts the heterostructure under biaxial tensile stress, forcing the vacancies to diffuse toward the surface and preventing them to participate to the interdiffusion. Depending on the UV laser irradiation fluence and number of pulse, the thermal shift was suppressed over range of 35 nm. Used in parallel with a SiO_2 dielectric mask, the stress field generated from the UV grown oxide, increased the sharpness between two different bandgap regions to a lateral resolution of about 1 μm or better. This ability to fabricate gallium oxide stressors on a wafer by a UV laser projection lithography technique has the potential to become a simple technology to manufacture multi-bandgap quantum well wafers.

In InP based heterostructures capped with an InP sacrificial layer, UV laser irradiation favours the desorption of surface atoms and breaks atomic bonds which generates new point defects. The extra concentration of point defects allows the UV laser quantum well intermixing

technology to control the intermixed bandgap over a range of ~ 125 nm by tuning the laser fluence and number of pulse. A phenomenological model was also developed to describe the intermixing enhancement due to the UV laser irradiation. For high number pulses, the degree of intermixing saturates and decreases. We attribute this suppression to the UV enhanced oxidation of the InP sacrificial layer and of the InGaAs contact layer and to the laser assisted amorphization of the heterostructure top layer. When compared, KrF and ArF laser were used to obtain blueshift of the order of 125 nm. However, to achieve the same blueshift extent, KrF laser irradiation was required to be held at a higher fluence and larger pulse number. Furthermore, KrF irradiated blueshifted samples were characterized by the formation of hot spots where the intermixing enhancement and suppression would happen at a faster rate than elsewhere. Because of this, we believe that ArF laser is a stronger candidate to achieve reproducible and spatially uniform multi-bandgap material InP based heterostructures.

The UV laser controlled quantum well intermixing technology was also applied to fabricate broad area laser diodes covering wavelengths ranging from 1440 to 1560 nm. The intermixed material obtained by UV laser quantum well intermixing demonstrated a quality comparable to the one of the reference material. After annealing, the photoluminescence from the irradiated sites was higher than from the untreated areas and the current threshold of the intermixed laser diodes was comparable, even lower, than the current threshold of the reference laser diodes.

9.2 Perspectives and future work

During KrF laser irradiation of GaAs, the importance of the physiorbed water vapour on the oxide stressor growth was highlighted. Under different environment, KrF laser irradiation led to the suppression of the thermal intermixing but, in contrast with experiments done in air

environment, it also led to the quenching of the photoluminescence signal. We explained this by the combined effect of the photoenhance oxide stressor growth and of the damage accumulation induced by the irradiation. Annealing the sample at ~ 125°C under nitrogen atmosphere should remove the adsorbed water vapour and should discriminate the effect of these two phenomenons. It would also allow us to determine the best irradiation and environmental conditions to efficiently enhance the quantum well intermixing in GaAs-based heterostructures.

In InP-based heterostructures, we also have identified two possible explanations for the intermixing suppression happening for large number of pulses under both ArF and KrF irradiation: the oxidation of the two top most layers and the amorphization of the InP sacrificial layer. The installation of an environmental chamber on ArF irradiation setup would allow us to differentiate the influence of both phenomenons. Such chamber would also allow us to generate point defect directly in InGaAs without oxidizing it and would also permit more selective control on the type of defects created in InP by properly choosing the environment gas.

UV laser irradiation demonstrated its potential to achieve quantum dot intermixing in InAs/InP quantum sticks. The blueshift range covered was of 50 nm. Although this is relatively small for quantum dot intermixing, nothing suggested that this was a limitation due to the UV laser technology. An optimization of the irradiation parameters and annealing conditions would certainly allow us to reach higher blueshift values.

One of biggest limitation of the UV laser quantum well intermixing technology is the control over the laser beam intensity. Unfortunately, this is an inherent limitation of the excimer laser itself. For low number of pulse, the uncertainty of the deposited energy per each pulse is relatively high and prevents accurate prediction of the induced blueshift. As we have seen, the

blueshift increases faster at the beginning of the irradiation. In such context, the pulse-to-pulse instability can have drastic consequences when trying to achieve a relatively low blueshift value. This could be counteracted indirectly by associating changes in surface properties to the intermixing extent. Although it is still dependant on the laser pulse-to-pulse stability, we have demonstrated that an in-situ monitoring system based on UV-excited photoluminescence is sensitive to surface condition changes. The implementation of a second laser for probing, would discard this issue. Furthermore, Raman spectroscopy or differential reflection measurements could also give a real-time assessment of the surface conditions and offer control over the desire bandgap shift. This however would require a better understanding on the relation between changes of the surface conditions and intermixing extent and it would also require standardize irradiation and annealing processes.

Up to now, we have obtained a moderate success in controlling quantum well intermixing in GaAs-based quantum well heterostructures with UV laser pulses in air environment. Although it suppresses the thermal shift with one micrometer lateral resolution, it doesn't demonstrate quantum well intermixing enhancement yet. The 35 nm blueshift suppression achieved would be enough to fabricate multi-wavelengths laser diode arrays or other simple integrated devices. However, since such bandgap increase is not enough to fabricate low loss waveguide, no complex photonic circuits could be fabricated using this technology. Controlling the environment during the irradiation might allow us to create point defect in GaAs with growing a surface stressor. Some preliminary results of low fluence irradiation under vacuum atmosphere led to a weak (20 nm) blueshift increase. We can expect that by improving our understanding of the surface stressor growth, we could establish irradiation conditions favourable to achieve blueshift over a broader range.

In contrast, the 125 nm blueshift obtained in InP-based quantum well heterostructures offers a sufficient range to fabricate monolithically integrated photonic circuits including active and passive devices. The passive waveguides would need to be fabricated in the regions demonstrating the highest shift. With the adequate plasma etching technology to define the waveguides, we can easily imagine a photonic chip including multiple lasers emitting on different channels and the multiplexing optics. The integration level achieved would permit the mass production of such chip for the information and communication market

Finally, because it can activate surface chemical reaction, UV laser irradiation in controlled environment has the potential to selectively generate point defects and form stressor that can enhance and inhibit their diffusion. In parallel with a projection lithography system, it could lead to the development of a global high resolution photonic integration technology which would be suitable for the new generation of photonic integrated circuits.